MULTIPLE ROLES OF RET SIGNALING IN MECHANOSENSORY NEURON DEVELOPMENT

Michael S. Fleming

A DISSERTATION

in

Neuroscience

Presented to the Faculties of the University of Pennsylvania

in

Partial Fulfillment of the Requirements for the
Degree of Doctor of Philosophy

2016

Supervisor of Dissertation

_____

Wenqin Luo, MD, PhD
Assistant Professor of Neuroscience

Graduate Group Chairperson

_____

Joshua I. Gold, PhD
Professor of Neuroscience

Dissertation Committee:

Gregory J. Bashaw, PhD, Professor of Neuroscience
Douglas J. Epstein, PhD, Professor of Genetics
Robert O. Heuckeroth, MD, PhD, Professor of Pediatrics
Steven S. Scherer, MD, PhD, Professor of Neurology

MULTIPLE ROLES OF RET SIGNALING IN MECHANOSENSORY NEURON DEVELOPMENT

COPYRIGHT

2016

Michael S. Fleming

ACKNOWLEDGEMENT

I would like to thank my mentor, Dr. Wenqin Luo. Wenqin has been an amazingly supportive and inspiring mentor over the past five years. Her insights and encouragement have been crucial in performing the work in this thesis. Wenqin is a brilliant scientist and our countless conversations about my project and science in general have been invaluable in teaching me how to think scientifically.

I would also like to thank members of the Luo lab for insightful comments, suggestions, and friendship. Thank you to Dr. Jingwen Niu, Dr. Lian Cui, Dr. Ishmail Abdus-Saboor, Dr. Nathan Fried, Will Olson, Peter Dong, Kim Kridsada, and Anna Vysochan for making the Luo lab such a great environment. Thank you to Dr. Minghong Ma and the members of her lab for helpful comments during joint lab meetings.

Many thanks to Drs. Greg Bashaw, Doug Epstein, Steve Scherer, and Robert Heuckeroth for serving on my thesis committee. Their expertise has been a valuable resource in designing and interpreting experiments, and their insights in and out of committee meetings have strengthened my thesis work in many ways.

Thank you to my family and friends for all of your support. My parents have always supported my interest in science and I want to thank them for encouraging me to pursue my goals. Most importantly, thank you to my wife, Melissa, for constant love, support, and understanding.

ABSTRACT

MULTIPLE ROLES OF RET SIGNALING IN THE DEVELOPMENT OF MECHANOSENSORY NEURONS

Michael S. Fleming

Wenqin Luo

Somatosensation is critical for interaction with the surrounding environment. Somatosensory stimuli are detected by primary somatosensory neurons of the dorsal root ganglia and trigeminal ganglia, which detect distinct classes of stimuli, such as temperature, pain, and pressure. In Chapters 2 and 3 of this thesis, we focus on rapidly adapting low-threshold mechanoreceptors (RALTMRs), which mediate the detection of light touch. RALTMRs are molecularly defined by the early embryonic expression of the receptor tyrosine kinase *Ret*. *Ret* is required for the development of central axonal projections of RALTMRs into the dorsal spinal cord. RET responds to the glial cell line-derived family of neurotrophic factors, which activate RET in combination with GPI-linked GFRα co-receptors. In vitro, RET can be activated by co-receptor expressed in the same cell (*cis* signaling) or by co-receptor expressed by neighboring cells (*trans* signaling), but previous studies suggest that *trans* RET signaling may not play a physiologically relevant role in vivo. Here, we show that RET in mouse RALTMRs can be activated by both GFRα2 expressed in the same cell (*cis* signaling) and GFRα1 expressed by neighboring cells (*trans* signaling), and that *trans* RET signaling is sufficient for the development of RALTMR central projections in vivo. Peripherally, *Ret*

is required for the development of vibration sensitive Pacinian corpuscle RALTMR end organs. We show that *Ret* mediates the neuronal expression of the ETS transcription factor *Er81*, which is also required for Pacinian corpuscle development, and that deficient axon/Schwann cell communication is the primary deficit in Pacinian corpuscle development in *Er81* mutant mice. Furthermore, we show that *Neuregulin-1*, an important mediator of axon/Schwann cell interactions, is required for Pacinian corpuscle development, and that *Er81* regulates the expression of specific *Neuregulin-1* isoforms. In total, we demonstrate that RET signaling drives the development of distinct developmental processes in both the central and peripheral axonal branches of RALTMRs. In Chapter 4, we describe the expression of itch-related neuropeptides GRP and NMB and their receptors in somatosensory neurons and the dorsal spinal cord.

TABLE OF CONTENTS

LIST OF TABLES

Chapter 2:

LIST OF ILLUSTRATIONS

Chapter 1:

Chapter 2:

Chapter 3:

Chapter 4:

CHAPTER 1

Introduction

This chapter was written by Michael S. Fleming. Portions of this chapter have been adapted from:

Fleming, MS and Luo W (2013). The anatomy, function, and development of mammalian Aß low-threshold mechanoreceptors. *Frontiers in Biology.* 8(4).

MAMALIAN SOMATOSENSATION

Light touch sensation is critical for our social interaction and daily lives. It allows for the detection of diverse stimuli, like a breeze, a kiss, a hug, the texture of fabric, or a shape, and is required for complex tasks, such as using a tool or reading Braille. These stimuli cause vibration, indentation or stretching of the skin, the movement of hair follicles, or some other physical change in the skin, which activate mechanosensory nerve fibers or the specialized mechanosensory end organs in the skin. There are several different types of mammalian low-threshold mechanosensory neurons (mechanoreceptors), including Aβ, Aδ, and C (distinguished according to their transduction velocity), which mediate various form of light touch sensation. In this introduction, I will focus on Aβ low-threshold mechanoreceptors, which are the main type of primary sensory neurons that mediate discriminative touch and tactile perception in mammals. Cell bodies of Aβ low-threshold mechanoreceptors are located in the trigeminal (TGs) and dorsal root ganglia (DRGs). Each neuron grows a single axon that bifurcates shortly after projecting from the cell body, with the peripheral axon innervating mechanosensory end organs and the central projection innervating the spinal cord and brain stem.

The morphologies and structures of Aβ low-threshold mechanosensory end organs have been extensively examined since their first discovery in the 1800s. Based on morphologies of these end organs, Aβ low-threshold mechanoreceptors are classified into several different subtypes, including Meissner's corpuscles, Pacinian corpuscles,

lanceolate endings, Merkel cells, and Ruffini corpuscles (Iggo and Andres, 1982; Rice and Albrecht, 2008). Physiological properties of Aβ low-threshold mechanoreceptors started to be characterized around the middle of 20th century. According to their rates of adaptation to sustained mechanical stimuli, Aβ low-threshold mechanoreceptors are classified as either rapidly adapting (RA) or slowly adapting (SA) (Iggo, 1985; Mountcastle, 1957). Interestingly, their end organ morphologies and physiological properties are very well correlated. Meissner's corpuscles, lanceolate endings, and Pacinian corpuscles are the RA mechanoreceptors (Iggo, 1985; Iggo and Ogawa, 1977), whereas Merkel cells and Ruffini corpuscles are the SA mechanoreceptors (Burgess, 1973; Iggo and Muir, 1969; Pare et al., 2002) (Figure 1). In the past two decades, advances in mouse genetic techniques have enabled the dissection of key molecules, mainly neurotrophic factors and transcription factors, involved in controlling the specification and development of different subtypes of mammalian Aβ low-threshold mechanoreceptors. In my thesis work, I have focused on the development of the RA mechanoreceptors, and in particular, the Pacinian corpuscles.

Recently, a specific molecular marker which exclusively marks RA mechanoreceptors has been identified. The receptor tyrosine kinase RET is expressed in 60% of adult mouse DRG neurons. The majority of RET^{+} neurons are small diameter neurons which begin to express *Ret* around E13.5 or later. However, a subset of large diameter neurons begins to express RET around E10.5, but their function remained unknown (Molliver et al., 1997). Recently, Luo, et al., used genetic tracing to show that the "early-RET^{+}"

neurons are RA mechanoreceptors (Luo et al., 2009). *Ret* also has an important role in the development of RA mechanoreceptors. In *Ret* mutants, central projections of RA mechanoreceptors reach the dorsal spinal cord, but fail to extend interstitial branches to innervate layers III-V of the dorsal horn (Bourane et al., 2009; Honma et al., 2010; Luo et al., 2009). In Chapter 2 of this thesis, I examine the RET signaling mechanisms which contribute to the growth of these central projections. *Ret* also has a role in the peripheral development of RA mechanoreceptors. In neural crest specific *Ret* mutants, Pacinian corpuscles do not form in the interosseous membrane surrounding the fibula, while Meissner's corpuscles and lanceolate endings appear mostly normal (Luo et al., 2009). In Chapter 3 of this thesis, I further examine the role of *Ret* in the development of Pacinian corpuscles.

MEISSNER'S CORPUSCLES

Anatomical location and morphology

Meissner's corpuscles are present in the glabrous (hairless) skin, including palms of the hand, soles of feet, and lips. They are located within the dermal papillae, which are conical protrusions of the dermis into the epidermis, with their long axis perpendicular to the surface of the skin (Munger and Ide, 1988). Meissner's corpuscles were first described in the fingers and palms of human hands by Georg Meissner and Rudolph Wagner in 1852 (Cauna, 1956), but a high-resolution description of their morphology was not possible until the advent of electron microscopy in the mid-20th century (Cauna

and Ross, 1960; Pease and Pallie, 1959). The oval shaped corpuscle structure is composed of disc-like lamellar stacks derived from Schwann cells, which is partially surrounded by a thin fibroblast capsule. In most cases, the corpuscle is innervated by a myelinated Aβ sensory fiber, which loses its myelination after traveling through the bottom third of the corpuscle (Zelena, 1994). The sensory axon takes a circuitous route within the corpuscle, weaving between stacks of lamellar cells. In addition to Aβ innervation, some Meissner's corpuscles are also innervated by C-fibers which have molecular profiles similar to nociceptors (Pare et al., 2001), but the functional relevance of this innervation is unclear.

A combination of physiological recording and horseradish peroxidase tracing has been employed to reveal morphologies of the central projections of mammalian Aβ low-threshold mechanoreceptors (Brown, 1981). Shortly after entering the spinal cord, their central axon bifurcates and sends projections in the rostral and caudal directions in the superficial layer of the spinal cord. Interstitial branches arise from these projections, and innervate deeper layers of the dorsal horn (Brown, 1981). In cats, Meissner's corpuscle afferents synapse mostly in the medial aspect of layers III-IV of the dorsal horn, while in rats they mostly innervate the medial aspect of layers III-V of the dorsal horn, with a small number of synapses made in the inner part of layer II (Brown, 1981; Semba et al., 1985; Shortland and Woolf, 1993).

Physiological properties and function

Meissner's corpuscles are classified as type I RA (RAI) mechanoreceptors. In single unit recordings from humans and monkeys, Meissner's corpuscle innervating fibers display a burst of activity upon the onset and offset of a stimulus, but remain silent during the static phase of stimulation (Talbot et al., 1968). They have an extremely low threshold for activation, responding to an indentation of the skin of less than 10μm (Iggo and Ogawa, 1977). In addition, Meissner's corpuscles have relatively small receptive fields and are most sensitive to low intensity stimuli of ~5-100Hz (Gardner and Palmer, 1990). When stimulated at frequencies within their optimal range, Meissner's corpuscle afferents produce action potentials in a nearly perfect one-to-one relationship with the stimulus and generate a "fluttering" feeling in human subjects (Talbot et al., 1968). Meissner's corpuscles may also function as velocity detectors to determine the rate of skin indentation (Willis and Coggeshall, 2004).

At present, the precise mechanical transduction mechanism for Meissner's corpuscles is unknown. A recent study has identified the KCNQ4 potassium channel, which is expressed in Meissner's corpuscle innervating Aβ low-threshold mechanoreceptors, as an important molecule to tune their sensitivity. KCNQ4 itself is not mechanically gated, but is important for setting the resting potential of neurons. Both mice and humans with KCNQ4 mutations display higher sensitivity to low frequency stimuli, which are mediated by Meissner's corpuscles (Heidenreich et al., 2012).

Development

Meissner's corpuscle innervating axons reach the dermal papilla around birth. Schwann cells associated with the axon begin to differentiate into the lamellar cells, which form the corpuscle structure around one week in rodents. Innervation is required for the development of the corpuscle structure, as corpuscles do not form if the footpad is denervated at birth (Zelena et al., 1990).

Meissner's corpuscles depend on the neurotrophic receptor tyrosine kinase TrkB for their development. TrkB is expressed in a subset of RA mechanoreceptor neurons starting at early developmental stages (Luo et al., 2009). In *TrkB* null mice, Meissner's corpuscles were not found in the dermal papilla of 2-3 week old mice (Gonzalez-Martinez et al., 2004). Examination of mice lacking the high affinity ligands of TrkB, brain derived neurotrophic factor (BDNF) or neurotrophin-4 (NT4), revealed that BDNF, but not NT4, is required for Meissner's corpuscle development (Gonzalez-Martinez et al., 2005). Since the number of DRG neurons is reduced by ~30% in *TrkB* and *BDNF* mutant mice in the second postnatal week, it is possible that BDNF-TrkB signaling supports the survival of Meissner's corpuscle neurons and the loss of Meissner's corpuscles is due to the death of innervating neurons (Perez-Pinera et al., 2008). However, the mechanism of TrkB signaling in controlling Meissner's corpuscle formation could be more complicated. Immunolocalization of TrkB in human digit skin shows that the receptor is expressed in

the lamellar cells of the corpuscle, but not on the innervating axon (Calavia et al., 2010) and the overexpression of NT4 or BDNF in the skin led to an increase in the size of Meissner's corpuscles, but no change in the number of sensory neurons in the DRG (Krimm et al., 2006; LeMaster et al., 1999). In addition, myelinated axons are present in the dermal papillae of neural crest specific *TrkB* mutants, even though no corpuscle structure is formed, and the central projections of Aβ low-threshold mechanoreceptors do not seem to be affected (Luo et al., 2009). These results suggests that at least some Meissner's corpuscle innervating neurons do not die in *TrkB* mutants, and the lack of corpuscles may be due to a pro-survival independent function of TrkB signaling. Future studies using tissue specific knockouts of *TrkB* and *BDNF* will be necessary to determine the spatial and temporal requirement of TrkB and its ligands in Meissner's corpuscle formation.

Meissner's corpuscles also express another neurotrophic receptor tyrosine kinase, *Ret*, during early development (early RET^+ RA mechanoreceptors) (Luo et al., 2009). Surprisingly, RET signaling is not essential for Meissner's corpuscle formation, as corpuscles are present, although somewhat underdeveloped, in neural crest specific *Ret* mutants. On the other hand, RET signaling is absolutely required for the central projections of all RA mechanoreceptors. In *Ret* mutants, central projections of RA mechanoreceptors reach the dorsal spinal cord, but fail to extend interstitial branches to innervate layers III-V of the dorsal horn (Bourane et al., 2009; Honma et al., 2010; Luo et al., 2009).

In addition to extrinsic neurotrophic signaling, intrinsic transcriptional programs play important roles to specify the neural identity of somatosensory neurons. One transcription factor, Shox2, is critical for the innervation and development of Meissner's corpuscles. Ablation of *Shox2* in mice leads to a lack of *TrkB* expression in two thirds of the DRG neurons which normally express the receptor during embryonic development (Abdo et al., 2011; Scott et al., 2011). As a result, *Shox2* mutant mice lack Meissner's corpuscles and show reduced innervation of the dermal papillae, while the heterozygous *Shox2* adult mice display an increased threshold for light touch detection (Abdo et al., 2011). Deletion of *Shox2* also caused reduced touch sensory axonal innervation to layers III/IV of the spinal cord (Scott et al., 2011). Additionally, two Maf family transcription factors, MafA and c-Maf, are expressed in the RET^{+} RA mechanoreceptors. RET and MafA reciprocally regulate the expression of each other, whereas c-Maf is upstream of *Ret* expression (Bourane et al., 2009; Hu et al., 2012; Wende et al., 2012). In *c-Maf* mutant mice, the number of Meissner's corpuscles is drastically reduced and the remaining corpuscles have a rudimentary structure, although the innervation of the dermal papillae isn't affected (Wende et al., 2012). A deficit in the formation of Meissner's corpuscles was not described in *MafA* mutant mice since these mutants were not examined any later than postnatal day zero (P0) (Bourane et al., 2009).

PACINIAN CORPUSCLES

Anatomical location and morphology

The anatomical location of Pacinian corpuscles varies greatly between species. In primates, Pacinian corpuscles are most prominently located in the subcutaneous fat pads of the fingers, palms, and soles (Zelena, 1994). They are also found in joints, tendons, interosseous membrane, and around some muscles and internal organs, such as the pancreas (Bell et al., 1994). Many early physiological and morphological studies of Pacinian corpuscles were performed on corpuscles isolated from the cat mesentery (Sato, 1961). In rodents, Pacinian corpuscles are not present in the skin but are enriched in the interosseous membrane around the fibula and ulna (Zelena, 1978). The Herbst corpuscle, a structure similar to the Pacinian corpuscle, is found in beak and interosseous membrane of birds (Saxod, 1996; Zelena et al., 1997).

Pacinian corpuscles were first described in the 18th century by Johannes Gottlieb Lehmann, and later rediscovered by Fillipo Pacini in 1841 (Bentivoglio and Pacini, 1995). They are oval shaped end organs and can reach sizes of up to 4 mm in length in adult human (Cauna and Mannan, 1958). Each Pacinian corpuscle is innervated by a single myelinated Aβ somatosensory neuron, which loses its myelination and assumes a relatively straight trajectory through the center of the corpuscle upon entering the corpuscle's inner core (Quilliam and Sato, 1955). Ultrastructural studies of the corpuscle have revealed that the inner core is composed of two "hemilamellae" on either side of the axon, with two clefts separating them, throughout the length of the inner core. Each

hemilamella of the mature corpuscle contains 40-80 layers of lamellar Schwann cells while the outer core is composed of ~30 layers of perinurial epithelial cells (Cauna and Mannan, 1958; Pease and Quilliam, 1957; Zelena, 1994). This layered construction produces an onion-like appearance in cross sections of Pacinian corpuscles.

Central projections of Pacinian afferents form synapses in two distinct regions: a larger dorsal region focused in layer III and outer layer IV with less dense innervation extending dorsally to inner layer II and ventrally to outer layer V, and a smaller ventral region concentrated in layer V but also sparsely innervating layers IV and VI (Brown, 1981; Brown et al., 1980; Semba et al., 1984).

Physiological properties and function

Pacinian corpuscles are classified as type II RA (RAII) mechanoreceptors, which, like Meissner's corpuscles, respond to mechanical stimuli at the onset and offset of stimuli. However, the RAI and RAII mechanoreceptors can be distinguished in two ways: 1) RAII mechanoreceptors have larger, less defined receptive fields, suggesting a poor ability of Pacinian corpuscles to localize stimuli (Palmer and Gardner, 1990); and 2) RAII mechanoreceptors respond to a higher frequency of vibration, and are most sensitive to stimuli in the 200-300Hz range (Burgess, 1973; Knibestol, 1973).

The precise mechanical transduction mechanism for Pacinian corpuscles is also unknown. The RA properties of Pacinian corpuscles are partly due to the corpuscle structure, which acts as a mechanical filter. Very low velocity or static stimuli cause compression of the outer layers of the corpuscle, but this compression does not reach the inner core. Instead, only the dynamic phase of compression results in deformation of the corpuscle to the inner core, evoking a response from the innervating axon (Hubbard, 1958). This model was supported by experiments in which removing the capsule of Pacinian corpuscles resulted in a prolonged generator potential upon a sustained mechanical stimulus. However, despite the prolonged generator potential, the innervating Aβ axon still only fired a few action potentials at the onset of stimulation. This suggests that inherent properties of these Aβ axons prevents a steady outward current from producing repetitive impulses, which is another potential mechanism underlying the RA response (Loewenstein and Mendelson, 1965; Mendelson and Lowenstein, 1964).

Pacinian corpuscles are exquisitely sensitive; in physiological preparations ambient vibrations in the building resulted in a response from the innervating axon (Hunt, 1961). These observations suggest that one potential function of Pacinian corpuscles, especially those in the interosseous membrane, may be to sense vibration transmitted through the skeletal system, either due to movement of the animal or due to external environmental vibrations, possibly generated by predators or prey. In humans, Pacinian corpuscles in the hand are tuned to sense the texture of an object or its dimensions indirectly through

the use of tools (Brisben et al., 1999). In addition, Pacinian corpuscles are important for detecting the fine texture of objects. Experiments with biomimetic sensors have shown that the normal spacing of fingerprints causes the amplification of vibrations in the ideal detection range of Pacinian corpuscles when scanning across a finely textured surface (Scheibert et al., 2009).

Development

Most studies regarding the development of Pacinian corpuscles have been performed on the corpuscles in the interosseous membrane of rodents. In rats and mice, an immature inner core and an outer capsule containing only a couple layers is present at birth (Zelena, 1994). The inner core becomes morphologically mature and more outer core layers are added in the first postnatal week. Outer core layers continue to be added during the first few weeks of life, and the corpuscle grows in size over the first few months. Innervation is required for the development of the corpuscle, as Pacinian corpuscles won't form if the leg is neonatally denervated (Zelena et al., 1990).

Pacinian corpuscle neurons arise from the early RET^{+} RA mechanoreceptors and are highly dependent on RET signaling for their development. In mice mutant for *Ret*, its co-receptor *Gfrα2*, or its ligand *Neurturin*, no Pacinian corpuscles are formed (Luo et al., 2009). The cause of the selective loss of Pacinian corpuscles, but not other subtypes of RA mechanoreceptors, in *Ret* mutant mice is currently unclear.

In addition, several transcription factors play critical roles in the development of Pacinian corpuscles. The ETS transcription factor Er81 is expressed in the inner core Schwann cells of Pacinian corpuscles, and no Pacinian corpuscles are formed in *Er81* null mice (Sedy et al., 2006). In *c-Maf* mutant mice, both the number of Pacinian corpuscles and axons in the interosseous nerve, which innervate Pacinian corpuscles, were greatly reduced. In addition, the remaining corpuscles display abnormal morphology (Hu et al., 2012; Wende et al., 2012). These results suggest that c-Maf is required in Pacinian corpuscle neurons for axonal growth/targeting or corpuscle formation. Interestingly, human patients with c-MAF missense mutations showed a somatosensory deficit specifically related to Pacinian corpuscles. These patients have a decreased sensitivity to high frequency vibration, which is detected by Pacinian corpuscles, while their detection of lower frequencies, which is mediated by Meissner's corpuscles, is not affected (Wende et al., 2012).

LANCEOLATE ENDINGS

Anatomical location and morphology

The innervation of hair follicles by low-threshold mechanosensory neurons is very complex. Aβ, Aδ, and C low-threshold mechanoreceptors all innervate hair follicles and form a palisade structure surrounding the follicle (Li et al., 2011; Lou et al., 2013). In addition, different types of hair are innervated by different combinations of sensory

fibers, and hair types vary by anatomical location and between species. In keeping with the scope of this introduction, we will only discuss the Aβ low-threshold mechanoreceptors in the hairy skin and whisker pad, which are Aβ lanceolate endings and Merkel cells (see below). Aβ lanceolate endings are associated with the awl and guard hairs of the hairy back skin and the whiskers, but not the zigzag hairs, which are the most numerous hair type in mouse hairy back skin (Li et al., 2011; Mosconi et al., 1993).

Hoggan and Hoggan originally described forked nerve endings surrounding hair follicles in 1893 (Hoggan and Hoggan, 1893). The lanceolate endings form a palisade-like structure which encircles the hair follicle. Individual endings have a flattened, oval shape, with the thin aspect directly abutting the hair follicle. Each ending is composed of a single oblong axonal fiber enclosed by flattened Schwann cells on either side of the axon. Axonal spikes protruding through the sheath where the two Schwann cell faces meet contact both the hair follicle and the surrounding connective tissue (Munger and Ide, 1988). Sparse genetic labeling of hair follicle innervating axons shows that the lanceolate endings which make up each palisade structure are innervated by more than one sensory afferent, and that individual mechanoreceptive neurons can innervate lanceolate endings surrounding multiple hair follicles (Suzuki et al., 2012).

Centrally, Aβ hair follicle afferents form distinct "flame-shaped" collateral arbors, which were first described by Ramon y Cajal and later characterized by Scheibel and Scheibel in 1968 (Scheibel and Scheibel, 1968). Upon entering the dorsal horn, the afferent fiber descends to layer IV or V, and then reverses direction and projects dorsally to the outer layer IV and layer III, where the collateral undergoes extensive branching and forms synapses with spinal neurons (Brown, 1981; Woodbury et al., 2001).

Physiological properties and function

Like Meissner's and Pacinian corpuscles, Aβ lanceolate endings also display RA properties. In recordings from cat whisker hair, two populations of RA afferents were found. The more numerous population responded only to high velocity stimuli, such as a flick of the hair or vibration from a tuning fork. This population could follow frequencies up to 1000 Hz and was not affected by the direction of the stimulus. A much smaller low velocity population of RA mechanoreceptors responded to stimuli from 5-200 Hz and exhibited some direction selectivity. They responded to hair deformation in any direction, but had a much lower activation threshold in the preferred direction (Gottschaldt et al., 1973). The RA hair follicle afferents are also extremely sensitive; in tests for the activation threshold using the skin nerve preparation, the activation threshold of more than half of the units recorded was below the level of resolution (0.07 mN) in mice (Woodbury et al., 2001).

Aβ lanceolate endings most likely function as velocity detectors for the deformation of hair. The mechanical transduction mechanism is unclear, but ultrastructural studies suggest that deformation of the lanceolate ending may occur upon movement of the hair, due to the connections of the Schwann cell structure to the hair follicle and surrounding tissue. This physical deformation may cause a response in the innervating axon (Takahashi-Iwanaga, 2000).

Development

Due to the complex innervation of hair follicles by different types of sensory neurons, it has been difficult to exclusively study the development of Aβ lanceolate endings. Most studies described below depend on pan-neural or Schwann cell markers to identify lanceolate endings. Therefore, the observed phenotypes in mutant mice may reflect deficits in neurons other than Aβ low-threshold mechanoreceptors. Recently, new mouse genetic tools have been developed to specifically label different classes of hair follicle innervating neurons (Li et al., 2011), which will help to identify molecular mechanisms that control development of different types of low-threshold mechanoreceptors in the future.

The trigeminal nerve approaches the site of whisker hair follicles by embryonic day 12 (E12) in mice and the lanceolate endings start to appear at E17 (Maklad et al., 2010). In the back skin, the development of lanceolate endings is slightly delayed; nerve fibers

reach the area of hair follicles around E14-E16 and immature lanceolate endings appear around birth (Peters et al., 2002). These anatomical studies correlate well with physiological recordings. Using the *ex vivo* skin nerve preparation, RA responses from hair follicle innervating neurons could be recorded at P0, and backfilled neurons displayed "flame-like" central innervation morphology typical of hair follicle receptors by P2 (Woodbury et al., 2001).

The role of neurotrophic signaling in controlling the development of Aβ hair follicle innervating neurons is less clear. Like the other low threshold RA mechanoreceptors, Aβ hair follicle innervating neurons express *Ret* during early development. In P14 neural crest specific *Ret* null mice, Luo et al. found that the morphology of lanceolate endings is disorganized, but the percentage of hair follicles that receive lanceolate ending innervation was not significantly different using a mixed pan-neuronal marker PGP9.5 and large diameter axon marker NFH (Luo et al., 2009). In P0 *Ret* null mice, Bourane et al. found that the total innervated area of NFH^+ lanceolate endings around the hair follicle is significantly reduced (Bourane et al., 2009). Although the conclusions from these two studies seem to be slightly different on the surface, which could well be explained by the different staining and quantification method, both studies in fact suggest that the normal morphology of Aβ lanceolate ending is dependent on *Ret* signaling.

Hair follicle innervation may also be dependent on *TrkB* signaling. In *TrkB* mutants, the morphology of lanceolate endings is affected to a similar extent as seen in *Ret* mutants. In addition, there was a reduction in the number of hair follicles innervated by lanceolate endings in *TrkB* null mice (Perez-Pinera et al., 2008), but the number of endings was not significantly changed in neural crest specific *TrkB* mutant mice (Luo et al., 2009). This discrepancy could be due to either the differences between *TrkB* null and neural crest conditional knockout mice or the technical difficulties of specifically identifying Aβ lanceolate endings and quantifying them. On the other hand, overexpression of TrkB ligands *BDNF* and *NT4* in the skin led to an increased density of hair follicle innervation (Krimm et al., 2006; LeMaster et al., 1999). Lastly, as discussed above, the transcription factor Shox2 promotes the expression of *TrkB* in DRG neurons. In *Shox2* null mice, lanceolate endings are disorganized, a phenotype very similar to the *TrkB* mutant phenotype (Abdo et al., 2011).

The proper formation of lanceolate endings may also depend on the activity of the innervating neurons. Woo et al. recently found that lanceolate ending innervating neurons express the vesicular glutamate transporter VGLUT2, while the Schwann cells which surround the innervating axons express NMDA receptors. Interestingly, ablating VGLUT2 from somatosensory neurons leads to a reduction in the frequency and organization of lanceolate forming Schwann cells at P0 (the latest stage the mice survived). Moreover, pharmacologically blocking glutamatergic transmission by injecting an NMDA receptor antagonist in the skin led to a reduction in the number and

organization of lanceolate Schwann cell processes in adult wild-type mice. Lastly, physiological tests of antagonist treated mice revealed a decrease in the sensitivity and conduction velocity of RA afferents innervating hair follicles (Woo et al., 2012). Collectively, these results suggest that communication between the innervating axon and the surrounding Schwann cell structure are crucial for the development and maintenance of lanceolate endings.

MERKEL CELLS

Anatomical location and morphology

Merkel cells are located in the basal epidermis of both glabrous and hairy skin of mammals. In glabrous skin, clusters of 4-40 Merkel cells are present in the epidermal pegs, which are protrusions of the epidermis into the dermis that surrounds the dermal papillae. In primates and marsupials, smaller clusters of Merkel cells are located at the base of the epidermal ridges which are responsible for the fingerprint pattern of the hands and feet (Halata et al., 2003). These clusters of Merkel cells in glabrous skin are often referred to as “touch spots” (Boulais and Misery, 2007). In hairy skin, Merkel cells are present in “touch domes”, which can be discerned by a slight elevation in the skin in some species, and can contain up to 150 Merkel cells. Touch domes may or may not be associated with a hair follicle (Zelena, 1994). In rodents, Merkel cells are closely associated with guard hair follicles, located in the epidermis in “collars” surrounding the

hair follicle, and whiskers, located in “cuffs” present underneath the glassy membrane of the follicle (Halata and Munger, 1980b; Zelena, 1994).

Merkel cells were first described as “touch cells” by Freidrich Sigmund Merkel in 1875 (Merkel, 1875). They are oval in shape and 10-15 μm in length along the long axis, which is the smallest among all mechanosensory endings discussed in this introduction. They can be differentiated from the surrounding epidermal cells by their large, multilobated nucleus which is oriented parallel to the dermis-epidermis junction. On the basal side of the cell, numerous dense core vesicles measuring 70-180 nm in diameter are located close to the cell membrane (Halata et al., 2003; Iggo and Muir, 1969; Tachibana and Nawa, 2002; Winkelmann and Breathnach, 1973). Most Merkel cells are associated with an innervating axon, forming a structure referred to as the Merkel cell-neurite complex. A nerve plate, which is formed by a myelinated axon which loses its myelin sheath upon entering the epidermis, directly opposes the vesicle dense basal membrane of the Merkel cell. This plate is separated from the Merkel cell by 15 nm, but in small regions they are separated by only 13 nm, and electron dense material is observed in both the Merkel cell and the nerve plate at these points (Halata et al., 2003; Iggo and Muir, 1969). A small number of Merkel cells do not make contact with an innervating axon. The function of these uninnervated Merkel cells is unknown, but it has been suggested they may have neuroendocrine or immune system functions (Boulais and Misery, 2007).

Central projections of Merkel cell innervating neurons bifurcate upon entering the spinal cord, and send collaterals into the dorsal horn as these branches travel anteriorly and posteriorly. The morphology of the collaterals innervating the dorsal horn are distinct form the RA mechanoreceptors. Individual collaterals dive into the dorsal horn perpendicular to the dorsal surface of the spinal cord. After reaching layer IV or V, the collaterals make a C- or L-shaped turn and then travel medially. During and after this turn, the collaterals gives off terminal arborizations in layers III-V (Brown, 1981).

Physiological properties and function

Merkel cell-neurite complexes are type I SA (SAI) mechanoreceptors. Unlike the RA mechanoreceptors discussed above, SA mechanoreceptors remain active during the static phase of stimuli. The innervating neuron is usually silent at rest, and responds to the onset of stimulation with a burst of activity, which is proportional to the velocity and displacement of the stimulus. After the initial phasic burst of activity, a tonic firing phase occurs for the duration of the application of the stimulus. The firing pattern during the tonic phase is irregular and can last for over 30 minutes (Iggo and Muir, 1969; Tapper, 1965; Willis and Coggeshall, 2004).

There has been a long-standing debate with regard to the exact role of Merkel cells in light touch sensation. Many studies suggested that the Merkel cell is critical for transducing the mechanical stimulus into a chemical signal to activate the innervating

neurite, while other studies proposed that Merkel cells may play a modulatory role and the neurite is primarily responsible for transducing the mechanical stimulus.

There is abundant biochemical evidence that Merkel cells produce neurotransmitters and the machinery required for synaptic release (Haeberle et al., 2004; Maksimovic et al., 2013; Tachibana and Nawa, 2002). Merkel cells also express voltage gated calcium channels, and calcium induced calcium release from internal stores occurs upon the entry of calcium into the cell, providing a potential mechanism for neurotransmitter release (Senok and Baumann, 1997; Yamashita et al., 1992). In addition, blocking glutamatergic transmission reduced the SA response evoked by activation of Merkel cell-neurite complexes, suggesting that excitatory neurotransmission is required for transducing the mechanical stimulus (Fagan and Cahusac, 2001). The most compelling evidence suggesting a mechanosensory function of Merkel cells comes from *Atoh1/Math1* conditional knockout mice, in which Merkel cells are not differentiated but the innervating fibers are still present in touch domes. Strikingly, although the total number of Aβ fibers is not significant changed, SAI responses could not be detected in these animals using the *ex vivo* skin nerve preparation (Maricich et al., 2009). These results suggest that Merkel cells are essential for mediating the SAI response. However, it is unclear whether these remaining fibers completely lost their mechanosensitivity or display physiological properties similar to RA mechanoreceptors.

On the other hand, using both ultrastructural and electrophysiological evidence, Gottschaldt and Vahle-Hinz argued that the ability of Merkel cell innervating neurites to follow high frequency stimuli up to 1200 Hz with a one-to-one response for up to 500 ms is incompatible with chemical communication, as neurotransmitter could not be released and cleared from the synapse quickly enough to produce such a precise response. In addition, the latency from application of stimulus to response in the innervating fiber was too fast for chemical transmission (Gottschaldt and Vahle-Hinz, 1981), further supporting their model that the innervating neurite acts as the mechanosensitive element.

Diamond's group also argued that Merkel cells are dispensable for mechanosensation. They found that touch domes were still mechanoresponsive after selective destruction of Merkel cells using quinacrine loading and ultraviolet (UV) light irradiation (Diamond et al., 1988). However, Ikeda et al. found that SAI responses evoked by touch dome stimulation were lost using a different irradiation procedure to eliminate Merkel cells (Ikeda et al., 1994). Further investigation revealed that quinacrine loading/UV irradiation is not selective and incomplete, leaving some Merkel cells relatively intact and damaging other nerve fibers in the skin (Senok et al., 1996). These conflicting results and technical issues make these experiments difficult to interpret.

Others have attempted to reconcile the conflicting findings regarding the role of the Merkel cell in mechanotransduction with a two-receptor-site model, in which both the innervating neurite and the Merkel cell are mechanosensitive. According to this model, the early phasic activity is mediated by the neurite while the late tonic phase is due to

chemical communication between the Merkel cell and the neurite (Maksimovic et al., 2013; Ogawa, 1996). A key to resolving this debate is to develop new tools, by which Merkel cell innervating axons can be specifically identified for physiological recording while Merkel cells are acutely and selectively ablated.

As a result of their small sizes, Merkel cell-neurite complexes have the smallest receptive fields among all mechanoreceptors and are best able to distinguish individual closely spaced objects. Due to these characteristics, Merkel cells are proposed to be essential for detecting the fine details of touched objects, such as shape, texture, and curvature (Johnson, 2001; Johnson et al., 2000). A recent study found that mice lacking Merkel cells were unable to detect certain textures with their feet (Maricich et al., 2012).

Development

In contrast to the RA mechanoreceptor end organs, Merkel cells appear in the skin prior to the arrival of innervating fibers (Saxod, 1996). Immature Merkel cells can be observed in the epidermis of the rat around E16, when innervating axons have only reached the dermis. Axons reach the epidermis and are found in close association with Merkel cells a day later (English et al., 1980).

Since Merkel cells share characteristics with both epidermal and neural cells, there has been argument concerning the embryological origins of Merkel cells in mammals (Lucarz and Brand, 2007). In birds, chick-quail chimera experiments offer strong support to a neural crest origin of Merkel cells (Grim and Halata, 2000). In addition, Merkel cells were labeled by LacZ when all neural crest derived cells were genetically labeled using *Wnt1*^{Cre} and *ROSA26R-β-Galactosidase* reporter mice, suggesting that mouse Merkel cells arose from a neural crest origin (Szeder et al., 2003). However, there is also genetic evidence to support an epidermal origin of Merkel cells. The transcription factor *Atoh1/Math1* is highly expressed and functionally required for the development of Merkel cells. Surprisingly, Merkel cells still form when *Atoh1* is conditionally ablated from neural crest cells. In contrast, when *Atoh1* is deleted from the basal layer of the epidermis using a *Keratin14*^{Cre} line, Merkel cells do not form, suggesting an epidermal origin for Merkel cells in mammals (Morrison et al., 2009). Nevertheless, this study could not exclude a cell non-autonomous effect for *Atoh1* in the development of Merkel cells, as *Atoh1* expression was also observed in some of the accessory cells surrounding Merkel cells.

Inherent transcriptional programs in the innervating neuron are also required for development of Merkel cell-neurite complex. Similar to Meissner's corpuscles and lanceolate endings, Merkel cells are dependent on the transcription factor Shox2 for sensory innervation during development. In *Shox2* mutants, Merkel cells are present in both glabrous and hairy skin, but there is a dramatic decrease in the percentage of Merkel

cells innervated by large diameter sensory fibers (Abdo et al., 2011). In addition, some mechanoreceptive DRG neurons co-express the Runt-related transcription factors *Runx1* and *Runx3* (Yoshikawa et al., 2013), and the number of Merkel cell-neurite complex surrounding the whiskers is greatly reduced in *Runx3* mutant mice (Senzaki et al., 2010). One plausible mechanism by which *Runx3* controls Merkel cell-neurite complex development is to regulate *TrkC* expression (Kramer et al., 2006b; Levanon et al., 2002; Nakamura et al., 2008).

In addition to transcriptional programs, Merkel cell-neurite complexes are highly dependent on several types of neurotrophic signaling for their development (Montano et al., 2010). One population of Merkel cells depends on TrkA/NGF signaling. The number of Merkel cells surrounding hair follicles and the number of innervating axons is reduced in *TrkA* mutants. However, remaining Merkel cells are maintained into adulthood, suggesting a TrkA independent Merkel cell population. Loss of the TrkA ligand NGF produces a similar, but less severe, phenotype (Fundin et al., 1997).

TrkC/NT3 signaling has a significant and complicated effect on Merkel cell development. *TrkC* is expressed in both Merkel cells and Merkel cell innervating somatosensory neurons. In mice lacking the kinase domain of TrkC, the number of Merkel cells is reduced at birth. In addition, those that are present at birth are not maintained during the first two postnatal weeks, suggesting that all Merkel cells become dependent on TrkC

signaling postnatally (Cronk, Wilkinson et al. 2002). Loss of NT3, the TrkC ligand, leads to a more severe deficit, with even fewer Merkel cells present at birth (Airaksinen et al., 1996). The phenotype becomes most severe when all isoforms of TrkC are eliminated in *TrkC* complete null mice, in which no Merkel cells or innervating fibers are present at birth, suggesting additional kinase-independent roles of TrkC in Merkel cell development (Cronk et al., 2002; Fundin et al., 1997).

TrkB signaling also has an effect on Merkel cell development. In *TrkB* mutant mice, the number of Merkel cells surrounding hair follicles and in the glabrous skin is greatly reduced (Perez-Pinera et al., 2008). When BDNF is overexpressed in the skin, the number of Merkel cells is increased in the glabrous but not hairy skin (LeMaster et al., 1999). Interestingly, the mechanical threshold of SAI mechanoreceptors increases eight fold in the *BDNF* heterozygous and null mice, although the number and morphology of Merkel cells was normal in touch domes of P14 *BDNF* null animals. This deficit could be rescued by injecting recombinant BDNF into *BDNF* heterozygous mice (Carroll et al., 1998).

Lastly, the low affinity neurotrophin receptor p75 also plays a role in Merkel cell development. p75 can bind NGF, BDNF, NT3, and NT4, and interact with the Trk receptors (Skaper, 2012). In *p75* mutant mice, Merkel cells develop normally during the first two postnatal weeks but then then slowly decrease in number over the following months until very few remain (Fundin et al., 1997; Kinkelin et al., 1999).

RUFFINI CORPUSCLES

Anatomical location and morphology

The Ruffini corpuscle is an elongated structure with tapered ends. Morphologically, it is quite similar to the Golgi tendon organs which are innervated by proprioceptors (Halata and Munger, 1980a). The corpuscle is usually encased in a capsule of 4-5 layers of perineural cells and contains an inner core of Schwann cells and collagen, which is innervated by a single large diameter myelinated axon that loses its myelination upon entry into the inner core. The axon gives off numerous terminal branches within the inner core (Chambers et al., 1972; Willis and Coggeshall, 2004). Collagen fibers associated with the inner core exit the poles of the Ruffini corpuscle and interact with collagen in the surrounding tissue, providing a potential mechanism for mechanically linking the inner core with the surrounding tissue (Halata, 1977).

The central projections of SA type II (SAII) mechanoreceptors, which are presumed to innervate Ruffini corpuscles, are distinct form other mechanoreceptors. Collaterals innervating the dorsal horn project to layer III, and then branch into at least two processes. These processes travel deeper into the dorsal horn and branch extensively, forming terminal arborizations from layer III-VI (Brown, 1981).

The first extensive morphological characterization of Ruffini corpuscles was performed on hairy skin of the cat (Chambers et al., 1972). However, the anatomical location and existence of Ruffini corpuscles between tissues and species is currently under debate. In many cases, numerous units with SAII responses can be recorded in nerve fibers innervating a tissue, but the Ruffini corpuscles cannot be found in the tissue following careful histological examination. For example, physiological recordings of nerves innervating the glabrous skin of raccoons and humans have shown a relatively high proportion of units exhibiting SAII responses (Johansson and Vallbo, 1979; Rasmusson and Turnbull, 1986). However, when glabrous skin from monkeys and raccoons was examined, no Ruffini corpuscles were found (Pare et al., 2002; Rice and Rasmusson, 2000). In humans, a single Ruffini corpuscle was found in the skin of the index finger, which is much less than what would be expected based on the physiological recordings (Pare et al., 2003). Notably, Pare, et al. observed innervation of blood vessels which looked morphologically similar to previous descriptions of Ruffini corpuscles. The authors suggest that previous studies may have misidentified these structures as Ruffini corpuscles, which could explain the discrepancy in previous findings (Pare et al., 2002). In mouse hairy skin, SAII fibers are also identified by physiological recordings but no definite Ruffini corpuscle structure has been reported (Wellnitz et al., 2010).

In many species, sensory endings which are morphologically similar to Ruffini corpuscles have been identified. In monkeys and raccoons, unencapsulated Ruffini-like endings were found at the base of the fingernail/claw (Pare et al., 2002; Rice and

Rasmusson, 2000). Ruffini corpuscles have also been found in association with hair follicles, where they are sometimes referred to as pilo-Ruffini complexes (Biemesderfer et al., 1978). Additionally, unencapsulated periodontal Ruffini-like corpuscles have been identified surrounding the teeth of rodents (Byers, 1985).

Physiology and function

Although not well defined morphologically, the physiology of SAII Aβ low-threshold mechanoreceptors have been extensively characterized in both humans and model organisms (Johansson and Vallbo, 1979; Wellnitz et al., 2010). Like the SAI response, the SAII responses is characterized by an early dynamic phase which is sensitive to both the velocity and displacement of the stimulus, followed by a static response phase that last throughout the application of stimulus. However, SAII responses can be differentiated from SAI responses because they usually display some background firing activity when no stimulus is applied, they fire at a much more regular rate during the static phase, and their maximum frequency of the response is less than that of the SAI response (Chambers et al., 1972).

SAII Aβ low-threshold mechanoreceptors are proposed to act primarily as stretch receptors. In psychophysical recordings SAII units were less sensitive than SAI units to skin indentation, but were much more sensitive to stretching of the skin (Johnson et al., 2000). The stretch receptors in the skin may have two functions. They may work in

combination with RA mechanoreceptors to sense movement of grasped objects. In addition, they may work in concert with proprioceptors to sense the position of the fingers and hand, as skin stretch will vary based on grasp (Johnson, 2001).

Development

Due to the difficulty in clearly identifying Ruffini corpuscles by morphology, relatively little work has been done to study their development compared to the other mechanoreceptors discussed in this review. Both periodontal Ruffini-like endings and those associated with whisker hair are dependent on TrkB neurotrophic signaling in mice. Periodontal Ruffini-like endings are absent in *TrkB* mutant mice, and mice lacking either *BDNF* or *NT4* show Ruffini-like endings with immature morphology (Hoshino et al., 2003; Maruyama et al., 2005; Matsuo et al., 2002). The Ruffini-like endings of whisker hairs are also absent in *TrkB* mutants. In addition, the number of whisker Ruffini-like endings is greatly reduced in *BDNF* mutants but is unaffected in *NT4* mutants. Furthermore, the number of Ruffini-like endings associated with whiskers is increased in NT3 mutant mice (Fundin et al., 1997).

RET STRUCTURE AND FUNCTION

The receptor tyrosine kinase RET (REarranged during Transfection) was first discovered in 1985 after DNA rearrangement conferred the ability to transform NIH3T3 cells upon

transfection with DNA from a human lymphoma (Takahashi et al., 1985). Since this time, research has revealed critical roles for RET in oncological and developmental diseases, including medullary thyroid carcinoma, multiple endocrine neoplasia, papillary thyroid carcinoma, and Hirschsprung disease (Amiel et al., 2008; Krampitz and Norton, 2014; Romei et al., 2016). Furthermore, RET signaling has critical roles in kidney development, spermatogenesis, and the development of enteric, sensory, autonomic, and motor neurons (Kramer et al., 2006a; Meng et al., 2000; Runeberg-Roos and Saarma, 2007; Schuchardt et al., 1994).

The RET protein contains four n-terminal cadherin-like domains. There is a calcium binding domain between the second and third cadherin-like domain, and calcium binding is required for proper folding and activation of RET (Anders et al., 2001). Following the cadherin-like domains is a cysteine-rich domain, followed by the transmembrane region. For many years, the extracellular domains required for association with the ligand/co-receptor complex has been controversial, with nearly all extracellular domains implicated in complex binding (Amoresano et al., 2005; Kjaer and Ibanez, 2003). Recent structural modeling work using low-angle X-ray scattering and electron microscopy data reconciles these results and suggests that RET associates with its co-receptors at four distinct sites distributed over the first three cadherin-like domains as well as the cysteine-rich domain (Goodman et al., 2014). The transmembrane domain of RET likely contributes to the dimerization of RET molecules, which is essential for activation of RET following ligand binding (Kjaer et al., 2006).

The intracellular domain contains a short juxtamembrane region, followed by the kinase domain and a c-terminal tail. Like other receptor tyrosine kinases, the intracellular domain of RET undergoes autophosphorylation of tyrosine residues following stimulation. Of the 18 intracellular tyrosine residues, 14 can be phosphorylated in vitro (Ibanez, 2013; Kawamoto et al., 2004). Phosphorylated tyrosine residues serve as docking sites for adapter proteins which activate downstream pathways including MAP kinase, PI3 kinase/AKT, Jun n-terminal kinase, and Phospholipase Cγ kinase pathways (Airaksinen et al., 1999; Borrello et al., 1996; Chiariello et al., 1998; van Weering and Bos, 1997; Worby et al., 1996).

Following the kinase domain is a cytoplasmic tail, which produces a short isoform (RET9) and long isoform (RET51) due to differential splicing. Both isoforms contain a critical tyrosine residue, Y1062, which is important for RET function in vivo (Durick et al., 1995). RET51 also contains an additional tyrosine, Y1096, which may compensate for the loss of Y1062 in some contexts (Degl'Innocenti et al., 2004; Jain et al., 2006). Generation of mice expressing only a single isoform of RET has produced conflicting results. In one study, mice expressing only a human/mouse chimera RET51 had deficient kidney development, while RET9 expressing mice had normal kidneys (de Graaff et al., 2001). In contrast, a more recent study of monoisoformic mice expressing human isoforms of RET9 or RET51 found no renal deficits in either mouse model (Jain et al.,

2006). Although RET9 and RET51 are identical up to their c-terminal tails, they are unable to associate with or activate each other upon stimulation with ligand (Tsui-Pierchala et al., 2002).

RET SIGNALING

RET is the receptor tyrosine kinase for the glial cell line-derived neurotrophic factor (GDNF) family of neurotrophic factors, which includes GDNF, neurturin (NRTN), artetmin, and persephin. RET is atypical among receptor tyrosine kinases in that it does not directly bind to its ligands. Instead, the ligands bind to GPI-linked GDNF-family receptor α (GFRα) co-receptors. The high affinity co-receptor/ligand pairs are GFRα1/GDNF (Jing et al., 1996; Treanor et al., 1996), GFRα2/NRTN (Baloh et al., 1997; Buj-Bello et al., 1997; Klein et al., 1997), GFRα3/artemin (Baloh et al., 1998), and GFRα4/persephin (Yang et al., 2007), although there is some crosstalk between nonmatching ligands and co-receptors, particularly at high ligand concentrations. The kinetics of ligand/co-receptor/RET binding remains poorly understood. Originally, it was proposed that ligand binds to GFRα co-receptor, which may exist as a dimer or may dimerize upon ligand binding. This ligand/co-receptor complex then binds to RET, leading to dimerization of RET and autophosphorylation of the RET intracellular domain (Jing et al., 1996). However, binding of RET and co-receptor has been observed in the absence of ligand, suggesting that RET and GFRα may associate prior to ligand binding (Cik et al., 2000; Eketjall et al., 1999).

The GPI-linked GFRα co-receptors also affect the subcellular localization of RET signaling. Like other GPI-linked proteins, GFRαs localize to lipid rafts. Under basal conditions, RET is mostly excluded from lipid rafts. However, upon stimulation with ligand, RET translocates to lipid rafts, where it becomes phosphorylated (Paratcha et al., 2001; Tansey et al., 2000). In cells expressing a version of GFRα1 containing a transmembrane domain, which is excluded from lipid rafts, stimulation with GDNF still led to phosphorylation of RET (Tansey et al., 2000). However, the activation of downstream effectors, such as MAP and Akt kinases, was reduced in these cells relative to cells containing GPI-linked GFRα1. The reduction in efficiency of RET signaling away from lipid rafts is likely due to the loss of colocalization with downstream effectors enriched in lipid rafts (Tansey et al., 2000). Furthermore, translocation to lipid rafts may segregate RET from cellular degradation machinery, increasing the perdurance of RET activation (Pierchala et al., 2006). Recently, a GFRα1-transmembrane domain knock-in mouse was generated and had kidney and enteric neuron phenotype which were similar to *Gfra1* null mice, suggesting that localization to lipid rafts is required for GFRα1 function in vivo (Tsui et al., 2015).

In addition to activation of RET by GFRα co-receptor expressed in the same cell (*cis* signaling), RET can also be activated by GFRα co-receptor expressed by other cells or soluble co-receptor present in the surrounding environment (*trans* signaling). The studies

which initially identified GFRα1 and GFRα2 as the RET co-receptor which binds GDNF/NRTN demonstrated that treatment with GDNF/NRTN and soluble co-receptor can activate RET in cultured cells, demonstrating that *trans* activation is possible in vitro (Jing et al., 1996; Klein et al., 1997; Treanor et al., 1996). In addition to expression in RET^+ cells, GFRα co-receptors (mostly *Gfrα1*) are also expressed in cells which do not express RET, but are adjacent to or in the axonal target fields or RET^+ cells (Enomoto et al., 2004; Trupp et al., 1997; Worley et al., 2000; Yu et al., 1998). These expression patterns suggest that GFRαs may activate RET in *trans* in vivo, that GFRαs have RET-independent functions, and/or that GFRαs in non-RET^+ cells may act to concentrate and present GDNF family ligands to RET^+ cells for activation in *cis*.

Although numerous studies have demonstrated the ability for GFRas to activate RET in *trans* in vitro and in tissue explants (Ledda et al., 2002; Paratcha et al., 2001; Patel et al., 2012; Tansey et al., 2000; Uesaka et al., 2013; Worley et al., 2000), whether *trans* signaling occurs in vivo has remained controversial. The strongest argument against a physiological role for *trans* RET signaling in vivo was presented by Enomoto, et al. (Enomoto et al., 2004). To determine whether RET-independent GFRα1 has a role in a variety of developmental processes, they generated a "*cis*-only" mouse model. In this model, *Gfrα1* expression was driven from the *Ret* locus in a *Gfrα1* null background. Therefore, *Gfra1* was expressed at a high level in all cells which express *Ret*, but in no other cells. In this model, a variety of RET/GFRα1 dependent developmental processes, including kidney formation and enteric and motor neuron development, appeared normal

and the mice survived to adulthood. Therefore, the authors concluded that *trans* RET activation is mostly irrelevant for normal in vivo development (Enomoto et al., 2004). However, in addition to a loss of *trans* expressed *Gfra1*, this model also produces a gain of function: *Gfra1* is expressed at a high level in all RET^{+} cells, including those which do not normally express the co-receptor. Therefore, any deficits due to the loss of *trans* RET signaling may be compensated for by the ectopic gain of *cis* GFRα1. Due to these concerns, an in vivo role for *trans* RET signaling has not been definitively ruled out. In Chapter 2 of my thesis, I show that both *cis* and *trans* activation of RET in RA mechanoreceptors contribute to the growth of axonal projections into the dorsal spinal cord.

ER81

ER81 (ETS-related 81, also known as ETV1) is a member of the PEA3 subfamily of the ETS (E26 transformation-specific) family of transcription factors (Monte et al., 1994; Oh et al., 2012). ER81 is comprised of an n-terminal transactivation domain, a central domain which partially inhibits the activity of ER81, an ETS DNA binding domain, and a c-terminal domain which acts as a second, weaker transactivation domain (Janknecht, 1996). The n-terminal transactivation domain is positively regulated by direct interaction with the MAP kinase pathway components, whereas the c-terminal transactivation domain can be indirectly activated through MAP kinase activity (Janknecht, 1996). Additionally, acetylation via p300 increases the DNA binding affinity of ER81 (Goel and

Janknecht, 2003). In contrast, phosphorylation of ER81 by protein kinase A negatively regulates the transactivation activity of ER81 (Wu and Janknecht, 2002). Chromosomal rearrangements involving ER81 have been implicated in Ewing's sarcoma and prostate cancer (Jeon et al., 1995; Tomlins et al., 2005). Furthermore, high levels of ER81 expression contribute to the development of gastrointestinal stromal tumors (Chi et al., 2010).

ER81 also plays a critical role in the development of motor circuits. Early experiments in chick demonstrated that ER81 and PEA3, another ETS transcription factor, were specifically expressed in distinct motor pools and proprioceptive neurons. Motor neurons and proprioceptive sensory neurons expressing ER81 innervated anterior limb muscles, whereas $PEA3^{+}$ neurons innervated posterior limb muscles (Lin et al., 1998). Loss of function data from mice demonstrated a functional role for ER81 in motor circuit development (Arber et al., 2000). *Er81* null mice display an uncoordinated motor phenotype within the first week of life and die around one month of age. A normal complement of motor neurons and proprioceptive neurons develop in *Er81* nulls. However, group Ia proprioceptive afferents, which usually extend a peripheral process which innervates muscle spindles and central process which innervates motor neurons, do not project to the ventral spinal cord to synapse on motor neurons in *Er81* mutants. Physiological recordings revealed that the monosynaptic stretch reflex circuit, normally mediated by Ia afferents, was severely disrupted due to the lack of ventral spinal cord innervation. In contrast to their central projections, the initial innervation of muscle

spindles by proprioceptors is normal in *Er81* mutants. In fact, excess muscle spindles are formed in distal limb muscles in *Er81* mutants, although the morphology of these spindles is abnormal (Kucera et al., 2002). Conditional ablation experiments support a neural specific requirement for *Er81* in the development of proprioceptive central projections (Patel et al., 2003).

Proprioceptive sensory neurons express TrkC, the receptor for the neurotrophin NT3. TrkC/NT3 signaling is required for the survival of proprioceptors, as well as proprioceptive projections to the ventral spinal cord (Klein et al., 1994; Tessarollo et al., 1994). In an apoptosis-deficient *Bax* null background, the loss of NT3 still lead to a deficit in the central projections of proprioceptors, despite the survival of proprioceptors (Patel et al., 2003). Furthermore, in a series of loss of function and gain of function experiments, Patel et al. demonstrated that TrkC signaling, potentiated by NT3 expressed peripherally, is required for the expression of ER81 in proprioceptors. In mouse dorsal root ganglia, ER81 is expressed in nearly all $TrkC^{+}$ proprioceptors (Arber et al., 2000). However, approximately 30% of $ER81^{+}$ neurons do not express TrkC, and their function currently remains unknown.

Pacinian corpuscles are also absent in *Er81* null mice (Sedy et al., 2006). It was previously reported that the afferents which innervate Pacinian corpuscles are present a few days before birth. However, these axons are not present at birth, and corpuscles do

not form. *Er81* is expressed in the Schwann cells which make up the inner core of the Pacinian corpuscle end organ, so it was proposed that a Schwann cell deficit led to the Pacinian corpuscle phenotype (Sedy et al., 2006). However, whether *Er81* also has a role in Pacinian corpuscle innervating neurons has not been investigated. In Chapter 3 of this thesis, I show that *Er81* is required in neurons for the development of Pacinian corpuscles.

SCHWANN CELLS AND NEUREGULIN-1

In the peripheral nervous system (PNS), motor and sensory neurons extend long axons to control movement and sense stimuli. Associated with these neurons are Schwann cells, which are composed of two broad classes: myelinating and non-myelinating Schwann cells. Myelinating Schwann cells produce the myelin sheath which insulates large diameter axons, while non-myelinating Schwann cells help to form specialized sensory and motor endings and bundle small diameter non-myelinated sensory neurons(Griffin and Thompson, 2008; Salzer, 2015). Neurons and Schwann cells interact closely to build the PNS, maintain its normal function, and regenerate the PNS when necessary (Mirsky et al., 2008; Stassart et al., 2013). Perturbations in neuron-Schwann cell interactions have significant effects on human health, manifesting in diseases such as Charcot-Marie-Tooth disease and other peripheral neuropathies (Scherer and Wrabetz, 2008).

An important mediator of communication between neurons and Schwann cells is the

primarily neuronal EGF-like protein Neuregulin-1 (NRG1) and its ERBB family of receptors expressed on Schwann cells (Birchmeier and Nave, 2008). The *Nrg1* gene locus produces at least 15 distinct isoforms via different transcriptional initiation or alternative splicing(Falls, 2003). The two most prevalent isoforms in the PNS are NRG1-Ig (NRG1 type I/II), which contains an extracellular Ig-like domain, and NRG1-CRD (NRG1 type III), which contains an extracellular cysteine rich domain (Buonanno and Fischbach, 2001). NRG1-CRD is crucial for axonal communication with myelinating Schwann cells. The level of NRG1-CRD expressed by a neuron is positively correlated with the thickness of its axonal myelination, with the largest diameter sensory neurons normally expressing the highest levels of Nrg1-CRD (Michailov et al., 2004). However, the upstream mechanisms which control the differential expression level of NRG1 in different types of neurons remain unknown.

In contrast to myelinating Schwann cells, the molecular mechanisms used by neurons to communicate with non-myelinating Schwann cells are largely unknown. *Nrg1* is also required for the differentiation and formation of muscle spindles, which are composed of muscle fibers, non-myelinating Schwann cells, and innervating proprioceptive axons(Hippenmeyer et al., 2002). In this case, isoforms other than NRG1-CRD, most likely NRG1-Ig, are required (Hippenmeyer et al., 2002). The precise cellular target of NRG1 signaling (i.e. muscle fibers or Schwann cells) in muscle spindle development remains unclear.

The juxtamembrane regions of both NRG1-CRD and NRG1-Ig can be cleaved by

proteases. The protease β-secretase 1 (BACE1) has been demonstrated to cleave NRG1, and contributes to the promyelinating and pro-muscle spindle development roles of *Nrg1-CRD* and *Nrg1-Ig*, respectively (Cheret et al., 2013; Hu et al., 2006; Willem et al., 2006). It has been proposed that cleavage of NRG1-Ig would release the EGF domain of NRG1 from the membrane and allow it to signal at a distance from its source, while cleavage of NRG1-CRD c-terminal to the EGF domain would produce a membrane tethered EGF domain, due to the membrane association of the CRD. However, recent work has demonstrated that ADAM family proteases can cleave NRG1-CRD between the CRD and EGF domains, allowing for the release of EGF domain following dual cleavage by both ADAM and BACE proteases (Fleck et al., 2013).

Pacinian corpuscle innervating neurons express NRG1 and corpuscle Schwann cells express ERBB receptors (Gonzalez-Martinez et al., 2007; Kopp et al., 1997). In addition, injection of NRG1-Ig into neonatally denervated limbs can rescue Pacinian corpuscles by preventing apoptosis of Schwann cells (Kopp et al., 1997). However, the role of NRG1 signaling in normal development and maintenance of Pacinian corpuscles has not been determined.

BOMBESIN-RELATED PEPTIDES AND ITCH

Itch, which is defined as producing a desire to scratch, represents significant clinical and quality-of-life issues. Itch perception is mediated by small diameter dorsal root ganglion and trigeminal ganglion neurons, which relay itch information to downstream neurons in the dorsal spinal cord or brainstem (Ikoma et al., 2011). For many years, the identity of

itch sensing neurons remained controversial. Some investigators supported an "intensity" model of itch, which suggested that itch and pain are detected by the same population of DRG neurons, with the intensity of the stimulus/firing rate output of the somatosensory neuron determining whether itch or pain is perceived (Patel and Dong, 2010). However, in recent years use of mouse genetic models to genetically label and manipulate molecularly defined classes of neurons has supported a "labeled-line" model, which suggests that distinct populations of somatosensory neurons specifically mediate itch transmission (Han et al., 2013; Liu et al., 2009).

Although populations of itch-specific neurons have been defined, the cellular mechanisms of itch sensation transmission remain controversial. Although itch-sensing neurons can release glutamate and blocking glutamatergic transmission in the spinal cord silences input from itch-sensing neurons, genetic ablation of glutamatergic transmission in itch-sensing neurons in mice does not eliminate itch (Koga et al., 2011; Lagerstrom et al., 2010; Liu et al., 2010). Therefore, other mechanisms in addition to glutamatergic transmission likely mediate itch sensation. The bombesin-related peptide gastrin related peptide (GRP) has been proposed as a potential mediator of itch transmission from somatosensory neurons to the dorsal spinal cord. GRP was found to be expressed in small diameter DRG neurons, and its receptor, *Grpr*, is expressed in superficial layers of the dorsal spinal cord. Intrathecal injection of GRP causes scratching behavior, and knocking out *Grpr* or ablating $GRPR^{+}$ cells in the dorsal spinal cord produced loss of itch behavior phenotypes (Sun and Chen, 2007; Sun et al., 2009).

GRP and neuromedin B (NMB) are the only members of the mammalian bombesin-like peptide family, identified based on their similarity to the bombesin peptide, originally isolated from the frog *Bombina bombina* (Jensen et al., 2008). GRP and NMB bind with high affinity to their G-protein coupled receptors, GRPR and NMBR, although GRP and NMB can bind to their non-matching receptor at high concentrations (Battey et al., 1991; Wada et al., 1991). Although GRP was detected in DRG neurons by immunostaining (Sun and Chen, 2007), other studies have failed to detect *Grp* transcript or protein in DRG neurons (Fleming et al., 2012; Mishra and Hoon, 2013; Solorzano et al., 2015). Therefore, GRP may play a role in itch transmission in local dorsal spinal cord circuits but may not act as a transmitter from primary sensory neurons (Gutierrez-Mecinas et al., 2014). In contrast to GRP, *Nmb* is highly expressed in somatosensory neurons (Allen Institute for Brain Science, 2016). Furthermore, intrathecal and intracerebroventricular injection of NMB produces a scratching response, demonstrating a potential role for NMB in the transmission of itch sensation (Su and Ko, 2011; Sukhtankar and Ko, 2013). In Chapter 4 of this thesis, we provide further evidence that GRP is expressed in the dorsal spinal cord, but is likely not expressed in DRG neurons. Furthermore, *Nmb* is highly expressed in DRG neurons which transmit itch and pain information.

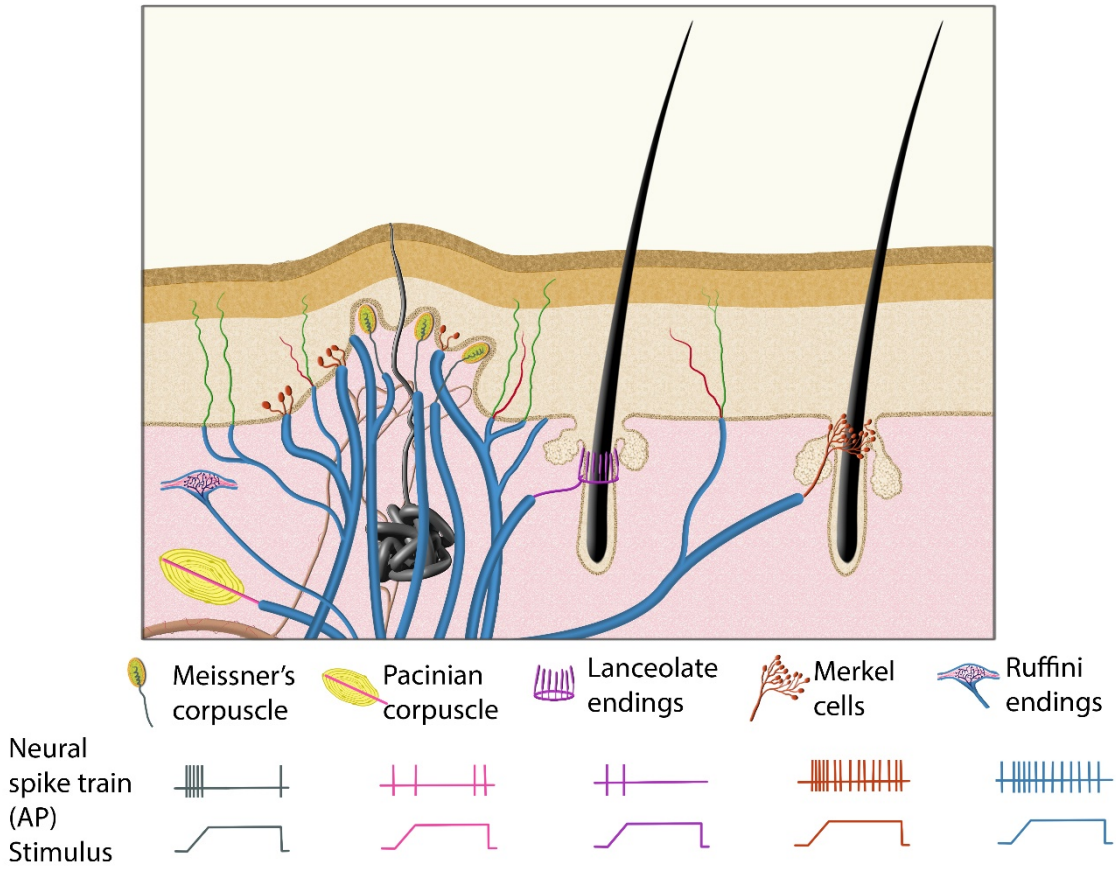

Figure 1. Illustration to demonstrate the morphologies and physiological properties of mammalian Aβ low-threshold mechanoreceptors. In glabrous skin (left side of the illustration), Meissner's corpuscles are located in the dermal papillae of the dermis, Merkel cells are located in the basal epidermis, Ruffini corpuscles are located in the dermis, and Pacinian corpuscles are located in the dermis, deeper than the other mechanosensory end organs. In hairy skin (right side of the illustration), hair follicles are surrounded by lanceolate endings and Merkel cells. The bottom panel shows the neural activity of different types of Aβ low-threshold mechanoreceptors in response to a sustained stimulus. Meissner's corpuscle, Pacinian corpuscle and lanceolate ending mechanoreceptors display rapidly adapting mechanosensitive physiological properties, while Merkel cell and Ruffini corpuscle mechanoreceptors display slowly adapting mechanosensitive properties, which fire action potentials (APs) throughout the duration of the stimulus.

CHAPTER 2

Cis and *trans* RET signaling control the survival and central projection growth of rapidly adapting mechanoreceptors

This chapter is adapted from:

Fleming, M.S., Vysochan, A., Paixao, S., Niu, J., Klein, R., Savitt, J.M., and Luo, W. (2015). Cis and trans RET signaling control the survival and central projection growth of rapidly adapting mechanoreceptors. *eLife 4*, e06828.

ABSTRACT

RET can be activated in *cis* or *trans* by its co-receptors and ligands *in vitro*, but the physiological roles of *trans* signaling are unclear. Rapidly adapting (RA) mechanoreceptors in dorsal root ganglia (DRGs) express *Ret* and the co-receptor *Gfra2* and depend on *Ret* for survival and central projection growth. Here, we show that *Ret* and *Gfra2* null mice display comparable early central projection deficits, but *Gfra2* null RA mechanoreceptors recover later. Loss of *Gfra1*, the co-receptor implicated in activating RET *in trans*, causes no significant central projection or cell survival deficit, but *Gfra1;Gfra2* double nulls phenocopy *Ret* nulls. Finally, we demonstrate that GFRa1 produced by neighboring DRG neurons activates RET in RA mechanoreceptors. Taken together, our results suggest that *trans* and *cis* RET signaling could function in the same developmental process and that the availability of both forms of activation likely enhances but not diversifies outcomes of RET signaling.

INTRODUCTION

The neurotrophic receptor tyrosine kinase RET plays critical roles in many biological processes, including kidney genesis, spermatogenesis, and development of enteric, sensory, autonomic, and motor neurons (Ibanez, 2013; Runeberg-Roos and Saarma, 2007). Loss of RET signaling leads to Hirschprung's disease, while RET gain of function has been implicated in various human carcinomas (Runeberg-Roos and Saarma, 2007; Santoro and Carlomagno, 2013). In addition, activation of the RET signaling pathway has potential applications in the treatment of Parkinson's disease and promotion of spinal cord regeneration following injury (Bespalov and Saarma, 2007; Deng et al., 2013). Therefore, it is critical to thoroughly understand RET signaling mechanisms.

RET is the common signaling receptor for the glial cell line-derived neurotrophic factor (GDNF) family of ligands (GFLs), which includes GDNF, neurturin (NRTN), artemin, and persephin. For RET activation and signaling, GFLs first bind to a GPI-linked GDNF family receptor alpha (GFRa), which then associates with RET to form an active signaling complex (Airaksinen and Saarma, 2002). In vertebrates, the GFRas and their high-affinity ligand pairs are GFRa1 and GDNF (Jing et al., 1996; Treanor et al., 1996), GFRa2 and NRTN (Baloh et al., 1997; Buj-Bello et al., 1997; Klein et al., 1997), GFRa3 and artemin (Baloh et al., 1998), and GFRa4 and persephin (Yang et al., 2007).

RET can be activated by GFRas expressed in the same cell (*cis* signaling) or by GFRas (mainly GFRa1) produced from other sources (*trans* signaling) *in vitro* (Ledda et al., 2002; Paratcha et al., 2001). The existence of both *cis* and *trans* activation has been proposed to diversify RET signaling by either recruiting different downstream effectors or changing the kinetics or efficacy of kinase activation (Paratcha et al., 2001; Tansey et al., 2000). Consistent with the *trans* signaling model, *Gfra1* is expressed in the target fields of many RET^{+} neurons during development and can promote axon growth upon GDNF treatment in culture (Paratcha et al., 2001; Trupp et al., 1997; Yu et al., 1998). However, the "*cis*-only" mouse model, in which *Gfra1* is expressed under the control of the *Ret* promoter in a *Gfra1* null background, produced no overt phenotypes in many *Ret*-dependent developmental processes, suggesting that *trans* signaling may not play a major physiological role (Enomoto et al., 2004). Recently, *trans* RET signaling has been implicated in the development of inhibitory cortical interneurons, nigral dopaminergic neurons, and enteric lymphoids, and in perineural invasion by cancer cells (Canty et al., 2009; He et al., 2014; Kholodilov et al., 2011; Patel et al., 2012). Nevertheless, the physiological functions of *trans* RET signaling and whether *cis* and *trans* signaling lead to the same or different biological outcomes *in vivo* remain largely unresolved.

Aβ Mechanoreceptors are large-diameter somatosensory neurons mediating discriminative touch, which innervate layers III-V of the spinal cord (SC). They can be broadly divided into rapidly-adapting (RA) and slowly-adapting (SA) mechanoreceptors based on their adaptation properties to sustained mechanical stimuli (Fleming and Luo,

2013). Previously, we and other labs identified that a small population of mouse DRG neurons, the early RET^{+} DRG neurons, develop into RA mechanoreceptors, and that *Ret* is required cell autonomously for the growth of their 3rd order central projections innervating the dorsal SC (dSC) (Bourane et al., 2009; Honma et al., 2010; Luo et al., 2009).

RET in RA mechanoreceptors encounters environments in which both *cis* and *trans* activation are possible, providing a good model system to study the physiological functions of *trans* RET signaling. RA mechanoreceptors express *Ret* and *Gfra2* (Bourane et al., 2009; Honma et al., 2010; Luo et al., 2009), whereas *Gfra1* is highly expressed in their target field (Treanor et al., 1996; Yu et al., 1998) and by neighboring DRG neurons during development (Honma et al., 2010; Luo et al., 2009). Here we found that the central projection deficit of RA mechanoreceptors is negligible in postnatal *Gfra2* and *Nrtn* mutant mice, which is in great contrast to the severely affected *Ret* mutant mice. By genetically tracing RA mechanoreceptors in different mutant mouse lines during development, we showed that the initial growth of the 3rd order central projections of RA mechanoreceptors depends on the *cis* activation of RET via GFRa2 and NRTN. However, central projections of *Gfra2* null RA mechanoreceptors gradually recover during development. *Gfra1* null mice show no obvious central projection deficit by itself, but *Gfra1*;*Gfra2* double null mice have similar cell death and central projection deficits to those of *Ret* null mice. Moreover, we showed that *Gfra1* is non-detectable in most RA mechanoreceptors, thus RET in RA mechanoreceptors is most likely activated

by GFRa1 in *trans*. Finally, we determined that RET in *Gfra2* null RA mechanoreceptors responds to GDNF in DRG explant culture, and this responsiveness is mediated by GFRa1 from neighboring DRG neurons (*trans* activation). Taken together, our results indicate that combinatorial *cis* and *trans* RET signaling promote survival and central projection growth of RA mechanoreceptors *in vivo*.

RESULTS

Expression of *Ret, Gfras,* and *GFLs* in the developing mouse spinal cord and DRGs

Since RET can be activated by GFLs/GFRas either in *cis* or in *trans* (mainly by GDNF/GFRa1) *in vitro*, we asked if the expression patterns of *Gfra1, Gfra2, Gdnf,* and *Nrtn* in the developing SC and DRGs would provide insight into RET signaling in RA mechanoreceptors *in vivo*. We performed *in situ* hybridization for *Ret, Gfra1, Gfra2, Gdnf,* and *Nrtn* on embryonic day 13.5 (E13.5) and E15.5 wild-type DRG and SC sections. Double *in situ* hybridizations that characterize the expression of *Gfra1* and *Gfra2* in different populations of DRG neurons have been previously conducted (summarized in Figure S1K (Luo et al., 2009)).

Similar to previous characterization (Luo et al., 2009; Luo et al., 2007; Molliver et al., 1997), *Ret* is expressed in motor neurons and a mix of small and large-diameter DRG neurons at E13.5 and E15.5 (Figure S1A-B). Most large diameter RET^{+} DRG neurons at

these stages are the early RET^+ DRG neurons, which develop into RA mechanoreceptors (Bourane et al., 2009; Luo et al., 2009). *Gfra1* is highly expressed in some DRG neurons and motor neurons as well, but these $GFRa1^+$ DRG neurons come from $NTRK1^+$ precursors and are not early RET^+ RA mechanoreceptors (Honma et al., 2010; Luo et al., 2009; Yu et al., 1998). In addition, *Gfra1* is highly expressed in the dorsal root entry zone and the dSC, which are the target fields of the central projections of RA mechanoreceptors (Figure S1C-D). *Gfra2* is expressed in a small number of large-diameter DRG neurons, which were previously shown to be RA mechanoreceptors (Bourane et al., 2009; Luo et al., 2009), and some SC cells and motor neurons at these stages (Figure S1E-F and (Oppenheim et al., 2000)).

Nrtn is diffusely expressed at a low level in the SC and DRGs at both E13.5 and E15.5; *Gdnf* transcript is barely detected at E13.5 but is clearly expressed in DRG and motor neurons at E15.5 (Figure S1G-J). Thus, based on the expression patterns of RET signaling components in the developing SC and DRGs, RET in the central projections and cell bodies of developing RA mechanoreceptors could potentially be activated in *cis* by NRTN/ GFRa2 or in *trans* by GDNF/ GFRa1, which may come from neighboring DRG neurons, dorsal root entry zone cells, or dSC cells.

Central projection deficit of RA mechanoreceptors is negligible in postnatal *Gfra2* and *Nrtn* null mice.

RA mechanoreceptors depend on RET for the growth of their 3rd order central projections innervating layers III-V of SC. In postnatal *Ret* mutant mice, VGLUT1^{+} puncta, which label pre-synaptic terminals of mechanoreceptors and proprioceptors (Hughes et al., 2004; Paixao et al., 2013), are greatly reduced in layers III-V, indicating deficits in the 3rd order central projections of RA mechanoreceptors (Luo et al., 2009). Since RA mechanoreceptors express a high level of *Gfra2* but not any other *Gfras* (Luo et al., 2009), it is likely that RET in RA mechanoreceptors is activated by NRTN/ GFRa2 in *cis*. Indeed, we previously found that Pacinian corpuscles, a subtype of RA mechanosensory end organs in the periphery, are not formed in *Ret*, *Gfra2*, or *Nrtn* mutant mice, supporting that NRTN/GFRa2-RET *cis* signaling occurs in RA mechanoreceptors (Luo et al., 2009). Here we asked if NRTN-GFRa2/RET *cis* signaling is required for the growth of RA mechanosensory central projections as well. We performed immunostaining of VGLUT1 with postnatal day 7 (P7) *Gfra2*$^{GFP/GFP}$ null and *Nrtn*$^{-/-}$ null SC sections. No significant decrease of VGLUT1^{+} puncta in layers III-V of SC is observed in *Gfra2* and *Nrtn* null mice (Figure 1A-C, Table1 (P=0.96), and data not shown). This result suggests that unlike RET signaling in the peripheral branches of RA mechanoreceptors, *cis* activation of RET by GFRa2 and NRTN may be dispensable for the normal development of central projections of RA mechanoreceptors.

To determine whether RA mechanoreceptors survive without *Gfra2*, we quantified the number of GFP^{+};NF200^{+} neurons per DRG section in P7 *Gfra2*$^{GFP/+}$ controls and *Gfra2*$^{GFP/GFP}$ nulls. GFP is expressed from the *Gfra2* locus and most of GFP^{+};NF200^{+}

neurons indicate RA mechanoreceptors in *Gfra2*^{GFP} mice. In agreement with our previous findings at P0 (Luo et al., 2009), we found a slight but non-significant decrease in RA mechanoreceptor number between controls and mutants (Figure 1D, Table 1, (P=0.34)). Therefore, *cis* RET signaling via GFRa2 does not seem to be critical for the early postnatal survival of RA mechanoreceptors.

Central projection deficit of *Ret* null mice at E13.5

To understand the mechanism of RET signaling that controls growth of RA mechanosensory central projections, we genetically traced RA mechanoreceptors in *Ret*, *Gfra1*, *Gfra2*, and *Nrtn* mutant mice at different developmental stages. We first used *Ret* mutant mice, which serve as a positive control for the central projection deficit, to determine a robust method for visualizing RA mechanosensory interstitial branches at E13.5. We compared two methods that have been previously used. One is immunostaining of neurofilament-200 (NF200), which is expressed by large diameter DRG neurons, including RA mechanoreceptors, SA mechanoreceptors, and proprioceptors (Bourane et al., 2009). The other is to use a knockin/null allele of *Ret* (Honma et al., 2010), *Ret*^{CFP} (Uesaka et al., 2008), in which cyan fluorescent protein (CFP, a variant of green fluorescent protein (GFP)) is expressed from the *Ret* locus. Although *Ret* is expressed in both RA mechanoreceptors and some other DRG neurons at E13.5 (Luo et al., 2009), central projections of non-RA mechanoreceptor RET^{+} neurons, most of which develop into nociceptors, do not innervate the dSC until E15.5 or later

(Ozaki and Snider, 1997). In addition, the expression of *Ret* in dSC neurons is not obvious until E15.5 (Figure S1B). Thus, the Ret^{CFP} allele may allow us to specifically visualize central projections of RA mechanoreceptors at E13.5.

To compare these two methods, we performed anti-NF200 and anti-GFP immunostaining on SC sections of E13.5 $Ret^{CFP/+}$ control and $Ret^{CFP/CFP}$ null embryos. We observed a decrease in the density of $NF200^+$ fibers in the dorsal horn (Figure S2B, E). This decrease of $NF200^+$ central projections, however, is not dramatic. This is because the NF200 antibody also recognizes central projections of SA mechanoreceptors and proprioceptors, which develop in a manner temporally comparable to RA mechanoreceptors. In contrast, CFP^+ fibers innervating the dSC display a dramatic reduction in *Ret* null mice (Figure S2C, F). *Ret* null CFP^+ fibers reach the dorsal surface of the SC but rarely grow interstitial branches innervating layers III-V. We quantified the number of CFP^+ pixels in the dorsal horn (displayed as percentage of CFP^+ pixels normalized to the control) as a proxy for the extent of axon growth and found a significant decrease in CFP^+ fibers in *Ret* mutant dorsal horn (Figure S2H and Table 2, ($P<.001$)). This result suggests that the Ret^{CFP} allele is a valid tool for visualizing central projection deficits of RA mechanoreceptors at E13.5.

Since *Ret* signaling can positively regulate the expression of its own signaling components or control neuronal survival (Baudet et al., 2008; Golden et al., 2010; Luo et

al., 2007), it is conceivable that the lack of dSC CFP^+ fibers could be due to a downregulation of *CFP* expressed in *Ret* null RA mechanoreceptors or death of RA mechanoreceptors. To exclude these possibilities, we quantified the number of CFP^+ neurons in DRGs. We found that the number of CFP^+ neurons per DRG section was not statistically different between *Ret* heterozygotes and null mice (Figure S2I and Table 2). In addition, the intensity of GFP^+ fibers at the dorsal surface of the SC is comparable between *Ret* mutant and control mice. Therefore, the loss of CFP^+ fibers in the dorsal horn of E13.5 *Ret* mutants must mainly be due to a deficit in growth of interstitial central axons, but not due to the down-regulation of *CFP* expression or the death of RA mechanoreceptors.

Central projections of RA mechanoreceptors are normal in E13.5 *Gfra1* null mice

The finding that dSC VGLUT1 staining is largely normal in postnatal *Gfra2* and *Nrtn* null mice suggests that *cis* RET signaling may be dispensable for RA mechanosensory central projections. To determine if the development of RA mechanosensory central projections depends on the *trans* activation of RET via GFRa1 and GDNF, we generated *Gfra1* null ($Gfra1^-$) mice (Figure S3A-B and Materials and Methods). *In situ* hybridization of *Gfra1* control and null DRG sections showed that *Gfra1* transcripts are not produced in mice homozygous for this mutant allele (Figure S3C-D). In addition, kidneys are not formed in these *Gfra1* null mice (data not shown), a phenotype consistent

with previously reported *Gfra1* null mice (Cacalano et al., 1998; Enomoto et al., 1998). Thus, the *Gfra1*$^{-}$ allele we generated is a null allele.

If *trans* activation of RET via GFRa1 is required for the growth of interstitial central projections of RA mechanoreceptors, we expect to see a decrease of central projections of RA mechanoreceptors in the dSC of *Gfra1* null mice. To test this idea, we generated E13.5 *Gfra1*$^{+/-}$*;Ret*$^{CFP/+}$ control and *Gfra1*$^{-/-}$*;Ret*$^{CFP/+}$ mutant embryos to examine RA mechanosensory central projections at this stage (Figures 1E-F). We found that innervation of dSC by CFP^{+} fibers was not reduced upon *Gfra1* ablation (Figure 1G, Table 2). Additionally, the lack of *Gfra1* function did not lead to a decrease of CFP^{+} DRG neurons (Figure 1H, Table2). Together, our results suggest that *trans* activation of RET via GFRa1 is not required for the survival or central projection growth of RA mechanosensory neurons at E13.5.

Gfra2 and _Nrtn_ mutant mice phenocopy central projection deficits of _Ret_ mutant mice at E13.5

Since no deficit was observed in the central projections of RA mechanoreceptors in E13.5 *Gfra1* mutants, we next asked whether *cis* RET signaling is required for the initial growth of RA mechanosensory 3rd order central projections. We crossed the *Ret*^{CFP} allele into *Gfra2* and *Nrtn* null mice and examined central projections of RA mechanoreceptors at E13.5 (Figures 2A-D). In contrast to what we observed at P7, at this early development

stage CFP^+ central projections of RA mechanoreceptors are greatly reduced in both *Gfra2* and *Nrtn* null SC sections (Figure 2E-F, Table 2, *Gfra2* mutant has 9.50±1.44% of control staining at thoracic levels ($P<0.001$)). In addition, similar to the E13.5 *Ret* mutant mice, the number of CFP^+ DRG neurons in *Gfra2* and *Nrtn* null mice is comparable to that of control mice (Figures 2G-H, Table 2), suggesting that the loss of CFP^+ fibers in the dSC of these mutant mice is due to a deficit in the interstitial central projection growth of RA mechanoreceptors. Thus, at E13.5, *Gfra2* and *Nrtn* null mice phenocopy the central projection deficit of *Ret* mutant mice, which suggests that RET is activated by NRTN/GFRa2 in *cis* for the initial growth of RA mechanosensory central projections.

Interstitial central projections of *Gfra2* null RA mechanoreceptors begin to recover from E15.5

If *Ret*, *Gfra2*, and *Nrtn* null mice phenocopy each other at E13.5, why do their postnatal VGLUT1 staining patterns look so different (Figure 1 and (Luo et al., 2009))? One possibility is that since *Ret* has a much broader expression pattern than *Gfra2* in the dSC and DRGs, the dramatic loss of VGLUT1 staining in layers III-V of SC may be caused by the loss of RET signaling both in RA mechanoreceptors and other RET^+ cells. For *Gfra2* and *Nrtn* mutant mice, though central projection deficits of RA mechanoreceptors may persist postnatally, $VGLUT1^+$ puncta from SA mechanoreceptors could mask the phenotype. Alternatively, RA mechanosensory central projections in *Gfra2* and *Nrtn*

mutant mice could recover at later developmental stages due to the function of other RET signaling mechanisms.

To differentiate these possibilities, we examined central projections of RA mechanoreceptors in *Gfra2* null mice through development. We focused on *Gfra2* instead of *Nrtn* mutant mice because: 1) the cell autonomous requirement of a co-receptor is the key to differentiate *cis* versus *trans* RET signaling; and 2) *Gfra2* and *Nrtn* null mice display very similar phenotypes of RA mechanoreceptors. Since *Ret* begins to be expressed in additional populations of DRG neurons (Luo et al., 2007; Molliver et al., 1997) and dSC cells (Figure S1B) from E15.5, we cannot use the Ret^{CFP} allele to visualize the central projections of RA mechanoreceptors at late developmental stages. To overcome this problem, we used a tandem allele (See Materials and Methods and Figure S4) of an inducible Cre allele of *Ret* (Ret^{CreERT}) and Rosa26 conditional red fluorescent protein ($Rosa^{Tdt}$). We combined these alleles with early (E11.5 and E12.5) 4-hydroxy tamoxifen (4-HT) treatment to specifically trace RA mechanoreceptors, as previously established (Luo et al., 2009).

We generated $Gfra2^{GFP/+}$; Ret^{CreERT}; $Rosa^{Tdt}$ control and $Gfra2^{GFP/GFP}$; Ret^{CreERT}; $Rosa^{Tdt}$ mutant mice and examined their SC and DRG sections at E15.5. Tdt^{+} fibers innervate layers III-V of the SC, which is consistent with specific genetic tracing of RA mechanoreceptors (Luo et al., 2009). In addition, the majority of Tdt^{+} DRG neurons are

RET^{+}, GFRa2^{+} (reported by the expression of GFP), but NTRK1^{-} at E15.5 (Figures 3A-J), further supporting the specific labeling of RA mechanoreceptors. We found that central projections of *Gfra2* null RA mechanoreceptors are also decreased at E15.5 (Figures 3K-P, Table 3, *Gfra2* mutant has 55.13±2.82% of control staining at the thoracic level (P<0.001)). Since the number of labeled DRG neurons is not significantly reduced in the mutant mice (*Gfra2* mutants have 79.52±8.39% of control cell number (P=0.06)), the central projection phenotype mostly reflects a growth deficit at this developmental stage. Noticeably, the relative reduction of innervation in *Gfra2* null mice at E15.5 is less severe compared to that of E13.5 mutants (Figure 2), suggesting that central projections of *Gfra2* null RA mechanoreceptors may start to recover at this stage.

Ret and _Gfra2_ null mice display different central projection and cell survival deficits at E18.5

To determine if RA mechanoreceptors require *Ret* but not *Gfra2* for their central projection growth at later developmental stages, we generated E18.5 $Ret^{CreERT/+};Rosa^{Tdt}$ control and $Ret^{CreERT/CreERT};Rosa^{Tdt}$ mutant embryos (Ret^{CreERT} is a null allele of *Ret*). Consistent with previous results (Bourane et al., 2009; Honma et al., 2010; Luo et al., 2009), we found that RA mechanosensory central projections are greatly reduced in the *Ret* mutant mice (Figures 4A, C, I, Table 4, *Ret* mutant has 35.86±4.97% of control staining at thoracic levels (P<0.001)). In addition, we counted the number of Tdt^{+} neurons in L4/L5 DRGs and found that the number of Tdt^{+} RA mechanoreceptors is

dramatically reduced as well (Figures 4B, D, J, *Ret* mutant has 52.52±7.76% of control cell number (P<0.001)). Taken together, these results suggest that *Ret* is absolutely required for both survival and central projection growth of RA mechanoreceptors at E18.5.

In contrast, central projections of Tdt^+ *Gfra2* null RA mechanoreceptors are only slightly reduced at E18.5 (Figures 4 E, G, I, Table 4, *Gfra2* mutant has 86.34±4.48% of control staining at thoracic levels (P=0.01)). At P7, almost no difference is observed (data not shown). Similarly, the number of Tdt^+ RA mechanoreceptors is only slightly reduced in *Gfra2* null mice (Figures 4 F, H, J *Gfra2* mutant has 84.01±5.16% of control cell number (P=0.04)), indicating that extensive cell death of RA mechanoreceptors resulting from an absence of RET signaling does not occur in *Gfra2* null mice. The discrepancy between E18.5 *Ret* and *Gfra2* mutant phenotypes suggests that RET signaling still occurs in neonatal *Gfra2* null RA mechanoreceptors. To demonstrate this, we quantified the expression of phospho-S6 ribosomal protein, which is downstream of RET/PI3K/mTOR signaling (Plaza-Menacho et al., 2010), in RA mechanoreceptors. We found that the proportion of GFP^+ RA mechanoreceptors which express phospho-S6 in P0 $Gfra2^{GFP/+}$ control and $Gfra2^{GFP/GFP}$ mutant DRGs was similar (Figure S5, (P=0.51)). This result is consistent with the idea that RET activation occurs in neonatal RA mechanoreceptors without *Gfra2*.

Collectively, our results suggest that *Gfra2* null RA mechanoreceptors display a central projection deficit at E13.5 but recover during later development, which explains the almost normal VGLUT1 staining in layers III-V of SC at P7. In addition, our data indicate that from E15.5, an additional GFRa2 independent but RET dependent mechanism begins to play a role in promoting the survival and central projection growth of RA mechanoreceptors.

RET in RA mechanoreceptors is activated via both GFRa1 and GFRa2

To determine if this GFRa2 independent but RET dependent mechanism requires GFRa1, we examined genetically labeled $Gfra1^{+/-};Ret^{CreERT/+};Rosa^{Tdt}$ control and $Gfra1^{-/-};Ret^{CreERT/+};Rosa^{Tdt}$ mutant SC and DRGs at E18.5. Similar to E13.5, neither RA mechanosensory central projections nor their number is significantly decreased in *Gfra1* null mice (Figures 5A-D, I-J, Table 4), suggesting that simply disrupting *trans* activation of RET via GFRa1 is not sufficient to block Ret signaling in RA mechanoreceptors.

The lack of *Ret*-mutant-like survival and central projection phenotypes of RA mechanoreceptors in both *Gfra1* and *Gfra2* single null mice made us wonder if *cis* and *trans* RET signaling function in the same developmental process and thus loss of one co-receptor can be compensated for by the other. To test this idea, we generated *Gfra1;Gfra2* double knockout mice, in which RA mechanoreceptors were specifically labeled with Tdt using the $Ret^{CreERT};Rosa^{Tdt}$ tandem allele. We examined control and

double null SC sections and DRGs at E18.5. We found that Tdt^+ RA mechanosensory central projections are greatly reduced in the dSC (Figures 5E, G, I, Table 4, *Gfra1;Gfra2* double mutant has 27.25±2.09% of control staining at thoracic levels ($P<0.001$)). In addition, fewer Tdt^+ RA mechanoreceptors remain in the double knockout DRGs (Figures 5F, H, J, *Gfra1;Gfra2* double mutant has 38.17±2.65% of control cell number ($P<0.001$)), indicating that a significant number of RA mechanoreceptors die in the absence of *Gfra1* and *Gfra2*. Strikingly, the extent of reduction in both cell number and central projections of RA mechanoreceptors is comparable between the *Ret* null and *Gfra1:Gfra2* double null mice. Thus, our *in vivo* analyses strongly suggest that RET in RA mechanoreceptors is activated via both GFRa1 and GFRa2.

Gfra1 is not upregulated in *Gfra2* null RA mechanoreceptors

Is RET in RA mechanoreceptors activated by GFRa1 in *cis* or *trans*? Although *Gfra1* is not widely expressed in RA mechanoreceptors in wild type mice, could it be upregulated to compensate for the loss of *Gfra2* in the *Gfra2* null mice? To address these questions, we conducted double fluorescent *in situ* hybridization of *Gfra1* and *GFP* with E14.5 $Gfra2^{GFP/+}$ control and $Gfra2^{GFP/GFP}$ null DRG sections. We found that a comparable low number of GFP^+ neurons expressed *Gfra1* transcript in both mutants and controls (Figures 6A-C ($P=0.52$)), suggesting that *Gfra1* is not upregulated in *Gfra2* null RA mechanoreceptors. In addition, we performed *in situ* hybridization of *Gfra1* with P0 $Gfra2^{GFP/+};Ntrk1^{+/-}$ control, $Gfra2^{GFP/+};Ntrk1^{-/-}$ null, and $Gfra2^{GFP/GFP};Ntkr1^{-/-}$ double

null DRG sections. We previously showed (Luo et al., 2009) that *Gfra1* is expressed in NTRK1^{+} DRG neurons and that the expression of *Gfra1* is completely lost in *Ntrk1* null mice. Here we found that while *Gfra1* expression was observed in *Gfra2*$^{GFP/+}$*;Ntrk1*$^{+/-}$ control DRGs, no *Gfra1* expression was observed in either *Gfra2*$^{GFP/+}$*;Ntkr1*$^{-/-}$ null or *Gfra2*$^{GFP/GFP}$*;Ntkr1*$^{-/-}$ double null DRGs (Figures 6D-F). This result indicates that the expression of *Gfra1* in *Gfra2* null DRG neurons still fully depends on NTRK1 signaling and thus it must be expressed in the non-RA mechanoreceptors. Moreover, we performed quantitative RT-PCR (QPCR) for *Gfra1* transcripts in DRGs from E13.5, E15.5, and E18.5 *Gfra2*$^{GFP/+}$ control and *Gfra2*$^{GFP/GFP}$ mutant embryos. We found no significant difference in the expression of *Gfra1* between control and mutant DRGs at any stage (Figures S6, Table 5), suggesting that *Gfra1* is not transcriptionally upregulated in DRG neurons upon *Gfra2* ablation.

GFRa1 produced by neighboring DRG neurons activates RET in RA mechanoreceptors *in trans*

Although *Gfra1* transcript in most RA mechanoreceptors is below the detection level of *in situ* hybridization, it remains possible that an undetectable amount of GFRa1 could function in *cis* to promote RET signaling in RA mechanoreceptors. To exclude this possibility and to demonstrate that RET in RA mechanoreceptors is indeed activated by GFRa1 in *trans*, we used DRG explants from E14.5 embryos of different mutant

backgrounds and treated these explants with NRTN, GDNF, GFRa1 plus GDNF , or GFRa1 alone.

In E14.5 explants harboring the *Ret*^{CFP} allele, the cell bodies and axons of RET^{+} neurons, some of which are RA mechanoreceptors, can be identified by anti-GFP immunostaining. We found that CFP^{+} neurons in *Ret*$^{CFP/+}$ control DRG explants grow long axons upon NRTN, GDNF, or GFRa1 plus GDNF, but not GFRa1 alone treatment (Figure S7A-D, I, Table 6). In addition, the number of CFP^{+} DRG neurons is reduced in GFRa1 alone culture (Figure S7J, Table 7), suggesting that either cell death or down-regulation of *Ret*, and thus *CFP* expression, occur in the absence of RET signaling. Similarly, CFP^{+} neurons in *Ret*$^{CFP/CFP}$ null DRG explants lost their responsiveness to GFLs completely (Figure S7E-H, I-J, Table 7), suggesting that this assay reflects RET dependent signaling.

Next, we examined DRG explants harboring the *Gfra2*^{GFP} allele, which drives a much lower level of GFP expression than *Ret*^{CFP}. Although some small diameter DRG neurons also express *Gfra2* around P0 or later (Luo et al., 2007), in this *Gfra2*^{GFP} mouse line GFP is mainly detected in the large diameter RA mechanoreceptors (Luo et al., 2009), which express a much higher level of *Gfra2*. Therefore, anti-GFP staining of E14.5 *Gfra2*^{GFP} DRG explants should specifically show RA mechanoreceptors. Since GFP^{+} axons of these explants could not be reliably imaged and quantified due to the low level of GFP expression, we approximated the extent of RET signaling in *Gfra2*^{GFP} DRG explants by

quantifying the number of discernable GFP^+ cell bodies. We found that *Gfra2*$^{GFP/+}$ control DRG neurons show robust responses upon GFL application (Figure 7A-D, Q, Table 7). Interestingly, *Gfra2*$^{GFP/GFP}$ null DRG neurons lost their responsiveness to NRTN, but retain GFP expression in the presence of either GDNF or GFRa1 plus GDNF (Figure 7 E-H, Q, Table 7). These results suggest that a GFRa2 independent but RET dependent mechanism can mediate GDNF responsiveness of RA mechanoreceptors.

How can *Gfra2* null RA mechanoreceptors retain their responsiveness to GDNF? It could be due to: 1) a very low level of GFRa1 is expressed in RA mechanoreceptors, which activates RET in *cis* in the presence of GDNF*;* or 2) GFRa1 expressed by neighboring DRG neurons binds GDNF and activates RET in RA mechanoreceptors in *trans.* To differentiate between these possibilities, we cultured E14.5 *Gfra2*$^{GFP/GFP}$*;Ntrk1*$^{-/-}$ double mutant DRGs. Since the expression of *Gfra1* in non-RA mechanoreceptor DRG neurons fully depends on NTRK1 signaling, as shown previously (Luo et al., 2009) and above (Figures 6 D-F), GFRa1 should be depleted from non-RA mechanoreceptors in *Gfra2*$^{GFP/GFP}$*;Ntrk1*$^{-/-}$ double mutant DRGs. Therefore, if GFRa1 is expressed at a low level in RA mechanoreceptors and activates RET *in cis*, the double null explants should retain their responsiveness to GDNF. On the other hand, if GFRa1 expressed by neighboring neurons activates RET in RA mechanoreceptors *in trans*, the GDNF responsiveness would be lost in the *Gfra2;Ntrk1* double nulls. Here we found that *Gfra2*$^{GFP/+}$*;Ntrk1*$^{-/-}$ control explants were responsive to NRTN, GDNF, and GDNF plus GFRa1, but not GFRa1 alone (Figures 7 I-L, R, Table 7). In contrast,

Gfra2$^{GFP/GFP}$*;Ntrk1*$^{-/-}$ double null explants only respond to GDNF plus GFRa1, but not to NRTN, GDNF, or GFRa1 (Figures 7 M-P, R, Table 7). The loss of responsiveness of RA mechanoreceptors to GDNF in *Gfra2;Ntrk1* double null DRG explants strongly suggests that *Gfra1* is not expressed at a functional level in RA mechanoreceptors and that RET in *Gfra2* null RA mechanoreceptors is activated by exogenous GFRa1 from the neighboring DRG neurons in *trans*.

GFRa1 and GFRa2 are normally shed by DRG neurons

Trans activation of RET could occur by direct contact between membranes of cells which express either RET or GFRa1, or by soluble GFRa1 which is shed from the cell surface. To determine whether GFRa1 is released by DRG neurons, we cultured dissociated DRGs from E18.5-P1 wild-type, *Gfra2*$^{-/-}$, and *Gfra1*$^{-/-}$ mice. We collected cell lysates and concentrated media from days 3-6 *in vitro* and then performed Western blot analysis.

Immunoblotting with anti-GFRa1 revealed a doublet at ~55-65 kDa in wild-type and *Gfra2*$^{-/-}$ cell lysates, which was absent in the *Gfra1*$^{-/-}$ samples (Figure 7S, lanes 1-3), confirming the specificity of the anti-GFRa1 antibody. A positive band of ~55kDa was present in concentrated supernatants of wild-type and *Gfra2*$^{-/-}$ but not *Gfra1*$^{-/-}$ cultures (Figure 7S, lanes 4-6), suggesting that soluble GFRa1 is shed from neonatal DRG cells. Together with reports of GFRa1 being shed by Sciatic nerve Schwann cells, immortalized neuronal progenitors (Paratcha et al., 2001), and adult DRG explants (He et al., 2014),

our findings indicate that GFRa1 can be released by many cell types during both developmental and adult stages. Therefore, it is possible that RET in RA mechanoreceptors is activated in *trans* by both soluble GFRa1 and GFRa1 tethered to the membranes of neighboring cells.

In addition, although there is no significant increase of *Gfra1* transcripts in *Gfra2* null DRGs by *in situ* or QPCR (Figures 6 and S6), it remains possible that post-transcriptional regulation may occur to alter the translation, perdurance, or release of GFRa1. To test this possibility, we quantified the amount of GFRa1 in cell lysates and supernatants of wild-type and *Gfra2*$^{-/-}$ cultures by densitometry. We found that the amount of GFRa1 expressed in the cell or shed into the media was not significantly different between wild-type and *Gfra2* null cultures (Figure 7U-V, Table 8). Therefore, *Gfra2* null DRGs do not produce or release more GFRa1 protein to compensate for the loss of *Gfra2*.

We also investigated whether GFRa2 is normally shed by DRGs. The specificity of the anti-GFRa2 antibody was confirmed by the absence of a ~75 kDa band from *Gfra2* null cell lysates, which was present in both wild type and *Gfra1* null cultures (Figure 7T, lanes 1-3). Furthermore, secreted GFRa2 band was also present in the supernatants of wild-type and *Gfra1* DRG cultures, but not in *Gfra2* null cultures. Therefore, both GFRa1 and GFRa2 are normally released by DRGs during early postnatal development.

Dynamic expression of *Gdnf* during development

As described above, the central projections of *Gfra2* null RA mechanoreceptors display a severe, *Ret*-like deficit at E13.5, but begin to recover from E15.5, which is due to compensation by *trans* signaling via GDNF/GFRa1. Why is *trans* RET signaling able to compensate for the loss of *cis* signaling during late embryonic development, but not at E13.5? One possible reason for the delay is the availability of *trans* signaling components. Our *in situ* hybridization data suggest that *Gfra1* is expressed at high levels at both E13.5 and E15.5, but the expression of *Gdnf* is greatly increased in DRGs from E13.5 to E15.5 (Figure S1). To provide additional evidence for the dynamic expression of *Gdnf* during development, we examined DRG and SC sections of E13.5 and E15.5 $Gdnf^{LacZ/+}$ (Moore et al., 1996) embryos using X-Gal staining. We found that the expression of LacZ increased significantly in DRGs from E13.5 to E15.5 (Figure 8 A-E ($P<0.001$), Figure S8). In addition, X-Gal staining was found in the E15.5 dorsal root, the pathway through which DRG central projections travel to reach the dSC (Figure 8 A-D, black arrows). Thus, the expression of *Gdnf* seems to significantly increase in both the DRG and dorsal root from E13.5 to E15.5, providing a possible explanation for why the *trans* compensation occurs from E15.5.

DISCUSSION

In summary, we used RA mechanoreceptors as a model system to study the physiological functions of *trans* RET signaling and whether *cis* and *trans* activation of RET lead to the

same or diversified biological outcomes *in vivo*. RA mechanoreceptors express *Ret* and *Gfra2* and depend on *Ret* for their survival and the growth of central axonal projections into SC, whereas *Gfra1* is highly expressed in the target field and neighboring DRG neurons. We found that the RA mechanosensory central projection deficit is negligible in postnatal *Gfra2* and *Nrtn* mutant mice. We examined central projections of genetically traced RA mechanoreceptors in *Ret, Gfra2, Nrtn, Gfra1,* and *Gfra1;Gfra2* double null mice and showed that only *Gfra1;Gfra2* double null mice display similar cell death and central projection deficits to those of neonatal *Ret* mutant mice, indicating that RET in RA mechanoreceptors can be activated by both GFRa1 and GFRa2. Since *Gfra1* is undetectable in control and *Gfra2* null RA mechanoreceptors, it most likely activates RET in RA mechanoreceptors *in trans*. Finally, using DRG explant cultures, we determined that *Gfra2* null RA mechanoreceptors respond to GDNF by utilizing GFRa1 produced by neighboring neurons, strongly suggesting that RET in RA mechanoreceptors is activated by GFRa1 in *trans*. Taken together, our results provide clear evidence that *cis* and *trans* RET signaling can function in the same development processes *in vivo* (Fig. 8F) and that the existence of both *cis* and *trans* activation is likely to enhance but not diversify outcomes of RET signaling.

Trans **activation of RET** ***in vivo***

Previous expression analyses revealed that *Gfra1* is expressed more broadly than *Ret*, and cells which express *Gfra1* usually lie adjacent to *Ret*-expressing cells (Trupp et al., 1997;

Yu et al., 1998). This expression pattern suggests that GFRa1 may have RET independent functions or that GFRa1 may interact with RET expressed on the surfaces of other cells *in trans*. Indeed, evidence for both ideas has been demonstrated. GFRa1 and GDNF interact with NCAM in neurons and Schwann cells to promote neurite outgrowth and Schwann cell migration (Nielsen et al., 2009; Paratcha et al., 2003). Additionally, GFRa1 and GDNF are required for the proper migration of cortical GABAergic interneurons and can act as ligand dependent adhesion molecules for synapse formation, independent of RET and NCAM (Ledda et al., 2007; Pozas and Ibanez, 2005). Recently, it was also shown that GFLs have additional roles in cortical development via interactions with Syndecan-3, likely independent of RET, GFRas, and NCAM (Bespalov et al., 2011). On the other hand, RET can be activated by GFRa1 and GDNF *in trans* using both heterologous cells and tissue explants (He et al., 2014; Ledda et al., 2002; Paratcha et al., 2001; Patel et al., 2012). *Trans* RET signaling may affect many cellular processes, including directional axonal outgrowth and promotion of axon regeneration (Airaksinen and Saarma, 2002; Ledda et al., 2002; Paratcha et al., 2001).

Evidence for physiologically relevant *in vivo* function of *trans* RET signaling, however, has remained less conclusive. Enomoto and colleagues generated a "*cis*-only" mouse model in which *Gfra1* is expressed in all RET-expressing cells, but not in cells that do not express RET (Enomoto et al., 2004). Using this model, they found that the major RET dependent developmental processes were completely normal, suggesting that *trans* signaling is likely to be irrelevant for most RET-dependent processes. Results from this

model, however, may not necessarily preclude a physiological role for *trans* signaling. Not only does this model present a loss of *trans* signaling, but it also presents a gain of function: *Gfra1* is expressed at a high level in RET^{+} cells which may not normally express this co-receptor. If *cis* and *trans* RET activation lead to similar physiological outcomes, any deficits due to the loss of *trans* signaling may be masked by a gain of *cis* signaling. Indeed, the gain-of-function of GFRa1 was recently demonstrated in enteric hematopoietic cells derived from *cis*-only mice (Patel et al., 2012). Thus, whether *trans* RET signaling has any physiological function in development has remained an open question.

We aimed to address this question by analyzing the survival and growth of RA mechanosensory central projections using loss-of-function mouse lines. Here, we found that loss of *cis* signaling, via ablation of either *Gfra2* or *Nrtn*, produces a central projection deficit during early embryonic development (Figure 2). Our findings are consistent with previous observations using a different *Ret* knock-in line and NRTN ectopic expression (Honma et al., 2010), but differ from the findings using anti-GFRa2 staining to visualize RA mechanosensory central projections at E13.5 (Bourane et al., 2009). This is likely due to different subcellular localization of CFP and GFRa2, as well as the expression of GFRa2 by some dSC cells (Figure S1 E, F), which may mask the RA mechanoreceptor phenotype. Interestingly, this phenotype recovers during late embryonic development and the central projections of *Gfra2* null mice seem nearly normal postnatally (Figures 1, 4). Thus, our results suggest that *cis* RET signaling is

required for the initial growth of RA mechanosensory central projections, but an additional *cis* signaling independent process takes place during later development. Indeed, the loss of both *cis* and *trans* signaling in *Gfra1;Gfra2* double mutants recapitulates the *Ret* phenotype (Figure 5, 6). Furthermore, using DRG explant and dissociated culture, we demonstrated that soluble GFRa1 is normally released by DRGs and that GFRa1 produced by $NTRK1^{+}$ DRG neurons present a potential source to activate RET in RA mechanoreceptors in *trans* to promote their survival (Figure 7). Taken together, our results suggest that *trans* RET signaling contributes to the development of RA mechanoreceptors *in vivo*.

Nevertheless, the exact subcellular locus of *trans* RET activation in RA mechanoreceptors remains speculative. The expression pattern of *Gfra1* suggests that *trans* RET activation is possible in the axons of RA mechanoreceptors along their path to dSC, and/or at the cell body within the DRG. Although individual DRG cell bodies are surrounded by satellite glial cells, large macromolecules and proteins are able to invade the space between the neuron and satellite cell (Hanani, 2005), suggesting *trans* RET activation by soluble GFRa1 could occur within DRGs.

RET signaling and the survival or RA mechanoreceptors

Signaling of neurotrophic RTKs, such as NTRK1, NTRK2, and NTRK3, are critical for the specification and survival of numerous classes of neurons (Ernsberger, 2009). RET

signaling also plays important roles in survival, differentiation, and specification of distinct neuronal classes (Enomoto, 2005). For example, RET signaling components are absolutely required for the survival of enteric neurons (Taraviras et al., 1999), but their roles in DRG neuron survival are more complicated to dissect. Previously, it was reported that the number of total DRG neurons is not significantly reduced in neonatal and early postnatal *Ret* mutants (Luo et al., 2007). At that time, specific molecular markers or genetic approaches for labeling RA mechanoreceptors had not been identified, so it was impossible to specifically assay the role of RET signaling in the survival of this neuronal population. Given that RA mechanoreceptors represent a very small proportion of the total DRG neurons (Luo et al., 2007; Molliver et al., 1997), a partial loss of this population may not lead to a significant change in cell counts of total DRG neurons.

In another paper (Luo et al., 2009), it was proposed that RA mechanoreceptors depend on NRTN-GFRa2/Ret signaling for their development. This was based on the findings that GFRa2 is the only co-receptor expressed in RA mechanoreceptors and that *Ret*, *Gfra2*, and *Nrtn* null mice display the same no-Pacinian-corpuscle phenotype. Since RET cannot be used as a molecular marker to quantify the number of RA mechanoreceptors in *Ret* null mice, the number of P0 RET^{+}/$NTRK1^{-}$ and $Gfra2^{GFP}$ DRG neurons, most of which indicate the RA mechanoreceptors, was quantified in *Nrtn* and *Gfra2* nulls. No significant change in cell number between mutants and controls was found, suggesting that *Gfra2* and *Nrtn* are not required for survival of neonatal RA mechanoreceptors. These results are interesting in light of the current findings. Here, we show that when *cis*

signaling via NRTN/GFRa2 is perturbed (as was tested in (Luo et al., 2009)), *trans* signaling via GDNF/GFRa1 can activate RET in RA mechanoreceptors to promote their survival and central projection growth. When the number of genetically labeled RA mechanoreceptors was quantified in different mutant backgrounds, we found only marginal changes in *Gfra2* nulls but drastic decreases in *Ret* mutants at E18.5 (Fig. 4). The slight difference between the current and previous findings regarding the loss of RA mechanoreceptors in *Gfra2* nulls at P0 (Luo et al., 2009) is likely due to different methods in identifying and quantifying RA mechanoreceptors. In short, the current study clarifies that RET signaling is required for RA mechanoreceptor survival but simple disruption of *cis* RET signaling components may not reveal this deficit.

Co-existence of *cis* and *trans* RET signaling

What is the purpose for RET to be activated both in *cis* and in *trans*? Do *cis* and *trans* signaling activate different cellular responses and influence distinct developmental processes, or do *cis* and *trans* signaling exert the same physiological effect? Here we found that, in RA mechanoreceptors, *cis* and *trans* signaling seem to produce similar biological outputs *in vivo*. Our results demonstrate that that *cis* and *trans* signaling can compensate for the loss of each other to promote both the central projection growth and survival of RA mechanoreceptors (Fig. 8F). This compensatory ability suggests that the existence of both *cis* and *trans* activation is likely to enhance but not diversify outcomes of RET signaling. Consistent with this notion, a recent study found that peripheral nerves

secrete both GDNF and GFRa1, which attracts perineural invasion of heterogeneous cancer cells, some of which expresses *Ret* and *Gfras*, while some express only *Ret* (He et al., 2014).

In an attempt to show that GFRa1 is normally released from wild-type DRG cells for *trans* RET signaling, we found the same for GFRa2 (Figure 7). Given that soluble GFRa2 could also activate RET in *trans* with NRTN (Worley et al., 2000), our finding raises many interesting questions, such as whether all GFRas are secreted and whether "*cis*" and "*trans*" RET signaling normally co-exist even when RET and GFRas are expressed in the same cells. It seems plausible that even for GFRas co-expressed with RET (usually defined as "*cis"* signaling), such as GFRa2 in RA mechanoreceptors, it could be secreted and then upon NRTN binding activates RET in the cell from which it was released ("*trans*" activation).

Although *cis* and *trans* activation of RET lead to a similar biological outcome in the growth and survival of RA mechanoreceptors, it worth noting that substantial differences likely exist between the signaling processes of *cis* and *trans* RET activation. *Cis* RET activation might be more efficient, given that GFRas and RET are located in the same membrane. In addition, *cis* and *trans* signaling could differ in the kinetics of recruitment of RET to lipid rafts upon GFLs stimulation, interactions with downstream associated proteins, and the longevity of activated RET and downstream effectors (Paratcha et al.,

2001; Tansey et al., 2000). Additionally, it remains possible that although the gross structure of the RA mechanosensory central projections seems mostly normal in mice lacking either *cis* or *trans* signaling, more precise aspects of circuit formation, such as specific synapse formation, which are beyond the resolution of current analysis, may differentially depend on *cis* or *trans* signaling. Finally, it will be interesting to see whether *cis* and *trans* signaling can produce similar biological outcomes in other systems, as we have shown here for RA mechanoreceptors. Future experiments to carefully dissect *cis* and *trans* RET signaling in other types of cells and tissues will address these issues.

MATERIALS AND METHODS

Mouse strains. Mice except $GDNF^{lacZ}$ line were raised in a barrier facility in Hill Pavilion, the University of Pennsylvania. All procedures were conducted according to animal protocols approved by Institutional Animal Care and Use Committee (IACUC) of the University of Pennsylvania and National Institutes of Health guidelines. $GDNF^{lacZ}$ mice were raised in accordance with the European Community Council Directive of November 24, 1986 (86/609/EEC), and approved by the ethics. Most mice used in this paper were described previously: Ret^{CreERT}, Ret^{CFP}, $Nrtn^{+/-}$ (purchased from the Jackson lab), $Gfra2^{GFP}$ (re-derived using sperm provided by Dr. Jeffery Milbrandt at the Washington University), $Rosa26^{Tdt}$, and $Gdnf^{LacZ}$ mice (Heuckeroth et al., 1999; Luo et al., 2009; Madisen et al., 2010; McDonagh et al., 2007; Moore et al., 1996; Uesaka et al., 2008). The $Ntrk1^{-}$ allele was generated by crossing the floxed $TrkA^{F592A}$ allele (Chen et al., 2005) to germline Cre mice. The generation of *Gfra1* conditional and null mice and

the *Ret*^{CreERT};*Rosa*^{Tdt} tandem allele are described below. All mice except *Gdnf*^{LacZ} were maintained on a mixed C57BL/6J and CD1 background. *Gdnf*^{LacZ} mice were maintained on a C57BL/6N background. Except for *Gfra1;Gfra2* double null animals (n=2), at least three animals per genotype were examined. N-values for explants are listed in Tables 7 and 8.

Generation of *Gfra1* conditional and null alleles. We generated *Gfra1* conditional knockout mice, in which loxP sites flank exon 6 of *Gfra1*, by homologous recombination. Mice harboring the floxed allele were crossed to germ line Cre mice, resulting in a *Gfra1* allele lacking exon 6. The loss of *Gfra1* transcript in *Gfra1*$^{-/-}$ mice was confirmed by *in-situ* hybridization of mutant and control DRGs (See Figure S3).

Generation of *Ret*^{CreERT};*Rosa*^{Tdt} tandem allele. Since *Ret* and *Rosa26* loci are located only ~5 megabases apart on mouse Chromosome 6, we generated a tandem configuration of *Ret*^{CreERT} and *Rosa*^{Tdt} alleles, which are linked during meiosis and became a great genetic advantage for our experiments (Figure S4). We used this tandem *Ret*^{CreERT};*Rosa*^{Tdt} allele to specifically label RA mechanoreceptors in different mutant mouse lines described in the text.

Genetic labeling of RA mechanoreceptors. We set up timed pregnancy mating for mice in the evening and checked mice for vaginal plugs the following morning. The time when a female mouse was found to have a plug was counted as embryonic day 0.5 (E0.5). We treated embryos harboring the $Ret^{CreERT};Rosa^{Tdt}$ reporter allele with 4-hydroxy-tamoxifen (4-HT, 2mg and 1mg at E11.5, and E12.5, respectively) by oral gavage to pregnant female mice to specifically label RA mechanoreceptor population.

Tissue preparation and histology. Spinal columns of embryos and neonatal mice at the desired developmental stages were dissected out and directly immersed in PBS/ 4% paraformaldehyde (PFA) for 2 to 4 hours at 4°C. Postnatal mice were sacrificed with CO_2, transcardially perfused with 4% PFA, and spinal columns were dissected out and post-fixed with 4% PFA for 2 hours at 4^{o}C. They were then cryo-protected in 1XPBS, 30% sucrose overnight. 20μm frozen sections of spinal cord and DRGs were cut using a Leica CM1950 cryostat. Immunostaining of spinal cords and DRG sections were performed as described previously (Niu et al., 2013). Antibodies used are as follows: rabbit anti-GFP (1:2000, Invitrogen, A-11122), chicken anti-GFP (1:1000, Aves, GFP-1020), chicken anti-NF200 (1:500, Aves, NF-H), rabbit anti-NF200 (1:1000, Sigma, N4142), rabbit anti-cRet (1:50, IBL, 18121), rabbit anti-NTRK1 (1:1000, Fisher/Millipore, 06-574), guinea pig anti-VGLUT1 (1:1000, Millipore, AB5905), rabbit anti-phospho-S6 (1:200, Cell Signaling, 2215s) and Alexa Fluorescent conjugated Goat or Donkey secondary antibodies (1:500, Invitrogen or Jackson ImmunoResearch).

LacZ color reaction. Embryos of the desired age were eviscerated and fixed in 1% PFA, 2mM $MgCl_2$, 5mM EGTA, 0.02% NP40 and 0.2% glutaraldehyde in phosphate buffer (pH 7.4) for 1.5 to 2 hours at 4°C. Vibratome sections were incubated for 30 min in washing solution (2mM MgCl2, 0.02% NP-40 in phosphate buffer pH 7.4).LacZ reaction was developed with X-gal (1mg/ml) at 37°C.

***In situ* hybridization.** DIG- or FITC-labeled riboprobes were synthesized using a DIG or FITC RNA labeling kit (Roche, 11175025910). Template for GFP was amplified by PCR and subcloned into vector pGEM-T Easy (Promega, A1360). Antisense RNA probes for *Ret, Gfra1, Gfra2, Gdnf,* and *Nrtn* were generated as previously described (Luo et al., 2009). The detailed procedures of *in situ* hybridization and double fluorescent *in situ* hybridization were performed as described previously (Fleming et al., 2012).

Quantitative RT-PCR. DRGs from E13.5, E15.5, and E18.5 $Gfra2^{GFP/+}$ and $Gfra2^{GFP/GFP}$ embryos were dissected and rapidly frozen on dry ice. RNA was extracted with the GeneJet RNA Purification Kit (Fermentas, K0731) and cDNAs were generated using Super-Script III First-Strand Synthesis System (Invitrogen, 18080-51). 500ng of total RNA was used for each RT reaction in a total volume of 25µL. QPCR reactions were performed in triplicate for three samples of each age and genotype. QPCR reactions

contained SYBR Green PCR master mix (Life Technologies, 4309155), 0.5 μM of each primer, and 3μL (for *Gfra1*) or 1μL (for *Gapdh*) of cDNA template per 15μL reaction. Reactions were run and analyzed on a StepOnePlus Real-Time PCR System (Applied Biosystems). Primers used were *Gapdh* (5'-CCACCAACTGCTTAGCCCCC-3' and 5'-GCAGTGATGGCATGGACTGTGG-3') and *Gfra1* (5'-TGTCTTTCTGATAATGATTACGGA-3' and 5'-CTACGATGTTTCTGCCAATGATA-3'). P-values between samples were calculated from ΔCT values with the Student's t-test, and relative concentrations were calculated by the $2^{-\Delta\Delta CT}$ method (Livak and Schmittgen, 2001).

DRG explant culture and immunostaining. E14.5 embryos were removed from the dam and placed in F-12 media (Invitrogen, 11765-047) on ice. Spinal cords with attached DRGs were dissected from the spinal column, and individual DRGs were removed and placed in fresh F-12 on ice. Using a dissecting needle, DRGs were cleaned and bisected, and then placed in fresh F-12. Explants were grown on Superfrost Plus slides (Fisher, 22-034-979) coated with poly-L-lysine (Sigma, P1274, 0.1 mg/mL in ddH2O overnight at 4°C) and laminin (BD, 354232, 20 μg/mL in HBSS (Invitrogen, 14170122) at 37°C for one to three hours). Immediately before placing explants on the slide, slides were washed with HBSS and DRG culture medium (Neurobasal medium (Invitrogen, 21103-049), 1X B27 (Invitrogen, 17504-044), 100 U/mL penicillin/streptomycin (Invitrogen, 15140-122), 2mM L-glutamine (Invitrogen, 25030-081), and 35mM glucose). DRG culture media supplemented with the appropriate

recombinant proteins (50 ng/mL Nrtn (R&D, 477-MN-025), 100 ng/mL GDNF (R&D, 512-GF-010), 300ng/mL GFRa1 (R&D, 560-GF-100), or 100 ng/mL GDNF and 300 ng/mL GFRa1) was added to the culture dish. Four to six DRG explants were placed on each slide and the culture dishes were carefully moved to a 37°C incubator and left undisturbed overnight. Following 16-24 hours of incubation, cultures were rinsed with PBS and fixed in 4% PFA in PBS for 30 minutes at room temperature. Immunofluorescence was then performed directly in the culture dish using antibody dilutions described above. Following secondary antibody, explant slides were mounted on microscope slides using Superglue, and coverslipped with Fluoromount-G (Southern Biotech, 0100-01) and 22x22mm coverglass.

Dissociated DRG cultures and biochemistry. DRGs from E18.5-P1 mice were collected into HBSS on ice. DRGs were first digested in 0.5mg/mL collagenase (Worthington, LS4186) plus 100 U/mL penicillin/streptomycin, 10mM HEPES, and 1X MEM vitamins (Sigma, M6895) in MEM (Invitrogen, 11095072) at 37°C for thirty minutes, followed by a second digestion with 0.05% trypsin (Invitrogen, 25200056) plus 100 U/mL penicillin/streptomycin, 10mM HEPES, and 1X MEM vitamins in MEM at 37°C for thirty minutes. Digestion was stopped by adding 5% FBS and 10mM HEPES in HBSS. Cells were then triturated with a fire polished Pasteur pipette to a homogenous solution. The cells were then pelleted at 500x*g* for 5 minutes and resuspended in DRG culture media, as described above, supplemented with 50 ng/mL NRTN, 100 ng/mL GDNF, and 50ng/mL NGF (R&D, 556-NG-100). Cells were plated in 6-well collagen

coated plates (Millipore, PICL06P05) and cultured at 37°C and 5% CO_2. After 2 days, media was removed and cells were rinsed with warmed Neurobasal media. 2mL of fresh DRG culture media supplemented with NRTN, GDNF, and NGF (but without B27) was added to each well. After 2 days, media was removed and saved at 4°C with added protease inhibitors (Sigma, P8340). Fresh media supplemented with growth factors but without B27 was then added to each well. After an additional 2 days, media was removed and pooled with previously collected media, and additional protease inhibitor was added. The cells were rinsed twice with PBS, and then lysed directly in the well by the addition of 70µL 2X sample buffer (0.125M Tris pH 6.8, 20% glycerol, 4% SDS, 0.16% bromophenol blue, 10% 2-mercaptoethanol) and scraping, followed by heating at 95°C for five minutes. All cell lysates were then brought to a total volume of 140µL with 1X PBS. Supernatants were centrifuged at 14,000xg for 15 minutes to clear cellular debris, and then were concentrated to ~30µL with Amicon 30kDa filters (Millipore, UFC503024), then mixed with an equal volume of 2X sample buffer and heated at 95°C for five minutes.

Duplicate 4-15% gradient mini-Protean TGX gels (Biorad, 456-1084) were used to run samples. 40µL of cell lysate of each genotype or one third of the total volume of concentrated supernatant of each genotype was used. Both gels were then transferred to nitrocellulose membrane and blocked in 3% BSA in TBS plus 0.1% Tween-20 (TBST) for one hour at room temperature. Membranes were then incubated overnight with either goat anti-GFRa1 (0.2µg/mL, R&D, AF560) or goat anti-GFRa2 (0.2µg/mL, R&D,

AF613) in blocking solution overnight at 4°C. Following washes with TBST, membranes were incubated with donkey anti-goat-AP (1:5000, Santa Cruz Biotechnology, SC-2022) in blocking solution for one hour at room temperature. After washes, AP was detected with CDP-Star (Applied Biosystems, T2218) and membranes were imaged with a Chemi-Doc system (BioRad).

Following imaging, membranes were stripped with 2x 10 minutes stripping buffer (0.2M glycine, 0.1% SDS, 1% Tween-20, pH 2.2), followed by 2x 10 minutes wash with PBS and 2x 5 minutes wash with TBST. Membrane was then probed with rabbit anti-β-actin (1:400, Santa Cruz Biotechnology, sc-130656) and goat anti-rabbit-AP (1:5000, Applied Biosystems, T2191) following the above procedure, except that all blocking and antibody incubations were performed in 5% milk in TBST.

Western blot densitometry was performed with ImageJ. Three cultures per genotype were analyzed. Densitometry measurements for each antibody were performed on three blots running independent culture samples. Relative quantifications were performed using β-actin in the cell lysates as a measure of total protein per lane, and optical density values for GFRa1 were scaled accordingly. Because an equal proportion of total lysates was run in each lane, total β-actin per cell lysate lane was used as a proxy for cell number, and was therefore used to normalize protein levels in the supernatant lanes (equal proportion of total supernatant volume were run in each lane). Cell lysate and

supernatant samples were scaled to wild-type quantifications of respective sample type and reported in arbitrary units. Student's t-test was used to measure significance of differences between genotypes.

Image acquisition. Fluorescent images of SC/DRG sections were acquired on a Leica SP5II confocal microscope. DRG explant cultures were imaged on Leica DM5000B microscope. Bright field images were taken using Leica DM5000B microscope.

Quantification and Statistics. For histological analysis, at least six sections per specified spinal/DRG level per animal were analyzed. For quantification of genetically labeled neuron number in E18.5 embryos, whole-mount L4/L5 DRGs were imaged and total Tdt^+ cell number was counted in each DRG. Except for *Gfra1;Gfra2* double null animals (n=2), at least three animals per genotype were examined. N-values for explants are listed in tables S6 and S7. Pixel counts for central projections were generated by counting the number of pixels at each intensity level (0-256) in an outlined immunoreactive area in ImageJ. Background staining was subtracted by counting pixel number of each intensity level in a non-immunoreactive region of the tissue. The minimal intensity level at which two consecutive levels displayed a pixel count of zero was taken as the threshold cut of background fluorescence. Pixel counts of real staining were then calculated by summing the pixel counts for all intensity levels above the defined background level. Column graphs were generated in GraphPad Prism 5. All error

bars are ± standard error of the mean (SEM), unless otherwise specified. All statistical analyses were performed using SAS version 9.3 (SAS Inc., Cary, NC). Due to differences in labeling efficiency across litters in 4-HT treated mice, quantification for spinal cord section staining and whole mount DRGs were performed by normalizing to controls within the same litter. For all explant quantifications, GFP^+ neuron number per 10,000μm^2 was calculated for each explant. For Ret^{CFP} explants, a circle with a radius 200μm larger than the explant was drawn around the explant in ImageJ, and the number of CFP^+ axons which crossed the circle was counted.

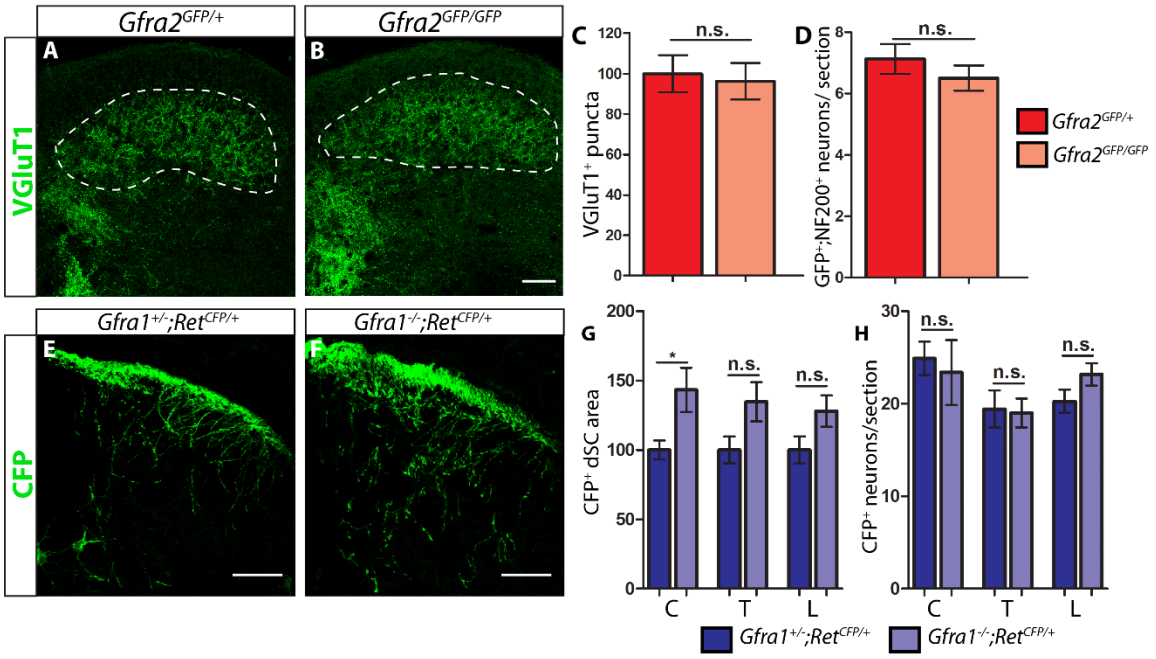

Figure 1: P7 *Gfra2* mutant mice show normal dSC VGLUT1 staining and *Gfra1* null mice display normal RA mechanoreceptor central projections at E13.5: (A-B) Anti-VGLUT1 immunostaining of P7 SC sections from *Gfra2*$^{GFP/+}$ control (**A**) and *Gfra2*$^{GFP/GFP}$ null (**B**) mice. VGLUT1 staining labels presynaptic terminals of mechanosensory neurons, which are found in layers III-V of the dSC (outlined in white). Note that GFP driven from the *Gfra2* locus cannot be visualized directly. Therefore, positive signal indicates presynaptic VGLUT1^{+} puncta and not GFRa2^{+} primary afferent axons. (**C**) Quantification of VGLUT1^{+} puncta in dSC, which is displayed as a percentage of VGLUT1^{+} pixels compared to the control pixel count. The similar density of VGLUT1^{+} puncta between mutant and control tissue suggests that *cis* RET signaling via GFRa2 is dispensable for the growth of RA mechanosensory central projections at P7. (**D**) Quantification of GFP^{+};NF200^{+} neurons, which indicate RA mechanoreceptors, per DRG section. The non-significant decrease in RA mechanoreceptor number per section in *Gfra2* nulls suggests that most RA mechanoreceptors are not dependent on *cis* RET signaling for survival. **(E-F)** Anti-GFP immunostaining of RA mechanoreceptor central projections in E13.5 *Gfra1*$^{+/-}$*;Ret*$^{CFP/+}$ control (**E**) and *Gfra1*$^{-/-}$*;Ret*$^{CFP/+}$ mutant (**F**) SC sections. The increased CFP signal in *Gfra1* null dSC is likely due to the precocious expression of *Ret* in some dSC neurons of *Gfra1* mutants. (**G**) Quantification of CFP^{+} pixel number in dSC. The lack of a reduction in CFP^{+} axons in *Gfra1* mutant dSC indicates that *trans* signaling via GFRa1 is not required for the initial growth of RA mechanosensory 3rd order central projections. (**H**) Quantification of number of CFP^{+} neurons per DRG section indicates no loss of RA mechanoreceptors in *Gfra1* mutants at E13.5. C: cervical level, T: thoracic level, L: lumbar level. Scale bars= 50µm. Error bars represent SEM. n.s.=P>0.05, *=P<0.05. Source data are provided in Tables 1 and 2.

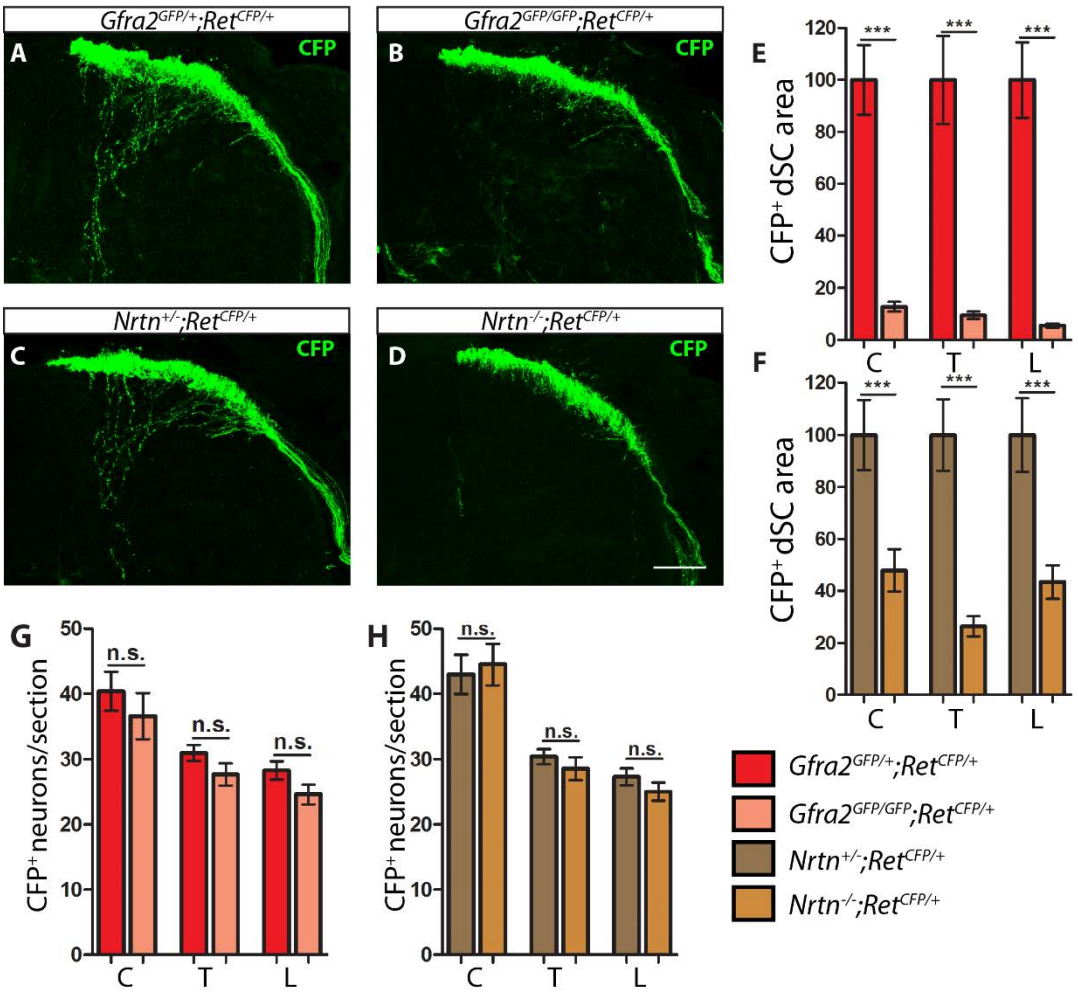

Figure 2: *Gfra2* and *Nrtn* null mice show reduced RA mechanoreceptor central projections at E13.5: (**A-D**) Anti-GFP immunostaining to visualize RA mechanosensory central projections in E13.5 dSC sections of $Gfra2^{GFP/+};Ret^{CFP/+}$ control (**A**), $Gfra2^{GFP/GFP};Ret^{CFP/+}$ mutant (**B**), $Nrtn^{+/-};Ret^{CFP/+}$ control (**C**), and $Nrtn^{-/-};Ret^{CFP/+}$ mutant (**D**) mice. (**E-F**) Quantification of CFP^+ pixel number in dSC of *Gfra2* (**E**) and *Nrtn* (**F**) mice. The dramatic reduction in CFP^+ axons in *Gfra2* and *Nrtn* nulls at E13.5 suggests that *cis* activation of RET is required for the initial growth of RA mechanosensory 3rd order central projections. (**G-H**) Quantification of number of CFP^+ neurons per DRG section in *Gfra2* (**G**) and *Nrtn* (**H**) mice. Similar number of CFP^+ DRG neurons between control and mutant mice indicates that cell death of RA mechanoreceptors or downregulation of Ret^{CFP} allele do not occur at E13.5 when *cis* RET signaling is ablated. Scale bar=50μm. Error bars represent SEM. n.s.=P>0.05, **=P<0.01 ***=P<0.001. Source data are provided in Figure 1-source data 2.

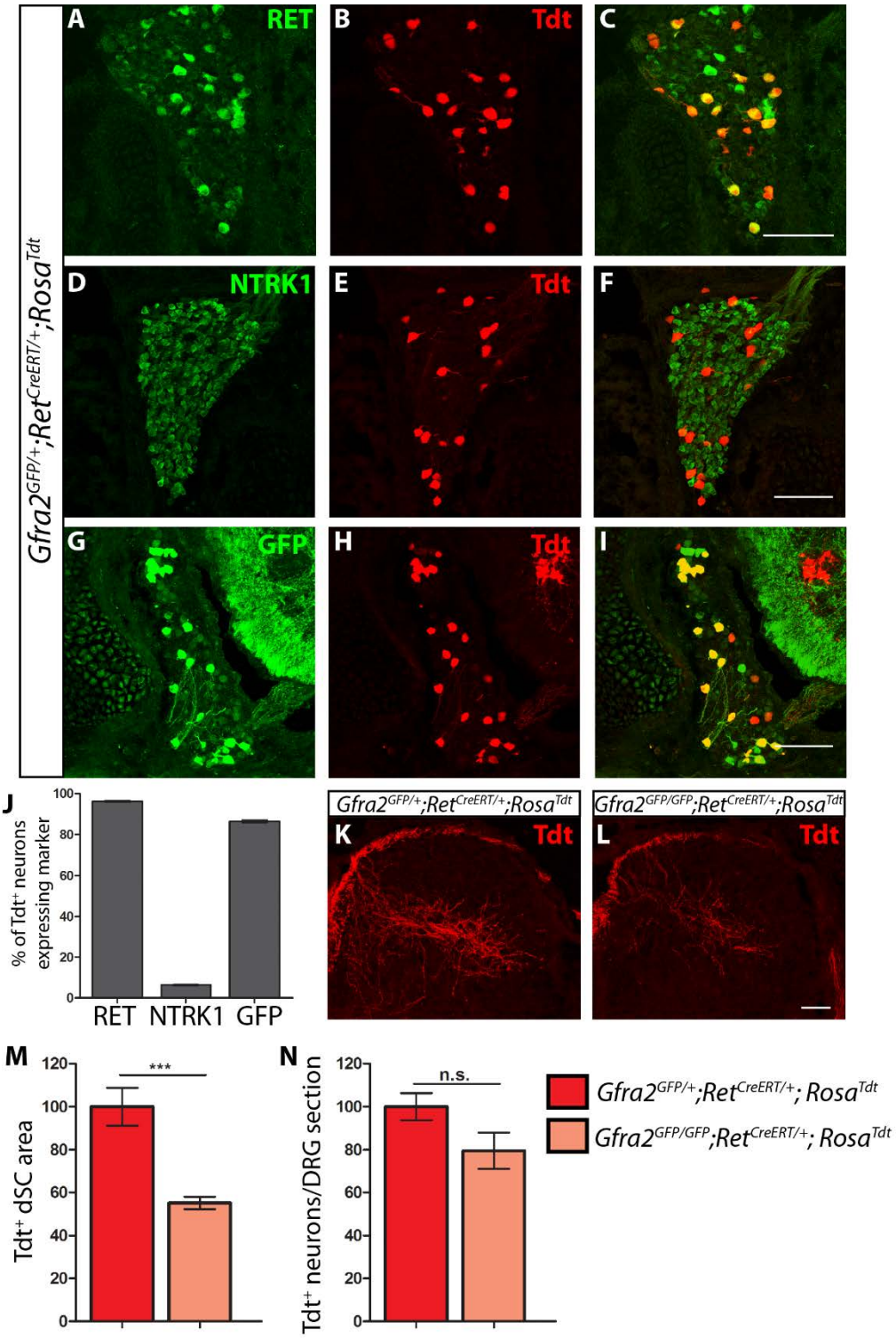

Figure 3: Central projection growth deficit of *Gfra2* null RA mechanoreceptors at E15.5: (**A-I)** E15.5 *Gfra2*$^{GFP/+}$;*Ret*$^{CreERT/+}$;*Rosa*^{Tdt} DRG sections stained with anti-RET (**A-C**), anti-NTRK1 (**D-F**), and anti-GFP (**G-I**). (**J**) Quantification of percentage of Tdt^{+} DRG neurons which co-express RET (96.16±0.28%), NTRK1 (6.56±0.18%), and GFP

driven from the *Gfra2* locus (86.48±0.55%). The expression profile of Tdt^+ neurons confirms that this genetic labeling strategy specifically labels RA mechanoreceptors. (**K-L**) Visualization of Tdt^+ RA mechanosensory central projections in dSC of E15.5 $Gfra2^{GFP/+}$; $Ret^{CreERT/+}$; $Rosa^{Tdt}$ control (**K**) and $Gfra2^{GFP/GFP}$; $Ret^{CreERT/+}$; $Rosa^{Tdt}$ mutant (**L**) SC sections. (**M**) Quantification of Tdt^+ pixels in dSC, which is displayed as a percentage normalized to dSC Tdt^+ pixels of the within litter controls. *Gfra2* mutant mice have 55.13±2.82% of control staining (P<0.001). Note that although *Gfra2* null RA mechanoreceptors still have a central projection deficit at E15.5, the reduction at this stage is less severe than the deficit observed at E13.5. (**N**) Quantification of number of Tdt^+ neurons per DRG section, which is displayed as a percentage normalized to Tdt^+ neurons of the within litter controls. *Gfra2* mutant mice have 79.52±8.39% of control cell number (P=0.06), which suggests that the survival of RA mechanoreceptors is not dependent on *cis* signaling at this stage. Scale bars= 100μm (A-I), 50μm (K-L). Error bars represent SEM. n.s.=P>0.05, ***=P<0.001. Source data are provided in Table 3.

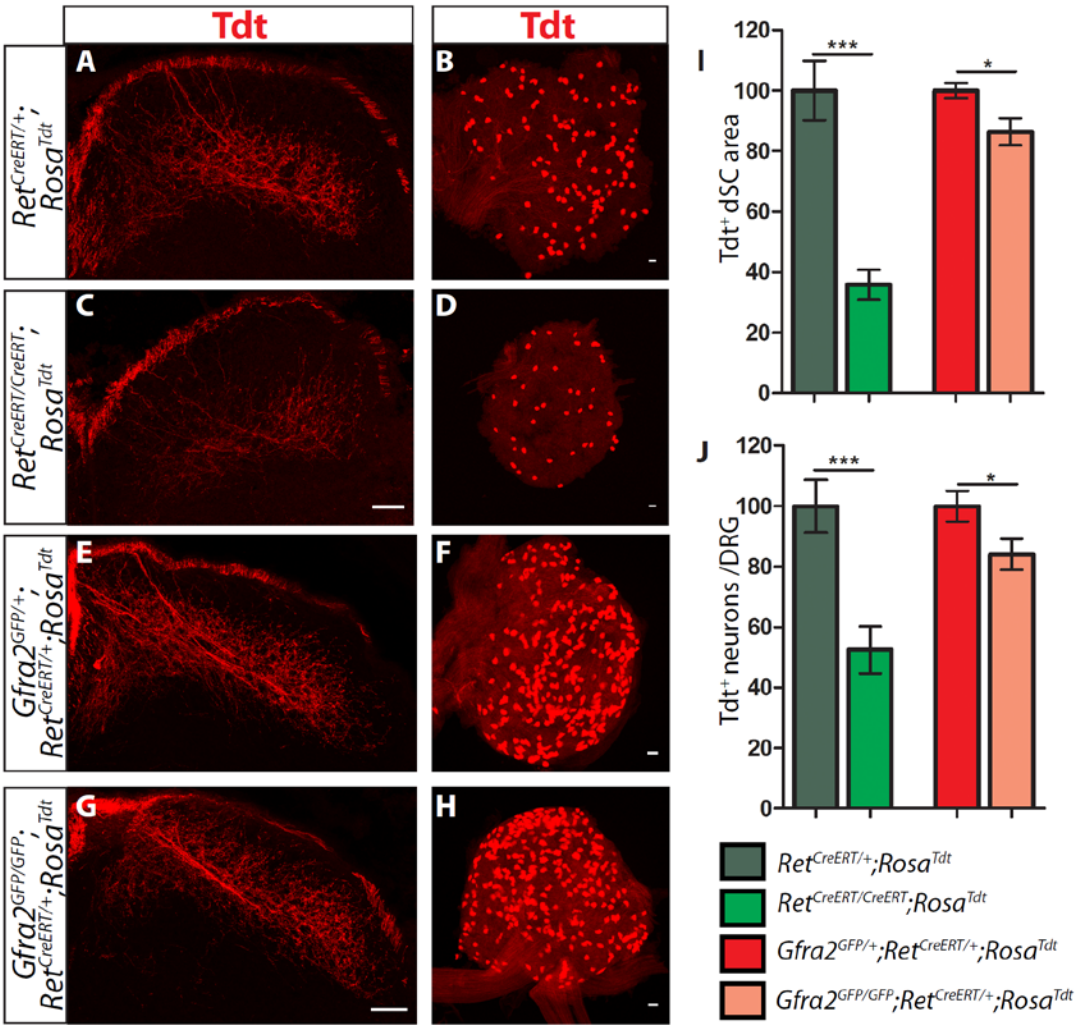

Figure 4: *Ret* and *Gfra2* null mice display different central projection and cell survival deficits at E18.5: (**A-H**) SC sections and whole mount L4/L5 DRGs of Tdt labeled RA mechanoreceptor from E18.5 $Ret^{CreERT/+};Rosa^{Tdt}$ control (**A-B**), $Ret^{CreERT/CreERT};Rosa^{Tdt}$ mutant (**C-D**), $Gfra2^{GFP/+};Ret^{CreERT/+};Rosa^{Tdt}$ control (**E-F**), and $Gfra2^{GFP/GFP};Ret^{CreERT/+};Rosa^{Tdt}$ mutant (**G-H**) embryos. **(I)** Quantification of Tdt^+ pixels in dSC, which is displayed as a percentage normalized to dSC Tdt^+ pixels of the within litter controls. (**J**) Quantification of the number of Tdt^+ DRG neurons per whole-mount L4/L5 DRG, which is displayed as a percentage normalized to Tdt^+ neurons of the within litter controls. *Ret* mutants have significant decreases in RA mechanosensory axons innervating the dSC and in the number of Tdt^+ RA mechanoreceptors, suggesting that *Ret* mutants have deficits in both the growth of 3rd order central projections and the survival of RA mechanoreceptors at E18.5. In contrast, *Gfra2* nulls have only minor deficits in RA mechanosensory central projection growth and the survival or RA mechanoreceptors, suggesting that an additional GFRa2 independent but RET dependent mechanism

functions in these processes. Scale bar=50μm. Error bars represent SEM. *.=P<0.05, ***=P<0.001. Source data are provided in Table 4.

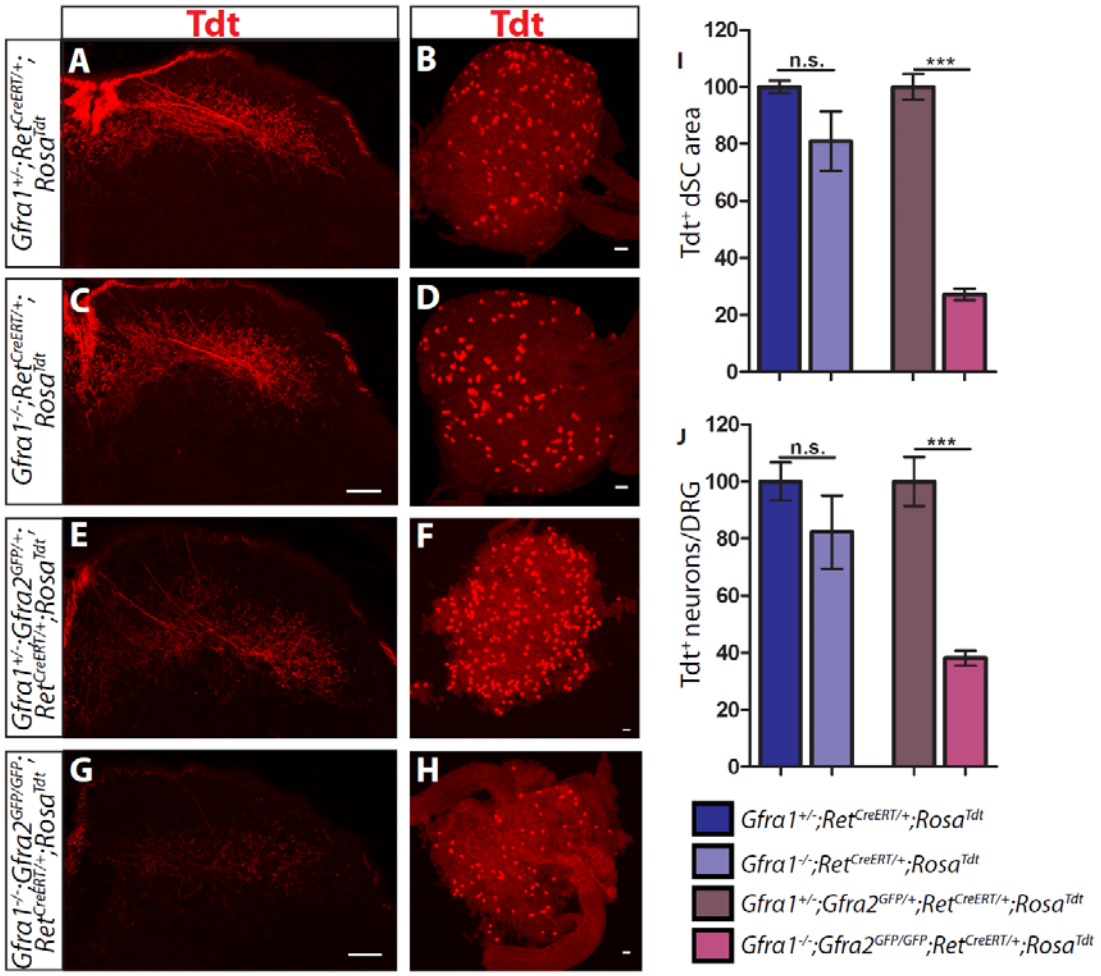

Figure 5: *Gfra1;Gfra2* double null mice phenocopy *Ret* mutants at E18.5: (**A-H**) SC sections and whole mount L4/L5 DRGs of Tdt labeled RA mechanoreceptors from E18.5 *Gfra1*$^{+/-}$;*Ret*$^{CreERT/+}$;*Rosa*^{Tdt} control (**A-B**), *Gfra1*$^{-/-}$;*Ret*$^{CreERT/+}$;*Rosa*^{Tdt} mutant (**C-D**), *Gfra1*$^{+/-}$; *Gfra2*$^{GFP/+}$;*Ret*$^{CreERT/+}$;*Rosa*^{Tdt} control (**E-F**) and *Gfra1*$^{-/-}$; *Gfra2*$^{GFP/GFP}$;*Ret*$^{CreERT/+}$;*Rosa*^{Tdt} double null (**G-H**) embryos. (**I**) Quantification of Tdt^{+} pixels in dSC, which is displayed as a percentage normalized to dSC Tdt^{+} pixels of the within litter controls. (**J**) Quantification of number of Tdt^{+} DRG neurons per DRG, which is displayed as a percentage normalized to Tdt^{+} neurons of the within litter controls. *Gfra1* mutants have no significant deficits in RA mechanosensory 3rd order projections or cell survival at E18.5, indicating that ablating *trans* signaling alone is not sufficient to disrupt the development of RA mechanoreceptors. However, loss of both *cis* and *trans* signaling in *Gfra1;Gfra2* double nulls leads to a significant loss of RA mechanosensory 3rd order projection growth and cell number, suggesting that both *cis* and *trans* RET signaling contribute to the development of RA mechanoreceptors. Scale bars=50µm. Error bars represent SEM. n.s..=P>0.05, ***=P<0.001. Source data are provided in Table 4.

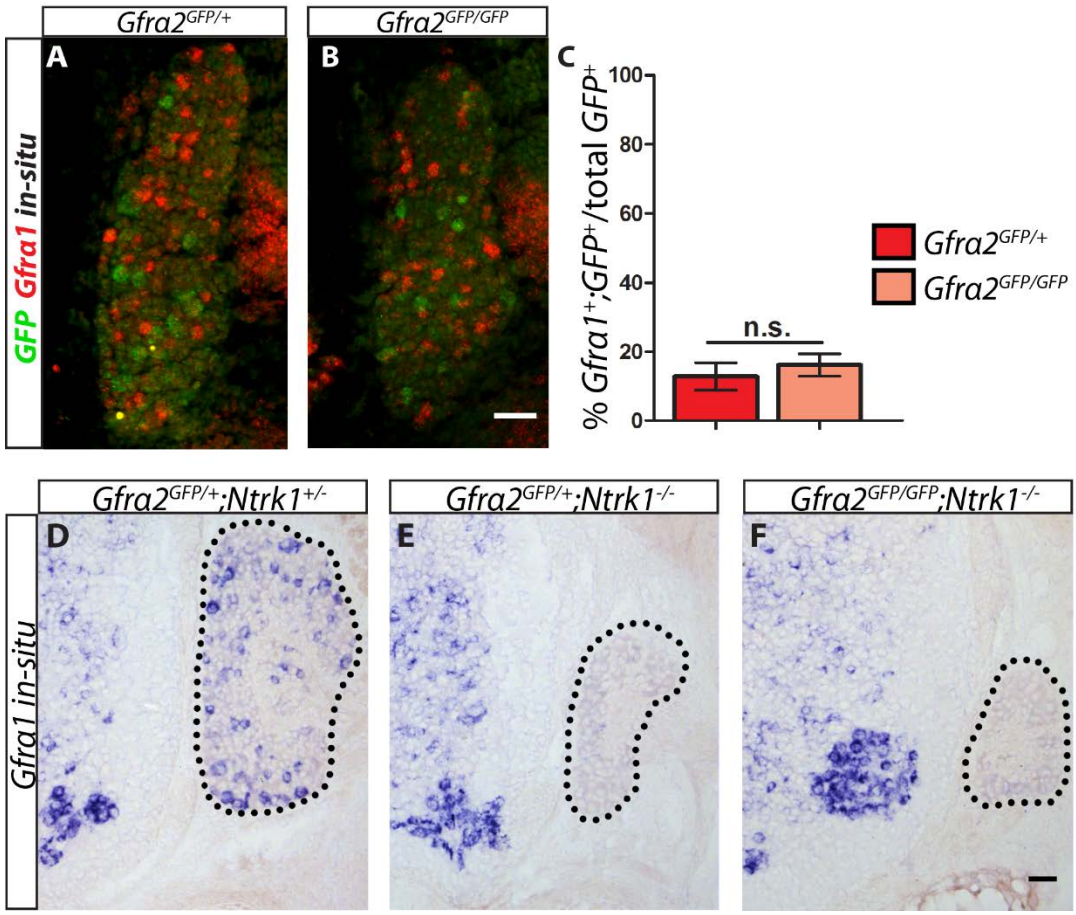

Figure 6: *Gfra1* is not upregulated in *Gfra2* null RA mechanoreceptors: (**A-B**) Double fluorescent *in situ* hybridization against *GFP* and *Gfra1* on E14.5 $Gfra2^{GFP/+}$ control (**A**) and $Gfra2^{GFP/GFP}$ null (**B**) DRG sections. (**C**) Quantification of percentage of GFP^+ neurons which co-express *Gfra1*. 12.81±3.92% of control GFP^+ neurons express *Gfra1*, and 16.17±3.31% of *Gfra2* null GFP^+ neurons express *Gfra1* (P=0.52). The comparable low number of DRG neurons co-expressing *GFP* and *Gfra1* in control and *Gfra2* nulls suggests that *Gfra1* normally is not expressed in most RA mechanoreceptors and that no upregulation of *Gfra1* occurs in *Gfra2* null RA mechanoreceptors. (**D-F)** *In situ* hybridization against *Gfra1* in P0 $Gfra2^{GFP/+};Ntrk1^{+/-}$ control (**D**), $Gfra2^{GFP/+};Ntrk1^{-/-}$ null (**E**), and $Gfra2^{GFP/GFP};Ntrk1^{-/-}$ double null **(F**) DRG and spinal cord sections. Black border outlines DRG. In control DRG sections, *Gfra1* is expressed in some DRG neurons. In $Gfra2^{GFP/+};Ntrk1^{-/-}$ null DRG sections, *Gfra1* transcript is not detected because the DRG neurons which normally express detectable levels of *Gfra1* don't survive in the absence of *Ntrk1*. In *Gfra2;Ntrk1* double null mice, no *Gfra1* expression is detected in DRG neurons as well, which further supports that upregulation of *Gfra1* doesn't occur in *Gfra2* null RA mechanoreceptors. Scale bars=50μm. Error bars represent SEM. n.s.=P>0.05

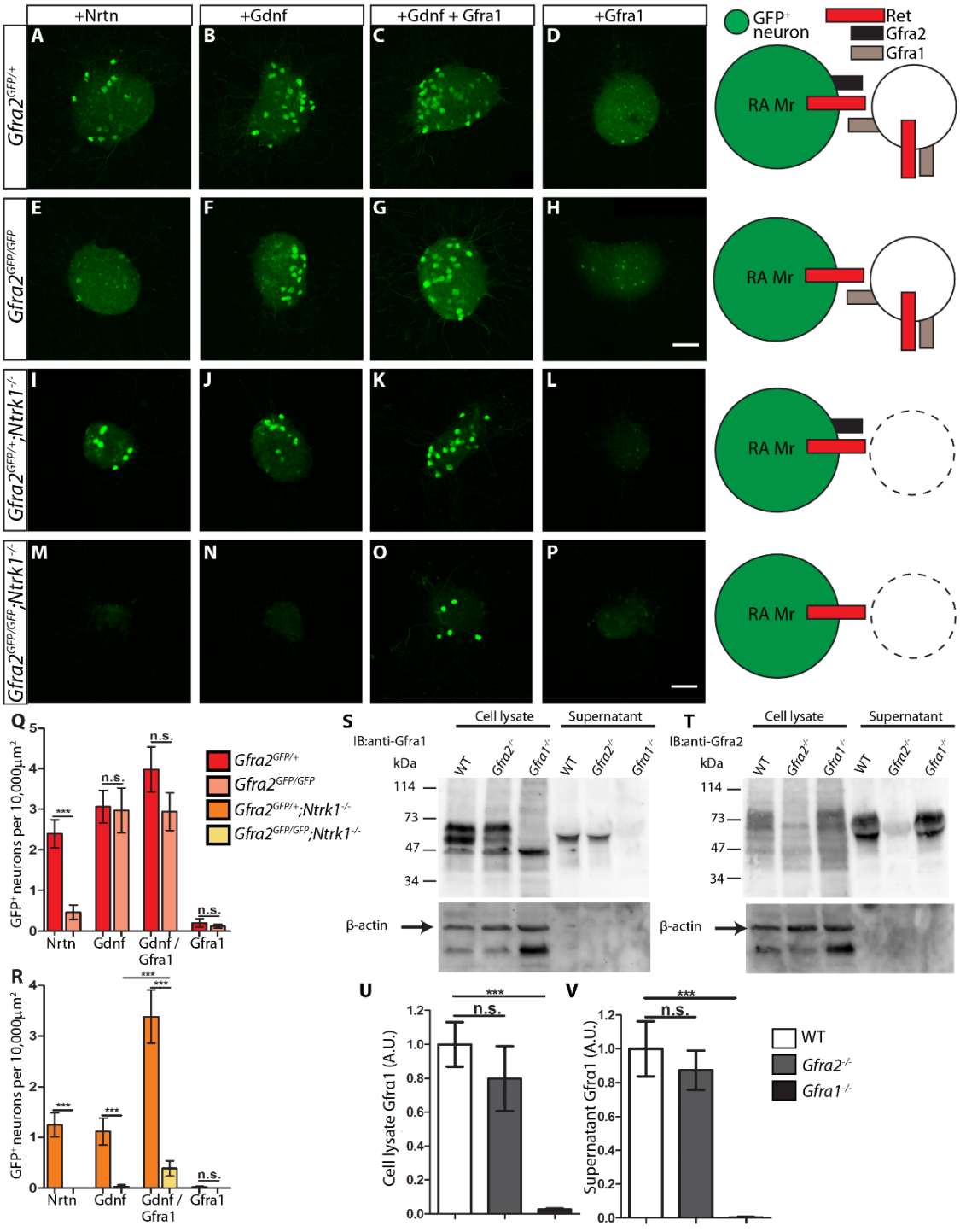

Figure 7: RA mechanoreceptors utilize GFRa1 produced by neighboring neurons to respond to GDNF: (**A-P**) DRG explants from *Gfra2*$^{GFP/+}$ control (**A-D**), *Gfra2*$^{GFP/GFP}$ null (**E-H**), *Gfra2*$^{GFP/+}$*;Ntrk1*$^{-/-}$ null (**I-L**), and *Gfra2*$^{GFP/GFP}$*;Ntrk1*$^{-/-}$ double null (**M-P**)

embryos grown for one day *in vitro* and stained with anti-GFP antibody. Explants were treated with NRTN (50ng/ml), GDNF (100ng/ml), GDNF (100ng/ml) plus GFRa1 (300ng/ml), or GFRa1 (300ng/ml), respectively. Schematic next to each genotype depicts the presence of RET and GFRas in each condition, and green color indicates cells detected by anti-GFP staining. (**Q**) Quantification of number of GFP^+ neurons per 10,000μm^2 of explant in *Gfra2*$^{GFP/+}$ control and *Gfra2*$^{GFP/GFP}$ null explants. GFP driven from the *Gfra2* locus indicates RET signaling activity. *Gfra2* control explants display many GFP^+ neurons upon NRTN, GDNF, and GDNF plus GFRa1 treatment, but do not respond to GFRa1 alone. *Gfra2* null explants lose their responsiveness to NRTN, but remain responsive to GDNF and GDNF plus GFRa1. (**R**) Quantification of number of GFP^+ neurons per 10,000μm^2 of explant in *Gfra2*$^{GFP/+}$*;Ntrk1*$^{-/-}$ null and *Gfra2*$^{GFP/GFP}$*;Ntrk1*$^{-/-}$ double null explants. In a *Ntrk1* null background, expression of *Gfra1* is lost in non-RA-mechanoreceptor DRG neurons. *Gfra2*$^{GFP/+}$*;Ntrk1*$^{-/-}$ null explants respond to NRTN, GDNF, and GDNF plus GFRa1. In this case, it is likely that GDNF activates RET signaling by interacting with GFRa2 (Jing et al., 1997; Rossi et al., 1999; Sanicola et al., 1997). In contrast, *Gfra2;Ntrk1* double null DRG explants show GFP expression upon treatment with a combination of GDNF and GFRa1, but completely lose their responsiveness to GDNF. These results indicate that *Gfra2* null RA mechanoreceptors do not express GFRa1 at a functional level and they depend on GFRa1 produced by neighboring $NTRK1^+$ neurons to respond to GDNF. See Figure 7-source data 2 for quantification. (**S-V**) Western blot analysis of cell lysates and concentrated supernatants from cultured dissociated DRG neurons of E18.5-P1 wild-type, *Gfra2* null, and *Gfra1* null mice. (**S**) The specificity of the anti-GFRa1 antibody was confirmed by the loss of a doublet at the predicted size of GFRa1 in *Gfra1* null cell lysates. GFRa1 was also detected in the supernatants of wild-type and *Gfra2* null cultures, but not *Gfra1* null cultures, indicating that GFRa1 is shed from the membrane of DRGs of both wild-type and *Gfra2* mutants. Note that the size of cleaved GFRa1 is slightly smaller than that tethered to cells, which is consistent with previous publication (Paratcha et al., 2001). Following detection of GFRa1, membranes were stripped and probed for β-actin, which served as a loading control and confirmation that the supernatant fraction was not contaminated with cells or cellular debris (lower panel). (**T**) The specificity of the anti-GFRa2 antibody was confirmed by the loss of a band ~75 kDa in *Gfra2* null cell lysates. The larger than predicted size of GFRa2 may be due to post-translational modifications. Two GFRa2 specific bands were also detected in the supernatants of wild-type and *Gfra1* null cultures, but not *Gfra2* null cultures, indicating that GFRa2 is also shed from DRG cell membranes. The size of cleaved GFRa2 is also smaller than that which is tethered to cells. (**U-V**) Densimetric quantification of anti-GFRa1 blots shows no significant change in the level of GFRa1 produced by cells (**U**) or released into the media (**V**), which suggests there is no compensation for the loss of GFRa2 through changes in the expression or release of GFRa1. See Figure 7-source data 3 for quantification. Error bars represent SEM. Scale bars=50μm. n.s.=P>0.05, ***=P<0.001. Source data are provided in Tables 7 and 8.

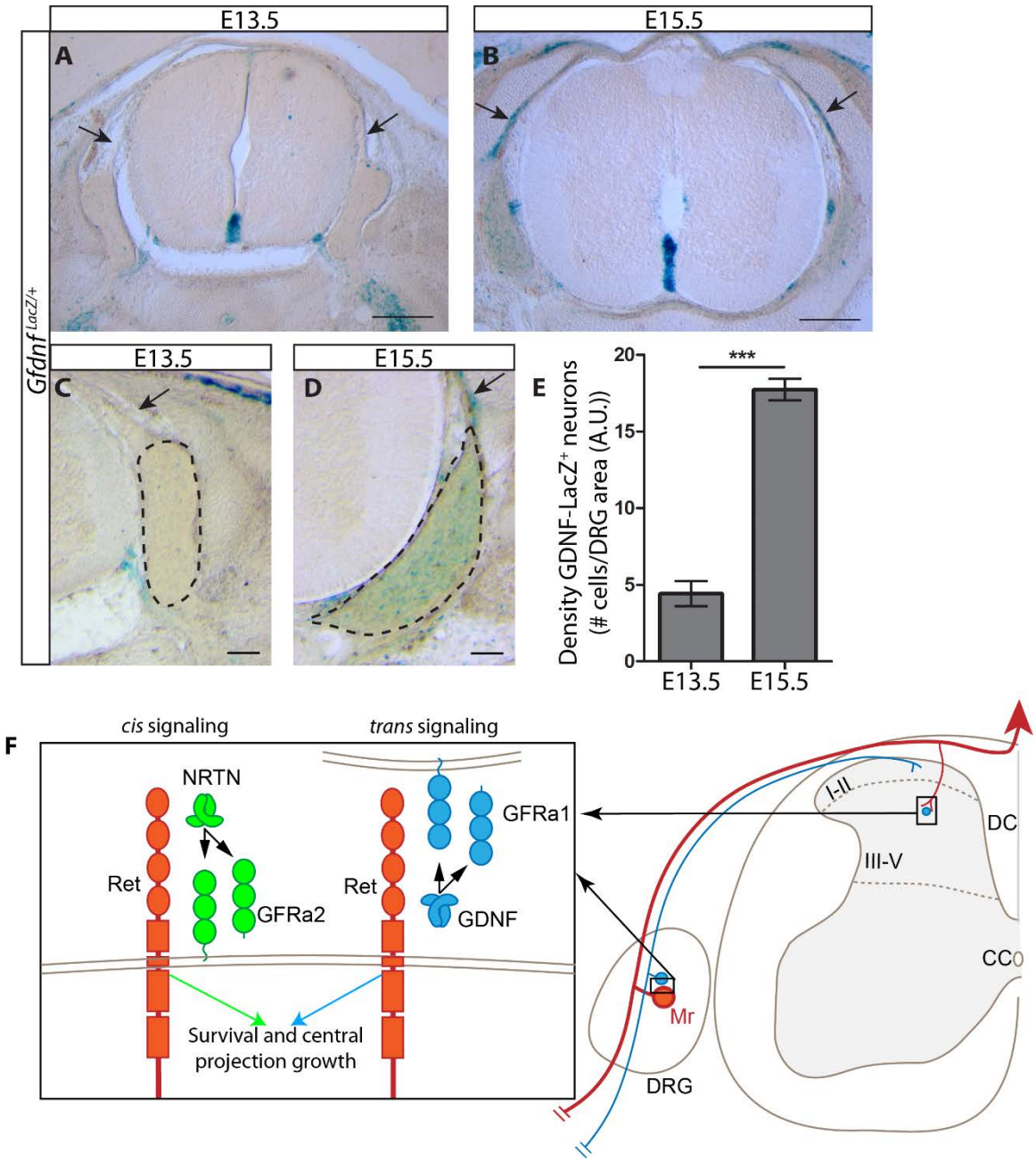

Figure 8: Dynamic expression of GDNF during development: (**A-D**) X-Gal staining of E13.5 (**A, C**) and E15.5 (**B, D**) *Gdnf*$^{LacZ/+}$ DRG and spinal cord sections (Also see Figure 8-figure supplement 1). Arrows indicate dorsal roots, which express *Gdnf* at E15.5, but not E13.5. (**E**) Quantification of LacZ^{+} cells per DRG section, normalized to DRG area, reveals a significant increase in the number of cells expressing *Gdnf* from E13.5 to E15.5. E13.5 embryos have 4.41±0.82 LacZ^{+} cells/unit area of DRG, E15.5 embryos have 17.73±0.70 LacZ^{+} cells/unit area of DRG (P<0.001). Error bars represent SEM. Scale bars=200μm (A-B), 100μm (C-D). ***=P<0.001 (**F**) Model of *cis* and *trans* signaling at cell bodies and central branches of RA mechanoreceptors. GFRa2 is

co-expressed with RET in RA mechanoreceptors and can activate RET in *cis.* GFRa2 can also be shed from the membrane and may activate RET in its soluble form. GFRa1 is expressed in neighboring DRG neurons, dorsal root entry zone cells, and dorsal SC cells. GFRa1 present at the membrane of these cells may directly contact the cell bodies or processes of RA mechanoreceptors to activate RET in *trans*. In addition, soluble GFRa1 released from these cells may also activate RET in RA mechanoreceptor in *trans*.

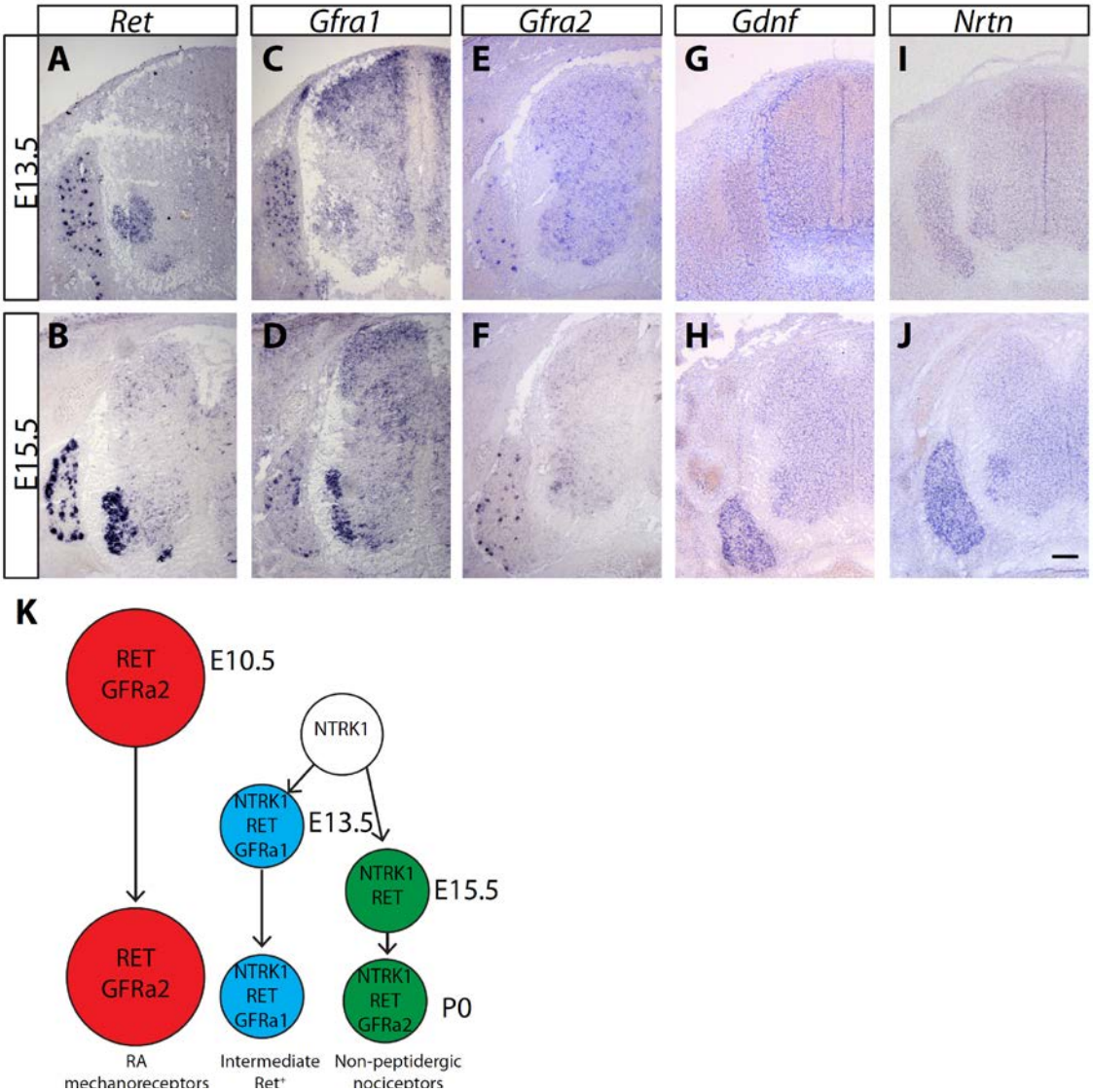

Figure S1: Expression of *Ret, Gfras,* and *Gfls* in developing spinal cord and DRG: (**A-J**) *In situ* hybridization of mouse spinal cord and DRG at E13.5 and E15.5 for *Ret* (**A-B)**, *Gfra1* (**C-D**), *Gfra2* (**E-F**), *Gdnf* (**G-H**), and *Nrtn* (**I-J**). *Ret* is expressed in DRG neurons and motor neurons at E13.5 and E15.5. *Ret* is also expressed in dSC from E15.5. *Gfra1* is expressed in DRG neurons, motor neurons, dorsal root entry zone, and dSC at both stages. Note that expression of *Gfra1* in the dorsal root entry zone and dSC is largely *Ret* independent. *Gfra2* is expressed in large diameter DRG neurons and in motor neurons. *Nrtn* and *Gdnf* are barely detected in DRG and SC at E13.5 and display increased expression in DRGs at E15.5. (**K**) Schematic of temporal expression of *Ret* and *Gfra* co-receptors in DRG neurons, which is adapted from previous studies (Luo et al., 2009; Luo et al., 2007; Molliver et al., 1997). RA mechanoreceptors (red cells) are early RET^+ DRG neurons, which begin to express *Ret* and *Gfra2* from E10.5 or earlier. All other RET^+ DRG neurons develop from $NTRK1^+$ precursors and depend on NTRK1 signaling for their expression of *Ret* and *Gfra*s. Intermediate RET^+ neurons (blue cells)

express *Ret* and *Gfra1* from E13.5. The late RET^{+} non-peptidergic nociceptors express *Ret* from E15.5, and begin to express a low level of *Gfra2* around P0. Scale bar= 100μm.

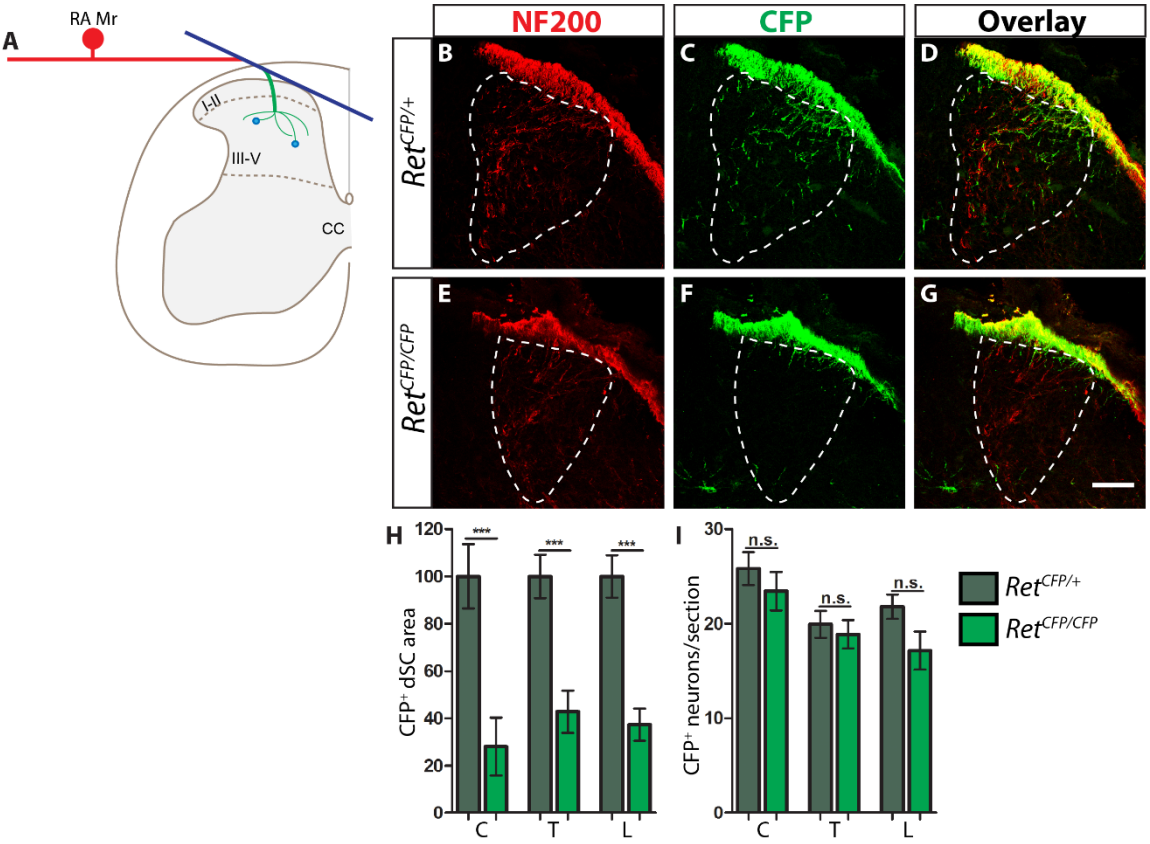

Figure S2: *Ret* is required for the growth of RA mechanosensory 3rd order central projections at E13.5: (**A**) Schematic of development of RA mechanosensory central projections. RA mechanoreceptors grow central and peripheral axons soon after neurogenesis, generating 1st order branches (red color). Upon reaching the dSC, the central axons bifurcate and send 2nd order longitudinal branches rostrally and caudally (blue color). Around E13.5, 3rd order interstitial projections (green color) from the longitudinal branches innervate layers III-V of the dSC and develop complex branching patterns. Synaptic connections between mechanoreceptors and dSC neurons (light blue dots) develop from E18.5. **(B-G)** Anti-NF200 and anti-GFP immunostaining of E13.5 $Ret^{CFP/+}$ (**B-D**) and $Ret^{CFP/CFP}$ (**E-G**) spinal cord. The dSC innervations of RA mechanosensory fibers are outlined by white dotted line. (**H**) Quantification of CFP^+ pixel number in the dSC, which is displayed as a percentage of pixel number relative to control. There is a significant decrease in CFP^+ axons innervating the SC in *Ret* mutants, suggesting that the initial growth of RA mechanosensory 3rd order projections depends on RET signaling. (**I**) Quantification of the number of CFP^+ neurons per DRG section. There is no significant change in the number of CFP^+ neurons per DRG section, suggesting that there is no cell death or downregualtion of CFP expression in E13.5 *Ret* null RA mechanoreceptors. Scale bar=50μm. C=Cervical, T=Thoracic, L=Lumbar. Error bars represent SEM. n.s.=P>0.05, ***=P<0.001. Source data are provided in Table 2.

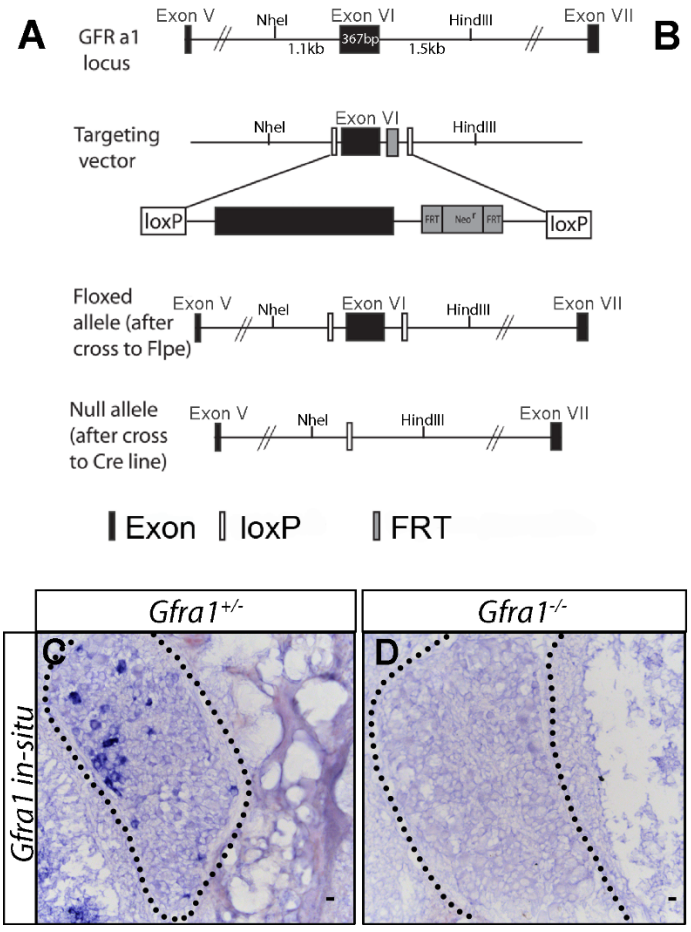

Figure S3: Generation of *Gfra1* conditional and null alleles: (**A**) Schematic of generation of *Gfra1* conditional and null alleles. See supplemental experimental procedures for additional details. (**B**) Predicted peptide sequence of the truncated GFRa1 protein after the excision of exon 6. Black letters represent amino acids which share identity with wild-type protein sequence. The loss of exon 6 causes a frame shift, leading to the inclusion of amino acids which do not match the wild-type sequence (blue letters). The frame shift also introduces a premature stop codon following amino acid 179. (**C-D**) *In situ* hybridization of *Gfra1* in P0 *Gfra1*$^{+/+}$ control (**C**) and *Gfra1*$^{-/-}$ null (**D**) DRG sections shows a complete loss of *Gfra1* transcript in *Gfra1* null tissue.

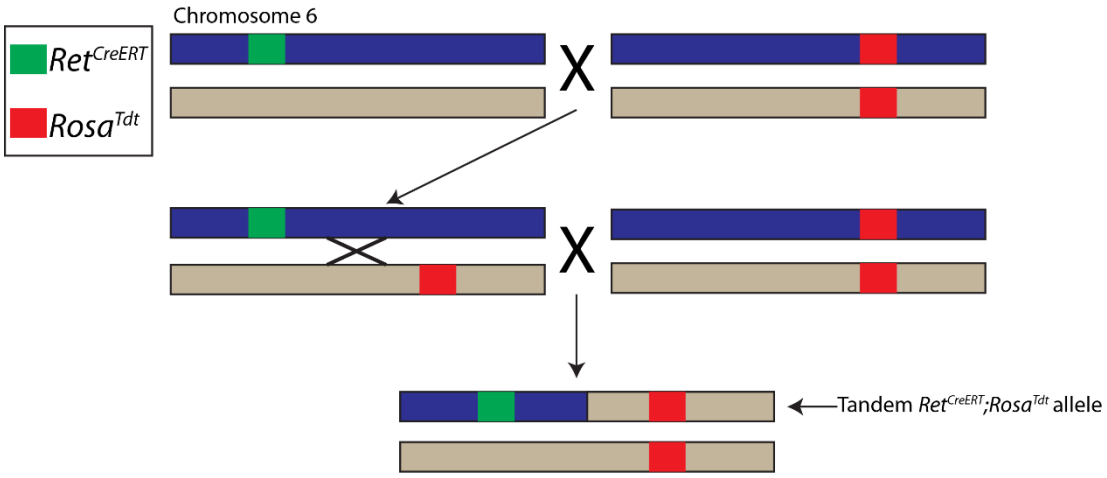

Figure S4: Generation of tandem *Ret*^{CreERT};*Rosa*^{Tdt} allele: The *Ret* and *Rosa* loci are located ~5 megabases apart on mouse Chromosome 6. *Ret*$^{CreERT/+}$ mice were crossed to *Rosa*$^{Tdt/Tdt}$ mice to generate *Ret*$^{CreERT/+}$;*Rosa*$^{Tdt/+}$ mice, which were crossed back to *Rosa*$^{Tdt/Tdt}$ mice. Occasionally, an interchromosomal recombination event occurred between the *Ret* and *Rosa* loci, which caused *Ret*^{CreERT} and *Rosa*^{Tdt} to be located on the same chromosome. Recombinants were identified by genotyping for the *Ret*^{CreERT} allele and the homozygous presence of the *Rosa*^{Tdt} allele. The chromosome containing both *Ret*^{CreERT} and *Rosa*^{Tdt} alleles is called the tandem *Ret*^{CreERT};*Rosa*^{Tdt} allele and maintained by mating with *Rosa*$^{Tdt/Tdt}$ mice.

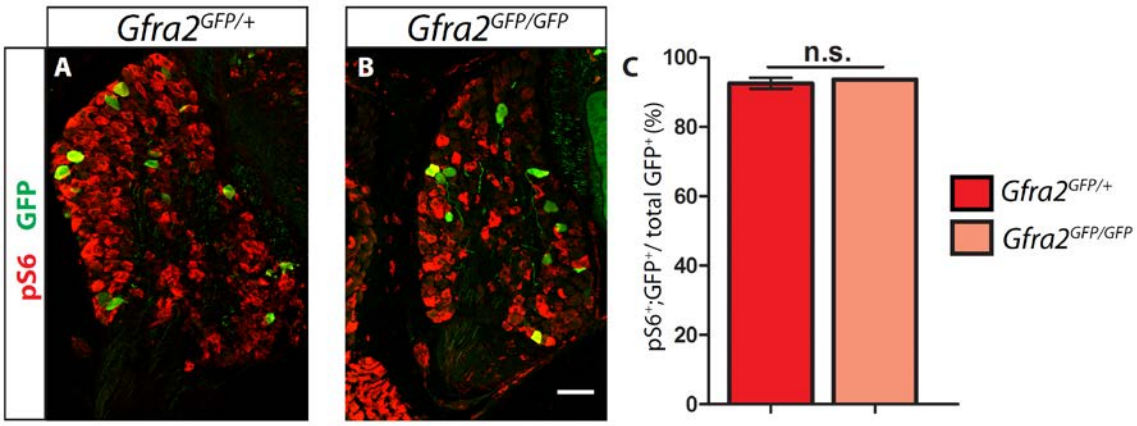

Figure S5: *Gfra2* null RA mechanoreceptors retain phospho-S6 expression: (**A-B**) Anti-GFP (green) and anti-phospho-S6 (red) staining of P0 *Gfra2*$^{GFP/+}$ control (**A**) and *Gfra2*$^{GFP/GFP}$ null (**B**) DRG sections. (**C**) Quantification of percentage of GFP^{+} neurons which express phospho-S6 shows no significant change in proportion of phospho-S6^{+} RA mechanoreceptors (92.53±1.55% of *Gfra2*$^{GFP/+}$ GFP^{+} DRG neurons express phospho-S6, 93.66±0.14% of *Gfra2*$^{GFPGFP+}$ GFP^{+} DRG neurons express phospho-S6, P=0.51). Therefore, active RTK signaling seems to still occur in *Gfra2* null RA mechanoreceptors.

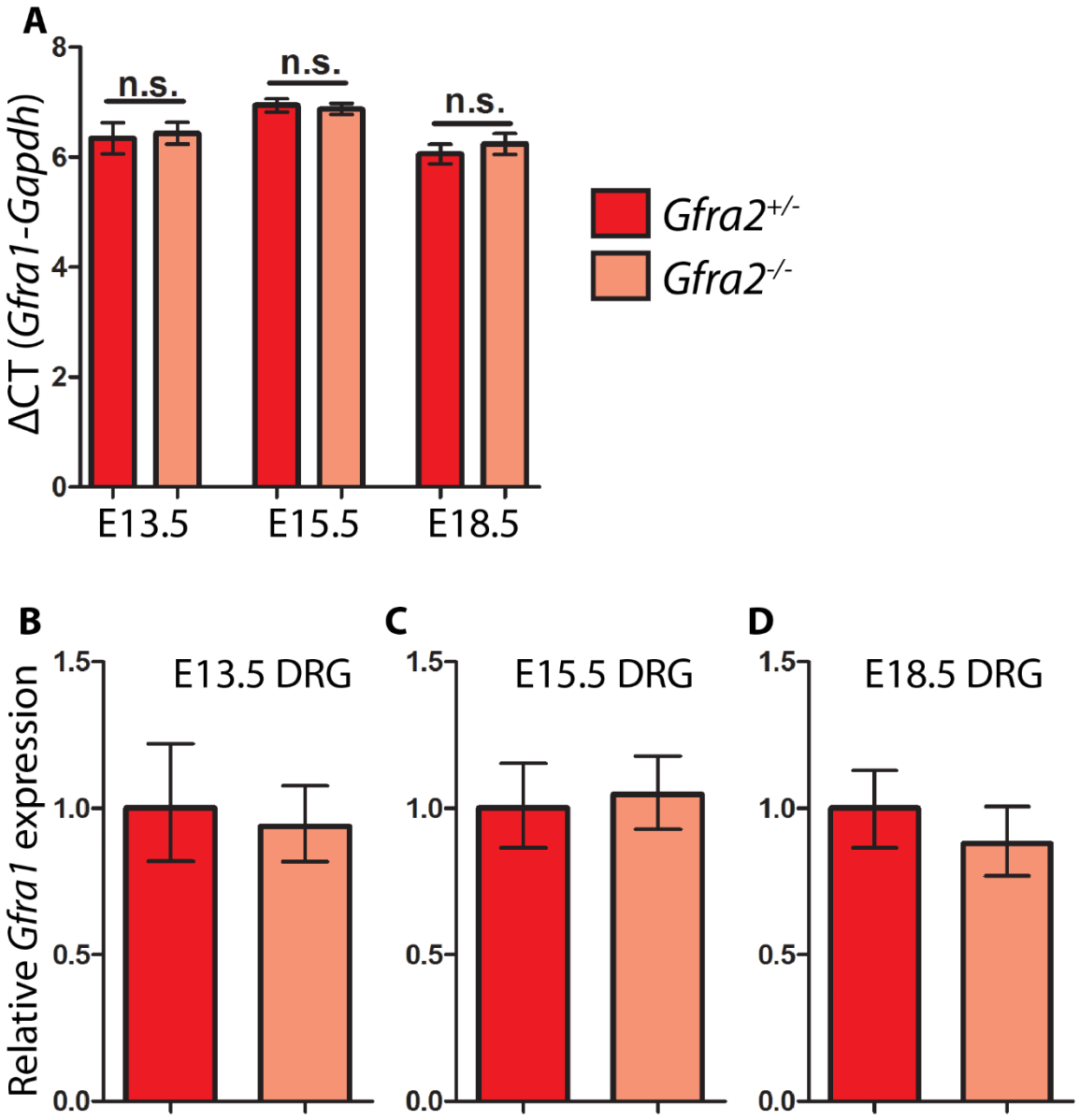

Figure S6: Quantitative RT-PCR of *Gfra1* in *Gfra2* null DRGs: QPCR for *Gfra1* from cDNAs generated from E13.5, E15.5, and E18.5 $Gfra2^{GFP/+}$ control and $Gfra2^{GFP/GFP}$ null DRGs. (**A**) ΔCT values (cycles to reach threshold for *Gfra1* minus cycles to reach threshold for *Gapdh*, a housekeeping gene) are not significantly different between control and mutant DRGs at E13.5, E15.5, or E18.5, suggesting that transcription of *Gfra1* is not changed in *Gfra2* mutants. Error bars represent standard deviation, n.s.=P>0.05. (**B-D**) Relative quantification of *Gfra1* expression levels at E13.5 (**B**), E15.5 (**C**), and E18.5 (**D**) calculated by $2^{-\Delta\Delta CT}$. Error bars represent range of expression based on $2^{-\Delta\Delta CT}$ calculated ± the standard deviation of CT. Source data are provided in Table 5.

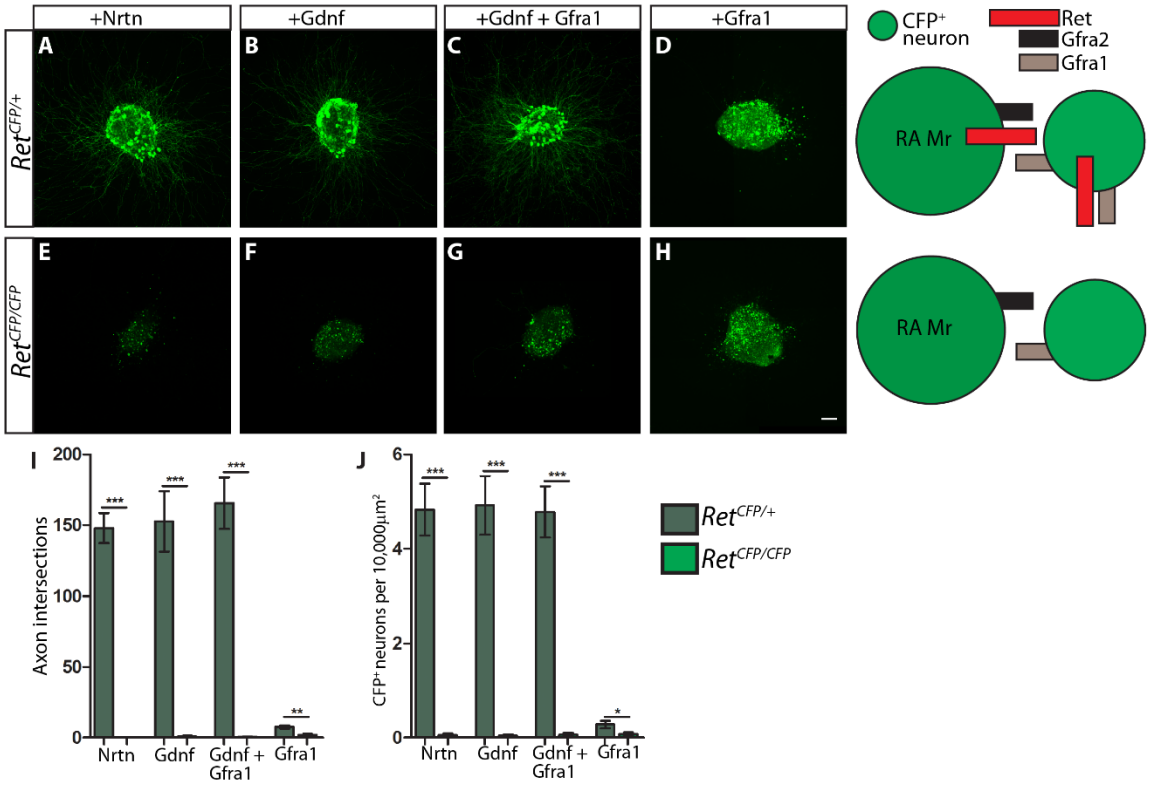

Figure S7: *Ret*^{CFP} null DRG explants lose responsiveness to GFLs: (**A-H**) DRG explants from E14.5 *Ret*$^{CFP/+}$ control (**A-D**) and *Ret*$^{CFP/CFP}$ null (**E-H**) embryos grown for one day *in vitro* and stained with anti-GFP antibody. Explants were treated with NRTN (50ng/ml), GDNF (100ng/ml), GDNF (100ng/ml) plus GFRa1 (300ng/ml), or GFRa1 (300ng/ml), respectively. Schematic next to each genotype depicts the presence of RET and GFRas in each condition, and green color indicates cells detected by anti-GFP staining. **(I**) Quantification of number of axonal intersections at a 200µm distance from the edge each explant for *Ret* control and null explants. CFP^{+} neurons in control explants grow numerous axons upon treatment with NRTN, GDNF, or GDNF plus GFRa1, but not in response to GFRa1 alone. *Ret* null explants do not grow axons upon treatment with GFLs. (**J**) Quantification of number of CFP^{+} neurons per 10,000µm^2 of explant in *Ret* control and null explants. Since RET signaling positively regulates *Ret* expression, CFP driven from the *Ret* locus serves as a readout of RET signaling activity as well. *Ret* control explants have many CFP^{+} neurons upon NRTN, GDNF, and GDNF plus GFRa1 treatment, but *Ret* null explants do not respond to treatment with GFLs. Scale= 50µm. Source data are provided in Tables 6 and 7.

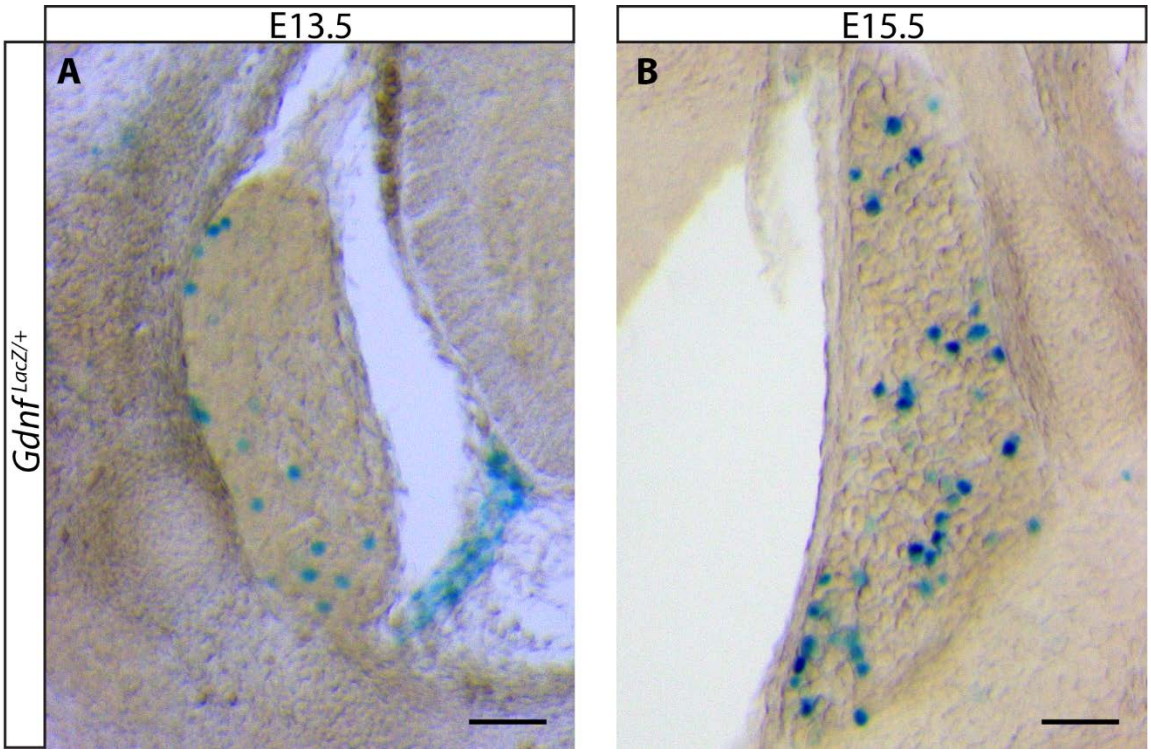

Figure S8: *Gdnf*^{LacZ} expression in DRGs at E13.5 and E15.5. DRG sections with large, strongly LacZ^{+} neurons were observed at both E13.5 (**A**) and E15.5 (**B**). Note that there are many more LacZ^{+} DRG neurons at E15.5. Sections with such cells were observed in all embryos and were usually found in distal anterior and distal posterior segments. Sections with smaller reactive cells, as shown in Figure 6, were observed more frequently. Scale= 100μm

Table 1: VGLUT1 dorsal spinal cord staining and RA mechanoreceptor number in P7 *Gfrα2* mutants

Control genotype	VGluT1$^+$ pixels (% of control)	Mutant genotype	VGluT1$^+$ pixels (% of control)	P-value
Gfrα2$^{GFP/+}$	100±9.12	*Gfrα2*$^{GFP/GFP}$	96.31±8.97	0.96

#Thoracic SC only

Control genotype	GFP$^+$;NF200$^+$ neurons/ DRG section	Mutant genotype	GFP$^+$;NF200$^+$ neurons/ DRG section	P-value
Gfrα2$^{GFP/+}$	7.13±0.48	*Gfrα2*$^{GFP/GFP}$	6.50±0.41	0.34

#L4/L5 DRGs only

Table 2: RA mechanoreceptor central projections and cell number in E13.5 *Ret, Gfrα1, Gfrα2,* and *Nrtn* mutants

SC Level	Control genotype	GFP$^+$ pixels (% of control)	Mutant genotype	GFP$^+$ pixels (% of control)	P-value
Cervical	*Ret$^{CFP/+}$*	100±13.61	*Ret$^{CFP/CFP}$*	28.12±12.25	<0.0001
Thoracic	*Ret$^{CFP/+}$*	100±9.18	*Ret$^{CFP/CFP}$*	42.88±8.93	0.0001
Lumbar	*Ret$^{CFP/+}$*	100±8.96	*Ret$^{CFP/CFP}$*	37.78±6.84	<0.0001
Cervical	*Gfrα1$^{+/-}$; Ret$^{CFP/+}$*	100±6.85	*Gfrα1$^{-/-}$;Ret$^{CFP/+}$* *	143.33±15.92	0.02
Thoracic	*Gfrα1$^{+/-}$; Ret$^{CFP/+}$*	100±9.68	*Gfrα1$^{-/-}$;Ret$^{CFP/+}$* *	134.65±14.14	0.05
Lumbar	*Gfrα1$^{+/-}$; Ret$^{CFP/+}$*	100±9.76	*Gfrα1$^{-/-}$;Ret$^{CFP/+}$* *	128.01±11.31	0.07
Cervical	*Gfrα2$^{+/-}$;Ret$^{CFP/+}$*	100±13.42	*Gfrα2$^{-/-}$;Ret$^{CFP/+}$*	12.78±1.86	<0.0001
Thoracic	*Gfrα2$^{+/-}$;Ret$^{CFP/+}$*	100±16.95	*Gfrα2$^{-/-}$;Ret$^{CFP/+}$*	9.50±1.44	<0.0001
Lumbar	*Gfrα2$^{+/-}$;Ret$^{CFP/+}$*	100±14.52	*Gfrα2$^{-/-}$;Ret$^{CFP/+}$*	5.57±0.77	<0.0001
Cervical	*Nrtn$^{+/-}$;Ret$^{CFP/+}$*	100±13.43	*Nrtn$^{-/-}$;Ret$^{CFP/+}$*	47.95±8.23	0.0002
Thoracic	*Nrtn$^{+/-}$;Ret$^{CFP/+}$*	100±13.64	*Nrtn$^{-/-}$;Ret$^{CFP/+}$*	26.47±3.84	<0.0001
Lumbar	*Nrtn$^{+/-}$;Ret$^{CFP/+}$*	100±14.12	*Nrtn$^{-/-}$;Ret$^{CFP/+}$*	43.47±6.49	0.002

*The slight increase of CFP$^+$ signal in *Gfrα1* mutant mice could be due to the precocious appearance of *Ret$^+$* dSC cells, which are also stained by anti-GFP antibody.

DRG Level	Control genotype	GFP$^+$ neurons per DRG section	Mutant genotype	GFP$^+$ neurons per DRG section	P-value
Cervical	*Ret$^{CFP/+}$*	25.81±1.74	*Ret$^{CFP/CFP}$*	23.44±2.03	0.38
Thoracic	*Ret$^{CFP/+}$*	19.94±1.42	*Ret$^{CFP/CFP}$*	18.88±1.50	0.61
Lumbar	*Ret$^{CFP/+}$*	21.81±1.29	*Ret$^{CFP/CFP}$*	17.16±2.01	0.06
Cervical	*Gfrα1$^{+/-}$;Ret$^{CFP/+}$*	24.89±1.82	*Gfrα1$^{-/-}$;Ret$^{CFP/+}$*	23.38±3.51	0.39
Thoracic	*Gfrα1$^{+/-}$;Ret$^{CFP/+}$*	19.43±2.02	*Gfrα1$^{-/-}$;Ret$^{CFP/+}$*	19.00±1.56	0.87
Lumbar	*Gfrα1$^{+/-}$;Ret$^{CFP/+}$*	20.27±1.24	*Gfrα1$^{-/-}$;Ret$^{CFP/+}$*	23.17±1.20	0.11
Cervical	*Gfrα2$^{+/-}$;Ret$^{CFP/+}$*	40.38±2.97	*Gfrα2$^{-/-}$;Ret$^{CFP/+}$*	36.57±3.53	0.41
Thoracic	*Gfrα2$^{+/-}$;Ret$^{CFP/+}$*	30.94±1.21	*Gfrα2$^{-/-}$;Ret$^{CFP/+}$*	27.67±1.69	0.13
Lumbar	*Gfrα2$^{+/-}$;Ret$^{CFP/+}$*	28.29±1.39	*Gfrα2$^{-/-}$;Ret$^{CFP/+}$*	24.59±1.53	0.09
Cervical	*Nrtn$^{+/-}$;Ret$^{CFP/+}$*	42.93±3.00	*Nrtn$^{-/-}$;Ret$^{CFP/+}$*	44.50±3.22	0.72
Thoracic	*Nrtn$^{+/-}$;Ret$^{CFP/+}$*	30.38±1.14	*Nrtn$^{-/-}$;Ret$^{CFP/+}$*	28.56±1.75	0.39
Lumbar	*Nrtn$^{+/-}$;Ret$^{CFP/+}$*	27.31±1.29	*Nrtn$^{-/-}$;Ret$^{CFP/+}$*	25.00±1.45	0.24

Table 3: RA mechanoreceptor central projections and cell number in E15.5 *Gfrα2* mutants

Control genotype	Tdt^+ dSC pixels (% of control)	Mutant genotype	Tdt^+ dSC pixels (% of control)	P-value
$Gfr\alpha2^{GFP/+}$; $Ret^{CreERT/+}$;$Rosa^{Tdt}$	100±8.80	$Gfr\alpha2^{GFP/GFP}$; $Ret^{CreERT/+}$;$Rosa^{Tdt}$	55.13±2.82	<0.0001

Thoracic spinal cord only

Control genotype	Tdt^+ neurons per DRG section (% of control)	Mutant genotype	Tdt^+ neurons per DRG section (% of control)	P-value
$Gfr\alpha2^{GFP/+}$; $Ret^{CreERT/+}$;$Rosa^{Tdt}$	100±6.32	$Gfr\alpha2^{GFP/GFP}$; $Ret^{CreERT/+}$;$Rosa^{Tdt}$	79.52±8.39	0.06

#L4/L5 DRGs only

Table 4: RA mechanoreceptor central projections and cell number in E18.5 *Ret, Gfrα2, Gfrα1,* and *Gfrα1;Gfrα2* mutants

Control genotype	Tdt^+ dSC pixels (% of control)	Mutant genotype	Tdt^+ dSC pixels (% of control)	P-value
$Ret^{CreERT/+}$; $Rosa^{Tdt}$	100±9.82	$Ret^{CreERT/CreERT}$; $Rosa^{Tdt}$	35.86±4.97	<0.0001
$Gfrα2^{GFP/+}$; $Ret^{CreERT/+}$;$Rosa^{Tdt}$	100±2.53	$Gfrα2^{GFP/GFP}$; $Ret^{CreERT/+}$;$Rosa^{Tdt}$	86.34±4.48	0.01
$Gfrα1^{+/-}$; $Ret^{CreERT/+}$;$Rosa^{Tdt}$	100±2.14	$Gfrα1^{-/-}$; $Ret^{CreERT/+}$;$Rosa^{Tdt}$	80.94±10.32	0.09
$Gfrα1^{+/-}$; $Gfrα2^{GFP/+}$; $Ret^{CreERT/+}$;$Rosa^{Tdt}$	100±4.49	$Gfrα1^{-/-}$; $Gfrα2^{GFP/GFP}$; $Ret^{CreERT/+}$;$Rosa^{Tdt}$	27.25±2.09	<0.0001

Thoracic spinal cord only

Control genotype	Tdt^+ neurons per DRG (% of control)	Mutant genotype	Tdt^+ neurons per DRG (% of control)	P-value
$Ret^{CreERT/+}$;$Rosa^{Tdt}$	100±8.71	$Ret^{CreERT/CreERT}$;$Rosa^{Tdt}$	52.52±7.76	0.0007
$Gfrα2^{GFP/+}$; $Ret^{CreERT/+}$;$Rosa^{Tdt}$	100±5.10	$Gfrα2^{GFP/GFP}$; $Ret^{CreERT/+}$;$Rosa^{Tdt}$	84.01±5.16	0.04
$Gfrα1^{+/-}$; $Ret^{CreERT/+}$;$Rosa^{Tdt}$	100±6.72	$Gfrα1^{-/-}$; $Ret^{CreERT/+}$;$Rosa^{Tdt}$	82.30±12.91	0.19
$Gfrα1^{+/-}$; $Gfrα2^{GFP/+}$; $Ret^{CreERT/+}$;$Rosa^{Tdt}$	100±8.61	$Gfrα1^{-/-}$; $Gfrα2^{GFP/GFP}$; $Ret^{CreERT/+}$;$Rosa^{Tdt}$	38.17±2.65	0.0002

#L4/L5 DRGs only

Table 5: QPCR of *Gfrα1* in embryonic *Gfrα2* null DRGs

Age	Genotype	ΔCT (*Gfrα1-Gapdh)*	ΔCT S.D.	Relative expression normalized to E13.5 *Gfrα2*$^{-/-}$ ($2^{-\Delta\Delta CT}$)
E13.5	*Gfrα2*$^{+/-}$	6.3449	0.2873	0.819-1.220
E13.5	*Gfrα2*$^{-/-}$	6.4359	0.1977	0.819-1.077
E15.5	*Gfrα2*$^{+/-}$	6.9424	0.2094	0.572-0.764
E15.5	*Gfrα2*$^{-/-}$	6.8770	0.1723	0.614-0.779
E18.5	*Gfrα2*$^{+/-}$	6.0577	0.1759	1.080-1.379
E18.5	*Gfrα2*$^{-/-}$	6.2467	0.1935	0.939-1.228

Population 1	Population 2	P-value
E13.5 *Gfrα2*$^{+/-}$	E13.5 *Gfrα2*$^{-/-}$	0.675
E15.5 *Gfrα2*$^{+/-}$	E15.5 *Gfrα2*$^{-/-}$	0.698
E18.5 *Gfrα2*$^{+/-}$	E18.5 *Gfrα2*$^{-/-}$	0.288

Table 6: Quantification of axonal growth in *Ret* mutant DRG explants

Treatment	Control genotype	Axon intersections at 200μm	Mutant genotype	Axon intersections at 200μm	p-value
NRTN	$Ret^{CFP/+}$	147.833±10.579 (n=6)	$Ret^{CFP/CFP}$	0 (n=8)	<0.0001
GDNF	$Ret^{CFP/+}$	152.500±21.165 (n=8)	$Ret^{CFP/CFP}$	0.875±0.543 (n=8)	<0.0001
GDNF+ GFRα1	$Ret^{CFP/+}$	165.375±18.029 (n=8)	$Ret^{CFP/CFP}$	0.375±0.246 (n=8)	<0.0001
GFRα1	$Ret^{CFP/+}$	7.428±1.104 (n=7)	$Ret^{CFP/CFP}$	1.875±0.695 (n=8)	0.0002

Table 7: GFP$^+$ neuron number in *Gfrα2* null and *Gfrα2;TrkA* double null explants

Treatment	Control genotype	GFP$^+$ neurons/ 10,000μm^2	Mutant genotype	GFP$^+$ neurons/ 10,000μm^2	p-value
NRTN	*Ret$^{CFP/+}$*	4.825±0.545 (n=6)	*Ret$^{CFP/CFP}$*	0.052±0.036 (n=8)	<0.0001
GDNF	*Ret$^{CFP/+}$*	4.917±0.619 (n=8)	*Ret$^{CFP/CFP}$*	0.045±0.022 (n=8)	<0.0001
GDNF + GFRα1	*Ret$^{CFP/+}$*	4.776±0.539 (n=8)	*Ret$^{CFP/CFP}$*	0.062±0.041 (n=8)	<0.0001
GFRα1	*Ret$^{CFP/+}$*	0.278±0.077 (n=7)	*Ret$^{CFP/CFP}$*	0.075±0.038 (n=8)	0.0245
NRTN	*Gfrα2$^{GFP/+}$*	2.394±0.344 (n=8)	*Gfrα2$^{GFP/GFP}$*	0.464±0.176 (n=7)	<0.0001
GDNF	*Gfrα2$^{GFP/+}$*	3.061±0.401 (n=8)	*Gfrα2$^{GFP/GFP}$*	2.968±0.554 (n=7)	0.7513
GDNF + GFRα1	*Gfrα2$^{GFP/+}$*	3.982±0.559 (n=7)	*Gfrα2$^{GFP/GFP}$*	2.941±0.461 (n=6)	0.1099
GFRα1	*Gfrα2$^{GFP/+}$*	0.201±0.103 (n=6)	*Gfrα2$^{GFP/GFP}$*	0.122±0.052 (n=6)	0.3635
NRTN	*Gfrα2$^{GFP/+}$; TrkA$^{-/-}$*	1.247±0.237 (n=12)	*Gfrα2$^{GFP/GFP}$; TrkA$^{-/-}$*	0 (n=6)	<0.0001
GDNF	*Gfrα2$^{GFP/+}$; TrkA$^{-/-}$*	1.113±0.268 (n=10)	*Gfrα2$^{GFP/GFP}$; TrkA$^{-/-}$*	0.033±0.031 (n=10)	<0.0001
GDNF + GFRα1	*Gfrα2$^{GFP/+}$; TrkA$^{-/-}$*	3.381±0.522 (n=11)	*Gfrα2$^{GFP/GFP}$; TrkA$^{-/-}$*	0.389±0.144 (n=8)	<0.0001
GFRα1	*Gfrα2$^{GFP/+}$; TrkA$^{-/-}$*	0.020±0.019 (n=9)	*Gfrα2$^{GFP/GFP}$; TrkA$^{-/-}$*	0 (n=6)	<0.0001

Genotype	Treatment	GFP$^+$ neurons/10,000μm^2	Treatment	GFP$^+$ neurons/10,000μm^2	p-value
Gfrα2$^{GFP/GFP}$; TrkA$^{-/-}$	GDNF + GFRα1	0.389±0.144 (n=10)	GDNF	0.033±0.031 (n=8)	0.0011

Table 8: Densimetric measurements of GFRα1 in DRG cell extracts and supernatants

Cell lysates

Genotype	**Band density (A.U.)**	**P-value (relative to wild type)**
Wild type	1±0.131	N/A
Gfrα2$^{-/-}$	0.798±0.192	0.434
Gfrα1$^{-/-}$	0.024±0.007	0.002

Supernatants

Genotype	**Band density (A.U.)**	**P-value (relative to wild type)**
Wild type	1±0.162	N/A
Gfrα2$^{-/-}$	0.873±0.116	0.556
Gfrα1$^{-/-}$	0.005±0.003	0.004

A.U.=arbitrary units

CHAPTER 3

A RET-ER81-Neuregulin1 signaling pathway drives the development of Pacinian corpuscles

Michael S. Fleming wrote this chapter and performed all experiments.

ABSTRACT

Rapidly adapting mechanoreceptors are somatosensory neurons responsible for the detection of light touch. All rapidly adapting mechanoreceptors are molecularly defined by the early embryonic expression of the receptor tyrosine kinase RET. However, in *Ret* mutants, only one type of rapidly adapting mechanoreceptor end organ, the Pacinian corpuscle, does not form. Pacinian corpuscles are also not formed in mice lacking the ETS transcription factor *Er81*. Pacinian corpuscles are composed of non-myelinating Schwann cells and are innervated by myelinated axons. A key mediator of axon-Schwann cell interactions is Neuregulin-1 (NRG1). The NRG1-CRD isoform is important for axonal communication with myelinating Schwann cells. In contrast, the NRG1-Ig isoform is required for the development of another somatosensory end organ, muscle spindles. Here, we show that *Ret* is required for the maintenance of *Er81* expression in Pacinian corpuscle innervating neurons, and that neural *Er81* expression is required for corpuscle formation. Furthermore, we find that the primary deficit in Pacinian corpuscle formation in *Er81* mutants is deficient axon-Schwann cell interactions, and that the expression of *Nrg1-Ig* is decreased in somatosensory neurons in *Er81* null mice. Finally, mechanosensory neuron specific *Nrg1* mutants lack Pacinian corpuscles, suggesting a RET-ER81-Nrg1 signaling pathway drives Pacinian corpuscle development.

INTRODUCTION

The mammalian somatosensory system is exquisitely tuned to detect and differentiate between diverse stimuli, such as pain, temperature, itch, and light touch. The primary somatosensory neurons which detect these stimuli have unique morphological and molecular properties and distinct developmental histories. Over the past few decades, great progress has been made in describing the intrinsic and extrinsic signaling pathways important for defining and driving the development of broad classes of somatosensory neurons, such as peptidergic and nonpeptidergic nociceptors, proprioceptors, and mechanoreceptors (Lallemend and Ernfors, 2012; Marmigere and Carroll, 2014). However, the molecular and cellular mechanisms which further differentiate these broad classes of neurons remain unclear.

The rapidly adapting (RA) low-threshold mechanoreceptors are one such broad class of somatosensory neurons. RA mechanoreceptors respond to light touch. RA mechanoreceptors have a unique molecular profile and developmental history. They are large diameter dorsal root ganglion (DRG) neurons which begin to express *Ret* and the RET co-receptor GFRα2 around E10.5, which is many days earlier than any other class of DRG neurons begin to express *Ret* (Bourane et al., 2009; Honma et al., 2010; Luo et al., 2009). RA mechanoreceptors can be further differentiated into three distinct classes based on the morphology and anatomical location of their end organs and the class of stimuli they are tuned to detect (Fleming and Luo, 2013). Lanceolate ending RA

mechanoreceptors innervate hair follicles and respond to deflection of the hair. Meissner's corpuscles are located in upper layers of the dermis and respond to low-frequency vibration. Pacinian corpuscles are present in deeper tissue, and respond to high frequency vibration. Despite these large functional and morphological differences between these classes of RA mechanoreceptors, how they are differentiated at the molecular level remains unknown.

Pacinian corpuscles are mechanosensory end organs which are present in the interosseous membrane surrounding the fibula and ulna in mice (Zelena, 1978). They are innervated by a single myelinated RA mechanosensory axon. Upon entering the corpuscle, the axon loses its contact with myelinating Schwann cells, and directly contacts the non-myelinating Schwann cells which comprise the inner core of the corpuscle (Pease and Quilliam, 1957). The inner core is surrounded by many layers of perineural epithelial cells (Zelena, 1994). In neural crest specific *Ret* mutant mice, Pacinian corpuscles do not form whereas Meissner's corpuscles and lanceolate endings are still present (Luo et al., 2009). Pacinian corpuscles are also absent in mice lacking the ETS transcription factor *Er81* (Sedy et al., 2006). In the peripheral nervous system, *Er81* is best known for its role in controlling the central and peripheral projections of proprioceptors, where it acts downstream of TrkC/NT3 neurotrophic signaling (Arber et al., 2000; Patel et al., 2003). Since *Er81* is expressed in corpuscle-forming Schwann cells, the loss-of-Pacinian corpuscle phenotype was previously attributed to the loss of *Er81* function in Schwann cells (Sedy et al., 2006). However, ~30% of $Er81^{+}$ DRG neurons are not proprioceptors

at E13.5 (Arber et al., 2000), raising the possibility that *Er81* may be expressed and function in Pacinian corpuscle neurons.

Here, we show that *Er81* is required in neurons for the development of Pacinian corpuscles. Furthermore, the maintenance of *Er81* expression in RA mechanoreceptors depends on RET signaling. Through morphological characterization of developing Pacinian corpuscles, we find that *Er81* mediates communication between axons and nonmyelinating Schwann cells of Pacinian corpuscles, likely via the regulation of *Neuregulin1-Ig*, but not interaction with myelinating Schwann cells.

RESULTS

Er81 is required for the development of Pacinian corpuscles, but not Meissner's corpuscles

Pacinian corpuscles and their innervating axons are absent in *Er81* mutant mice around birth (Sedy et al., 2006). The lack of Pacinian corpuscles in *Er81* mutants was previously attributed to a Schwann cell deficit, due to the expression of *Er81* in the inner core nonmyelinating Schwann cells of Pacinian corpuscles. Meissner's corpuscles are another RA mechanoreceptor end organ composed of nonmyelinating Schwann cells (Fleming and Luo, 2013; Zelena, 1994), however it is unclear whether they require *Er81* for their development. Using an $Er81^{LacZ}$ reporter allele (Arber et al., 2000), we confirmed that *Er81* is expressed in Pacinian corpuscle inner core Schwann cells (Figure 1A)(Sedy et al.,

2006). Sections of mouse glabrous skin revealed that *Er81* is also expressed in the nonmyelinating Schwann cells of the lamella comprising the Meissner's corpuscle inner core (Figure 1B).

Due to the expression of *Er81* in Meissner's corpuscle Schwann cells, we asked whether *Er81* is required for Meissner corpuscle development. We examined glabrous skin sections from postnatal day 21 (P21) control and *Er81* null mice and found $S100^{+}$ corpuscles were present in the mutant dermal papillae (Figure 1C-D). Therefore, like *Ret*, *Er81* is required for the development of Pacinian corpuscles but not Meissner's corpuscles. Due to the lack of a Meissner's corpuscle phenotype despite the expression of *Er81* in the corpuscle Schwann cells, it's possible that *Er81* may act in tissue other than Schwann cells to promote Pacinian corpuscle end organ formation.

_Er81_ is expressed in Pacinian corpuscle innervating neurons

Although the function of ER81 in proprioceptive DRG neurons has been established, approximately 30% of $ER81^{+}$ DRG neurons are not proprioceptors and have an unknown identity. We hypothesized that a portion of these $Er81^{+}$ non-proprioceptors may be Pacinian corpuscle innervating neurons. We first asked whether ER81 is expressed in limb innervating RA mechanoreceptors. We quantified the proportion of RA mechanoreceptors which are immunopositve for ER81 in $Ret^{CFP/+};TrkA^{-/-}$ DRG sections. In this genetic background, all Ret^{+} neurons can be identified with anti-GFP

immunostaining. Additionally, because all *Ret*$^{+}$ DRG neurons besides RA mechanoreceptors depend on NGF/TrkA signaling for their survival and expression of *Ret*, all CFP^{+} neurons in these sections should be RA mechanoreceptors (Luo et al., 2009; Luo et al., 2007). We found that ~40% of RA mechanoreceptors in hindlimb innervating DRGs (L4 and L5) express ER81, while only ~10% of RA mechanoreceptors in surrounding DRGs (L3 and L6) express ER81 (Figure 2A-E). Therefore, we conclude that ER81 is expressed in hindlimb innervating RA mechanoreceptors.

To directly visualize the axons of *Er81*$^{+}$ neurons, we crossed a tamoxifen inducible Cre recombinase driven from the *Er81* locus to a *Tau*^{GFP} conditional reporter allele, and treated pregnant dams with tamoxifen at E15.5 and E16.5 to permanently label a subset of *Er81*$^{+}$ neurons with GFP. At P15, tamoxifen treated mice displayed GFP expression in a subset of ER81^{+} DRG neurons (Figure 2F). GFP^{+} axons innervated layers III-V of the dorsal spinal cord, the dorsal spinal cord target zone of mechanosensory neurons (Figure 2G). Additionally, whole mount staining of the interosseous membrane showed that a subset of Pacinian corpuscles are innervated by GFP^{+} axons (Figure 2H). The lack of GFP^{+} axons innervating all Pacinian corpuscles is likely due to the recombination efficiency of the inducible Cre. Therefore, we conclude that *Er81* is expressed in Pacinian corpuscle innervating DRG neurons.

Er81 is required in neurons, but not Schwann cells, for Pacinian corpuscle development

To determine where *Er81* is required for Pacinian corpuscle development, we combined an *Er81* conditional allele with tissue specific *Cre* lines. We generated conditional mutants with $Nestin^{Cre}$ which drives recombination in Pacinian corpuscle innervating neurons but not corpuscle Schwann cells (Figure 3A). Anti-ER81 immunostaining was absent from DRG sections of $Nestin^{Cre};Er81^{f/-}$ mice, demonstrating efficient recombination of the *Er81* allele in DRG neurons (Figure 3B-C). Serial sections of the hindlimbs revealed a complete absence of Pacinian corpuscles around the fibula (Figure 3D-E). Therefore, we conclude that *Er81* is required in neurons for Pacinian corpuscle development.

As *Er81* is also expressed in the Schwann cells which comprise the Pacinian corpuscle end organ, we next asked if *Er81* is required in Schwann cells for Pacinian corpuscle development. We employed a *Dessert Hedgehog*^{Cre} (Dhh^{Cre}) transgenic line, which drives recombination in Pacinian corpuscle Schwann cells but not their innervating neurons, to ablate *Er81* (Figure 4A). $Dhh^{Cre};Er81^{f/-}$ mice had significantly fewer and smaller Pacinian corpuscles (Figure 4B-E). However, the phenotype in the Schwann cell specific mutants is much less severe than the neural specific mutant phenotype. Therefore, we conclude that *Er81* in Schwann cells contributes to, but is not absolutely required for, Pacinian corpuscle development.

Although innervation is required for the initial formation of Pacinian corpuscles (Zelena, 1980), denervated Pacinian corpuscles in the adult survive until they are reinnervated (in the case of nerve crush/injury) or for up to one year without re-innervation (in the case of nerve transection) (Zelena, 1982, 1984). We asked whether *Er81* in the corpuscle Schwann cells has a role in maintaining the Pacinian corpuscle following the loss of innervation. We performed unilateral tibial nerve transection on 2-4 month old $Dhh^{Cre};Er81^{f/-}$ conditional mutants and $Er81^{f/-}$ control mice, and examined Pacinian corpuscles two weeks after surgery. We confirmed denervation by the loss of NFH^{+} fibers in Pacinian corpuscles (Figure 5A-B). We found that there was no decrease in the number of corpuscles per leg in the transected leg compared to the contralateral non-operated leg, in either the controls or conditional mutants (Figure 5C). Therefore, we conclude that *Er81* is not necessary for the survival of Pacinian corpuscle Schwann cells following denervation. Additionally, the deficit in Pacinian corpuscle number observed at P7 (Figure 4E) in the conditional mutant relative to the control is no longer present in adults, suggesting development of Pacinian corpuscles may simply be delayed in $Dhh^{Cre};Er81^{f/-}$ mice.

The loss of Pacinian corpuscles in *Ret* mutants is not caused by cell death

The common Pacinian corpuscle phenotype between *Ret* and *Er81* mutants suggests they may act in a common molecular pathway to promote corpuscle formation. In

proprioceptors, *Er81* expression is downstream of TrkC/NT3 neurotrophic signaling (Patel et al., 2003). We aimed to test the hypothesis that an analogous RET/neurturin signaling pathway may control the expression of *Er81* in Pacinian corpuscle innervating RA mechanoreceptors.

One potential confound when examining the effects of neurotrophin signaling is the death of neurons which lack neurotrophic support. Due to this well characterized role of neurotrophins (Snider and Silos-Santiago, 1996), it's possible that Pacinian corpuscles may not form in *Ret* mutants because the innervating neurons do not survive due to a lack of RET signaling. To eliminate this possibility, we examined *Ret* mutants and controls in a *Bax* null background. *Bax* is a component of the apoptotic pathway. Elimination of *Bax* allows for the investigation of cell-survival independent effects of loss of neurotrophin or neurotrophic receptor function (Patel et al., 2000). We examined *Ret;Bax* double mutants at P0, the latest they survive due to kidney agenesis. Because S100 is not yet expressed in immature Schwann cells at P0, we examined rudimentary Pacinian corpuscle formation by hematoxylin and eosin (H&E) staining of serial leg sections. We found rudimentary corpuscles present around the fibula of $Ret^{CFP/+};Bax^{-/-}$ single mutants, but no rudimentary corpuscles in the $Ret^{CFP/CFP};Bax^{-/-}$ double mutants (Figure 6A-B). Additionally, we performed immunostaining against CFP driven from the *Ret* locus to examine the axons of the interosseous nerve which innervate Pacinian corpuscles. These axons were present in the $Ret^{CFP/+};Bax^{-/-}$ single mutants, but absent in the $Ret^{CFP/CFP};Bax^{-/-}$ double mutants (Figure 6C-D). Therefore, we conclude that the lack

of Pacinian corpuscles in *Ret* mutants is independent of RET's pro-survival function, and that the innervating axons of Pacinian corpuscles never reach their target in *Ret* mutants, likely due to axon guidance or growth deficits.

Er81 expression is downstream of *Ret* in Pacinian corpuscle innervating neurons

The number of Pacinian corpuscles formed per leg is highly conserved between mice. If *Ret* and *Er81* act in a common genetic pathway, reducing the dosage of both genes may augment the effect on corpuscle formation. We examined the number of Pacinian corpuscles per leg in wild type, $Ret^{+/-}$, $Er81^{+/-}$; and $Ret^{+/-};Er81^{+/-}$ mice. We found that *Ret* and *Er81* single heterozygotes did not have a significant decrease in the number of Pacinian corpuscles relative to wild-type mice. In contrast, *Ret;Er81* double heterozygotes had significantly fewer Pacinian corpuscles per leg than all other genotypes, and the deficit in Pacinian corpuscles was greater than the additive deficit exhibited by *Ret* and *Er81* single mutants (Figure 7). Therefore, *Ret* and *Er81* may act in common or parallel pathways for Pacinian corpuscles development.

To test the hypothesis that *Ret* regulates the expression of *Er81*, we performed double fluorescent *in-situ* hybridization against *CFP* (driven from the *Ret* locus) and *Er81* in L4/L5 DRG sections. At E13.5, shortly after *Er81* begins to be expressed in DRG neurons (Arber et al., 2000), we did not observe a change in the proportion of CFP^{+} neurons which express *Er81* in $Ret^{CFP/CFP}$ mutants compared to $Ret^{CFP/+}$ controls (Figure

8A-C). Therefore, *Ret* is not required for the initiation of *Er81* expression in RA mechanoreceptors. Because cell death due to lack of neurotrophic support begins during late embryonic development, we used a *Bax* null background to compare the expression of *Er81* in RA mechanoreceptors in *Ret* heterozygotes and mutants. At P0, we found a significant decrease in the proportion of large diameter CFP^{+} neurons expressing *Er81* in $Ret^{CFP/CFP};Bax^{-/-}$ mutants compared to $Ret^{CFP/+};Bax^{-/-}$ controls (Figure 8D-F). Therefore, RET signaling is required for the maintenance, but not initiation, of *Er81* expression in limb level RA mechanoreceptors.

Conversely, it is possible that *Er81* regulates the expression of *Ret*. To examine this possibility, we performed *Ret*/*TrkA* double fluorescent in situ hybridization combined with anti-neurofilament heavy-chain (NFH) immunostaining. We then quantified the number of $Ret^{+}/TrkA^{-}/NFH^{+}$ RA mechanoreceptors per L4/L5 DRG section in *Bax* null and *Er81/Bax* double mice from P3-P5 (Figure 8G). If *Er81* positively regulated the expression of *Ret* we would predict a decrease in the number of Ret^{+} RA mechanoreceptors in *Er81* mutants. However, we found that the number of Ret^{+} RA mechanoreceptors was not significantly different from *Bax* single null controls in the double mutants, suggesting that *Er81* does not regulate the expression of *Ret* in RA mechanoreceptors.

The *Er81* Pacinian corpuscle phenotype arises from deficient axon-Schwann cell interactions

Why do Pacinian corpuscles fail to form in *Er81* mutants? We hypothesized that there could be three potential causes for the lack of Pacinian corpuscles in mutant mice. First, it's possible that Pacinian corpuscle innervating neurons or corpuscle Schwann cells depend on *Er81* for their survival. Alternatively, it's possible that Pacinian corpuscle innervating neurons never reach their target in *Er81* mutants. Finally, if innervating neurons reach the proper target and Schwann cell precursors are present, then a breakdown in communication between the axon and the Schwann cells could prevent corpuscles from forming. We addressed each of these possibilities in a series of experiments.

Loss of DRG neurons during the early postnatal period in *Er81* mutants has previously been reported (de Nooij et al., 2013; Kucera et al., 2002). To determine if *Er81* acts solely to promote the survival of neurons or Schwann cells, we examined *Er81* mutant and control legs in a *Bax* null background. We performed immunostaining for S100, which marks Schwann cells, and NFH, which marks large diameter axons, at P3, shortly after Pacinian corpuscles can be clearly identified by anti-S100 staining (Figure 9A-B). We found that although $S100^{+}$ Pacinian corpuscles were present in the double mutants, they were more than halved in number and size (Figure 9C-D). Additionally, the expression level of S100, which is a marker of Schwann cell maturation, was just above

the threshold of detection in the double mutants, but strongly expressed in the *Er81*$^{+/-}$*;Bax*$^{-/-}$ control corpuscles. Therefore, we conclude that the primary deficit in *Er81* mutants is not the failure of neurons or Schwann cells to survive. Furthermore, all present corpuscles were innervated by a single NFH^{+} axon in controls and double mutants, suggesting that targeting and growth of Pacinian corpuscle axons is not affected by the loss of *Er81*.

To determine whether axonal growth and pathfinding is affected in *Er81* single mutants, we also performed anti-NFH staining on P2 control and mutant serial leg sections. We found that NFH^{+} fibers are present in the interosseous membrane near the fibula, just distal to the appearance of Pacinian corpuscles (Figure 10A-B). Therefore, Pacinian corpuscle innervating neurons survive and their axons reach their target in *Er81* mutants, even when cell death is not prevented by the ablation of *Bax*.

If innervating axons reach their target in *Er81* mutants, do they begin the process of generating Pacinian corpuscles? We performed H&E and anti-S100/anti-NFH staining on P2 leg serial sections. In *Er81*$^{+/-}$ controls, we observed well-formed rudimentary corpuscles by H&E staining, as well as strongly S100^{+} Schwann cells surrounding innervating fibers around the fibula. In contrast, *Er81* mutants had hypotrophic rudimentary Schwann cells by H&E staining, and Pacinian corpuscle-like anti-S100 staining was not present around axonal fibers innervating the fibula (Figure 10C-F).

Therefore, we conclude that in *Er81* mutants Pacinian corpuscle innervating axons reach their target and are in contact with immature Schwann cells. However, the Schwann cells do not properly differentiate and form Pacinian corpuscles, likely due to a breakdown in communication between the innervating axon and the Schwann cells.

Interactions with myelinating Schwann cells appear normal in *Er81* mutants

The inner core of the Pacinian corpuscles are composed of nonmyelinating Schwann cells (Griffin and Thompson, 2008; Monk et al., 2015), which do not form properly in *Er81* mutants. Is the development of the most prevalent Schwann cell type in the PNS, myelinating Schwann cells, also affected by the loss of *Er81*? We performed transmission electron microscopy on the L5 dorsal roots of $Er81^{+/-}$ controls and $Er81^{-/-}$ mutants and calculated the g-ratio of individual axonal fibers (Figure 11). At P21, which is near the maximum lifespan of most *Er81* mutants, there was no significant difference in the g-ratio between controls and mutants, and there were no obvious defects in the morphology of the myelin sheath. Therefore, *Er81* is not required for proper myelination, or for communication between axons and myelinating Schwann cells.

***Nrg1* is required in neurons for Pacinian corpuscle formation**

One major effector of axon-Schwann cell communication in the PNS is Neuregulin-1 (NRG1). NRG1 contains an EGF-like domain which acts through ErbB receptors, which

are expressed on Schwann cells, muscle fibers, and other targets of NRG1 signaling (Birchmeier and Nave, 2008). *Nrg1* is a complex gene with more than 15 isoforms produced through differential splicing and the use of different transcriptional start sites (Falls, 2003). In the PNS, isoforms of *Nrg1* containing a cysteine rich domain (*Nrg1-CRD*) are crucial for axonal interactions with myelinating Schwann cells (Michailov et al., 2004). The level of *Nrg1-CRD* expressed by a neuron is directly correlated with its myelination thickness. In contrast, the expression level of *Nrg1* isoforms with Ig-like domains (*Nrg1-Ig*) has no effect on myelination thickness. Instead, *Nrg1-Ig* is likely required in neurons for the formation of proprioceptive muscle spindles (Hippenmeyer et al., 2002). Interestingly, muscle spindles also depend on *Er81* for their development (Arber et al., 2000; Kucera et al., 2002).

Pacinian corpuscle innervating neurons express NRG1 and corpuscle Schwann cells express ERBB (Gonzalez-Martinez et al., 2007; Kopp et al., 1997). However, it is unclear whether NRG1 signaling contributes to Pacinian corpuscle development. To determine if neuronal *Nrg1* expression is required for Pacinian corpuscle formation, we ablated *Nrg1* from rapidly adapting mechanoreceptors by combining a floxed allele of *Nrg1* with a tamoxifen inducible $Ret^{CreERT2}$ line. At P3, Pacinian corpuscles and innervating axons were present in the $Ret^{CreERT2};Nrg1^{+/-}$ controls. In $Ret^{CreERT2};Nrg^{f/-}$ conditional mutants, $S100^{+}$ Pacinian corpuscles were completely absent. NFH^{+} innervating axons persisted, suggesting Pacinian corpuscle axons reach their target and survive until at least P3 when they lack *Nrg1* expression (Figure 12). Therefore, *Nrg1* is

required in Pacinian corpuscle innervating neurons for the development of Pacinian corpuscles.

To confirm the neural requirement for *Nrg1* in Pacinian corpuscle formation, we also ablated *Nrg1* from mechanosensory neurons with a $Split^{Cre}$ transgenic line. $Split^{Cre}$ drives recombination in RA mechanoreceptors (Rutlin et al., 2014). At P7 and P21, $Split^{Cre};Nrg1^{f/-}$ conditional mutants have approximately half the number of Pacinian corpuscles of $Split^{Cre};Nrg1^{f/+}$ controls (Figure 12A-B). The incomplete phenotype observed in $Split^{Cre}$ conditional mutants may be due to incomplete ablation of *Nrg1* in mechanosensory neurons due to transient or low-level expression of recombinase, or due to late ablation of *Nrg1* in some neurons after a critical period. Examination of paw skin at P21 revealed no obvious defects in the development of Meissner's corpuscles, suggesting that Meissner's corpuscles may not depend on neuronal *Nrg1* for their development (Figure 12C-D).

Nrg1-Ig expression is reduced in *Er81* null DRG neurons

As ER81 is a transcription factor, it is unlikely that it acts directly in the communication between axons and nonmyelinating Schwann cells. Due to the similar Pacinian corpuscle phenotypes in *Er81* nulls and *Nrg1* conditional mutants, we asked whether *Er81* may regulate the expression of *Nrg1*. We performed isoform specific in situ hybridization for *Nrg1-Ig* and *Nrg1-CRD* transcripts. We found that the expression of *Nrg1-Ig*, but not

Nrg1-CRD, transcript was reduced in *Er81* null L4/L5 DRGs (Figure 14). Therefore, we conclude that *Er81* specifically regulates *Nrg1-Ig* expression. This finding is in agreement with the g-ratio data, which showed no deficits in myelination in *Er81* mutants. Due to the tight correlation between myelination and *Nrg1-CRD* expression (Michailov et al., 2004), it seems unlikely that *Nrg1-CRD* expression would be reduced in *Er81* mutants due to the lack of a myelination deficit.

Bace1 contributes to Pacinian corpuscle development

The juxtamembrane regions of both *Nrg1-CRD* and *Nrg1-Ig* can be cleaved by proteases (Fleck et al., 2013; Nave and Salzer, 2006). These cleavage events may potentiate the ability of the EGF domain of NRG1 to interact with ERBB. The protease β-secretase 1 (Bace1) cleaves NRG1, and contributes to the promyelinating and pro-muscle spindle development roles of *Nrg1-CRD* and *Nrg1-Ig*, respectively (Cheret et al., 2013; Hu et al., 2006; Willem et al., 2006). We examined the legs of *Bace1* nulls and littermate controls and found a slight but significant decrease in the number of Pacinian corpuscles per leg (Figure 15). A decrease, rather than a total absence of corpuscles, is in line with partial reductions in myelination and muscle spindle formation observed in *Bace1* mutants (Cheret et al., 2013; Hu et al., 2006; Willem et al., 2006). This partial phenotype is likely due to redundancy in proteases which are capable of processing Nrg1 *in vivo* or activity of uncleaved NRG1.

Nrg1 in Schwann cells is not required for Pacinian corpuscle maintenance following injury

Although *Nrg1* is not normally expressed at detectable levels in Schwann cells, it has recently been reported that myelinating Schwann cells begin to express *Nrg1* following nerve injury, and that autocrine NRG1 signaling allows for the dedifferentiation and survival of Schwann cells after the loss of innervation (Stassart et al., 2013). This allows for the survival of the Schwann cells until re-innervation can occur and the Schwann cell can again receive trophic support from the innervating axon. We wanted to address whether a similar mechanism exists in Pacinian corpuscle nonmyelinating Schwann cells. We generated Schwann cell specific $Dhh^{Cre};Nrg1^{f/f}$ mutants, and performed unilateral tibial nerve transection. We confirmed denervation by a lack of NFH^{+} innervating fibers, and found that there was no decrease in the number of corpuscles per leg in the denervated leg relative to the contralateral leg three months after surgery (Figure 16). This suggests that the cellular mechanisms for survival following nerve injury differs between myelinating and nonmyelinating Schwann cells.

DISCUSSION

The specification of somatosensory neurons is a complicated, multi-factorial process which is incompletely understood. For many classes of somatosensory neurons, a combination of extrinsic signaling via neurotrophic factors integrates with and alters the intrinsic transcriptional programs of somatosensory neurons, driving the transcription of

genes which produce distinct morphological and physiological properties. Here, we have described such a signaling pathway in the development of Pacinian corpuscles, which mediate the detection of high-frequency vibration.

Previous studies have shown that the receptor tyrosine kinase RET and the ETS transcription factor ER81 both are essential for the development of Pacinian corpuscles (Luo et al., 2009; Sedy et al., 2006). Here, we have shown that *Er81* is required in Pacinian corpuscle innervating neurons, and its expression is partly mediated by *Ret*. Furthermore, we found that *Nrg1*, a major mediator of axon-Schwann cell communication, is also required for Pacinian corpuscle formation, and that the expression of specific *Nrg1* isoforms are partly mediated by *Er81*.

The findings in these studies raise interesting parallels with proprioceptors, another class of somatosensory neurons (Figure 17). *Er81* is required in proprioceptors to establish appropriate connections with motor neuron targets in the spinal cord (Arber et al., 2000). Similar to the observed *Er81* null Pacinian corpuscle phenotype, the initial proprioceptive projections to the periphery are normal in *Er81* mutants, but the morphology and specification of proprioceptive end organs goes awry in the early postnatal period (Arber et al., 2000; Kucera et al., 2002). Future studies with enhanced genetic tools to specifically trace the central projections of Pacinian corpuscle innervating neurons may

reveal a similar deficit in the central projections of Pacinian corpuscle innervating neurons in *Er81* mutants.

Another interesting parallel between proprioceptive and Pacinian corpuscle innervating neurons is in their reliance on neurotrophic signaling to support expression of *Er81*. Proprioceptors are highly dependent on TrkC/NT3 signaling for their survival and development (Klein et al., 1994; Tessarollo et al., 1994). TrkC/NT3 signaling is necessary and sufficient to drive ER81 expression in proprioceptors (Patel et al., 2003). Pacinian corpuscle innervating neurons express the neurotrophin receptor RET, and *Ret* is required for the formation of Pacinian corpuscles. In *Ret* mutants, we found that the expression of *Er81* is reduced in Pacinian corpuscles innervating neurons. Therefore, these two distinct classes of neuron utilize distinct signaling pathways to converge on a similar cellular output. Notably, the *Er81* null proprioceptive and Pacinian corpuscle phenotypes are less severe than the $NT3^{-/-};Bax^{-/-}$ and $Ret^{-/-};Bax^{-/-}$ phenotypes (Patel et al., 2003), suggesting both cell types employ additional mediators other than *Er81* downstream of neurotrophic signaling.

Lastly, both proprioceptors and Pacinian corpuscles have similar reliance on *Nrg1* for the development of their respective end organs. In neural specific *Nrg1* mutants, early stages of muscle spindle induction do not occur (Hippenmeyer et al., 2002). Through a lack of a phenotype in *Nrg1-CRD* isoform specific mutants and the enriched expression of *Nrg1-Ig*

in proprioceptive neurons, Hippenmeyer, et al., inferred that *Nrg1-Ig* is specifically required for muscle spindle development. Here, we have shown that Pacinian corpuscles do not form when *Nrg1* is ablated from *Ret*-expressing DRG neurons. Due to the death of isoform specific *Nrg1* mutants at stages before obvious Pacinian corpuscles develop, we are unable to directly examine the roles of distinct isoforms in Pacinian corpuscle development. However, examination of *Er81* mutants suggests that *Nrg1-Ig*, but not *Nrg1-CRD*, is expressed downstream of *Er81* in DRG neurons. Therefore, it is possible that *Er81* specifically controls the expression of *Nrg1-Ig* in both proprioceptors and Pacinian corpuscle innervating neurons to effect proper end organ development. In sum, the data presented here and in previous studies supports a neurotrophin receptor-ER81-Nrg1-Ig signaling pathway which drives the development of both Pacinian corpuscles and proprioceptors.

ACKNOWLEDGMENTS

We would like to thank Dr. Joel Li for assistance with tissue processing and image acquisition for electron microscopy experiments. Mouse strains and tissue were provided by Drs. Silvia Arber, Shin-ichi Abe, and Tong Li.

MATERIALS AND METHODS

Mouse strains. All mice except for surgical animals were raised in a barrier facility in Hill Pavilion at the University of Pennsylvania. Surgical animals were raised in a conventional facility in John Morgan Building at the University of Pennsylvania. All procedures were conducted according to animal protocols approved by the Institutional Animal Care and Use Committee of the University of Pennsylvania and National Institutes of Health guidelines. Previously described mouse lines include $Er81^{LacZ}$ (Arber et al., 2000), $TrkA^{-}$ (Fleming et al., 2015), Ret^{CFP} (Uesaka et al., 2008), $Er81^{CreERT2}$ (Taniguchi et al., 2011), $Tau^{f(GFP)}$ (Hippenmeyer et al., 2005), $Nestin^{Cre}$ (Tronche et al., 1999), $Er81^{f}$ (Patel et al., 2003), $Rosa^{tdTomato}$ (Madisen et al., 2010), Dhh^{Cre} (Jaegle et al., 2003), Bax^{-} (Knudson et al., 1995), $Ret^{CreERT2}$ (Luo et al., 2009), $Nrg1^{f}$ (Zhang et al., 2011), and $Bace1^{-}$ (Savonenko et al., 2008). The $Nrg1^{-}$ allele was generated by crossing $Nrg1^{f}$ to a germline Cre female.

Tissue preparation, histology, and in situ hybridization. For immunostaining of spinal columns and DRGs, mice were anesthetized with 100mg/kg ketamine, 16mg/kg xylazine, and 1mg/kg acerpromazine by IP injection. Mice were then transcardially perfused with PBS, followed by perfusion with 4% PFA in PBS. Spinal columns were then dissected and post-fixed in 4% PFA in PBS for 2-4 hours at 4°C, followed by overnight cryoprotection in 30% sucrose in PBS at 4°C. In mice processed only for leg and skin tissue for cryosectioning, mice were sacrificed with CO_2 followed by cervical dislocation/decapitation. Paw skin was fixed overnight in 4% PFA in PBS at 4°C, followed by cryopreservation. Legs were fixed 2-4 hours in 4% PFA in PBS at 4°C, and

then decalcified overnight (Luo et al., 2009), followed by cryopreservation. Preserved tissue was then embedded in NEG-50, and sectioned at 20µm (spinal columns/DRGs), 30-40µm (leg/skin tissue for immunostaining), or 10-15µm (leg tissue for H&E staining). For spinal columns, care was taken in embedding and sectioning process to ensure collection of specific lumbar DRG levels. Serial leg sections from ankle to knee were collected to ensure collection of all Pacinian corpuscles. Cryosection immunostaining was performed as previously reported (Fleming et al., 2015). Whole mount interosseous membranes were dissected from hindlimbs following above perfusion procedure, and then postfixed for 2-4 hours as above. Following fixation, whole mount membranes were permeablized 3X10 minutes with PBS with 1% TritonX-100 and 1% Tween-20. Antibody incubation was performed overnight at room temperature with rocking in PBS plus 5% lamb serum, 1% TritonX-100, and 1% Tween-20. The following day, sections were washed 3X1 hour with PBS plus 1% Tween-20. Secondary antibody incubation was performed overnight at room temperature with rocking in PBS plus 5% lamb serum and 1% Tween-20. Sections were then washed 3X1 hour in PBS plus 1% Tween-20, and then cleared in 50% glycerol in PBS for 30minutes, followed by 75% glycerol in PBS for 30 minutes, and then mounted and imaged in 75% glycerol in PBS. Antibodies used were chicken anti-LacZ (1:500, Aves, BGL-1040), chicken anti-GFP (1:500, Aves, GFP-1020), chicken anti-NFH (1:500, Aves, NF-H), guinea pig anti-VGLUT1 (1:1000, Millipore, AB5905), Rabbit anti-S100 (1:400, Dako, Z031129-2), rabbit anti-ER81 (Arber et al., 2000) (1:1000, gift from Silvia Arber), and Alexa Fluorescent conjugated goat or donkey raised secondary antibodies (1:500, Invitrogen or Jackson ImmunoResearch). H&E staining was performed as previously described (Luo et al.,

2009). In situ hybridization was performed as previously described (Fleming et al., 2015).

Image acquisition. Fluorescent images were collected on a Leica SP5II confocal microscope and a Leica DM5000B microscope. Bright field images were collected with a Leica DM5000B microscope. Electron micrographs were collected on a Jeol-1010 transmission electron microscope.

Animal surgery. Two-four month old mice were anesthetized with the inhalation of ~3% isoflurane in the induction chamber and then maintained on 1-2% isoflurane through a nose cone throughout the procedure. Before making the surgical incision, a very small volume (no more than 2 mg/kg) of bupivacaine (0.25%) will be injected with a 25 gauge needle at equidistant places approximately 0.5-1cm apart, in an ellipse around the incision site. Following incision, the overlying muscle will be dissected and the right tibial nerve was doubly ligated with 5-O silk threads, and transected between the ligations with iridectomy scissors. The proximal and distal ends will be separated by a gap and attached to an adjacent muscle with a suture. The skin was then sutured with 5-O silk threads. Following surgery, mouse is given subcutaneous (S.C.) injection of ~1ml of lactated Ringer's solution to prevent dehydration and are kept on a heating pad until fully recovered from anesthesia. Meloxicam was given (2mg/kg S.C.) at the time of anesthesia

induction and every 12 hours for two days post-surgery. Mice were then processed for collection of leg tissue 2 weeks-3 months following surgery as above.

Tamoxifen treatment. Timed pregnancies were set up in the evening and female mice were checked for vaginal plug the following morning. The time that vaginal plug was observed was considered embryonic day 0.5 (E0.5). Pregnant dams carrying the *Er81*^{CreERT2} embryos were treated with 10mg of tamoxifen dissolved in sunflower oil by oral gavage at E14.5 and E15.5. Pregnant dams carrying the *Ret*^{CreERT2} embryos were treated with 5mg of tamoxifen, 5µg ß-estradiol, and 2.5mg progesterone by oral gavage at E13.5 and E14.5.

Quantification and statistics. For histological analysis of DRG neurons, at least 6 sections per animal were quantified. Image names were randomized after collection to blind experimenter to genotype of images. Pacinian corpuscle counts were performed by manually scanning slides of serial cryosections. Pacinian corpuscles which appeared at similar locations in consecutive sections were not double counted. Pacinian corpuscle size measurements were obtained by imaging every 5th serial section, to avoid double counting individual corpuscles which span multiple sections. The area of individual corpuscle cross sections were then measured by manually tracing the S100^{+} corpuscles in ImageJ. G-ratios were calculated by manually measuring the area of individual fibers and their axons in ImageJ, and then calculating the diameter of fibers based on assuming

the measured areas corresponded to a circle. Statistical analysis was performed with GraphPad Prism software.

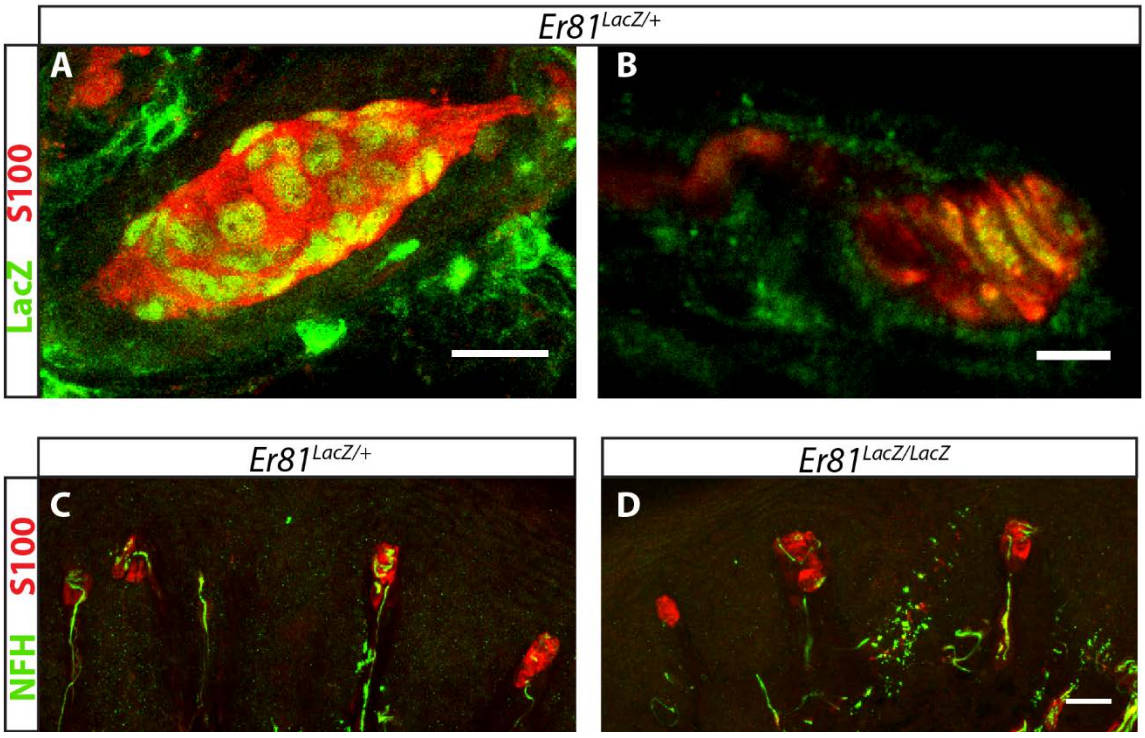

Figure 1: *Er81* is not required for the development of Meissner's corpuscles: (**A**) Nuclear *LacZ* driven from the *Er81* locus labels the nuclei of *Er81*$^{+}$ cells. Anti-LacZ (green) immunostaining combined with ant-S100 (red) staining reveals *Er81* expression in the inner core Schwann cells of Pacinian corpuscles in whole-mount staining of the interosseous membrane at P7. (**B**) Anti-LacZ and anti-S100 immunostaining of hindpaw glabrous skin sections from P21 *Er81*$^{LacZ/+}$ mice reveals expression of *Er81* in the Schwann cells of Meissner's corpuscle end organs. (**C-D**) Anti-S100 and anti-NFH staining of glabrous skin sections from P21 *Er81*$^{LacZ/+}$ control and *Er81*$^{LacZ/LacZ}$ null mice reveals no obvious deficit in the formation or innervation of Meissner's corpuscles in *Er81* nulls relative to controls. n=3 animals per genotype. Scale=20μm (A, C,D), 5μm (B).

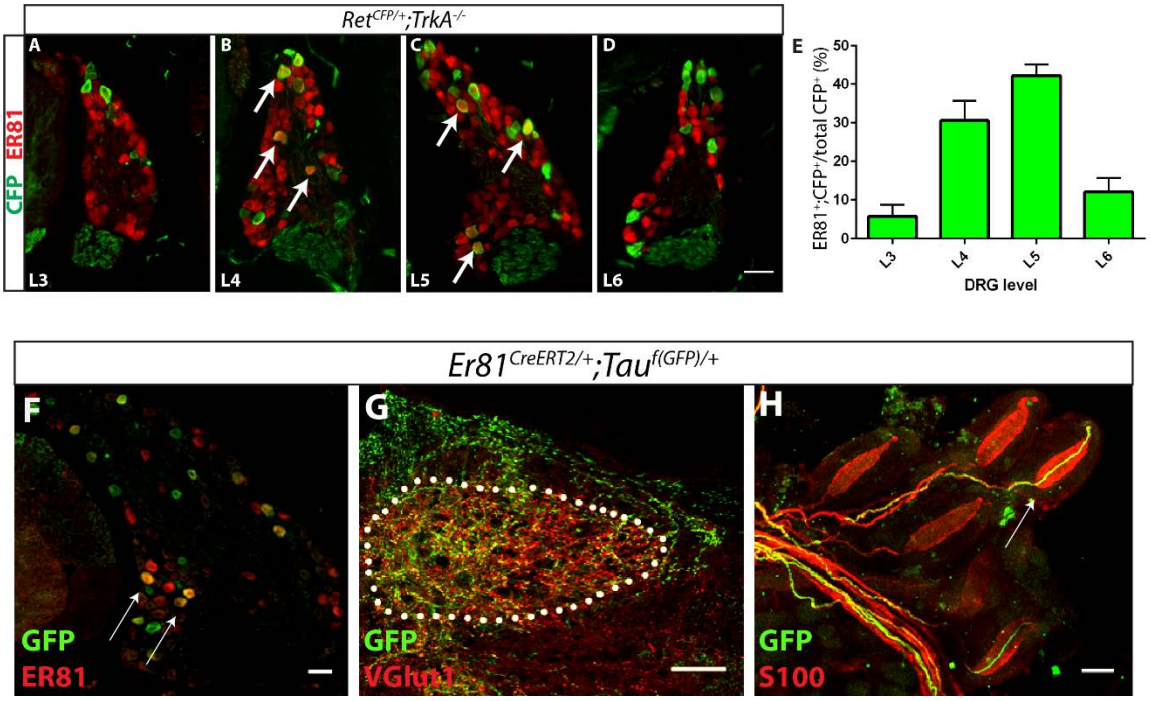

Figure 2: ER81 is expressed in Pacinian corpuscle innervating neurons: (**A-E**) In *Ret*$^{CFP/+}$;*TrkA*$^{-/-}$ mice, CFP driven from the *Ret* locus marks *Ret* expressing cells. Additionally, all *Ret*$^{+}$ DRG neurons except RA mechanoreceptors do not survive due to the lack of *TrkA* mediated neurotrophic support. Therefore, all CFP^{+} DRG neurons in this genetic background are RA mechanoreceptors. Anti-CFP (green) and anti-ER81 (red) immunostaining of limb-innervating (L4 and L5) and neighboring (L3 and L6) DRG sections at P0 reveals a high degree of ER81 expression in limb-innervating RA mechanoreceptors relative to non-limb innervating RA mechanoreceptors (5.71±2.43% of L3, 30.57±4.19% of L4, 42.30±2.37% of L5, and 12.08±2.98% of L6 RA mechanoreceptors express ER81). (**F**) *Er81*$^{ERT2/+}$;*Tau*$^{f(GFP)/+}$ mice were treated with tamoxifen at E14.5 and E15.5, permanently labeling a subset of *Er81*$^{+}$ cells with GFP, and analyzed at P15. Anti-GFP (green) and anti-ER81 (red) immunostaining of DRG sections revealed that a subset of ER81^{+} neurons express GFP. (**G**) Dorsal spinal cord immunostaining with anti-VGlut1 (red), which labels presynaptic terminals of mechanosensory neurons, reveals that GFP^{+} neurons innervate mechanosensory specific layers III-V of the dorsal spinal cord. (**H**) Whole mount anti-S100 (red) and anti-GFP staining of interosseous membrane shows Pacinian corpuscles innervated by GFP^{+} fibers. n=3 animals per genotype. Scale=50μm. Error bars represent SEM.

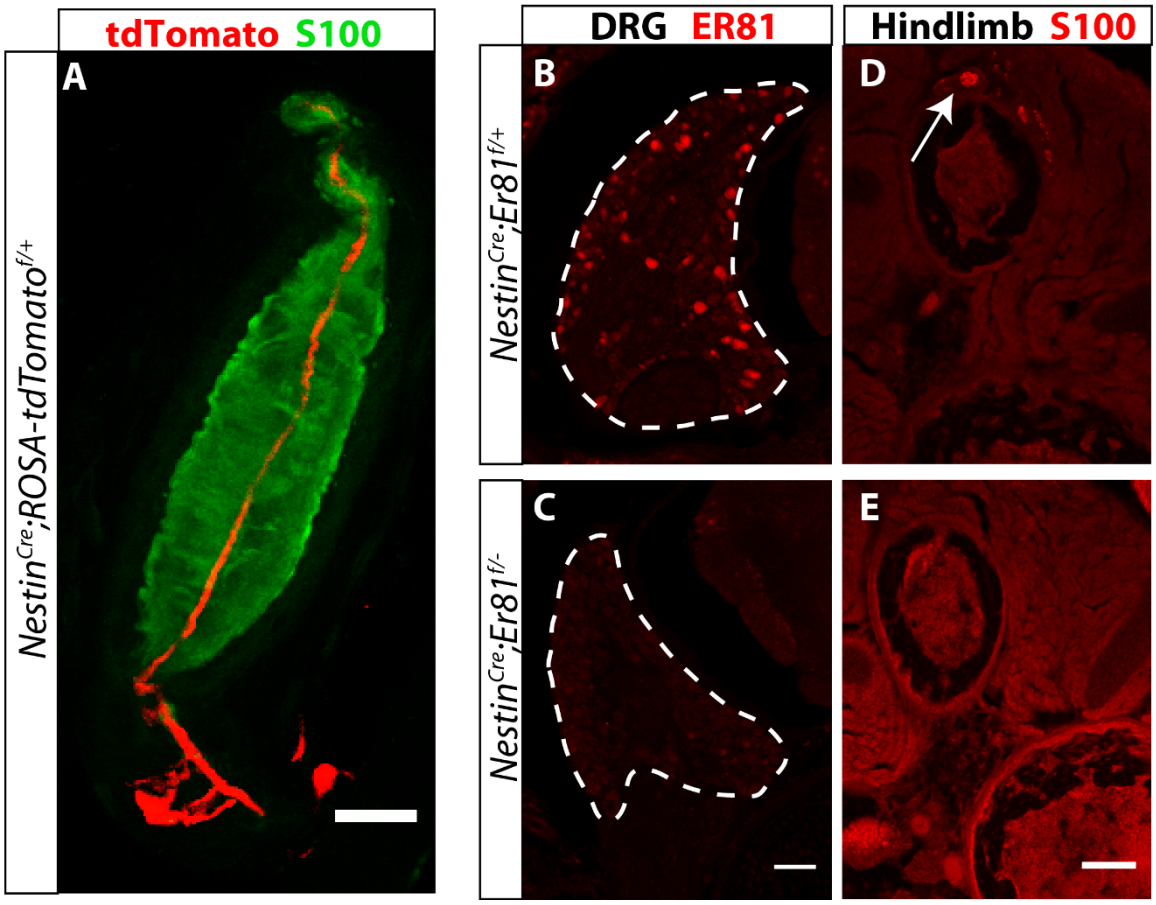

Figure 3: *Er81* is required in neurons for Pacinian corpuscle development: (**A**) Nestin^{Cre} crossed to a ROSA-tdTomato (red) reporter allele exhibits recombination in innervating fibers of Pacinian corpuscles, but not in the S100^{+} (green) Schwann cells of the Pacinian corpuscle end organ. (**B-C**) Anti-ER81 immunostaining of DRG sections from P7 *Nestin^{Cre};Er81$^{f/+}$* control (B) and *Nestin^{Cre};Er81$^{f/-}$* conditional mutant (C) shows ablation of ER81 expression in neurons in the mutant mice. (**D-E**) Anti-S100 staining of hindlimb sections from P7 control (D) and conditional mutant (E) mice shows a lack of S100^{+} Pacinian corpuscles surrounding the fibula in conditional mutant mice. n=3 animals per genotype. Scale=20µm (A), 50µm (B-E).

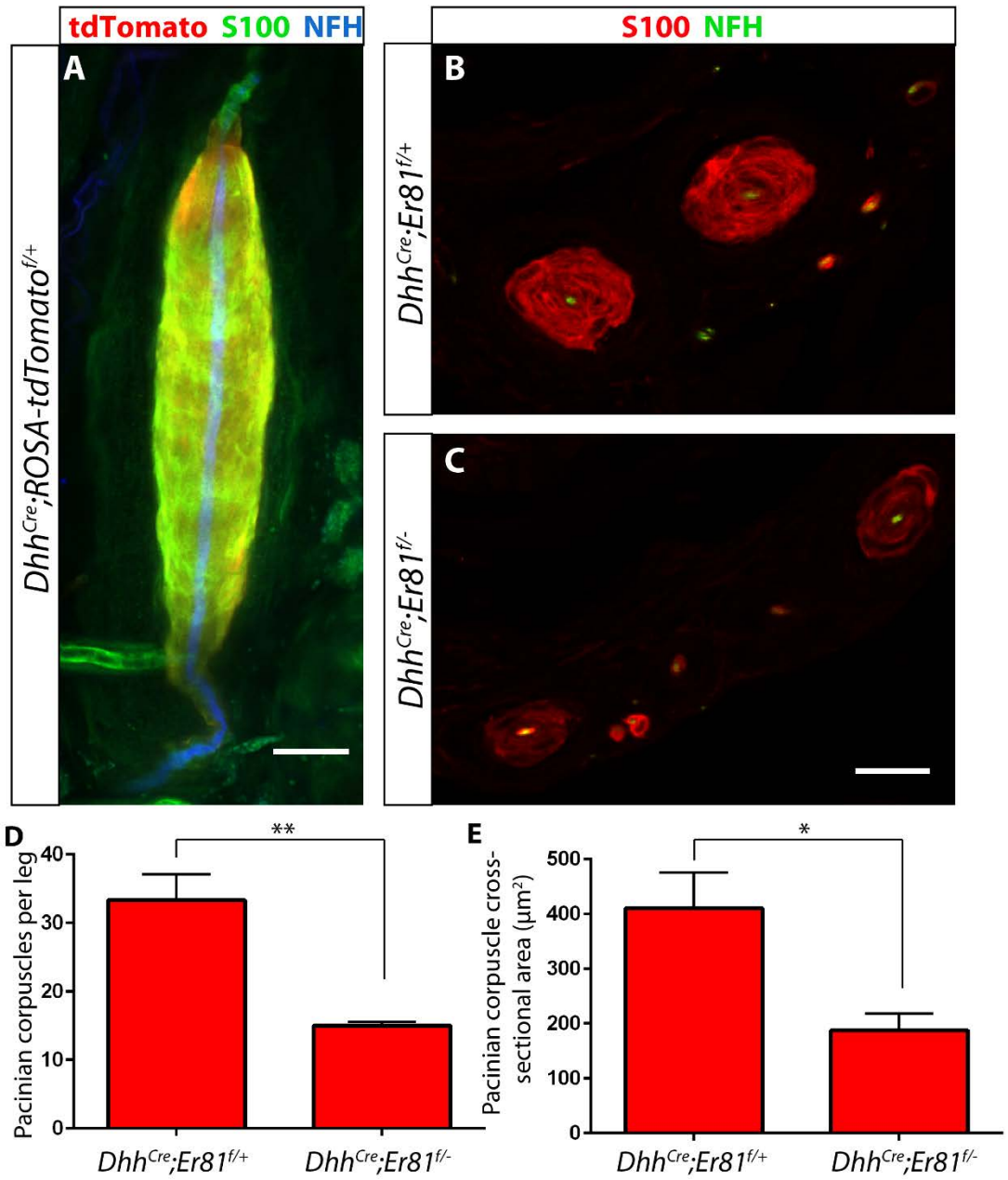

Figure 4: *Er81* in Schwann cells contributes to, but is not required for, Pacinian corpuscle development: (**A**) Dhh^{Cre} crossed to a ROSA-tdTomato (red) reporter allele produces reporter activity in $S100^{+}$ (green) Schwann cells of the Pacinian corpuscle inner core, but not in the NFH^{+} (blue) innervating fiber. (**B-C**) Pacinian corpuscles are present around the fibula in $Dhh^{Cre};Er81^{f/+}$ control (B) and $Dhh^{Cre};Er81^{f/-}$ conditional mutant (C) mice at P7. (**D**) Quantification of serial leg sections revealed a significant decrease in the number of Pacinian corpuscles per leg in Schwann cell specific *Er81* mutants compared to controls (33.33±3.756 PC per leg in $Dhh^{Cre};Er81^{f/+}$ controls, 15.00±0.58 PC per leg in $Dhh^{Cre};Er81^{f/-}$ conditional mutants, p=0.009). (**E**) The average size of Pacinian corpuscles, measured by cross-sectional area, is significantly reduced in Schwann cell

specific *Er81* mutants (410.1±65.3μm^2 in *Dhh^{Cre};Er81$^{f/+}$*controls, 187.9±30.9μm^2 in *Dhh^{Cre};Er81$^{f/-}$* conditional mutants, p=0.037). n=3 animals, 6 legs per genotype. Scale=20μm. *=p<0.05, **=p<0.01. Error bars represent SEM.

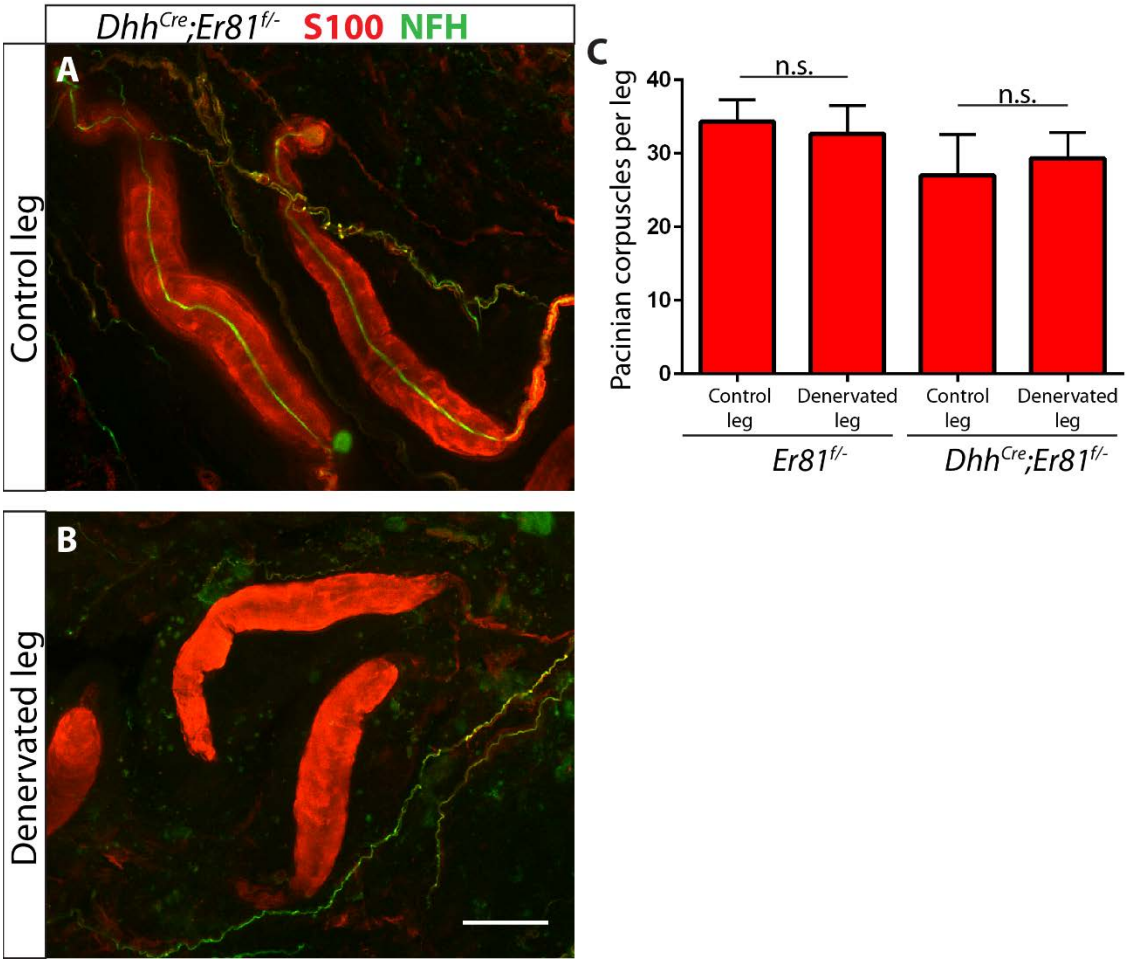

Figure 5: *Er81* in Schwann cells is not required for maintenance of Pacinian corpuscle following denervation: 2-4 month old *Er81*$^{f/-}$ control and *Dhh*^{Cre};*Er81*$^{f/-}$ conditional mutants underwent unilateral tibial nerve transection and recovered for 2 weeks prior to tissue processing. (**A-B**) Denervation was confirmed by the loss of NFH^{+} (green) axons innervating S100^{+} (red) Pacinian corpuscles in the denervated limb (B), in contrast to NFH^{+} innervation in the non-surgical limb (A). (**C**) Quantification of S100^{+} Pacinian corpuscles in serial hindlimb sections in *Er81*$^{f/-}$ controls (34.33±2.96 corpuscles per non-surgical limb, 32.67±3.84 corpuscles per denervated limb, p=0.75) and *Dhh*^{Cre};*Er81*$^{f/-}$conditional mutants (27.00±5.57 corpuscles per non-surgical limb, 29.33±3.53 corpuscles per denervated limb, p=0.74) shows that loss of Schwann cell *Er81* does not cause a deficit in the maintenance of Pacinian corpuscles following denervating injury. n= 3 legs per condition. n.s.=p≥0.05. Error bars represent SEM. Scale=50μm.

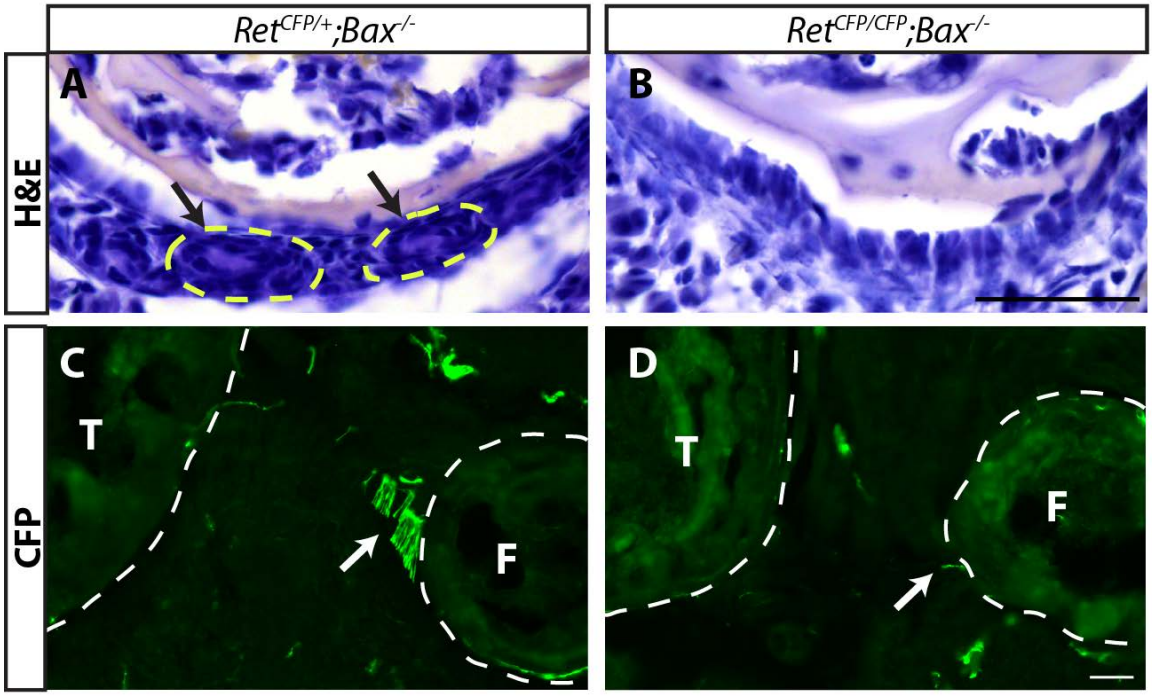

Figure 6: The *Ret* null Pacinian corpuscle phenotype is independent of cell death: (**A-B**) Hematoxylin and eosin (H&E) stained sections of P0 $Ret^{CFP/+};Bax^{-/-}$ control (A) and $Ret^{CFP/CFP};Bax^{-/-}$ double mutant (B) hindlimbs. Arrow indicates rudimentary Pacinian corpuscles, which are present in the $Ret^{CFP/+};Bax^{-/-}$ control but not $Ret^{CFP/CFP};Bax^{-/-}$ double mutant hindlimbs. (**C-D**) Anti-CFP staining of P0 $Ret^{CFP/+};Bax^{-/-}$ and $Ret^{CFP/CFP};Bax^{-/-}$ hindlimbs, which labels the axons of RA mechanoreceptors. Arrow indicates axons of interosseous nerve, which are absent in double mutant. T=tibia, F=fibula, n=3 animals per genotype. Scale= 50µm.

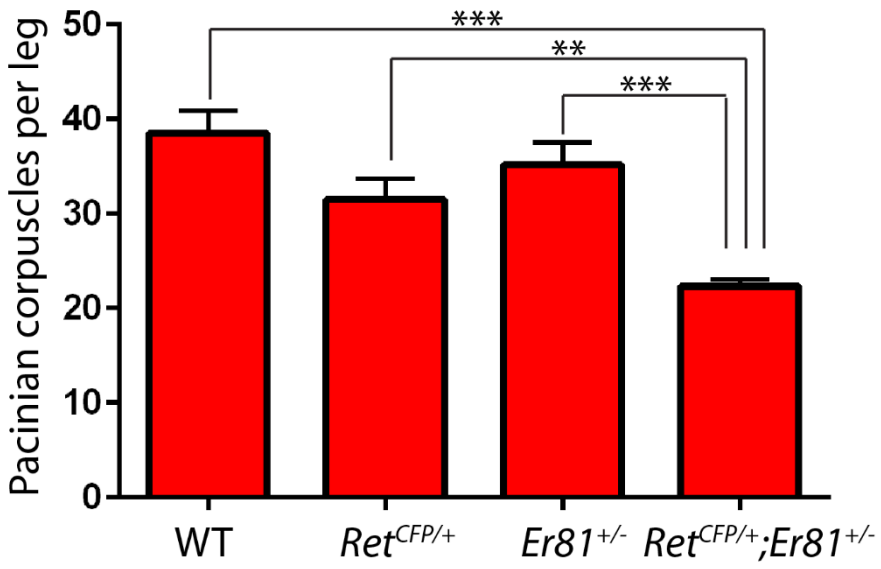

Figure 7: The number of Pacinian corpuscles per limb is significantly reduced in *Ret*;*Er81* double heterozygotes: The number of $S100^{+}$ Pacinian corpuscles per limb was quantified in serial sections of P14-P21 wild type (38.50±2.36 Pacinian corpuscles per limb), $Ret^{CFP/+}$ (31.50±2.23 Pacinian corpuscles per limb), $Er81^{+/-}$ (35.17±2.40 Pacinian corpuscles per limb), and $Ret^{CFP/+};Er81^{+/-}$ (22.33±0.71 Pacinian corpuscles per limb) hindlimbs. The number of Pacinian corpuscles in $Ret^{CFP/+};Er81^{+/-}$ double heterozygotes is significantly less than in all other genotypes. n=6 limbs per genotype **=p<0.01, ***=p<0.001. Error bars represent SEM.

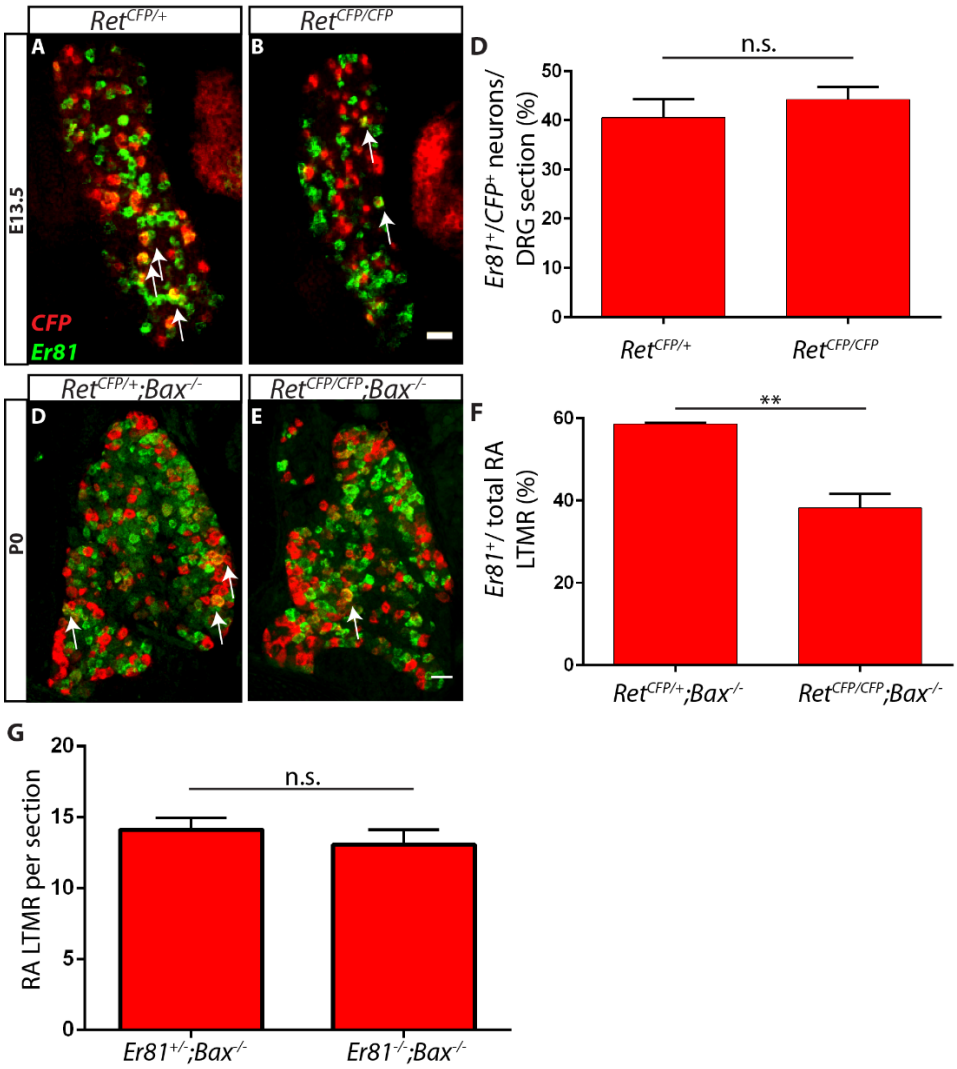

Figure 8: *Ret* is required for the maintenance, but not initiation, of *Er81* expression in RA mechanoreceptors: (**A-C**) Double fluorescent in situ hybridization against *CFP* (red) driven from the *Ret* locus and *Er81* (green) in L4/L5 DRGs of $Ret^{CFP/+}$ and $Ret^{CFP/CFP}$ embryos at E13.5. The percentage of CFP^+ neurons expressing *Er81* is similar between controls and mutants (40.55±3.74% in $Ret^{CFP/+}$ DRGs, 44.19±2.65% in $Ret^{CFP/CFP}$ DRGs, p=0.47, n=3) . (**D-F**) *CFP/Er81* double fluorescent in situ hybridization of P0 *Ret* mutants and controls in an apoptosis deficient background shows a significant decrease in the percentage of RA mechanoreceptors which express *Er81* in *Ret* mutants (58.69±0.26% in $Ret^{CFP/+};Bax^{-/-}$ DRGs, 38.24±3.40% in $Ret^{CFP/CFP}; Bax^{-/-}$ DRGs, p=0.004, n=3). (**G**) The number of $Ret^{+};TrkA^{-};NFH^{+}$ rapidly adapting mechanoreceptors per L4/L5 DRG section was similar between *Er81* mutants and controls in an apoptosis deficient background at P3-P5, suggesting *Er81* does not mediate the expression of *Ret* in RA mechanoreceptors (14.12±0.82 RA mechanoreceptors per section in $Er81^{+/-};Bax^{-/-}$ controls, 13.06±1.06 RA mechanoreceptors per section in

Er81$^{-/-}$*;Bax*$^{-/-}$ double mutants, p=0.47, n=3). n=3 animals per condition, ≥8 sections per animal. **=p<0.01, n.s.=p≥0.05. Error bars represent SEM. Scale=50μm.

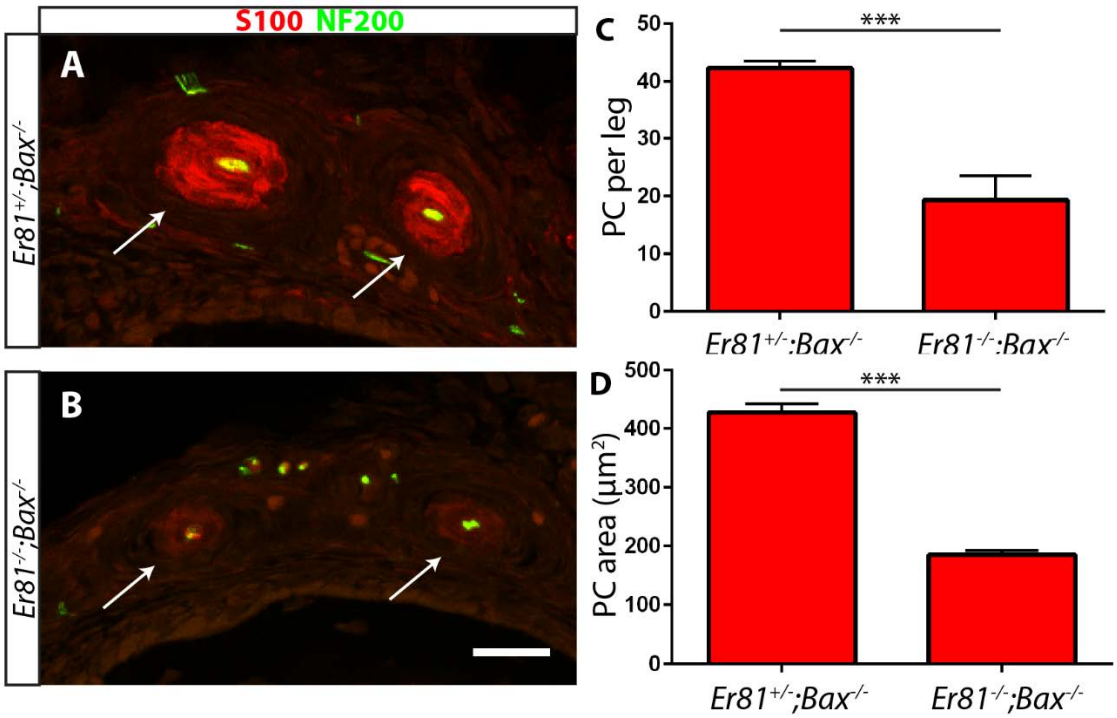

Figure 9: The *Er81* Pacinian corpuscle phenotype is independent of cell death: (**A-B**)Anti-S100 (red) and anti-NFH (green) staining of P3 *Er81*$^{+/-}$*;Bax*$^{-/-}$ control(A) and *Er81*$^{-/-}$*;Bax*$^{-/-}$ double mutant(B) hindlimb sections. Arrows indicate Pacinian corpuscles. Note the lower expression level of S100 in double mutant Pacinian corpuscles relative to controls. (**C**) Quantification of S100^{+} Pacinian corpuscles in serial leg sections reveals a significant decrease in the number of corpuscles formed in double mutants relative to controls (42.33±1.20 PC per leg in *Er81*$^{+/-}$*;Bax*$^{-/-}$ controls, 19.33±4.18 PC per leg in *Er81*$^{+/-}$*;Bax*$^{-/-}$ double mutants, p=0.006). (**D**) Quantification of average cross-sectional area of Pacinian corpuscles reveals a significant decrease in the size of the remaining PCs in double mutants (427.3±14.7µm^2 in *Er81*$^{+/-}$*;Bax*$^{-/-}$ controls, 185.3±6.7µm^2 in *Er81*$^{+/-}$*;Bax*$^{-/-}$ double mutants, p=0.0001). n=3 animals, 6 legs per genotype. ***=p<0.001. Error bars represent SEM. Scale= 20µm.

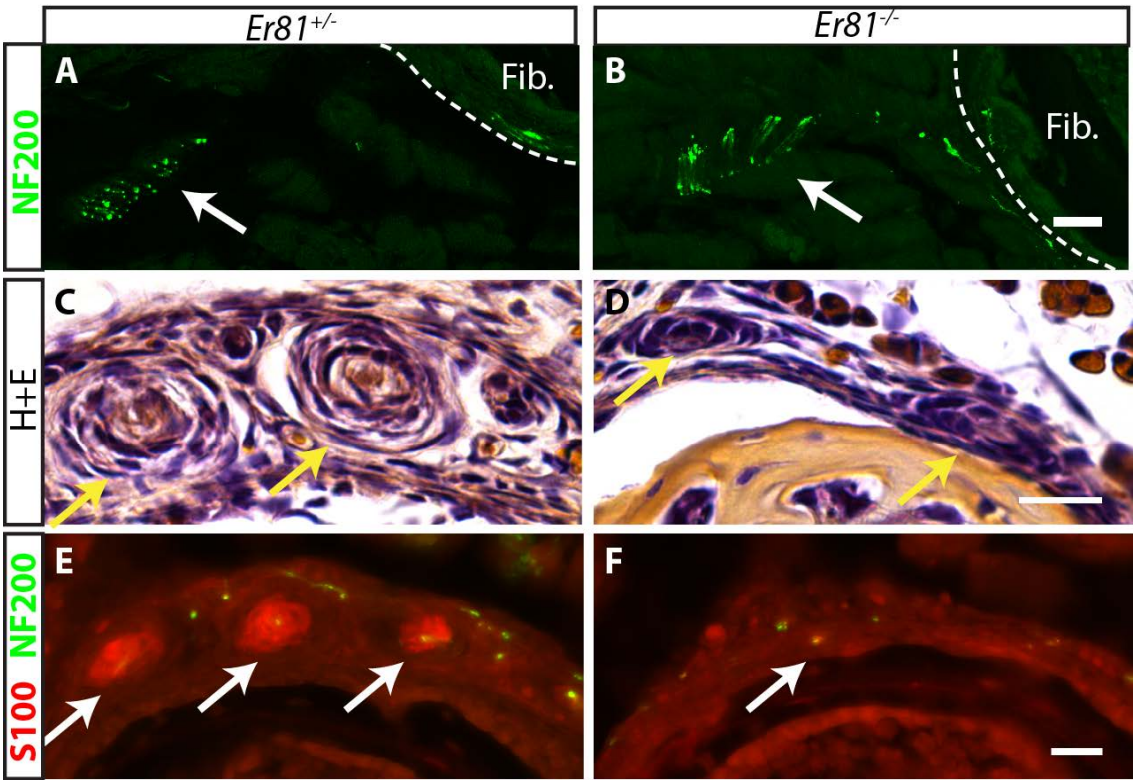

Figure 10: The primary deficit in Pacinian corpuscle formation in *Er81* mutants is deficient axon/Schwann cell communication: (**A-B**) Anti-NFH staining of P2 interosseous nerve shows intact innervation of fibula/interosseous membrane in both *Er81*$^{+/-}$ control (A) and *Er81*$^{-/-}$ mutant (B) mice. (**C-D**) H&E staining of P2 hindlimbs shows early Pacinian corpuscles forming in the *Er81*$^{+/-}$ control (C). Schwann cells form much smaller, rudimentary Pacinian corpuscles in the *Er81*$^{-/-}$ mutant (D). (**E-F**) Anti-S100 (red) and anti-NFH (green) staining shows that mature Schwann cells are present in corpuscles by P2 in the control (E) but are absent in the mutant (F). n=3 animals per genotype. Scale= 20μm.

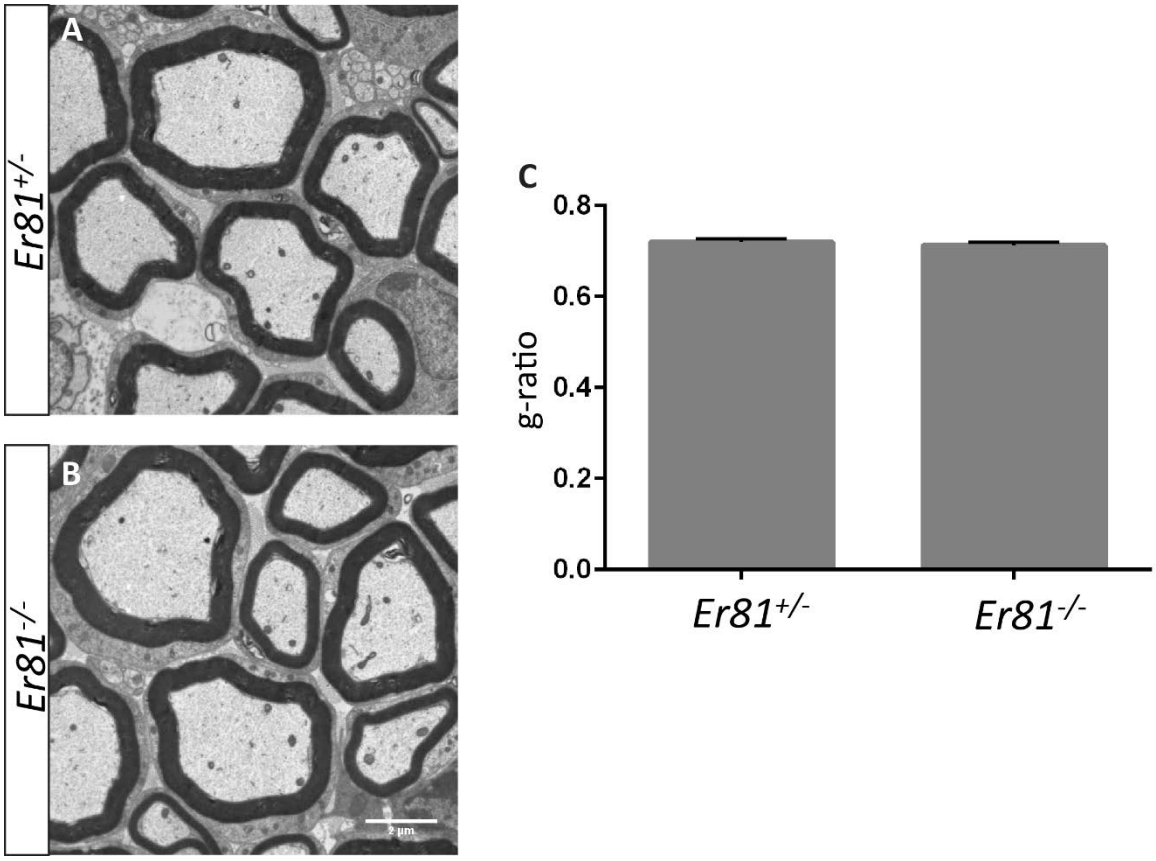

Figure 11: Interactions with myelinating Schwann cells are intact in *Er81* mutant sensory neurons: (**A-B**) Transmission electron micrographs of L5 dorsal roots from P21 *Er81*$^{+/-}$ control and *Er81*$^{-/-}$ mutants reveal no defect in the morphology of the myelin sheath surrounding large-diameter sensory neurons in mutant mice. (**C**) The g-ratios of myelinated axonal fibers are similar between *Er81* mutants and controls (0.720±0.007 in *Er81*$^{+/-}$ controls, 0.7132±0.006 in *Er81*$^{-/-}$ mutants, p=0.50). n=3 animals per genotype, >100 fibers per animal. Error bars represent SEM. Scale=2µm.

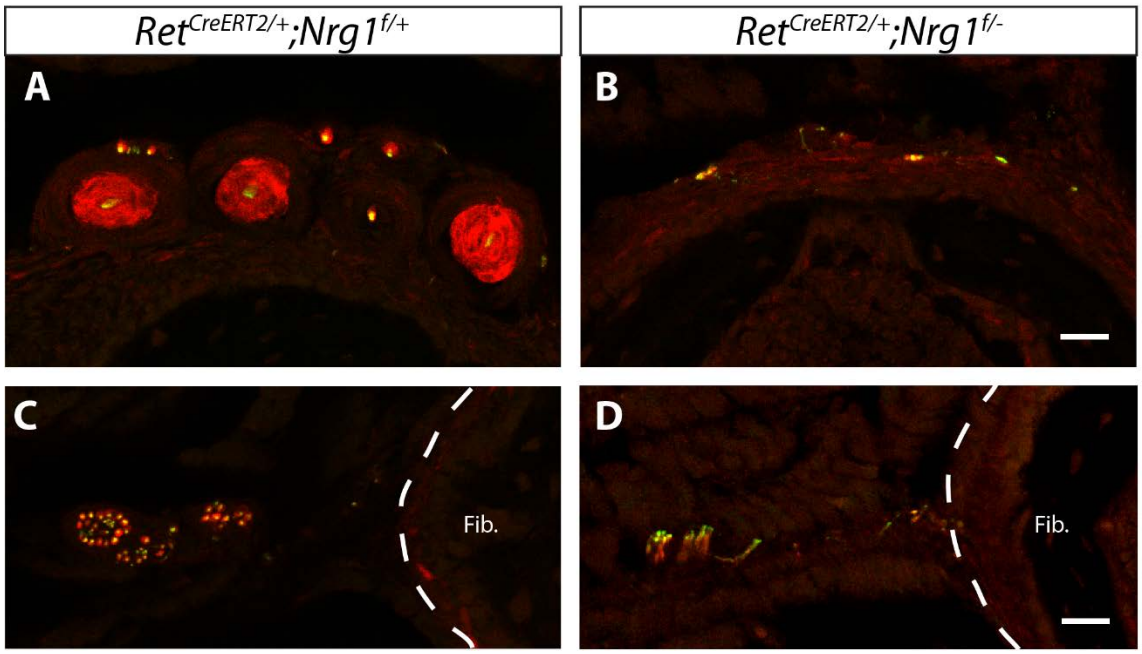

Figure 12: *Nrg1* is required in neurons for Pacinian corpuscle formation: *Ret*$^{CreERT2/+}$;*Nrg1*$^{f/+}$ controls and *Ret*$^{CreERT2/+}$;*Nrg1*$^{f/-}$ mutants were treated with tamoxifen at E13.5 and E14.5 to drive recombination in *Ret*$^{+}$ cells, including Pacinian corpuscle innervating neurons. (**A-B**) Anti-S100 (red) and anti-NFH (green) staining of P5 hindlimb sections showed a lack of S100^{+} Pacinian corpuscles in the *Nrg1* conditional mutant mice. (**C-D**) Staining of hindlimb sections proximal to the appearance of Pacinian corpuscles around the fibula showed axons of the interosseous nerve, which innervate Pacinian corpuscles, in both mutant and control mice. n=2 animals, 4 legs per genotype. Scale=20μm.

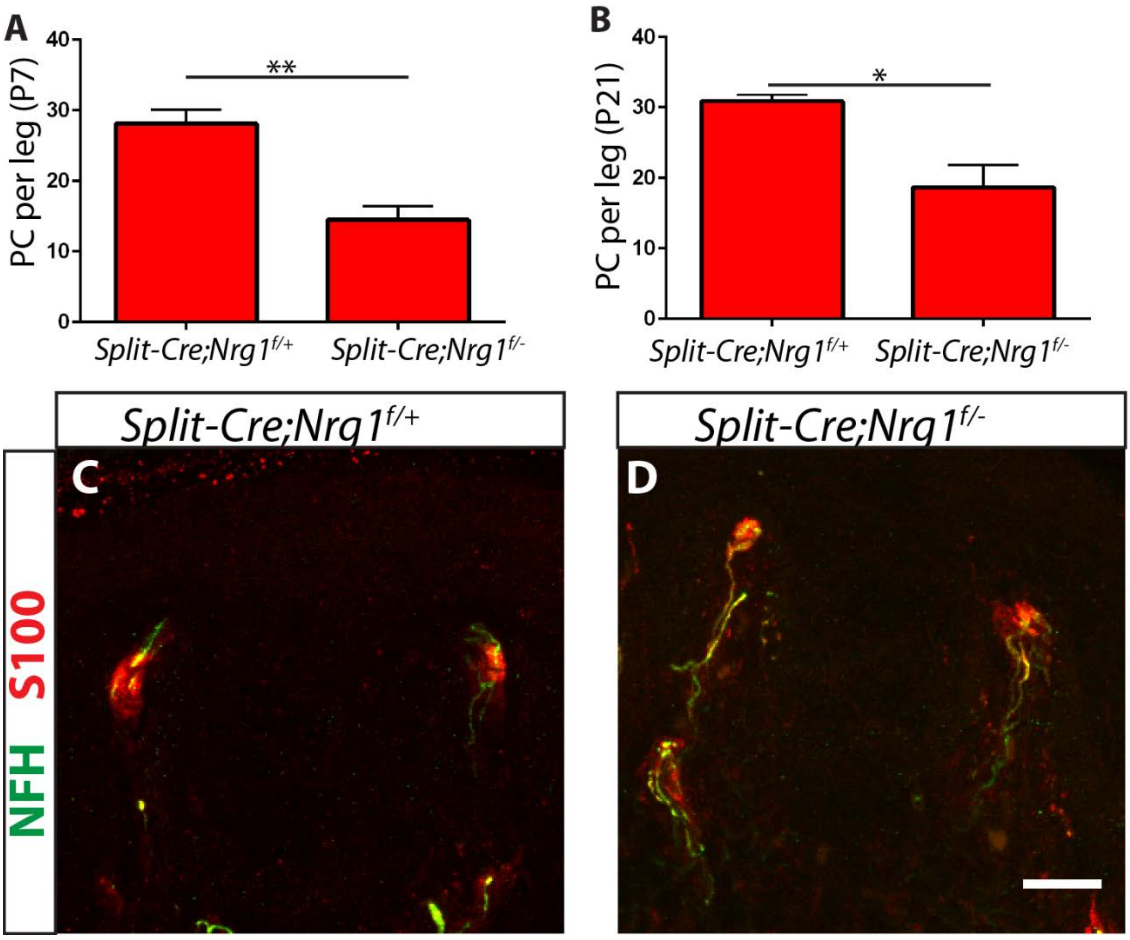

Figure 13: Neuronal *Nrg1* is not required for Meissner's corpuscle development: (**A-B**) *Split*^{Cre} , which drives recombination in rapidly adapting mechanoreceptors, produced a partial, but significant, decrease in the number of Pacinian corpuscles per leg when combined with a conditional *Nrg1* allele at both P7 and P21 (*Split*^{Cre}*;Nrg1*$^{f/+}$ controls have 28.13±1.98 corpuscles per leg at P7, *Split*^{Cre}*;Nrg1*$^{f/-}$ mutants have 14.50±1.92 corpuscles per leg at P7, p=0.002; *Split*^{Cre}*;Nrg1*$^{f/+}$ controls have 30.83±1.01 corpuscles per leg at P21, *Split*^{Cre}*;Nrg1*$^{f/-}$ mutants have 18.67±3.18 corpuscles per leg at P21, p=0.02). (**C-D**) Glabrous skin sections from P21 *Split*^{Cre}*;Nrg1*$^{f/+}$ controls (C) and *Split*^{Cre}*;Nrg1*$^{f/-}$ mutants (D) showed no obvious change in the appearance or number of Meissner's corpuscles in mutants relative to controls. n=3 animals, 6 legs/glabrous skin samples per genotype. *=p<0.05, **=p<0.01. Error bars represent SEM. Scale=20μm.

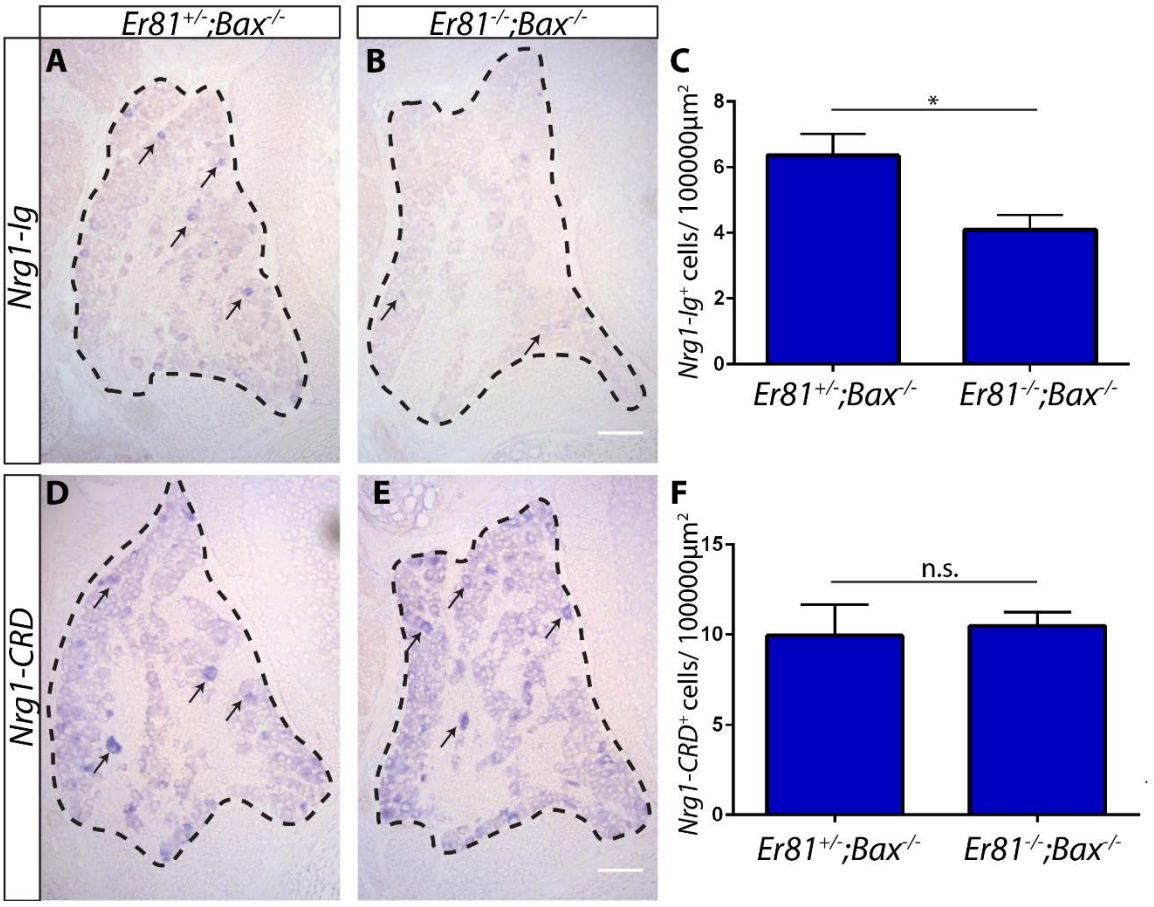

Figure 14: *Nrg1-Ig*, but not *Nrg1-CRD*, expression is reduced in *Er81* null DRG neurons: (**A-C**) Isoform specific in situ hybridization against *Nrg1-Ig* showed a significant decrease in the number of cells expressing *Nrg1-Ig* transcript in L4/L5 DRGs from P3-P5 *Er81* mutants in an apoptosis deficient background relative to controls (6.36±0.65 *Nrg1-Ig*$^{+}$ cells per 100,000µm^{2} in *Er81*$^{+/-}$*;Bax*$^{-/-}$ controls, 4.09±0.48 *Nrg1-Ig*$^{+}$ cells per 100,000µm^{2} in *Er81*$^{+/-}$*;Bax*$^{-/-}$ controls, p=0.04). (**D-F**) Isoform specific in situ hybridization against *Nrg1-CRD* showed no difference in the number of DRG neurons expressing a high level of *Nrg1-CRD* transcript between controls and mutants (9.94±1.76 *Nrg1-CRD*$^{+}$ cells per 100,000µm^{2} in *Er81*$^{+/-}$*;Bax*$^{-/-}$ controls, 10.47±0.77 *Nrg1-CRD*$^{+}$ cells per 100,000µm^{2} in *Er81*$^{+/-}$*;Bax*$^{-/-}$ controls, p=0.79). n=3 animals per genotype, ≥8 sections per animal. *=p<0.05, n.s.=p≥0.05. Error bars represent SEM. Scale=100µm.

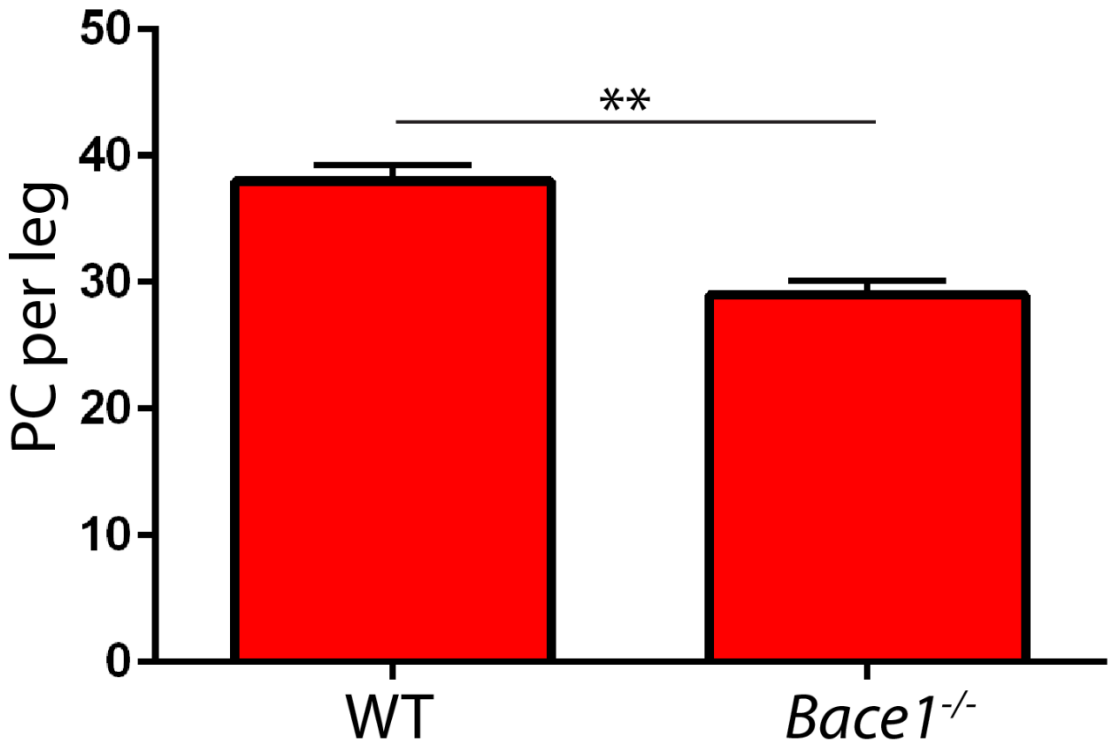

Figure 15: *Bace1* contributes to the development of Pacinian corpuscles: 3-4 week old *Bace1* null mice have significantly fewer $S100^{+}$ Pacinian corpuscles per leg quantified from serial sections of hindlimbs relative to wild-type littermate controls (*Bace1*$^{+/+}$ mice have 38±1.31 Pacinian corpuscles per leg, *Bace1*$^{-/-}$ mice have 29±1.10 Pacinian corpuscles per leg, p=0.006). n=3 animals, 6 legs per genotype. Error bars represent SEM.

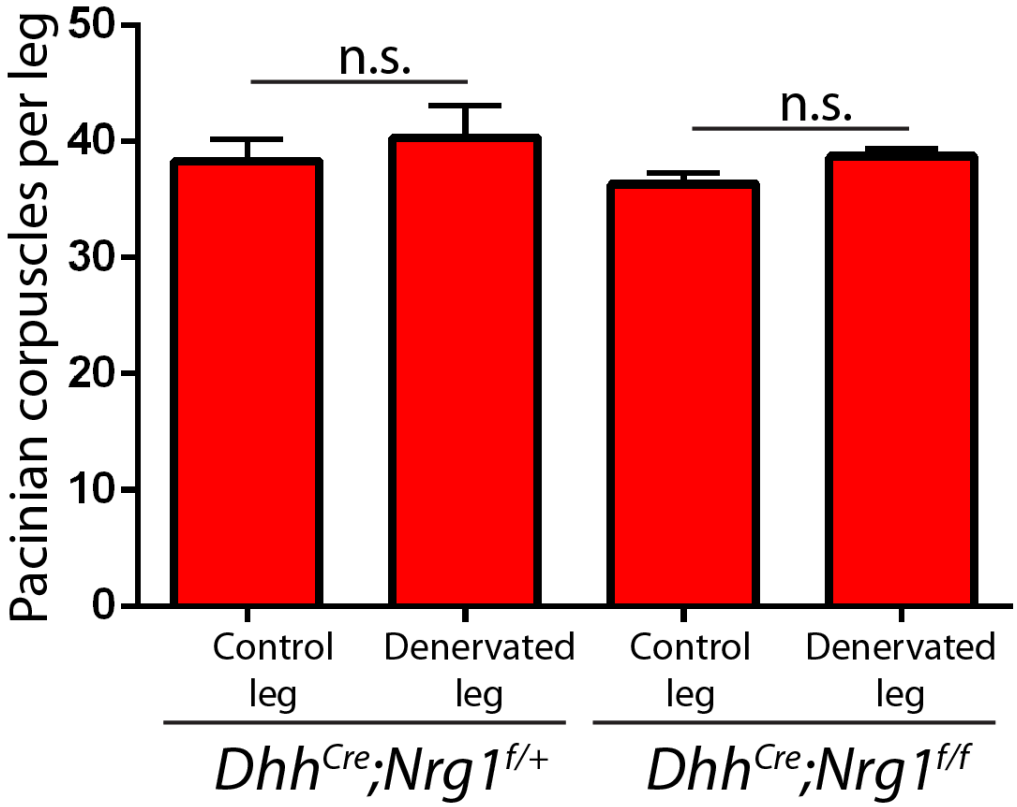

Figure 16: Schwann cell derived *Nrg1* is not required for maintenance of Pacinian corpuscle following denervation: Two-four month old *Dhh*^{Cre};*Nrg1*$^{f/+}$ control and *Dhh*^{Cre};*Nrg1*$^{f/f}$ conditional mutants underwent unilateral tibial nerve transection and recovered for three months prior to tissue processing. Quantification of S100^{+} Pacinian corpuscles in serial hindlimb sections in *Dhh*^{Cre};*Nrg1*$^{f/f}$ controls (38.33±1.86 corpuscles per non-surgical limb, 40.33±2.73 corpuscles per denervated limb, p=0.58) and *Dhh*^{Cre};*Nrg1*$^{f/f}$ conditional mutants (36.33±0.88 corpuscles per non-surgical limb, 38.67±0.67 corpuscles per denervated limb, p=0.10) shows that loss of Schwann cell *Nrg1* does not cause a deficit in the maintenance of Pacinian corpuscles following denervating injury. n=3 legs per condition. n.s.=p≥0.05. Error bars represent SEM.

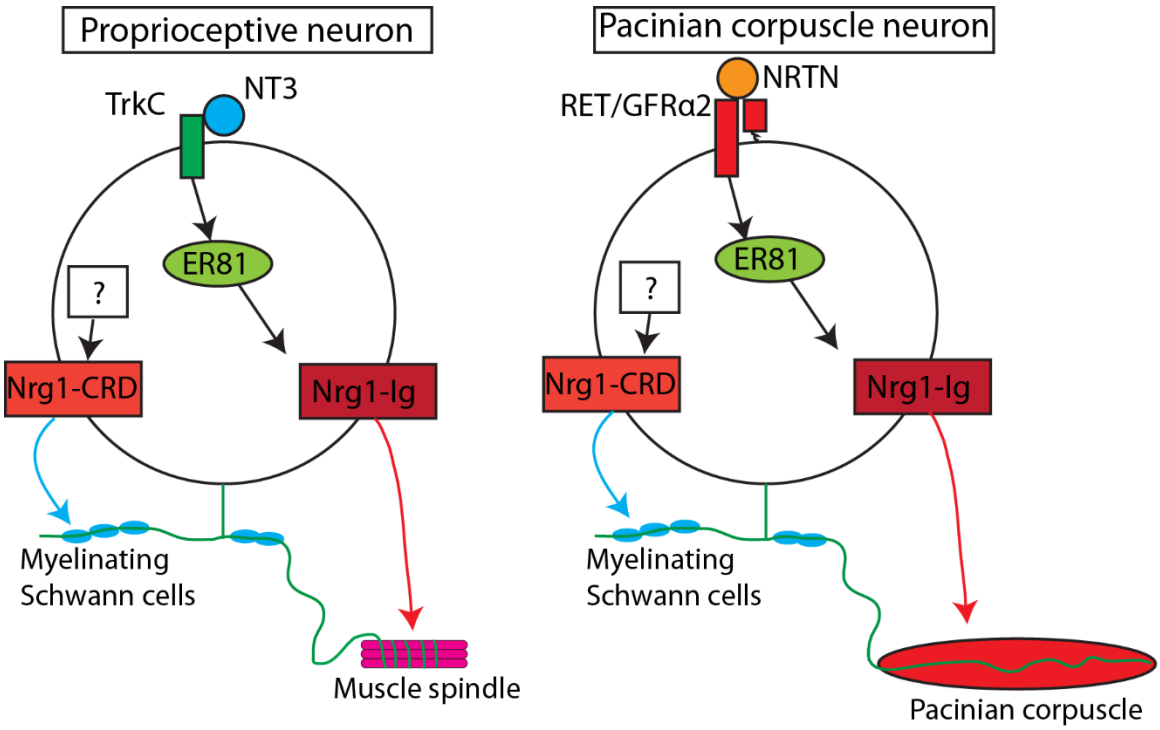

Figure 17: The roles of neurotrophic signaling, ER81, and Neuregulin1 in muscle spindle and Pacinian corpuscle development: In muscle spindle innervating DRG neurons, the expression of ER81 lies downstream of TrkC/NT3 neurotrophic signaling (Patel, et al., 2003). In Pacinian corpuscle innervating neurons, the expression of ER81 lies downstream of RET/GFRα2/NRTN signaling. In both cell types, ER81 regulates the expression of Nrg1-Ig. In proprioceptors, proprioceptive neuron derived Nrg1 (likely Nrg1-Ig) contributes to the development of muscle spindle end organs (Hippenmeyer, et al., 2002). In Pacinian corpuscle innervating neurons, Nrg1 (likely Nrg1-Ig) contributes to the development of Pacinian corpuscle end organs. In both cell types, Nrg1-CRD is critical for interactions with myelinating Schwann cells (Michailov, et al., 2004), but the upstream transcriptional regulators remain unknown.

CHAPTER 4

The majority of dorsal spinal cord gastrin releasing peptide is synthesized locally whereas neuromedin B is highly expressed in pain- and itch-sensing somatosensory neurons

This chapter is adapted from:

Fleming, M.S., Ramos, D., Han, S.B., Zhao, J., Son, Y.J., and Luo, W. (2012). The majority of dorsal spinal cord gastrin releasing peptide is synthesized locally whereas neuromedin B is highly expressed in pain- and itch-sensing somatosensory neurons. Mol Pain *8*, 52.

ABSTRACT

Itch is one of the major somatosensory modalities. Some recent findings have proposed that gastrin releasing peptide (Grp) is expressed in a subset of dorsal root ganglion (DRG) neurons and functions as a selective neurotransmitter for transferring itch information to spinal cord interneurons. However, expression data from public databases and earlier literatures indicate that *Grp* mRNA is only detected in dorsal spinal cord (dSC) whereas its family member neuromedin B (*Nmb*) is highly expressed in DRG neurons. These contradictory results argue that a thorough characterization of the expression of *Grp* and *Nmb* is warranted. We found that *Grp* mRNA is highly expressed in dSC but is barely detectable in DRGs of juvenile and adult mice. Anti-bombesin serum specifically recognizes Grp but not Nmb. Grp is present in a small number of small-diameter DRG neurons and in abundance in layers I and II of the spinal cord. The reduction of dSC Grp after dorsal root rhizotomy is significantly different from those of DRG derived markers but similar to that of a spinal cord neuronal marker. Double fluorescent *in situ* of *Nmb* and other molecular markers indicate that *Nmb* is highly and selectively expressed in nociceptive and itch-sensitive DRG neurons. Therefore, the majority of dSC Grp is synthesized locally in dorsal spinal cord neurons. On the other hand, *Nmb* is highly expressed in pain- and itch-sensing DRG neurons. Our findings provide direct anatomic evidence that Grp could function locally in the dorsal spinal cord in addition to its roles in DRG neurons and that Nmb has potential roles in nociceptive and itch-sensitive neurons. These results will improve our understanding about roles of Grp and Nmb in mediating itch sensation.

INTRODUCTION

Itch is one of the major somatosensory modalities. Pruritogenic stimuli are detected by somatosensory neurons in the dorsal root ganglia (DRG) and trigeminal ganglia, which transmit itch information to the central nervous system (CNS) by synapsing with dorsal spinal cord (dSC) or medulla interneurons (Ikoma et al., 2011). At present, neuronal mechanisms mediating itch sensation are under intensive investigation in order to identify novel targets for itch therapeutics. Some recent studies have proposed that Grp selectively mediates the transmission of itch information from the DRG to the dSC (Sun and Chen, 2007; Sun et al., 2009).

Grp belongs to the mammalian bombesin-like peptide family, which contains two known members: Grp and Nmb. Grp and Nmb share 80% and 70% identity with bombesin, respectively (Matusiak et al., 2005), and selectively bind with high affinity to their respective G-protein coupled receptors, gastrin releasing peptide receptor (Grpr) and neuromedin B receptor (Nmbr) (Jensen et al., 2008). Grp, Nmb and their receptors are broadly expressed in mammals and their functions have been implied in metabolic regulation, stress response, and cancer pathogenesis (Majumdar and Weber, 2011; Moody and Merali, 2004; Patel et al., 2006; Wada et al., 1990; Wada et al., 1992). Interestingly, both Grp and Nmb have also been found to induce itching behaviors (Su and Ko, 2011; Sun and Chen, 2007; Sun et al., 2009).

The hypothesis that Grp functions as a selective neurotransmitter for itch sensation is supported by the complementary expression pattern of *Grp* and *Grpr* in adult mice, as Grp is detected in a subset of small diameter DRG neurons and their nerve terminals innervating the dSC, where *Grpr* is expressed. In addition, co-injection of a Grpr antagonist with Grp negated the pruritogenic effect of Grp. Furthermore, *Grpr* null mice or mice with ablated bombesin-binding dSC neurons exhibited a specific reduced response to pruritogenic compounds (Sun and Chen, 2007; Sun et al., 2009).

Despite strong evidence in support of the function of Grpr in mediating itch sensation, some concerns exist about the expression pattern of Grp in DRG and dSC neurons. First, *in situ* hybridization data from the Allen Spinal Cord Atlas shows that *Grp* is highly expressed in postnatal day 4 (P4) mouse dSC but it is barely detected in DRG neurons (Allen Spinal Cord Atlas, 2016). In addition, the antibody used by previous studies to detect Grp was a rabbit polyclonal antibody generated against the bombesin peptide (Lagerstrom et al., 2010; Liu et al., 2010; Ross et al., 2010; Sun and Chen, 2007; Sun et al., 2009). Given the very high similarity between mouse Grp and Nmb peptide sequences, it is conceivable that this antibody may recognize both peptides. Indeed, *Nmb* is highly expressed in DRG neurons (Allen Spinal Cord Atlas, 2016). Lastly, recent physiological, pharmacological, and genetic studies have demonstrated that glutamate functions as a neurotransmitter of itch-sensing neurons to activate dSC neurons, including Grp-responsive dSC neurons (Koga et al., 2011; Lagerstrom et al., 2010; Liu et al., 2010;

Ross et al., 2010). Thus, it is necessary to thoroughly re-examine the expression of *Grp* and *Nmb* in DRG and dSC to resolve some current controversies.

In this study, we used a combination of approaches, including *in situ* hybridization, reverse transcriptase PCR (RT-PCR), real time PCR, immunohistochemistry, and dorsal root rhizotomy to investigate the expression of *Grp* and *Nmb* in DRG and dSC neurons. We found that *Nmb* is highly expressed in DRG neurons and the majority of dSC Grp is synthesized locally in spinal cord neurons. In addition, we found that *Nmb* is specifically expressed in a subpopulation of nociceptive and itch sensitive DRG neurons. Our results suggest that Grp has additional local function in the dSC and Nmb may have potential functions in itch- and pain-sensing DRG neurons.

RESULTS

Expression of *Grp* mRNA in juvenile and adult mouse

As mentioned above, *Grp* mRNA is found to be highly expressed in P4 mouse dSC but it is barely detectable in DRG neurons using *in situ* hybridization. On the other hand, Grp has been shown to be specifically expressed in a small population of adult itch-sensing mouse DRG neurons using immunohistochemistry, and dSC Grp is suggested to be transported from DRG neurons (Sun and Chen, 2007). At least two possibilities can explain these inconsistent results: one is that they reflect the normal dynamic expression

pattern of *Grp* from early postnatal days to adulthood, and the other is that *Grp* is expressed at a low level in DRG neurons and these results reflect the sensitivity or detection threshold of different techniques.

To address these two different possibilities, we first characterized the expression pattern of *Grp* mRNA in juvenile and adult mice using *in situ* hybridization, RT-PCR, and real time PCR. In addition, we investigated the expression pattern of Grpr, the receptor for Grp, and the other mammalian bombesin-related peptide, Nmb, and its receptor, Nmbr. We performed *in situ* hybridization for *Grp*, *Grpr*, *Nmb*, and *Nmbr* on juvenile (P14-P21) wild-type DRG and dSC tissue (n=3 mice). In agreement with the Allen Spinal Cord Atlas P4 expression data, we found that *Grp* and *Grpr* mRNA could be detected in superficial layers of juvenile mouse dSC, but not in DRG neurons (Figure 1A-1D). In contrast, *Nmb* is highly expressed in ~50% of DRG neurons, but not in dSC (Figure 1E-1F). We could not detect the expression of *Nmbr* in either DRG or dSC at this age, even with very high concentration of antisense probe (Figure 1G-1H). This result is different from the Allen Spinal Cord Atlas P4 data, which shows some expression of *Nmbr* in superficial layers of the dSC. This difference could be due to the dynamic expression of *Nmbr* as mice mature.

To examine the expression pattern of these transcripts by a more sensitive approach, we performed RT-PCR on RNA acutely isolated from either DRGs or dSC of adult wild-type

mice (n=4 mice). In agreement with our *in situ* hybridization data from juvenile mice, we found that *Grp* and *Grpr* could be readily amplified from adult dSC cDNA whereas *Nmb* was robustly amplified from adult DRG cDNA (Figure 1I). Notably, a faint *Grp* band was detected in DRG samples in four out of seven trials. This band was consistently much fainter than the *Grp* product amplified from dSC. As an amplification control, a ubiquitously expressed gene, *Gapdh*, was detected at similar levels in DRG and dSC. The fact that *Grp* cDNA cannot be consistently amplified from freshly isolated adult DRG transcripts indicates that *Grp* is present in DRG neurons at a very low level. This notion is also supported by evidence that *Grp* could not be amplified from a commercially prepared adult DRG cDNA library using PCR, although *Nmb* was readily amplified from the same library (data not shown). To further quantify the relative abundance of *Grp* mRNA in dSC and DRG, we performed real time PCR with dSC and DRG cDNA. We found that *Grp* transcript was present at a much higher concentration in dSC relative to DRG (range=63-1155 fold difference, n=3 mice, 4 trials per sample) (Figure 1J). In addition, we noted that faint *Nmb* and *Nmbr* bands were amplified from dSC cDNA (Figure 1I). These slightly different results obtained using *in situ* hybridization and RT-PCR can be explained by the fact that *in situ* hybridization is usually less sensitive compared to reverse transcriptase-and real time PCR. Taken together, our results reveal that *Grp* and *Grpr* mRNA are highly expressed in dSC in both juvenile and adult mice whereas *Nmb* mRNA is highly expressed in DRG neurons. Additionally, *Grp* mRNA is expressed in juvenile and adult mouse DRG neurons at a very low level, which is near the detection threshold of RT-PCR but below that of *in-situ* hybridization.

Characterization of the specificity of anti-bombesin antiserum

The bombesin family of peptides contains two known family members in mouse: Grp and Nmb. These peptides share 80% and 70% identity, respectively, with the originally characterized member of this family, *Bombina bombina* bombesin (Figure 2A). Previous studies (Lagerstrom et al., 2010; Liu et al., 2010; Ross et al., 2010; Sun and Chen, 2007; Sun et al., 2009) have used a rabbit polyclonal anti-bombesin serum (Immunostar, 20073) to detect the presence of Grp. However, it has not been formally determined whether this anti-bombesin serum selectively recognizes Grp. It is conceivable that this polyclonal antibody detects both Grp and Nmb, given the high similarity among bombesin, Grp, and Nmb. To address this issue, we first characterized the specificity of this polyclonal antibody *in vitro*. In HEK293T cells, we expressed EGFP or EGFP with C terminal fusion of bombesin, Grp, or Nmb. We found that cells expressing EGFP-bombesin and EGFP-Grp were stained by the anti-bombesin antiserum, whereas cells expressing EGFP-Nmb or EGFP alone were not recognized by the antiserum (Figure 2B-2M). These findings indicate that the polyclonal antibody used in this and previous studies selectively recognizes Grp but not Nmb, which is quite surprising given the high level of identity between these peptides and the immunizing antigen.

Characterizing the expression of Grp in DRG neurons and dSC using immunostaining

After establishing that the anti-bombesin antiserum selectively recognizes Grp *in vitro*, we next examined the staining pattern of the antiserum *in vivo*. In wild-type P14-P21 mice, we observed that a small number of small-diameter DRG neurons are immunopositive for the anti-bombesin serum (1.79±0.04% of lumbar DRG neurons, n=3 mice) (Figure 3A-3J). Consistent with previously published results, these Grp^+ neurons are a subpopulation of peptidergic nociceptors, as they are also $Cgrp^+$ (marker of peptidergic nociceptive DRG neurons), but Pap^-, $IB4^-$ (markers of nonpeptidergic nociceptors), and $VGlut1^-$ (marker for mechanoreceptors and proprioceptors). This small number of immunopositive neurons is consistent with our finding that *Grp* mRNA is expressed at a very low level in juvenile mouse DRG neurons.

In contrast to DRG neurons, we readily detected the abundant presence of Grp in superficial layers of the dorsal spinal cord. Notably, the immunostaining signal of Grp in dSC is much stronger than that of DRG neurons. We found that Grp is mainly present in layer I and the outer layer of layer II (IIo) of the spinal cord, as the intense Grp signal overlaps with layers innervated by Cgrp, a marker of peptidergic nociceptive DRG afferents terminating in laminae I-IIo of the dorsal horn (Figure 3K-3L) . Some less intense Grp signal also overlaps with markers of nonpeptidergic nociceptors, such as Pap and IB4, which terminate in lamina IIi of the dorsal horn, and Pkcγ, which is expressed in spinal cord neurons located in lamina IIi and IIIo (Figures 3O-3R and 4A-4C) (Molliver et al., 1997; Polgar et al., 1999; Taylor-Blake and Zylka, 2010). However, Grp immunostaining signal does not overlap with $VGlut1^+$ puncta, which are formed by Aβ

mechanoreceptors innervating layers III-V (Figure 3S-3T) (Hughes et al., 2004). High magnification images of dSC Grp staining show that discrete Grp^+ puncta are present around $NeuN^+$ dSC nuclei, indicating that *Grp* is expressed in dSC neurons (Figure 3U). Taken together, our results reveal that Grp is present at a high level in spinal cord superficial layer neurons.

To further confirm the specificity of immunoreactivity in dSC and DRG, we preabsorbed anti-bombesin antiserum with either bombesin or Grp peptide, and used the supernatant to stain wild type mouse DRGs and spinal cord (n= 3). We found a loss of Grp immunostaining in both dSC and DRG after preabsorbing the antiserum, suggesting that the immunoreactivity we detected in these regions was not due to nonspecific antibodies in the antiserum (Figure 3C-3D and 3M-3N). Unfortunately, the *Grp* null mouse, which would definitively address the *in vivo* specificity of this anti-bombesin serum, is not currently available to us.

Source of dSC Grp

Even though Grp is present at a high level in layers I and II of the spinal cord, its source is still unclear. It could be synthesized locally in dorsal spinal cord neurons, as suggested by the *Grp* mRNA expression pattern observed in the Allen Spinal Cord Atlas and our own results, or it could be synthesized in and transported from DRG neurons, as previously proposed (Sun and Chen, 2007). Interestingly, Grp is barely detected in

dorsal root axons with this anti-bombesin serum (Figure 3V-3X). In contrast, we found that Cgrp, Pap, and IB4, which are known markers carried by nociceptive afferents, intensely stain dorsal root axons (Figure 3U-3W and data not shown). These findings suggest that the amount of GRP transported from DRG neurons to dSC, if any, is below the detection threshold of our method. So far, our data support that most dSC Grp is synthesized in dSC neurons because: 1) abundant *Grp* transcript is detected in dSC using *in-situ* hybridization and RT-PCR; 2) consistent with the mRNA distribution, a high level of Grp is detected in dSC by immunostaining; 3) a very low level of *Grp* transcript is detected in DRG neurons; 4) a small number of Grp^+ neurons are present in DRGs; and 5) Grp is barely detected in dorsal root axons.

To further determine the source of dSC Grp, we performed immunostaining on spinal cord following a unilateral dorsal rhizotomy of L4/L5/L6 dorsal roots of adult mice (n=3). If the primary source of dSC Grp is due to its synthesis in and release from somatosensory afferents, we predict that immunostaining signal for dSC Grp would be greatly decreased following the dorsal rhizotomy. However, if the primary source of dSC Grp is spinal cord neurons, the change in immunostaining signal for dSC Grp following dorsal root rhizotomy should not be as dramatic. We sacrificed the animals two weeks after rhizotomy to ensure that robust degeneration of dorsal root axons had occurred. Spinal cord sections were immunostained with anti-bombesin serum and other antibodies marking DRG sensory axons or spinal cord neurons. The change in immunofluorescence intensity on the transected side was normalized to that of the control

side (See methods for details). We found that following L4/L5/L6 dorsal root transection, the intensity of bombesin immunoreactivity is decreased (58.52±8.00% fluorescent intensity, transected/control). Importantly, this decrease is not significantly different from the change of immunoreactivity of Pkcγ (65.91±12.78% fluorescent intensity transected/control), a protein known to be highly expressed in dorsal spinal cord neurons (P=0.44). The modest reduction of dSC Pkcγ and Grp could be due to the loss of DRG neuron derived Pkcγ and Grp and the denervation response of dSC neurons (Tessler et al., 1984; Wang et al., 1991). On the other hand, the immunofluorescence intensity of dSC Pap (24.95±5.58% fluorescent intensity transected/control) and Cgrp (18.25±7.84% fluorescent intensity transected/control), markers primarily transported from nonpeptidergic and peptidergic nociceptors, were dramatically reduced (Figure 4A-4S). Remarkably, the signal reduction of Grp and Pkcγ are significantly different from that of Cgrp and Pap ($P < 0.01$). Taking all findings together, we conclude that the majority of dSC Grp is synthesized locally.

Nmb is mainly expressed in small-diameter DRG neurons

Though *Grp* is only expressed in a few DRG neurons, the other mammalian bombesin-like peptide, *Nmb*, is highly expressed (Figure 1F). This specific expression pattern suggests that Nmb may play a role in somatosensation. Indeed, administration of Nmb has been shown to induce scratching behavior, which can be blocked by administration of an Nmbr antagonist (Su and Ko, 2011). To further determine a role for Nmb in the itch

pathway or other somatosensory modalities, it is important to characterize which subpopulation of DRG neurons expresses *Nmb*. Since there is no commercially available antibody that can reliably and specifically detect Nmb (assay with EGFP-Nmb fusion protein in HEK293 cells, data not shown), we performed double fluorescent *in situ* hybridization (FISH) and FISH combined with immunohistochemistry to establish the molecular profile of Nmb^+ DRG neurons in P21 mice.

We first examined whether *Nmb* is expressed in large- or small-diameter DRG neurons. DRG neurons with different soma sizes have different developmental origins, molecular profiles, physiological properties, and functional modalities. Small-diameter, unmyelinated or thinly-myelinated DRG neurons, which express the intermediate filament peripherin, are mostly nociceptors. On the other hand, medium- to large-diameter, highly-myelinated DRG neurons, which express the intermediate filament neurofilament heavy chain (Nfh), are mostly mechanoreceptors and proprioceptors. To characterize the size distribution of Nmb^+ neurons, we performed FISH for *Nmb* and combined it with immunostaining for either peripherin or Nfh. We found that most Nmb^+ neurons are small-diameter DRG neurons as they are also $peripherin^+$ (76.89±6.62% Nmb^+ neurons express peripherin; 51.53±4.59% $peripherin^+$ neurons express *Nmb*; Figure 5A-5D). In addition, about a quarter of Nmb^+ neurons are large-diameter and Nfh^+ (28.53±3.23% Nmb^+ neurons express Nfh; 28.73±7.42% Nfh^+ neurons express *Nmb*; Figure 5E-5H). Furthermore, we measured the size of Nmb^+ DRG neurons and plotted their size distribution with regard to those of $peripherin^+$ and Nfh^+ neurons.

Our data illustrates a skewed distribution in the size of Nmb^+ neurons, with a majority of neurons showing a size distribution similar to $peripherin^+$ neurons and a small proportion having larger areas comparable to Nfh^+ neurons (Figure 5I). These results suggest that *Nmb* is expressed in both small and large diameter DRG neurons, but most Nmb^+ neurons have small-diameter somata.

Nmb is expressed in both peptidergic and non-peptidergic nociceptors

As mentioned above, most small diameter DRG neurons are nociceptors. To address whether *Nmb* is expressed in pain- and itch-sensing DRG neurons, we first examined *Nmb* expression in two broadly defined classes of pain-sensitive neurons: peptidergic and nonpeptidergic nociceptors. During embryonic development, all nociceptors express TrkA, the neurotrophic receptor tyrosine kinase for nerve growth factor (NGF). In the first two postnatal weeks, however, DRG neurons that differentiate into nonpeptidergic nociceptors extinguish their expression of *TrkA* and express another receptor tyrosine kinase, Ret, while peptidergic nociceptors retain their expression of *TrkA* into adulthood (Luo et al., 2007; Molliver et al., 1997). We performed double FISH for *Nmb* and *Ret* or *TrkA* to determine which classes of nociceptors express *Nmb*. Almost all $TrkA^+$ neurons (41.99±2.01% of Nmb^+ neurons express *TrkA*; 94.59±1.14% of $TrkA^+$ neurons express *Nmb*) and majority of Ret^+ neurons (72.14±2.54% of Nmb^+ neurons express *Ret*; 75.04±1.58% of Ret^+ neurons express *Nmb*) express *Nmb* (Figure 6A-H). The Ret^+ DRG neurons are comprised of both small-diameter nonpeptidergic nociceptors and larger-

diameter rapidly adapting (RA) mechanoreceptors (Luo et al., 2009). Interestingly, all large-diameter Ret^+ RA mechanoreceptors are Nmb^- (arrow, Figure 6B-6C), and the proportion of Ret^+ neurons that co-express *Nmb* is very similar to the proportion of Ret^+ DRG neurons that are nociceptors (Bennett et al., 1998; Molliver et al., 1997). Additionally, we found that almost all Nmb^+ neurons express either *Ret* or TrkA (98.78±0.12% of total NMB^+ neurons) when we combine double FISH for *Nmb* and *Ret* with immunohistochemistry for TrkA (Figure 6I-6M). We also note that $Nmb^+/TrkA^+$ neurons are larger than Nmb^+/Ret^+ neurons. In short, these results indicate that *Nmb* is specifically expressed in both peptidergic and non-peptidergic nociceptors.

To further confirm the expression of *Nmb* in nonpeptidergic nociceptors we combined *Nmb* FISH with immunostaining for Pap or binding of isolectin-B4, markers that exclusively label nonpeptidergic nociceptors. *Nmb* was expressed in nearly all DRG neurons that bind IB4 (49.20±2.98% of Nmb^+ neurons bind IB4; 98.47±0.25% of IB4-binding neurons express *Nmb*) or that are Pap^+ (72.61±2.79% of Nmb^+ neurons express Pap; 97.28±0.23% of Pap^+ neurons express *Nmb*) (Figure 6N-6U). Additionally, we examined the expression of *Nmb* in neurons that express the G-protein coupled receptor *MrgprD*, which comprise a large subset of nonpeptidergic nociceptors which mediate the sensation of mechanical pain (Cavanaugh et al., 2009). *Nmb* was expressed in all DRG neurons which express *MrgprD* (49.89±1.24% of Nmb^+ neurons express MrgprD; 100±0% of $MrgprD^+$ neurons express Nmb) (Figure 6V-6Y). Taken together, our data indicate that *Nmb* is expressed in nearly all peptidergic and nonpeptidergic nociceptors.

Nmb is expressed in itch-sensing neurons

Itch-sensing neurons have been suggested to be a subpopulation of nociceptors. We next asked whether *Nmb* is present in potential itch-sensing DRG neurons. The transient receptor potential channel TrpV1 was originally characterized as the channel mediating the burning sensation associated with capsaicin administration (Caterina et al., 1997). Additionally, $TrpV1^+$ neurons have been shown to play important roles in the detection of noxious heat and mediation of itch sensation in response to histaminergic stimuli (Imamachi et al., 2009; Shim et al., 2007). Double FISH revealed that *Nmb* is expressed in approximately half of $TrpV1^+$ DRG neurons (20.94±0.56% of Nmb^+ neurons express *TrpV1*; 53.72±3.66% of $TrpV1^+$ neurons express *Nmb*) (Figure 7A-D).

To further investigate the expression of *Nmb* in itch-sensing DRG neurons, we performed double FISH for *Nmb* and *MrgprA3*. MrgprA3 is a G-protein coupled receptor which is expressed in a subset of small diameter DRG neurons and is activated by chloroquine, a non-histaminergic pruritogen (Liu et al., 2009). Remarkably, we found that almost all $MrgprA3^+$ DRG neurons co-express *Nmb*, even though MrgprA3 is expressed in only a small proportion of Nmb^+ neurons(15.10±0.93% Nmb^+ neurons express *MrgprA3*; 99.19±0.81% $MrgprA3^+$ neurons express *Nmb*) (Figure 7E-H). In summary, our results suggest that *Nmb* is expressed in populations of DRG neurons that mediate itch sensation.

Nmb is not expressed in cold-sensing and low-threshold mechanosensory neurons

Subsets of small-diameter DRG neurons have been shown to respond optimally to various stimuli, including pruritogens, noxious thermal, mechanical, or chemical stimuli, innocuous temperature, or light touch. To test if the expression of *Nmb* is specific to pain- and itch-sensing neurons, we also performed double FISH for *Nmb* and molecular markers that identify temperature- or light touch-sensing neurons. One such marker is the transient receptor potential channel, TrpM8. TrpM8 has been shown to be important for the detection of environmental, but not noxious, cold (temperatures ~15°-26°C), and to be activated by chemicals which induce a cooling sensation, such as methanol and icilin (Dhaka et al., 2007). Interestingly, expression of *Nmb* is almost completely non-overlapping with that of *TrpM8* (0.08±0.08% Nmb^+ neurons express *TrpM8*; 0.61±0.61% of $TrpM8^+$ neurons express *Nmb*) (Figure 8A-D).

To further test our hypothesis that *Nmb* is specifically expressed in pain- and itch-sensing neurons, we compared the expression of *Nmb* to markers of low-threshold mechanosensitive neurons, which mediate the sensation of light touch, texture, form, vibration, and body position. Low-threshold mechanosensory neurons contain several different groups of DRG neurons, each of which have distinct molecular and developmental profiles. We examined the expression of *Nmb* with regard to three classes of low-threshold mechanosensitive neurons: Aδ low-threshold mechanoreceptors (Aδ LTMRs), c-fiber low-threshold mechanoreceptors (C-LTMRs), and proprioceptors.

Aδ LTMRs, which are also known as D-hair, express the neurotrophic tyrosine kinase receptor TrkB postnatally (Li et al., 2011). We found that the expression of *TrkB* and *Nmb* mRNA is completely non-overlapping in juvenile mouse DRG neurons (0±0% Nmb^+ neurons express *TrkB*; 0±0% $TrkB^+$ neurons express *Nmb*) (Figure 8E-8H). We also examined the overlap between *Nmb* and tyrosine hydroxylase (Th), a marker that is expressed postnatally in intermediately adapting, small-diameter C fiber LTMRs (Li et al., 2011). Even though most Nmb^+ neurons have small-diameter somata, we found minimal overlap between *Nmb* and Th expression (0.37±0.26% Nmb^+ neurons express Th; 1.64±1.09% Th^+ neurons express *Nmb*) (Figure 8I-8L). Moreover, we have shown in the previous section that *Nmb* is not expressed in large-diameter Ret^+ neurons, which are Aβ RA mechanoreceptors (Figure 6C). Taken together, our results strongly suggest that *Nmb* is not expressed in LTMRs, which is consistent with our hypothesis that *Nmb* is expressed exclusively in pain- and itch- sensing neurons.

We next examined the expression of *Nmb* in neurons which express the neurotrophic receptor tyrosine kinase TrkC, which is commonly used as a marker of proprioceptive and Aβ slowly adapting mechanosensitive DRG neurons. We found that a very small percentage of Nmb^+ neurons co-express *TrkC* (4.81±0.93% Nmb^+ neurons express *TrkC*; 22.86±1.16% $TrkC^+$ neurons express *Nmb*) (Figure 8M-8P). Attempts to further clarify whether *Nmb* is expressed in proprioceptors were unsuccessful, as another classical

immunohistochemical marker of proprioceptors, parvalbumin, did not work in combination with our *in-situ* hybridization protocol. At present, we are uncertain about the functional identity of these $Nmb^+/TrkC^+$ neurons. Nevertheless, our hypothesis that *Nmb* is specifically expressed in pain- and itch- sensing neurons should still be true, as $Nmb^+/TrkC^+$ neurons are only a very small percentage of total Nmb^+ neurons (less than 5%).

DISCUSSION

In this paper, we have presented evidence demonstrating that Grp, which has been proposed to act as a selective neurotransmitter of itching sensation from the DRG to the dSC, is also highly expressed in dSC neurons. In addition, we have found that Nmb, a homologue of Grp, is highly and selectively expressed in pain- and itch-sensing DRG neurons. Our anatomical characterization suggests that Grp can function intraspinally in dSC neurons in addition to its potential roles in DRG neurons and Nmb could play roles in pain- and itch-sensing neurons.

Grp is highly expressed in dSC neurons

By employing multiple methods to detect *Grp* mRNA and protein, we found that *Grp* is robustly expressed in dSC neurons. Even though a previous publication suggests that no *Grp* mRNA is detected in adult mouse spinal cord by *in situ* hybridization (Sun and

Chen, 2007), we detected abundant *Grp* mRNA in both juvenile and adult mouse dorsal spinal cord using *in situ* hybridization, RT-PCR, and real time PCR. We cannot make a comparison or suggest possible explanations for these different results because the *in situ* hybridization data of *Grp* in the previous publication is not shown. Nevertheless, our results are in line with the P4 *in situ* hybridization data of the Allen Mouse Spinal Cord Atlas, suggesting that the expression pattern of *Grp* in DRG and SC neurons is fairly stable from early postnatal days to adulthood (Allen Spinal Cord Atlas, 2016). Our results are also consistent with the P7 and adult *Grp* expression pattern provided by the St. Jude Brain Gene Expression Map (BGEM) using a radioactive *in situ* hybridization method (Magdaleno et al., 2006). Furthermore, *Grp* mRNA was shown to be highly expressed in dSC in adult rat (Wada et al., 1990). Taken together, our results and information from public databases strongly support the conclusion that *Grp* mRNA is highly expressed in postnatal dSC neurons.

In agreement with the low level of *Grp* mRNA found in DRG neurons (Figure 1B and (Allen Spinal Cord Atlas, 2016;Wada et al., 1990)), we only detected a small number of Grp^+ DRG neurons using immunostaining (Figure 3A-3G). The Grp^+ neurons we detected are much less than that found in a previous publication (8.6% of lumbar DRG neurons (Sun and Chen, 2007)). This difference could be due to different fixation conditions. Though we detected a robust level of Grp peptide in dSC neurons using immunostaining (Figure 3K, O, Q, S) , we barely detect any Grp in dorsal root nerve (Figure 3V), the only pathway between DRG neurons and dSC, indicating that the

amount of Grp synthesized and transported from DRG to dSC is minimal and below the detection level of our methods.

To further confirm the source of dSC Grp, we also conducted the dorsal root rhizotomy. Since proteins or peptides derived from DRG neurons need to be transported through the dorsal root, their presence in the spinal cord should dramatically decrease following central root rhizotomy. On the other hand, reduction of proteins or peptides that are primarily synthesized in dSC neurons should not be as dramatic. Indeed, we found ~80% decrease of markers originating from DRG neurons, such as Cgrp and Pap, and only found ~ 35% decrease of a spinal neuron marker, Pkcγ. Importantly, the change of dSC Grp is significantly different from DRG neuron derived markers but similar to that of Pkcγ (Figure 4S), suggesting that the majority of Grp is synthesized locally in dSC neurons. This result is consistent with the expression pattern of *Grp* mRNA. Taking all data into consideration, our results strongly argue that a majority of dSC Grp is synthesized locally in spinal cord neurons.

***Nmb* is specifically expressed in pain- and itch-sensing DRG neurons**

In contrast to *Grp*, we found that the other known mammalian bombesin peptide, *Nmb*, is highly expressed in DRG neurons. By co-staining with molecular markers for different modalities of somatosensory neurons, we found that *Nmb* is selectively expressed in pain- and itch-sensing neurons. This specific expression pattern suggests that Nmb may play a

role in these neurons. In addition to its potential role as a neurotransmitter in pain- and itch-sensing neurons, as discussed below, another interesting possibility is that DRG neuron derived Nmb may be released by peripheral axons and functions peripherally. In fact, we detected some expression of *Nmbr* in mouse glabrous skin by *in situ* hybridization (data not shown). Moreover, *Nmbr* mRNA levels were found to be increased following mechanical wounding and bombesin can promote keratinocyte mitosis and migration *in vitro* (Baroni et al., 2008). These observations and our anatomical characterization raise the intriguing possibility that Nmb could be released from free nerve terminals upon injury to promote skin regeneration and wound healing.

Neurotransmitter for itch-sensing somatosensory neurons

Which chemical do itch-sensing somatosensory neurons use as the pruritogenic neurotransmitter? This is an important question as a pruritogenic specific neurotransmitter would be a potential target for treating patients with pruritic disease. Some recent studies have proposed glutamate and Grp as two candidate neurotransmitters for itch-sensing somatosensory neurons (Koga et al., 2011; Lagerstrom et al., 2010; Liu et al., 2010; Sun and Chen, 2007). One anatomical requirement for a chemical to function as the pruritogenic neurotransmitter is that it is synthesized in DRG neurons, transported to dSC, and activates its receptor, which is expressed in postsynaptic neurons. We found that *Grp* mRNA is expressed at a low level in DRG neurons and a small amount of Grp is transported from DRG neurons to dSC. Interestingly, we found that a

high level of Grp is synthesized in dSC neurons, which may also contribute to normal itch perception by modulating the spinal cord local circuits. Future molecular and behavior analysis with *Grp* null or DRG vs. dSC specific *Grp* knockout mice will help to address the expression and function of DRG neuron and dSC neuron derived Grp.

On the other hand, Nmb, the other mammalian bombesin-related peptide, could be an interesting candidate neurotransmitter to modulate pain and itch sensation, given its high and selective expression in DRG neurons. Though we did not detect significant amount of *Nmbr* mRNA in dSC using *in situ* hybridization at P21, intrathecal injection of Nmb induces itching behavior (Su and Ko, 2011). This response may be conducted through Nmbr, which could be expressed in dSC at a low level. Alternatively, Nmb could be acting though Grpr, which Nmb can bind to with a low affinity (Jensen et al., 2008). Thus, a good antibody against Nmbr or behavior analysis with *Nmb* and *Nmbr* knockout mice in the future will help to address the localization of Nmbr and physiological roles of DRG neuron derived Nmb.

Conclusions

We have found that *Grp* transcript is highly expressed in dSC neurons and the majority dSC Grp is synthesized locally. On the other hand, *Grp* transcript is expressed at a low level in DRG neurons, and that the contribution of DRG neuron-derived Grp to the total amount of Grp observed in the dSC is relatively small. In addition, we have shown that

Nmb, the other mammalian bombesin-related peptide, is highly expressed in pain- and itch-sensing DRG neurons. Taken together, our results suggest that intraspinally synthesized Grp may have a local function in addition to potential functions of DRG neuron-derived Grp and that *Nmb* may play a role in itch- or pain-sensing neurons. This anatomical characterization of Grp and *Nmb* will improve our understanding about roles of Grp and Nmb in mediating itch sensation.

MATERIALS AND METHODS

Animals. Mice were raised in a barrier facility in the Hill Pavilion, University of Pennsylvania. All animal procedures were conducted according to animal protocols approved by the Institutional Animal Care and Use Committee (IACUC) of the University of Pennsylvania. For *in-situ* hybridization and antibody characterization studies, six P14-P21 wild type mice of both sexes with a mixed CD1/C57Bl/6J background were used. For RT-PCR experiments, four 4-6 month wild type mice of both sexes with a mixed CD1/C57Bl/6J background were used. For dorsal rhizotomy experiments, we used *2* month old C57Bl/6J mice of either sex and the survival surgery was conducted in Shriners Hospitals Pediatric Research Center, Temple University. All surgical and postoperative procedures were performed in accordance with Temple's Institutional Animal Care and Use Committee and National Institutes of Health guidelines.

***In situ* hybridization.** DIG-labeled riboprobes were synthesized using a DIG RNA labeling kit (Roche, 11175025910). Template for Nmb probe was amplified from a mouse DRG cDNA library (BD, Ref#630022) and subcloned into vector pGEM-T Easy (Promega, A1360). Mouse IMAGE clones for Grp (GenBank: BC024515), Grpr (GenBank: BC113145), and Nmbr (GenBank: BC119237) were purchased from Open Biosystems, and PCR products were subcloned into pGEM-T Easy. Primers used to amplify cDNA were: Nmb (5'-GGCAAGCAGGGAGCTCTT-3' and 5'-CTGGTGACCCAACCAGAA-3'), Grp (5'-CACGGTCCTGGCTAAGATGTAT-3' and 5'-CCAGTAGAGTTGACGTTTGCAGA-3'), Nmbr (5'-AGGTCTCTCTCCAACCTCTCCT-3' and 5'-ACCAGAACAATCTTAGCCAGGCG-3'), and Grpr (5'-ATGGCTCCAAATAATTGTTCCCA-3' and 5'-TTTAGTCTAGACATACCCCTCAT-3'). FITC-labeled probes for c-Ret, TrkB, TrkC, TrpV1, MrgprA3, MrgprD, and TrpM8 were generated as previously described (Dong et al., 2001; Luo et al., 2007).

Intact lumbar spinal column was dissected from euthanized wild-type P14-P21 mice and rapidly frozen in OCT on a dry-ice/ethanol bath. 20µm cryosections were collected on Superfrost Plus slides (Fisher, 22-034-979) and allowed to dry for at least 2 hours at room temperature before *in-situ* hybridization. All steps prior to hybridization were carried out under RNase free conditions. Cryosections were immersion-fixed in freshly made 4% PFA in PBS for 20 minutes at room temperature. Slides were then washed in fresh-DEPC PBS (1:1000 DEPC in PBS immediately before use), followed by wash in DEPC-

pretreated PBS (1:1000 DEPC in PBS overnight (O/N), followed by autoclaving). An antigen retrieval step, often used for immunohistochemistry, was found to increase the signal of many probes. Citric acid buffer (10mM citric acid, 0.05% Tween-20, pH6.0) was boiled in a microwave, and DEPC (1:1000) was added to freshly boiled solution. Slides were immersed in solution in a 95°C waterbath for 20 minutes, and then allowed to cool at room temperature for 30 minutes. Sections were then washed in DEPC pretreated PBS (1X 5 minutes), incubated in Proteinase K (25µg/mL in DEPC-pretreated H_2O) for five minutes, followed by washes in fresh-DEPC PBS (1X 5 minutes) and DEPC pre-treated PBS (1X 5 minutes). Sections were then acetylated at room temperature for ten minutes in freshly made acetylation solution (0.1M triethanolamine, 0.25% acetic anhydride in DEPC pre-treated H_2O). Slides were then prehybridized in hybridization buffer (50% formamide, 5XSSC, 0.3mg/mL yeast tRNA, 100µg/mL heparin, 1X Denhardt's, 0.1% Tween-20, 0.1% CHAPS, 5mM EDTA in RNase free H_2O) at 62°C in a humidified chamber for 30 minutes. Following prehybridization, excess hybridization buffer was removed from slides and 1-2ng/µl of DIG and/or FITC labeled riboprobe diluted in hybridization buffer was placed on the slide. Slides were incubated O/N under Parafilm coverslips at 62°C. Slides were then washed in 0.2X SSC at 68°C (1X 15 minutes, 2X 30 minutes).

For colorimetric reaction, slides were blocked in PBT (PBS, 0.1% TritonX-100) and 20% lamb serum at room temperature for one hour. Sections were then incubated with AP-conjugated anti-DIG antibody (1:1000; Roche, 11093274910) in blocking buffer O/N at

4°C. Slides were washed in PBT (3X 10 minutes) and incubated O/N in darkness in alkaline phosphatase buffer (100mM Tris pH9.5, 50mM $MgCl_2$, 100mM NaCl, 0.1% Tween-20, 5mM levamisole, 0.34mg/mL 4-Nitro blue tetrazolium (NBT)(Roche, 11383213001), 0.17mg/mL 5-bromo-4-chloro-3-indolyl-phosphate(BCIP)(Roche, 1138221001)). Following color reaction, slides were rinsed repeatedly in PBS and then fixed for 20 minutes in 4% PFA in PBS at room temperature. Slides were then repeatedly rinsed in ddH_2O, dried at 37°C for 1 hour, dehydrated in xylenes (3X 2 minutes), and coverslipped with Permount (Fisher, SP15).

For double fluorescent in-situ hybridization (FISH), slides were blocked for one hour at room temperature with 0.5% Blocking Reagent (Roche, 11096176001) in PBS. Sections were incubated in anti-FITC-POD (1:100 in .5% Blocking Reagent; Roche, 11426346910) O/N at 4°C. Slides were then washed in PBT (3X10 minutes) and incubated in 0.1% BSA in PBS for 15 minutes. FITC riboprobes were then developed using the TSA Plus system (Perkin Elmer, NEL741001KT), by diluting fluorescein tyramide into 1X amplification buffer (1:100) and incubating slides in working solution for 10-15 minutes, followed by washes in PBS (3X 10 minutes). Slides were then blocked in PBT containing 20% lamb serum for 1 hour at room temperature, and incubated O/N at 4°C with AP-conjugated anti-DIG antibody (1:500 in PBT +20% lamb serum). Slides were washed in TNT (100mM Tris-HCl, 150mM NaCl, 0.05% Tween-20, pH7.5) (3X 10 minutes), then in detection buffer (100mM Tris-HCl, 100mM NaCl, 10mM $MgCl_2$, pH8.0) (2X 10 minutes). DIG-labeled riboprobes were then developed

using HNPP/Fast Red TR system (Roche, 11758888001). Sections were incubated in detection solution (10µL HNPP stock solution, 10µL of 25mg/mL FastRed per 1mL of detection buffer, filtered through 0.2µM nylon filter) (3x30 minutes), with TNT rinses between incubations. Slides were then rinsed in PBS and mounted with Flourmount (Southern Biotech, 0100-01).

For FISH combined with immunofluorescence, normal hybridization procedure was followed, using DIG-labeled probe. After 0.2X SSC washes, sections were blocked for one hour in PBT containing 20% lamb serum. Sections were then incubated with AP-conjugated anti-DIG (1:500) and primary antibody at the appropriate dilution (described below) at 4°C O/N in 20% lamb serum blocking solution. Slides were washed in PBT (3X 10 minutes), then incubated in species appropriate Alexa 488 conjugated secondary antibody (1:500 in 5% lamb serum in PBT) for one hour at RT. HNPP/FastRed detection was then performed as described above, beginning with initial TNT washes.

Immunohistochemistry. For characterization of anti-bombesin antibody, P14-P21 mice were deeply anesthetized with CO_2 and perfused with 4% PFA in PBS. Intact lumbar spinal columns were dissected and post-fixed for 2-4 hours in 4% PFA in PBS at 4°C, cryoprotected in 30% sucrose in PBS O/N at 4°C, and embedded in OCT. 20µm cryosections of lumbar spinal cord and DRG were collected on Superfrost Plus slides, and allowed to dry at room temperature for at least two hours. For dorsal rhizotomy samples, 30µm free floating cryosections were collected in PBT and processed for

immunohistochemistry in solution. Sections were washed in PBT (3X 10 minutes), and then blocked in PBS containing 5% lamb serum and 0.3% TritonX-100 for 1 hour at room temperature. Primary antibodies were diluted in the same buffer, and incubated O/N at 4°C, then washed in PBT (3X 10 minutes). Secondary antibodies were incubated in blocking buffer at 1:1000 dilution for one hour at room temperature. Slides were then washed in PBT (3X 10 minutes) and mounted with Flourmount. Primary antibodies used include rabbit anti-bombesin (1:1000; ImmunoStar, 20073), chicken anti-Gfp (1:2000; Aves, GFP-1020), guinea pig anti-Cgrp (1:250; Bachem, T-5053), mouse anti-Pkcγ (1:50, Invitrogen, 13-3800), chicken anti-Pap (1:1000; Aves, PAP), rabbit anti-peripherin (1:1000; Millipore, AB1530), rabbit anti-Nfh (1:2000; Sigma, N4142), rabbit anti-TrkA (1:1000; Millipore, 06-574), rabbit anti-tyrosine hydroxylase (1:100; Millipore, AB152), mouse anti-NeuN (1:1000, Millipore, MAB377), and Alexa 488 conjugated IB4 (1:200; Invitrogen, I21411). Secondary antibodies used were Alexa 488, Alexa 594, or Alexa 647 conjugated goat anti-rabbit antibody, Alexa 488 conjugated goat anti-mouse antibody, Alexa 488 conjugated goat anti-chicken antibody, and Alexa 488 conjugated goat anti-guinea pig antibody. All secondary antibodies were purchased from Invitrogen.

Peptide Preabsorption. Anti-bombesin and anti-Cgrp antibodies at the concentrations described above were added to PBS containing 5% lamb serum, 0.3% TritonX-100, and bombesin peptide (50µg/mL; American Peptide Company, 16-7-10A) or GRP peptide (50µg/mL; American Peptide Company, 62-3-10) and incubated O/N at 4°C with gentle

agitation. Solutions were centrifuged at high speed (~16,000 x g) for ten minutes, and supernatant was used for immunohistochemistry, as described above.

Reverse transcriptase PCR. 4-6 month old wild type mice were deeply anesthetized with CO_2, transcardially perfused with sterile, RNAse free, ice-cold PBS, then decapitated. Lumbar and thoracic DRGs and dorsal spinal cord were dissected under RNase free conditions and rapidly frozen on dry ice. RNA was isolated using the GeneJet RNA Purification Kit (Fermentas, K0731), and cDNA was synthesized with oligo-dt primers using the SuperScript First-Strand Synthesis system (Invitrogen, 11904018). PCR was performed on cDNA synthesized from DRG or dorsal spinal cord cDNA with primers for Nmb (5'- CCGAGGGACCAGAGACTACA-3' and 5'-ACTTCACCAGGGAAGCAAGA), Grp (5'-CACGGTCCTGGCTAAGATGTAT-3' and 5'-CCAGTAGAGTTGACGTTTGCAGA-3'), Nmbr (5'-AGGTCTCTCTCCAACCTCTCCT-3' and 5'-ACCAGAACAATCTTAGCCAGGCG-3'), Grpr (5'-ATGGCTCCAAATAATTGTTCCCA-3' and 5'-TTTAGTCTAGACATACCCCTCAT-3'), and Gapdh (5'-GGTGAAGGTCGGTGTGAACG-3' and 5'-CTCGCTCCTGGAAGATGGTG-3').

Real time PCR. *Grp* mRNA from DRG or dSC were measured by quantitative real-time PCR under the ABI 7500 Fast Real-Time PCR system (Applied Biosystems, Foster City, CA), with *Gapdh* as an internal reference gene. The reaction mixture contained 250 nM

of each primer, 1×SYBR Green PCR Master Mix (ABI), and 1µl of cDNA. Relative concentration of *Grp* present in each cDNA sample was calculated by the comparative C(T) method (Schmittgen and Livak, 2008). Real time PCR was performed on cDNA isolated from three adult wild type mice, and was repeated four times per sample. Primers used were Grp primers listed above, and Gapdh (5'-TCGGTGTGAACGGATTTGGC-3'and 5'- TCCCATTCTCGGCTTGACT-3').

Plasmid construction. Plasmids were constructed to express bombesin, Grp, or Nmb fused to the C terminus of EGFP. The coding regions of the peptides were constructed by annealing oligonucleotides coding for the open reading frame of each peptide with EcoRI (5') and SalI (3') sticky ends. Primers used for this procedure were: bombesin (5-AATTCCAGCAGAGGCTGGGGAATCAGTGGGCAGTGGGTCACTTGATGTGAG-3' and 5'-TCGACTCACATCAAGTGACCCACTGCCCACTGATTCCCCAGCCTCTGCTGG-3') Grp (5'-AATTCATGTATCCGCGCGGCAGTCACTGGGCTGTGGGACACTTAATGTGAG-3' and 5'-TCGACTCACATTAAGTGTCCCACAGCCCAGTGACTGCCGCGCGGATACATG-3') and Nmb (5'AATTCGGCAACCTCTGGGCGACCGGTCACTTCATGTGAG-3' and 5'-TCGACTCACATGAAGTGACCGGTCGCCCAGAGGTTGCCG-3'). Oligonucleotides were phosphorylated with T4 polynucleotide kinase (PNK) (NEB, M0201) for 20 minutes at 37°C, and then PNK was heat inactivated at 65°C for 20

minutes. Phosphorylated oligonucleotides were annealed by heating to 95°C for five minutes, then allowing them to cool to room temperature. Annealed oligonucleotides were then ligated into pPMS93 (a gift from Dr. Jeremy Nathans lab at Johns Hopkins University, CMV promoter to drive the expression of EGFP C-terminal fusion protein) pre-digested with EcoRI and SalI. Ligated plasmids were transformed into DH5-α, and grown overnight at 37°C on agarose plates supplemented with 100µg/mL carbenicillin. Individual colonies were then selected and grown overnight in 2XYT containing 100µg/mL carbenicillin, and then mini-prepped (Fermentas, K0503). Correct insertions were confirmed by DNA sequencing.

Cell culture and immunocytochemistry. QBI HEK293 cells were grown on 12mm circle coverslips in HEK293 growth media (10% FBS (Invitrogen, 10082147), 1% Penicillin/Streptomycin (Invitrogen, 15140122) in DMEM (Invitrogen, 11965084)) in 6-well tissue culture plates. Coverslips were coated with 100µg/mL poly-D-lysine solution to help cell adhesion. Individual cultures were transfected with 1µg/mL of pRK5-EGFP, pPMS-bombesin, pPMS-Grp, or pPMS-Nmb EGFP fusion plasmid with Lipofectamine LTX (Invitrogen, 15338100). Eighteen to twenty four hours after transfection, coverslips were then rinsed gently with PBS and fixed in 4% PFA in PBS for 1.5 hours at room temperature. Coverslips were then processed for immunohistochemistry as described above.

Dorsal root rhizotomy and postoperative procedures. The surgical procedure was standard (Di Maio et al., 2011). Mice were anesthetized with an intraperitoneal injection of xylazine (8 mg/kg) and ketamine (120 mg/kg). Supplements were given during the procedure as necessary. A 2- to 3-cm-long incision was made in the skin of the back; the spinal musculature was reflected; and the L5 spinal cord segments were exposed by hemi-laminectomies. The cavity made by the laminectomies was perfused with warm sterile Ringer's solution. A small incision was made in the dura overlying the L3-L5 dorsal roots; a fine spring scissor (501778, World Precision Instruments) was introduced subdurally and L4, L5, and L6 dorsal roots were cut. The laminectomy site was covered with a piece of thin synthetic matrix membrane (Biobrane, Bertek Pharmaceuticals), which was then stabilized with a layer of thicker artificial dura (Gore Preclude MVP Dura Substitute, W.L. Gore and Associates). Animals are given subcutaneous injections of lactated Ringer's solution to prevent dehydration and are kept on a heating pad until fully recovered from anesthesia. Buprenex is given as post-operative analgesia (0.05mg/kg S.C. every 12 hours for 2 days). On the 15^{th} day after dorsal rhizotomy, mice were perfused transcardially with 0.9% heparinized saline solution followed by 4% paraformaldehyde in PBS.

Imaging. All images were acquired on a Leica DM5000B or Leica TCS SP5 II and processed using Adobe Photoshop CCS version 12.0.

Quantification and Statistics. For dorsal rhizotomy experiments, adjacent sections of the spinal cord lumbar enlargement were used for different marker staining. Images of each dorsal horn of individual sections were acquired using identical exposure conditions. Using ImageJ, the bombesin reactive and Cgrp, Pkcγ, or Pap (costain) reactive regions of dorsal spinal cord were outlined. Pixel counts for each fluorescence intensity value (0-255) within the outlined region were generated by ImageJ. In addition, background pixel intensity values were generated from a non-reactive area of the dorsal spinal cord for each image. Background pixel counts were clustered around low intensity values and showed a normal distribution, and the threshold for background fluorescence cutoff was established as the first highest intensity value that had a pixel count of zero. To calculate total fluorescence intensity, the pixel count for each intensity above background level was multiplied by its intensity, and the results of these calculations were summed. In cases where the immunostaining signal was greatly reduced on transected side, the stain area was approximated based on the control side. The difference between the control and transected side was calculated as percentage change in fluorescent intensity ([fluorescent intensity transected/fluorescent intensity control]*100). This value was calculated for three sections per marker per animal. The average and SEM for each marker across all sections was calculated, and P-values were calculated using a two-tailed student's t-test.

Cell size calculations. ImageJ software was used to calculate size of DRG neurons. All images were taken at 20x magnification. To avoid bias in counting, the first 25 positive cells in each image from left to right were counted. In total, 225 cells per marker were

counted (n=3 animals, 9 DRG per animal). Using ImageJ, cells were outlined using the lasso tool and the area was obtained. For graphical representation, cells were divided into $100um^2$ bins.

Expression profile quantification. Expression profile of Nmb^+ DRG neurons was evaluated by counting the number of cells that were positive for Nmb, co-staining markers, or both in 3 wild-type P14-P21 animals (6-8 lumbar DRG sections per animal). Total number of positive cells in each category was calculated for each animal, and the percentages of double positive neurons with regard to total Nmb^+ neurons (Nmb^+; $costain^+$ /total Nmb^+) or to total co-staining-marker-positive neurons (Nmb^+; $costain^+$ positive/total $costain^+$) were calculated. The average and SEM of these percentages between animals were then calculated.

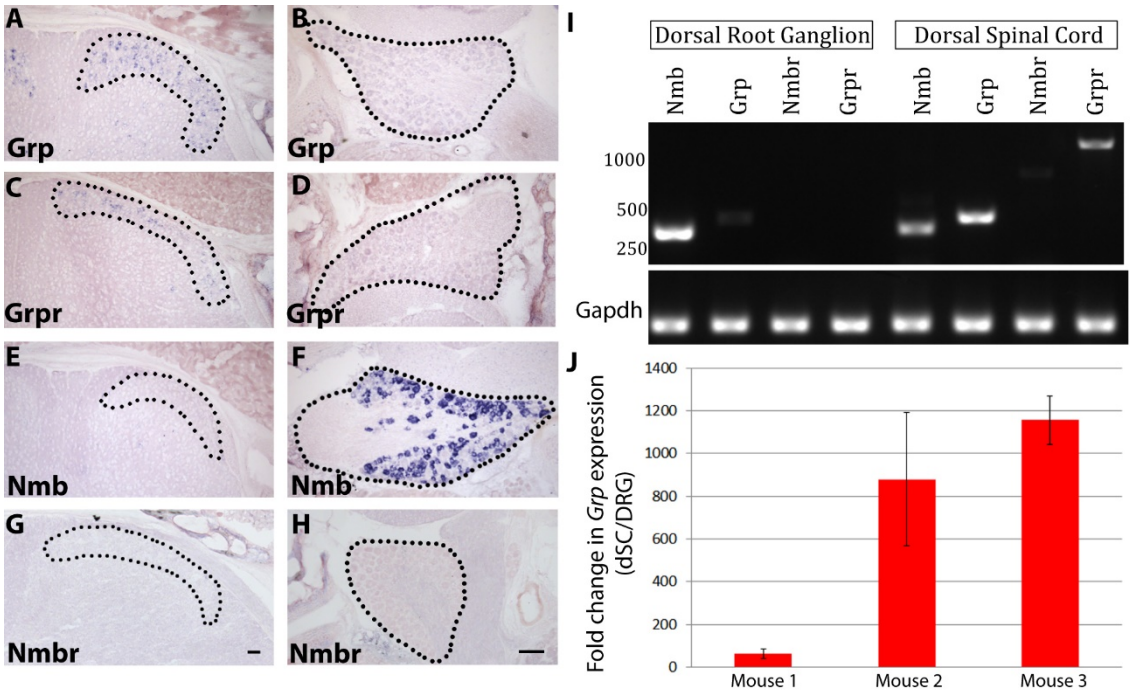

Figure 1: Expression of *Grp*, *Grpr*, *Nmb*, and *Nmbr* mRNA in dSC and DRG neurons. (A-H) *in situ* hybridization with P21 wild type mouse dSC and DRG for *Grp* **(A-B)**, *Grpr* **(C-D)**, *Nmb* **(E-F)**, and *Nmbr* **(G-H)**. dSC and DRGs are outlined with black dots. Scale bars=50 µm. **(I)** RT-PCR performed on RNA acutely isolated from wild type adult mouse dSC and DRG. cDNA was amplified with primers specific for *Nmb*, *Grp*, *Nmbr*, and *Grpr*. Lower bands are cDNA amplified with primers specific for *Gapdh*, which served as a loading control. **(J)** Graphical representation of real time RT-PCR for *Grp* performed on dSC and DRG RNA isolated from adult mice (n=3 animals, 4 replicates per animal). Quantification represents fold difference between dSC Grp relative to that of DRG. Relative abundance of cDNA was calculated in comparison to Gapdh housekeeping gene by the $2^{(-\Delta\Delta C_T)}$ method (see details in method).

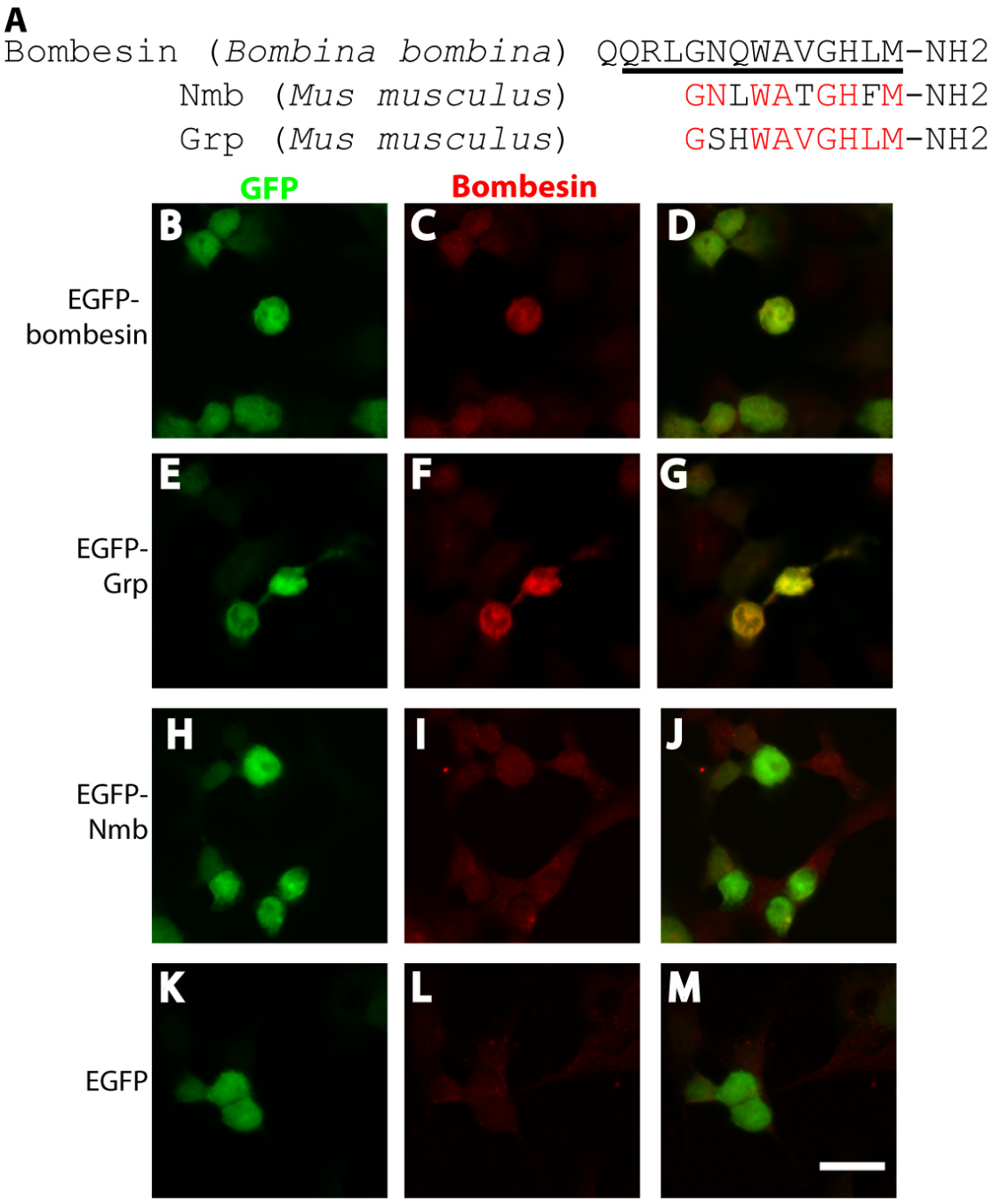

Figure 2: *In vitro* characterization of anti-bombesin antiserum specificity. (A) Alignment of *Bombina bombina* bombesin, *Mus musculus* Grp, and *Mus musculus* Nmb peptide sequences. Black bar underneath the bombesin peptide sequence indicates the immunizing peptide used for developing the rabbit anti-bombesin antiserum. Grp and Nmb residues that share identity with the immunizing peptide are highlighted in red. **(B-M)** HEK293 cells were transfected with EGFP-bombesin (B-D), EGFP-Grp (E-G), EGFP-Nmb (H-J), or EGFP alone (K-M) and immunostained with anti-bombesin antiserum (red) and anti-GFP antibody (green). Scale bar= 25µm.

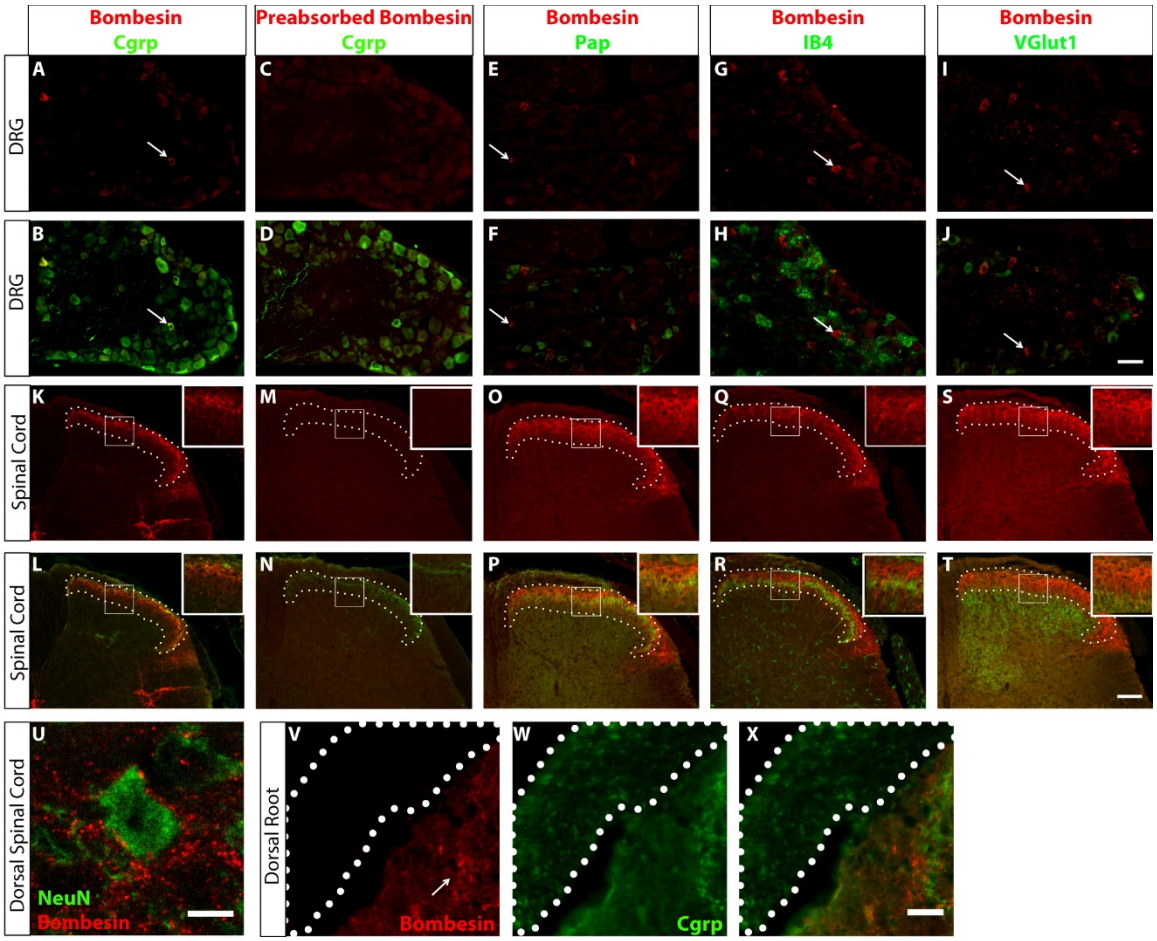

Figure 3: Characterizing the localization of Grp in DRG, spinal cord, and dorsal root using anti-bombesin antiserum. **(A-B)** DRGs immunostained with antibodies against bombesin (red) and Cgrp (green). Arrow indicates a bombesin^{+};Cgrp^{+} neuron. **(C-D)** DRG neurons in adjacent sections are immunostained with anti-bombesin antiserum preabsorbed with purified Grp (red) and anti-Cgrp antibody (green). Preabsorption results in a complete loss of anti-bombesin immunoreactivity. **(E-F)** DRG neurons immunostained with antibodies against bombesin (red) and Pap (green). **(G-H)** DRG neurons immunostained with anti-bombesin anti-serum (red) and fluorescently-conjugated IB4 (green). **(I-J)** DRG neurons immunostained with antibodies against bombesin (red) and VGlut1 (green). Arrows in (E-J) indicate bombesin^{+} neurons that are not immunopositive for the costaining marker. **(K-L)** dSC section immunostained with antibodies against bombesin (red) and Cgrp (green). The dSC layers positive for bombesin are outlined with white dots and higher magnification of the staining is shown in the inset. **(M-N)** dSC section immunostained with anti-bombesin antiserum preabsorbed with purified Grp (red) and anti-Cgrp antibody (green), showing a complete loss of anti-bombesin immunoreactivity. **(O-P)** dSC section immunostained with antibodies against bombesin (red) and Pap (green). **(Q-R)** dSC section immunostained with anti-bombesin serum (red) and fluorescently-conjugated IB4 (green). **(S-T)** dSC

section immunostained with antibodies against bombesin (red) and VGlut1 (green). **(U)** A high magnification confocal image of adult dSC immunostained with anti-bombesin (red) and anti-NeuN (green). **(V-X)** A higher magnification of wild type adult dorsal root immunostained with antibodies against bombesin (red) and Cgrp (green) reveals the presence of Cgrp, but not Grp, in axons projecting from the DRG to dSC. Dorsal root is outlined by dotted line. Arrow indicates the dSC anti-bombesin immunoreactivity. Scale bars= 50µm (A-J), 100µm (K-T), 5µm (U), 30µm (V-X).

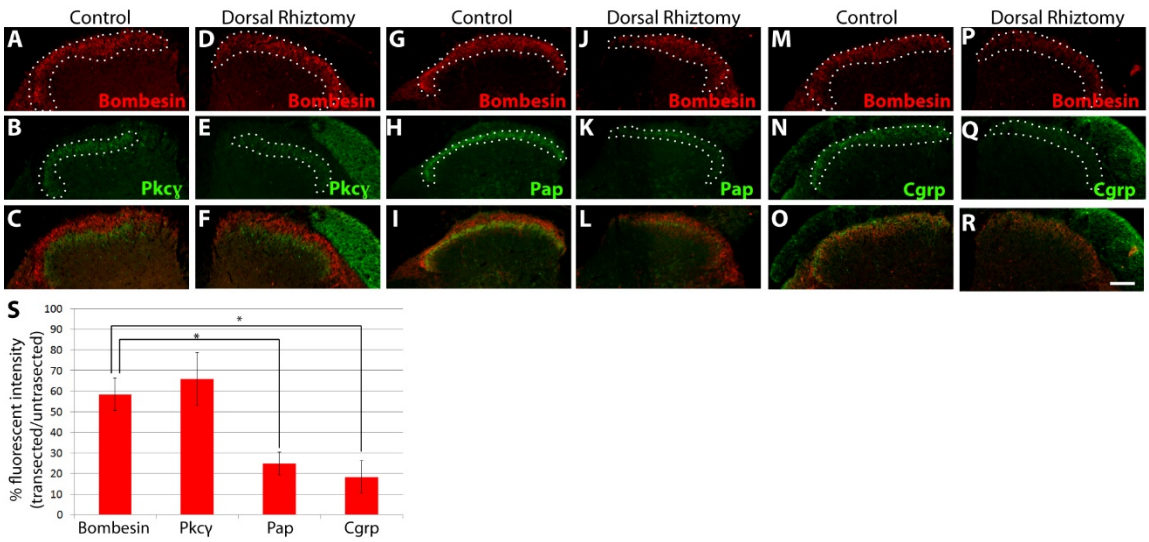

Figure 4: Dorsal root rhizotomy causes a dramatic loss of Pap and Cgrp but significantly smaller changes of bombesin and Pkcγ in dSC. L4, L5, and L6 central roots of two month old wild type mice were transected, and mice were examined two weeks following surgery. Sections of the lumbar enlargement were immunostained to examine the loss of proteins and peptides caused by dorsal root axonal degeneration and the contralateral side of the same spinal cord section was used as the control. **(A-F)** Sections were immunostained with antibodies against bombesin (red) and Pkcγ (green), a protein highly synthesized in dSC neurons (control side (A-C) and transected side (D-F)). Comparable and modest loss of both bombesin and Pkcγ immunoreactivity are found after the dorsal root rhizotomy. Enhanced green fluorescence and abnormal morphology of the transected dorsal root were also noted, which may be caused by axonal inflammation after injury. **(G-L)** Sections immunostained with antibodies against bombesin (red) and Pap (green). As noted, dSC Pap is dramatically decreased after the dorsal root rhizotomy. **(M-R)** Sections immunostained with antibodies against bombesin (red) and Cgrp (green), another marker derived from DRG neurons. Similar to Pap, dSC Cgrp is also greatly reduced following the dorsal root rhizotomy. Scale bar= 100µm. **(S)** Quantification and statistical analysis of dynamic changes of dSC Grp, Pkcγ, Pap, and Cgrp following the dorsal root rhizotomy. The loss of dSC Grp after dorsal root rhizotomy is significantly different from those of Pap and Cgrp ($P < 0.01$), and the same is true for dSC Pkcγ. In contrast, no significant differences are found between Grp and Pkcγ ($P=0.44$) or Pap and Cgrp ($P=0.25$).

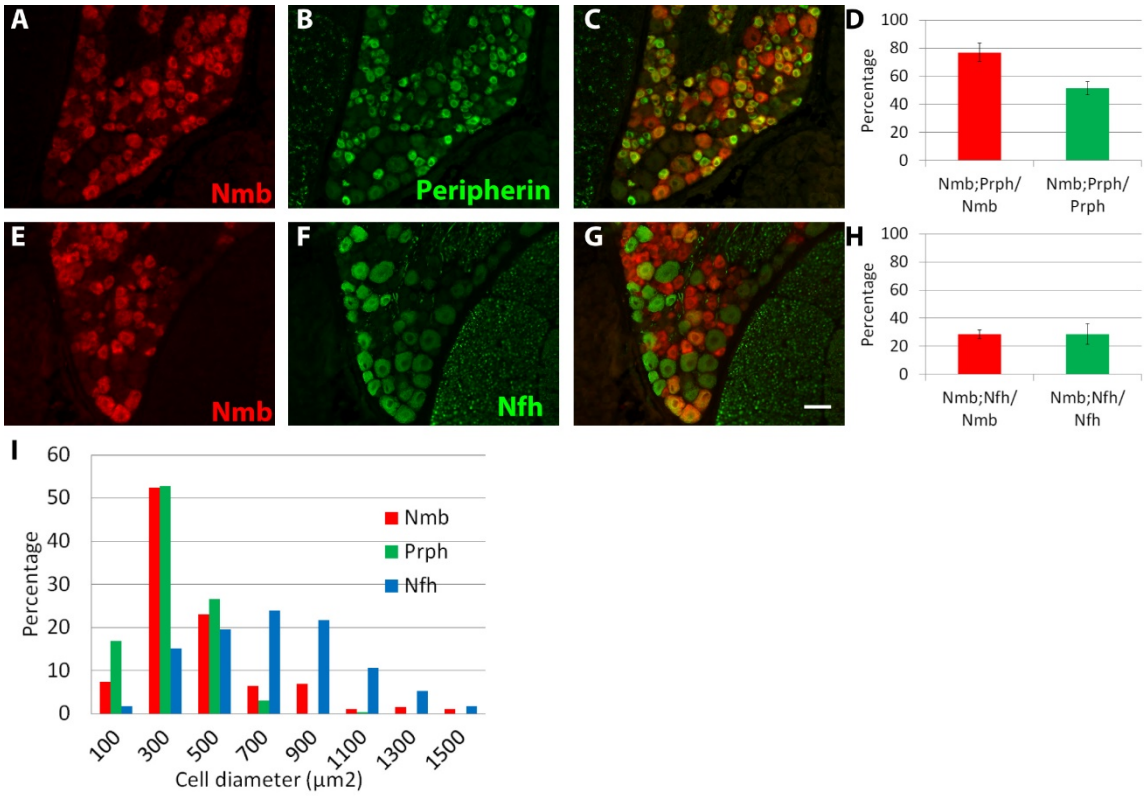

Figure 5: *Nmb* is expressed in small and large diameter DRG neurons. (A-D) FISH for *Nmb* (red) and immunostaining for peripherin (green), an intermediate filament that is present in small diameter DRG neurons. Histogram shows the percentage of Nmb^+ neurons that express peripherin (red bar) and the percentage of $Peripherin^+$ neurons that express Nmb (green bar). Mean ± SEM. **(E-H)** FISH for *Nmb* (red) and immunostaining for NF200 (green), a marker of large diameter myelinated neurons, and quantification of overlapping expression. Scale bar= 50µm **(I)** Distribution of soma sizes of Nmb^+, $Peripherin^+$, and $NF200^+$ DRG neurons, in 100μm^2 bins.

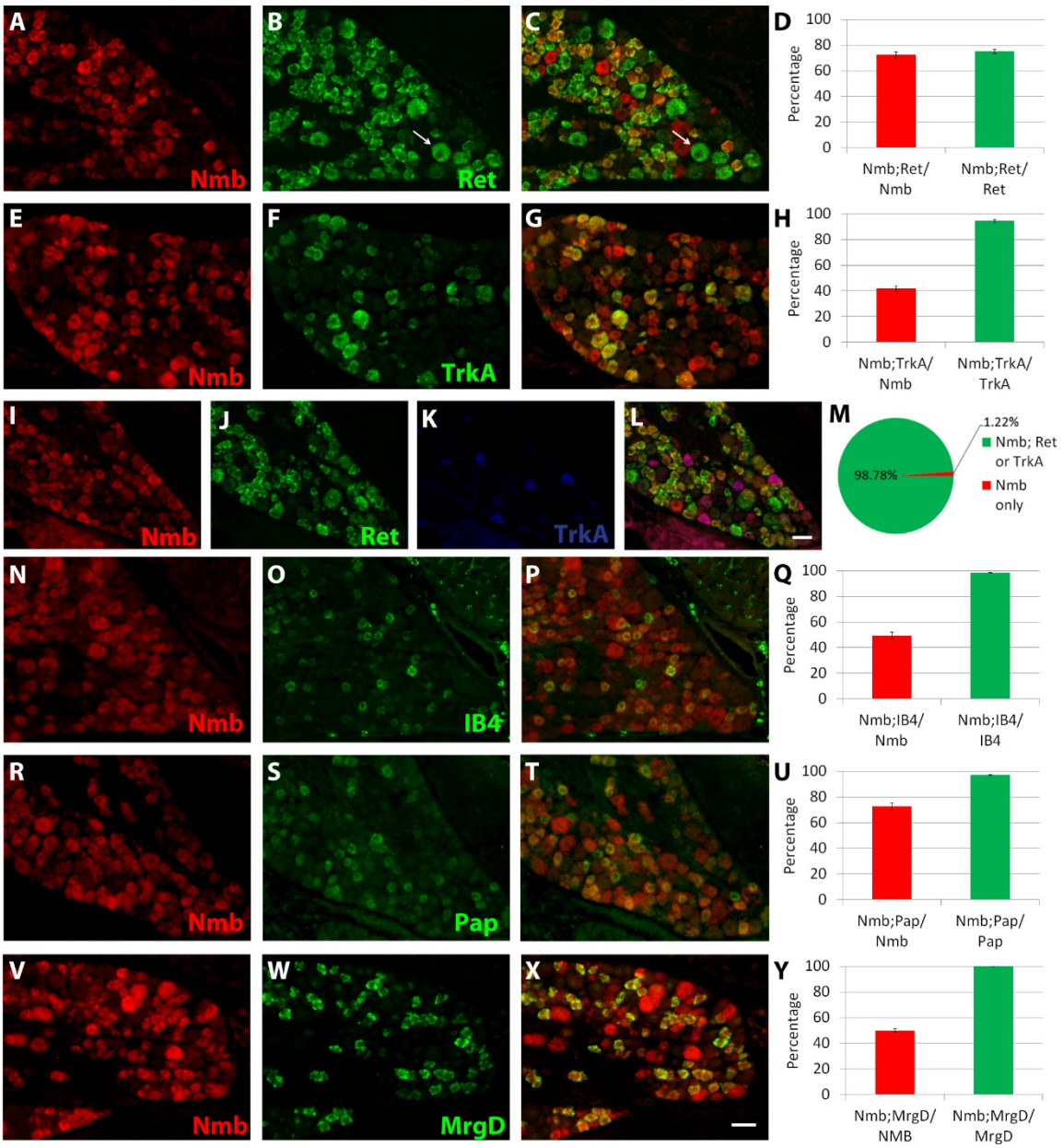

Figure 6: *Nmb* is expressed in peptidergic and nonpeptidergic nociceptors. (A-D) FISH for *Nmb* (red) and *Ret* (green), a marker for small diameter nonpeptidergic nociceptors and RA mechanoreceptors. Arrow indicates a large diameter, Ret^+ neuron, all of which are Nmb^-. **(E-H)** FISH for *Nmb* (red) and *TrkA* (green), a marker for peptidergic nociceptors. **(I-M)** FISH for *Nmb* (red) and *Ret* (green), combined with immunostaining for TrkA (blue). Quantification shows the percentages of Nmb^+ neurons which also express Ret or TrkA (green), or which express neither marker (red). **(N-Q)** FISH for *Nmb* (red) and binding of IB4 (green). **(R-U)** FISH for *Nmb* (red) combined with immunostaining for Pap (green). **(V-Y)** FISH for *Nmb* (red) and *MrgprD* (green). Scale bar= 50µm

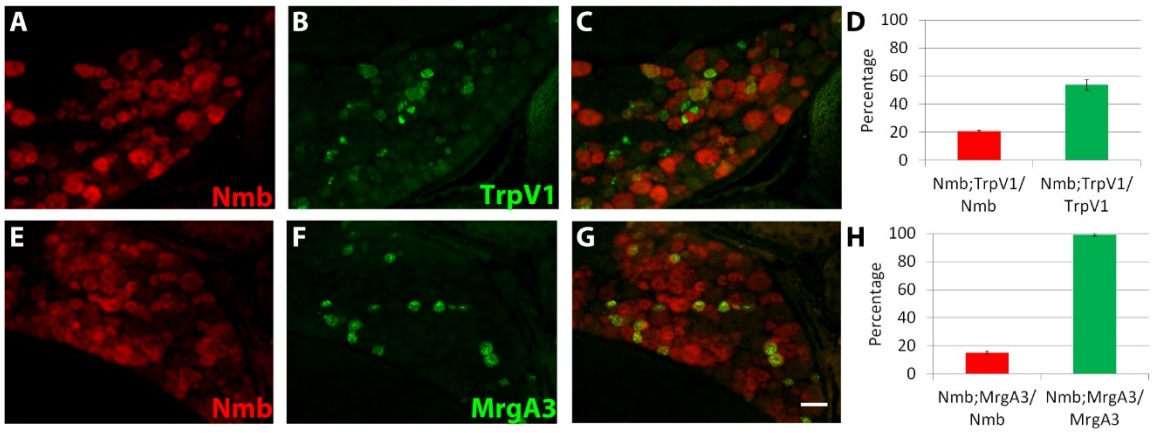

Figure 7: *Nmb* is expressed in itch-sensitive DRG neurons. **(A-D)** FISH for *Nmb* (red) and *TrpV1* (green), a marker of neurons responding to noxious and histaminergic itch stimuli. **(E-H)** FISH for *Nmb* (red) and *MrgprA3* (green), a marker of neurons responding to nonhistaminergic itch. Scale bar= 50µm

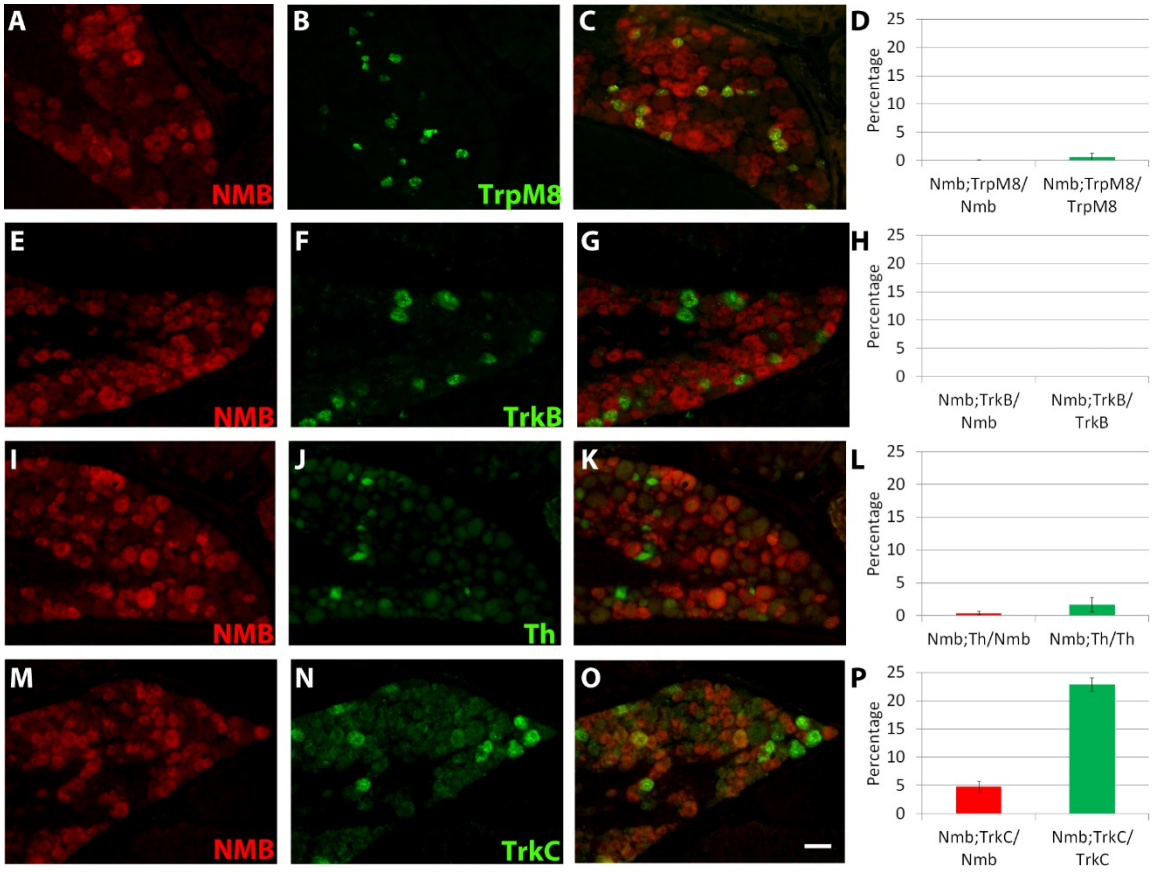

Figure 8: *Nmb* is not expressed in DRG neurons responding to innocuous thermal or mechanical stimuli. (A-D) FISH for *Nmb* (red) and *TrpM8* (green), a marker of neurons responding to innocuous cold stimuli. **(E-H)** FISH for *Nmb* (red) and *TrkB* (green), a marker of Aδ LTMRs. **(I-L)** FISH for *Nmb* (red) and *TH* (green), a marker of a population of intermediately adapting C fiber LTMRs. **(M-P)** FISH for *Nmb* (red) and *TrkC* (green), a marker of slowly adapting mechanoreceptors and proprioceptors. Scale bar= 50µm

CHAPTER 5

Conclusions and Future Directions

THE DISTINCTION BETWEEN *CIS* AND *TRANS* RET SIGNLAING

In Chapter 2, we demonstrated that either *cis* or *trans* RET signaling is sufficient for RA mechanoreceptors to grow to their termination zone in the dorsal spinal cord. Previous studies have suggested that *cis* and *trans* RET signaling may lead to activation of distinct downstream processes (Paratcha et al., 2001; Tansey et al., 2000). Additionally, a "*cis*-only" mouse model, in which *Gfra1* is expressed in all Ret^{+} cells in an otherwise *Gfra1* null background showed no developmental deficits in many RET-dependent developmental processes (Enomoto et al., 2004). However, in the particular developmental process examined here, both *cis* and *trans* signaling produce the same cellular output, suggesting they may be functionally interchangeable in vivo. It is currently unclear whether *trans* signaling alone this will be sufficient for other RET-dependent developmental processes.

One observation in our studies which suggests *cis* and *trans* activation may be interchangeable relates to the constitutive release of GFRα co-receptors. Conditioned media from cultured DRG neurons contained high levels of both GFRα1 and GFRα2. Another recent study has shown that GFRα1 can be released from neuronal membranes not only via cleavage of the GPI-tether by phospholipases, but also by matrix metalloproteinases (Tsui et al., 2015). Therefore, it is possible that under basal conditions, GFRα co-receptors are rapidly processed and released from the membrane. If

so, "*cis*" expressed GFRα may commonly be shed by the cell and interact with RET in a manner similar to GFRα expressed in *trans* from a neighboring cell.

The generation of a "*trans*-only" mouse model could further clarify whether *cis* and *trans* RET signaling are interchangeable for development in vivo. The GFRα1 pro-protein contains an n-terminal ER targeting sequence for entrance into the secretory pathway and a c-terminal GPI signal sequence which interacts with the GPI-transamidase complex (Eisenhaber et al., 1999). This c-terminal domain is then cleaved from the protein and the GPI anchor is covalently linked to the c-terminal amino acid (S436 in GFRα1). If the GPI signal sequence is removed from the pro-protein, GFRα1 will not become GPI-anchored and will be constitutively secreted. GFRα1Δ437 lacks a GPI signal sequence and cannot interact with the transamidase complex, and has been shown to be biologically active *in trans* in vitro (Worley et al., 2000). Additionally, I have performed preliminary biochemical and immunostaining experiments to demonstrate that GFRα1Δ437 is constitutively secreted and not retained at the cell surface when expressed in HEK 293 cells (data not shown). These preliminary data and previous studies suggest a knock-in mouse expressing GFRα1Δ437 from the *Gfra1* locus could be a valuable genetic model. If RET-dependent developmental processes, such as kidney and enteric neuron development, are normal in the homozygous "*trans*-only" mouse, these data would strongly suggest *cis* and *trans* RET signaling produce similar biological outputs across many cell types in vivo. In contrast, a negative result would suggest *cis* and *trans*

RET signaling produce different outputs in some cell types, or that constitutive secretion lowers the local concentration of GFRα1and diminishes the efficiency of RET signaling.

Trans RET activation as a therapeutic approach

Hirschsprung disease is characterized by a lack of enteric neurons in the distal bowel, resulting in bowel motility problems in children affected by the disease. RET mutations contribute to ~50% of familial cases of Hirschsprung disease (Parisi and Kapur, 2000). These patients have only a partial loss of RET function, often due to heterozygous hypomorphic mutations, so a low level of RET signaling occurs in enteric neural crest-derived cells (ENCCs) (Pan and Li, 2012). Therefore, one plausible treatment strategy is to increase RET signaling in these precursor cells to increase their proliferation and migration. This may lead to the colonization of the distal bowel and prevent more invasive treatments, such as surgical resection of the distal bowel.

One potential treatment which could increase RET signaling is treatment with soluble GFRα1/GDNF. Previous studies have shown that treatment of wild-type ENCCs with a combination of GFRα1 and GDNF increased the number of enteric neurons differentiated in vitro (Worley et al., 2000). Additionally, treatment of *Gfra1* conditional mutant gut explants with soluble GFRα1 improved the differentiation and migration of enteric neuron precursors (Uesaka et al., 2013). However, it is unclear if such treatment would be effective in *Ret* hypomorphs, as any residual RET in ENCCs may already be

maximally activated. The effectiveness of this treatment approach can be tested using ENCCs from *Ret*$^{9/-}$ mice, which combines a *Ret* null and hypomorphic allele to recapitulate the distal bowel aganglionosis observed in Hirschsprung disease patients (Uesaka et al., 2008). In vitro treatment of ENCCs derived from these embryos with a combination of GFRα1 and GDNF may increase their proliferative or differentiation capacities. Additionally, treatment of hypomorphic embryos with viral vectors expressing *trans* signaling components or via transgenic expression of *Gfra1* from the surrounding tissue will further clarify the feasibility of this approach.

THE ROLE OF PACINAIN CORPUSCLES ACROSS SPECIES

In rodents, Pacinian corpuscles are primarily studied in the interosseous membrane surrounding the limb bones (Zelena, 1978). However, the anatomical location of Pacinian corpuscles varies widely between mammalian species (Bell et al., 1994). Unlike rodents, primates and some other mammalian species have Pacinian corpuscles in the glabrous skin (Zelena, 1994). Pacinian corpuscles in the human hand assist in the differentiation of fine textures (Srinivasan et al., 1990). In addition, it has been proposed that Pacinian corpuscles are important for tool usage (Brisben et al., 1999). Vibrations transferred through a tool can be sensed by Pacinian corpuscles may assist in interpreting the shape of an object which is not directly touched by the hand. The evolutionary changes that produced Pacinian corpuscles in the glabrous skin remain unclear.

In Chapter 3 of this thesis, we showed that expression of *Er81* and *Nrg1* by rapidly adapting mechanoreceptors is critical for the development of Pacinian corpuscles in the interosseous membrane of the mouse. One intriguing possibility is that the expression of *Er81* and/or high levels of *Nrg1* in RA mechanoreceptors may be sufficient to produce large Pacinian corpuscle end organs. The expansion of the population of RA mechanoreceptors expressing these genes to include those which project to the glabrous skin may be one factor contributing to the dermal localization of Pacinian corpuscles in higher mammals. To test this hypothesis, mouse models which transgenically overexpress *Er81* or *Nrg1* in RA mechanoreceptors should be generated. Examination of the paw skin of these animals may reveal Pacinian corpuscle-like structures, which are larger and located in deeper skin tissue than Meissner's corpuscles.

The role of interosseous Pacinian corpuscles in somatosensation remains unclear. It has been proposed that interosseous Pacinian corpuscles may sense vibrations transferred through the ground, which may be important for sensing approaching predators (Mcintyre, 1980). Additionally, Pacinian corpuscles have been implicated in detecting joint position in human subjects. In both the hand and foot, application of high frequency vibration to the skin inhibited the ability of human subjects to estimate the angle of nearby joints, including in the fingers and ankle, likely due to a masking of important information mediated by Pacinian corpuscles by "noisy" stimulation (Mildren and Bent, 2016; Weerakkody et al., 2007; Weerakkody et al., 2009). Although it was proposed that cutaneous Pacinian corpuscles mediate this ability due to the location of the stimulation,

it's possible that interosseous Pacinian corpuscles were also disrupted by this stimulus and that they may also contribute to the detection of joint angle.

To investigate the role of interosseous Pacinian corpuscles, a mouse model which selectively eliminates *Er81* from RA mechanoreceptors should be generated. Currently available Cre lines, such as $Ret^{CreERT2}$, $Nestin^{Cre}$, and $Wnt1^{Cre}$, cannot be used for this purpose as they will also eliminate *Er81* from motor neurons, proprioceptors, and/or Schwann cells, producing confounding motor deficits. $Split^{Cre}$, which is exclusively expressed in mechanosensory neurons (Rutlin et al., 2014), may work for this purpose, but its efficiency in ablating *Er81* from RA mechanoreceptors needs to be tested. If mechanosensory neurons specific *Er81* mutants can be generated, I predict they will lack Pacinian corpuscles but have intact proprioceptive/motor circuits. Behavioral tests of such animals, including detection of vibration applied directly to the paw, detection of vibration applied to the ground, and motor tests, such as rotarod, horizontal ladder, and gait analysis, may provide further insight into the role of interosseous Pacinian corpuscles.

BIBLIOGRAPHY

Abdo, H., Li, L., Lallemend, F., Bachy, I., Xu, X.J., Rice, F.L., and Ernfors, P. (2011). Dependence on the transcription factor Shox2 for specification of sensory neurons conveying discriminative touch. Eur J Neurosci *34*, 1529-1541.

Airaksinen, M.S., Koltzenburg, M., Lewin, G.R., Masu, Y., Helbig, C., Wolf, E., Brem, G., Toyka, K.V., Thoenen, H., and Meyer, M. (1996). Specific subtypes of cutaneous mechanoreceptors require neurotrophin-3 following peripheral target innervation. Neuron *16*, 287-295.

Airaksinen, M.S., and Saarma, M. (2002). The GDNF family: signalling, biological functions and therapeutic value. Nat Rev Neurosci *3*, 383-394.

Airaksinen, M.S., Titievsky, A., and Saarma, M. (1999). GDNF family neurotrophic factor signaling: four masters, one servant? Mol Cell Neurosci *13*, 313-325.

Allen Institute for Brain Science (2016). Allen Spinal Cord Atlas [Internet]. Available from: http://mousespinal.brain-map.org.

Amiel, J., Sproat-Emison, E., Garcia-Barcelo, M., Lantieri, F., Burzynski, G., Borrego, S., Pelet, A., Arnold, S., Miao, X., Griseri, P., *et al.* (2008). Hirschsprung disease, associated syndromes and genetics: a review. J Med Genet *45*, 1-14.

Amoresano, A., Incoronato, M., Monti, G., Pucci, P., de Franciscis, V., and Cerchia, L. (2005). Direct interactions among Ret, GDNF and GFRalpha1 molecules reveal new insights into the assembly of a functional three-protein complex. Cell Signal *17*, 717-727.

Anders, J., Kjar, S., and Ibanez, C.F. (2001). Molecular modeling of the extracellular domain of the RET receptor tyrosine kinase reveals multiple cadherin-like domains and a calcium-binding site. J Biol Chem *276*, 35808-35817.

Arber, S., Ladle, D.R., Lin, J.H., Frank, E., and Jessell, T.M. (2000). ETS gene Er81 controls the formation of functional connections between group Ia sensory afferents and motor neurons. Cell *101*, 485-498.

Baloh, R.H., Tansey, M.G., Golden, J.P., Creedon, D.J., Heuckeroth, R.O., Keck, C.L., Zimonjic, D.B., Popescu, N.C., Johnson, E.M., Jr., and Milbrandt, J. (1997). TrnR2, a novel receptor that mediates neurturin and GDNF signaling through Ret. Neuron *18*, 793-802.

Baloh, R.H., Tansey, M.G., Lampe, P.A., Fahrner, T.J., Enomoto, H., Simburger, K.S., Leitner, M.L., Araki, T., Johnson, E.M., Jr., and Milbrandt, J. (1998). Artemin, a novel member of the GDNF ligand family, supports peripheral and central neurons and signals through the GFRalpha3-RET receptor complex. Neuron *21*, 1291-1302.

Baroni, A., Perfetto, B., Canozo, N., Braca, A., Farina, E., Melito, A., De Maria, S., and Carteni, M. (2008). Bombesin: a possible role in wound repair. Peptides *29*, 1157-1166.

Battey, J.F., Way, J.M., Corjay, M.H., Shapira, H., Kusano, K., Harkins, R., Wu, J.M., Slattery, T., Mann, E., and Feldman, R.I. (1991). Molecular cloning of the bombesin/gastrin-releasing peptide receptor from Swiss 3T3 cells. Proc Natl Acad Sci U S A *88*, 395-399.

Baudet, C., Pozas, E., Adameyko, I., Andersson, E., Ericson, J., and Ernfors, P. (2008). Retrograde signaling onto Ret during motor nerve terminal maturation. J Neurosci *28*, 963-975.

Bell, J., Bolanowski, S., and Holmes, M.H. (1994). The structure and function of Pacinian corpuscles: a review. Prog Neurobiol *42*, 79-128.

Bennett, D.L., Michael, G.J., Ramachandran, N., Munson, J.B., Averill, S., Yan, Q., McMahon, S.B., and Priestley, J.V. (1998). A distinct subgroup of small DRG cells express GDNF receptor components and GDNF is protective for these neurons after nerve injury. J Neurosci *18*, 3059-3072.

Bentivoglio, M., and Pacini, P. (1995). Filippo Pacini: a determined observer. Brain Res Bull *38*, 161-165.

Bespalov, M.M., and Saarma, M. (2007). GDNF family receptor complexes are emerging drug targets. Trends Pharmacol Sci *28*, 68-74.

Bespalov, M.M., Sidorova, Y.A., Tumova, S., Ahonen-Bishopp, A., Magalhaes, A.C., Kulesskiy, E., Paveliev, M., Rivera, C., Rauvala, H., and Saarma, M. (2011). Heparan sulfate proteoglycan syndecan-3 is a novel receptor for GDNF, neurturin, and artemin. J Cell Biol *192*, 153-169.

Biemesderfer, D., Munger, B.L., Binck, J., and Dubner, R. (1978). The pilo-Ruffini complex: a non-sinus hair and associated slowly-adapting mechanoreceptor in primate facial skin. Brain Res *142*, 197-222.

Birchmeier, C., and Nave, K.A. (2008). Neuregulin-1, a key axonal signal that drives Schwann cell growth and differentiation. Glia *56*, 1491-1497.

Borrello, M.G., Alberti, L., Arighi, E., Bongarzone, I., Battistini, C., Bardelli, A., Pasini, B., Piutti, C., Rizzetti, M.G., Mondellini, P., *et al.* (1996). The full oncogenic activity of Ret/ptc2 depends on tyrosine 539, a docking site for phospholipase Cgamma. Mol Cell Biol *16*, 2151-2163.

Boulais, N., and Misery, L. (2007). Merkel cells. J Am Acad Dermatol *57*, 147-165.

Bourane, S., Garces, A., Venteo, S., Pattyn, A., Hubert, T., Fichard, A., Puech, S.,

Boukhaddaoui, H., Baudet, C., Takahashi, S., *et al.* (2009). Low-threshold mechanoreceptor subtypes selectively express MafA and are specified by Ret signaling. Neuron *64*, 857-870.

Brisben, A.J., Hsiao, S.S., and Johnson, K.O. (1999). Detection of vibration transmitted through an object grasped in the hand. Journal of neurophysiology *81*, 1548-1558.

Brown, A.G. (1981). Organization in the spinal cord : the anatomy and physiology of identified neurones (Berlin ; New York: Springer-Verlag).

Brown, A.G., Fyffe, R.E., and Noble, R. (1980). Projections from Pacinian corpuscles and rapidly adapting mechanoreceptors of glabrous skin to the cat's spinal cord. J Physiol *307*, 385-400.

Buj-Bello, A., Adu, J., Pinon, L.G., Horton, A., Thompson, J., Rosenthal, A., Chinchetru, M., Buchman, V.L., and Davies, A.M. (1997). Neurturin responsiveness requires a GPI-linked receptor and the Ret receptor tyrosine kinase. Nature *387*, 721-724.

Buonanno, A., and Fischbach, G.D. (2001). Neuregulin and ErbB receptor signaling pathways in the nervous system. Curr Opin Neurobiol *11*, 287-296.

Burgess, P.R., and Pearl, E.R. (1973). Cutaneious mechanoreceptors and nociceptors. In Handbook of Sensory Physiology, A. Iggo, ed. (Berlin: Springer), pp. 29-78.

Byers, M.R. (1985). Sensory innervation of periodontal ligament of rat molars consists of unencapsulated Ruffini-like mechanoreceptors and free nerve endings. J Comp Neurol *231*, 500-518.

Cacalano, G., Farinas, I., Wang, L.C., Hagler, K., Forgie, A., Moore, M., Armanini, M., Phillips, H., Ryan, A.M., Reichardt, L.F., *et al.* (1998). GFRalpha1 is an essential receptor component for GDNF in the developing nervous system and kidney. Neuron *21*, 53-62.

Calavia, M.G., Feito, J., Lopez-Iglesias, L., de Carlos, F., Garcia-Suarez, O., Perez-Pinera, P., Cobo, J., and Vega, J.A. (2010). The lamellar cells in human Meissner corpuscles express TrkB. Neurosci Lett *468*, 106-109.

Canty, A.J., Dietze, J., Harvey, M., Enomoto, H., Milbrandt, J., and Ibanez, C.F. (2009). Regionalized loss of parvalbumin interneurons in the cerebral cortex of mice with deficits in GFRalpha1 signaling. J Neurosci *29*, 10695-10705.

Carroll, P., Lewin, G.R., Koltzenburg, M., Toyka, K.V., and Thoenen, H. (1998). A role for BDNF in mechanosensation. Nature neuroscience *1*, 42-46.

Caterina, M.J., Schumacher, M.A., Tominaga, M., Rosen, T.A., Levine, J.D., and Julius, D. (1997). The capsaicin receptor: a heat-activated ion channel in the pain pathway. Nature *389*, 816-824.

Cauna, N. (1956). Nerve supply and nerve endings in Meissner's corpuscles. Am J Anat *99*, 315-350.

Cauna, N., and Mannan, G. (1958). The structure of human digital pacinian corpuscles (corpus cula lamellosa) and its functional significance. J Anat *92*, 1-20.

Cauna, N., and Ross, L.L. (1960). The fine structure of Meissner's touch corpuscles of human fingers. J Biophys Biochem Cytol *8*, 467-482.

Cavanaugh, D.J., Lee, H., Lo, L., Shields, S.D., Zylka, M.J., Basbaum, A.I., and Anderson, D.J. (2009). Distinct subsets of unmyelinated primary sensory fibers mediate behavioral responses to noxious thermal and mechanical stimuli. Proceedings of the National Academy of Sciences of the United States of America *106*, 9075-9080.

Chambers, M.R., Andres, K.H., von Duering, M., and Iggo, A. (1972). The structure and function of the slowly adapting type II mechanoreceptor in hairy skin. Q J Exp Physiol Cogn Med Sci *57*, 417-445.

Chen, X., Ye, H., Kuruvilla, R., Ramanan, N., Scangos, K.W., Zhang, C., Johnson, N.M., England, P.M., Shokat, K.M., and Ginty, D.D. (2005). A chemical-genetic approach to studying neurotrophin signaling. Neuron *46*, 13-21.

Cheret, C., Willem, M., Fricker, F.R., Wende, H., Wulf-Goldenberg, A., Tahirovic, S., Nave, K.A., Saftig, P., Haass, C., Garratt, A.N., *et al.* (2013). Bace1 and Neuregulin-1 cooperate to control formation and maintenance of muscle spindles. Embo J *32*, 2015-2028.

Chi, P., Chen, Y., Zhang, L., Guo, X., Wongvipat, J., Shamu, T., Fletcher, J.A., Dewell, S., Maki, R.G., Zheng, D., *et al.* (2010). ETV1 is a lineage survival factor that cooperates with KIT in gastrointestinal stromal tumours. Nature *467*, 849-853.

Chiariello, M., Visconti, R., Carlomagno, F., Melillo, R.M., Bucci, C., de Franciscis, V., Fox, G.M., Jing, S., Coso, O.A., Gutkind, J.S., *et al.* (1998). Signalling of the Ret receptor tyrosine kinase through the c-Jun NH2-terminal protein kinases (JNKS): evidence for a divergence of the ERKs and JNKs pathways induced by Ret. Oncogene *16*, 2435-2445.

Cik, M., Masure, S., Lesage, A.S., Van Der Linden, I., Van Gompel, P., Pangalos, M.N., Gordon, R.D., and Leysen, J.E. (2000). Binding of GDNF and neurturin to human GDNF family receptor alpha 1 and 2. Influence of cRET and cooperative interactions. J Biol Chem *275*, 27505-27512.

Cronk, K.M., Wilkinson, G.A., Grimes, R., Wheeler, E.F., Jhaveri, S., Fundin, B.T., Silos-Santiago, I., Tessarollo, L., Reichardt, L.F., and Rice, F.L. (2002). Diverse dependencies of developing Merkel innervation on the trkA and both full-length and truncated isoforms of trkC. Development *129*, 3739-3750.

de Graaff, E., Srinivas, S., Kilkenny, C., D'Agati, V., Mankoo, B.S., Costantini, F., and Pachnis, V. (2001). Differential activities of the RET tyrosine kinase receptor isoforms during mammalian embryogenesis. Genes Dev *15*, 2433-2444.

de Nooij, J.C., Doobar, S., and Jessell, T.M. (2013). Etv1 inactivation reveals proprioceptor subclasses that reflect the level of NT3 expression in muscle targets. Neuron *77*, 1055-1068.

Degl'Innocenti, D., Arighi, E., Popsueva, A., Sangregorio, R., Alberti, L., Rizzetti, M.G., Ferrario, C., Sariola, H., Pierotti, M.A., and Borrello, M.G. (2004). Differential requirement of Tyr1062 multidocking site by RET isoforms to promote neural cell scattering and epithelial cell branching. Oncogene *23*, 7297-7309.

Deng, L.X., Deng, P., Ruan, Y., Xu, Z.C., Liu, N.K., Wen, X., Smith, G.M., and Xu, X.M. (2013). A novel growth-promoting pathway formed by GDNF-overexpressing Schwann cells promotes propriospinal axonal regeneration, synapse formation, and partial recovery of function after spinal cord injury. J Neurosci *33*, 5655-5667.

Dhaka, A., Murray, A.N., Mathur, J., Earley, T.J., Petrus, M.J., and Patapoutian, A. (2007). TRPM8 is required for cold sensation in mice. Neuron *54*, 371-378.

Di Maio, A., Skuba, A., Himes, B.T., Bhagat, S.L., Hyun, J.K., Tessler, A., Bishop, D., and Son, Y.J. (2011). In vivo imaging of dorsal root regeneration: rapid immobilization and presynaptic differentiation at the CNS/PNS border. J Neurosci *31*, 4569-4582.

Diamond, J., Mills, L.R., and Mearow, K.M. (1988). Evidence that the Merkel cell is not the transducer in the mechanosensory Merkel cell-neurite complex. Prog Brain Res *74*, 51-56.

Dong, X., Han, S., Zylka, M.J., Simon, M.I., and Anderson, D.J. (2001). A diverse family of GPCRs expressed in specific subsets of nociceptive sensory neurons. Cell *106*, 619-632.

Durick, K., Yao, V.J., Borrello, M.G., Bongarzone, I., Pierotti, M.A., and Taylor, S.S. (1995). Tyrosines outside the kinase core and dimerization are required for the mitogenic activity of RET/ptc2. J Biol Chem *270*, 24642-24645.

Eisenhaber, B., Bork, P., and Eisenhaber, F. (1999). Prediction of potential GPI-modification sites in proprotein sequences. J Mol Biol *292*, 741-758.

Eketjall, S., Fainzilber, M., Murray-Rust, J., and Ibanez, C.F. (1999). Distinct structural elements in GDNF mediate binding to GFRalpha1 and activation of the GFRalpha1-c-Ret receptor complex. Embo J *18*, 5901-5910.

English, K.B., Burgess, P.R., and Kavka-Van Norman, D. (1980). Development of rat Merkel cells. J Comp Neurol *194*, 475-496.

Enomoto, H. (2005). Regulation of neural development by glial cell line-derived neurotrophic factor family ligands. Anat Sci Int *80*, 42-52.

Enomoto, H., Araki, T., Jackman, A., Heuckeroth, R.O., Snider, W.D., Johnson, E.M., Jr., and Milbrandt, J. (1998). GFR alpha1-deficient mice have deficits in the enteric nervous system and kidneys. Neuron *21*, 317-324.

Enomoto, H., Hughes, I., Golden, J., Baloh, R.H., Yonemura, S., Heuckeroth, R.O., Johnson, E.M., Jr., and Milbrandt, J. (2004). GFRalpha1 expression in cells lacking RET is dispensable for organogenesis and nerve regeneration. Neuron *44*, 623-636.

Ernsberger, U. (2009). Role of neurotrophin signalling in the differentiation of neurons from dorsal root ganglia and sympathetic ganglia. Cell and tissue research *336*, 349-384.

Fagan, B.M., and Cahusac, P.M. (2001). Evidence for glutamate receptor mediated transmission at mechanoreceptors in the skin. Neuroreport *12*, 341-347.

Falls, D.L. (2003). Neuregulins: functions, forms, and signaling strategies. Exp Cell Res *284*, 14-30.

Fleck, D., van Bebber, F., Colombo, A., Galante, C., Schwenk, B.M., Rabe, L., Hampel, H., Novak, B., Kremmer, E., Tahirovic, S., *et al.* (2013). Dual cleavage of neuregulin 1 type III by BACE1 and ADAM17 liberates its EGF-like domain and allows paracrine signaling. J Neurosci *33*, 7856-7869.

Fleming, M.S., and Luo, W. (2013). The anatomy, function, and development of mammalian Abeta low-threshold mechanoreceptors. Front Biol (Beijing) *8*.

Fleming, M.S., Ramos, D., Han, S.B., Zhao, J., Son, Y.J., and Luo, W. (2012). The majority of dorsal spinal cord gastrin releasing peptide is synthesized locally whereas

neuromedin B is highly expressed in pain- and itch-sensing somatosensory neurons. Mol Pain *8*, 52.

Fleming, M.S., Vysochan, A., Paixao, S., Niu, J., Klein, R., Savitt, J.M., and Luo, W. (2015). Cis and trans RET signaling control the survival and central projection growth of rapidly adapting mechanoreceptors. Elife *4*, e06828.

Fundin, B.T., Silos-Santiago, I., Ernfors, P., Fagan, A.M., Aldskogius, H., DeChiara, T.M., Phillips, H.S., Barbacid, M., Yancopoulos, G.D., and Rice, F.L. (1997). Differential dependency of cutaneous mechanoreceptors on neurotrophins, trk receptors, and P75 LNGFR. Dev Biol *190*, 94-116.

Gardner, E.P., and Palmer, C.I. (1990). Simulation of motion on the skin. III. Mechanisms used by rapidly adapting cutaneous mechanoreceptors in the primate hand for spatiotemporal resolution and two-point discrimination. Journal of neurophysiology *63*, 841-859.

Goel, A., and Janknecht, R. (2003). Acetylation-mediated transcriptional activation of the ETS protein ER81 by p300, P/CAF, and HER2/Neu. Mol Cell Biol *23*, 6243-6254.

Golden, J.P., Hoshi, M., Nassar, M.A., Enomoto, H., Wood, J.N., Milbrandt, J., Gereau, R.W.t., Johnson, E.M., Jr., and Jain, S. (2010). RET signaling is required for survival and normal function of nonpeptidergic nociceptors. J Neurosci *30*, 3983-3994.

Gonzalez-Martinez, T., Farinas, I., Del Valle, M.E., Feito, J., Germana, G., Cobo, J., and Vega, J.A. (2005). BDNF, but not NT-4, is necessary for normal development of Meissner corpuscles. Neurosci Lett *377*, 12-15.

Gonzalez-Martinez, T., Germana, A., Catania, S., Cobo, T., Ochoa-Erena, F.J., de Carlos, F., Diaz-Esnal, B., and Vega, J.A. (2007). Postnatal developmental changes in the expression of ErbB receptors in murine Pacinian cospucles. Neurosci Lett *420*, 90-95.

Gonzalez-Martinez, T., Germana, G.P., Monjil, D.F., Silos-Santiago, I., de Carlos, F., Germana, G., Cobo, J., and Vega, J.A. (2004). Absence of Meissner corpuscles in the digital pads of mice lacking functional TrkB. Brain Res *1002*, 120-128.

Goodman, K.M., Kjaer, S., Beuron, F., Knowles, P.P., Nawrotek, A., Burns, E.M., Purkiss, A.G., George, R., Santoro, M., Morris, E.P., *et al.* (2014). RET recognition of GDNF-GFRalpha1 ligand by a composite binding site promotes membrane-proximal self-association. Cell Rep *8*, 1894-1904.

Gottschaldt, K.M., Iggo, A., and Young, D.W. (1973). Functional characteristics of mechanoreceptors in sinus hair follicles of the cat. J Physiol *235*, 287-315.

Gottschaldt, K.M., and Vahle-Hinz, C. (1981). Merkel cell receptors: structure and transducer function. Science *214*, 183-186.

Griffin, J.W., and Thompson, W.J. (2008). Biology and pathology of nonmyelinating Schwann cells. Glia *56*, 1518-1531.

Grim, M., and Halata, Z. (2000). Developmental origin of avian Merkel cells. Anat Embryol (Berl) *202*, 401-410.

Gutierrez-Mecinas, M., Watanabe, M., and Todd, A.J. (2014). Expression of gastrin-releasing peptide by excitatory interneurons in the mouse superficial dorsal horn. Mol Pain *10*, 79.

Haeberle, H., Fujiwara, M., Chuang, J., Medina, M.M., Panditrao, M.V., Bechstedt, S., Howard, J., and Lumpkin, E.A. (2004). Molecular profiling reveals synaptic release machinery in Merkel cells. Proceedings of the National Academy of Sciences of the United States of America *101*, 14503-14508.

Halata, Z. (1977). The ultrastructure of the sensory nerve endings in the articular capsule of the knee joint of the domestic cat (Ruffini corpuscles and Pacinian corpuscles). J Anat *124*, 717-729.

Halata, Z., Grim, M., and Bauman, K.I. (2003). Friedrich Sigmund Merkel and his "Merkel cell", morphology, development, and physiology: review and new results. Anat Rec A Discov Mol Cell Evol Biol *271*, 225-239.

Halata, Z., and Munger, B.L. (1980a). The sensory innervation of primate eyelid. Anat Rec A Discov Mol Cell Evol Biol *198*, 657-670.

Halata, Z., and Munger, B.L. (1980b). Sensory nerve endings in rhesus monkey sinus hairs. J Comp Neurol *192*, 645-663.

Han, L., Ma, C., Liu, Q., Weng, H.J., Cui, Y., Tang, Z., Kim, Y., Nie, H., Qu, L., Patel, K.N., *et al.* (2013). A subpopulation of nociceptors specifically linked to itch. Nat Neurosci *16*, 174-182.

Hanani, M. (2005). Satellite glial cells in sensory ganglia: from form to function. Brain Res Brain Res Rev *48*, 457-476.

He, S., Chen, C.H., Chernichenko, N., Bakst, R.L., Barajas, F., Deborde, S., Allen, P.J., Vakiani, E., Yu, Z., and Wong, R.J. (2014). GFRalpha1 released by nerves enhances cancer cell perineural invasion through GDNF-RET signaling. Proceedings of the National Academy of Sciences of the United States of America *111*, E2008-2017.

Heidenreich, M., Lechner, S.G., Vardanyan, V., Wetzel, C., Cremers, C.W., De Leenheer, E.M., Aranguez, G., Moreno-Pelayo, M.A., Jentsch, T.J., and Lewin, G.R. (2012). KCNQ4 K(+) channels tune mechanoreceptors for normal touch sensation in mouse and man. Nature neuroscience *15*, 138-145.

Heuckeroth, R.O., Enomoto, H., Grider, J.R., Golden, J.P., Hanke, J.A., Jackman, A., Molliver, D.C., Bardgett, M.E., Snider, W.D., Johnson, E.M., Jr., *et al.* (1999). Gene targeting reveals a critical role for neurturin in the development and maintenance of enteric, sensory, and parasympathetic neurons. Neuron *22*, 253-263.

Hippenmeyer, S., Shneider, N.A., Birchmeier, C., Burden, S.J., Jessell, T.M., and Arber, S. (2002). A role for neuregulin1 signaling in muscle spindle differentiation. Neuron *36*, 1035-1049.

Hippenmeyer, S., Vrieseling, E., Sigrist, M., Portmann, T., Laengle, C., Ladle, D.R., and Arber, S. (2005). A developmental switch in the response of DRG neurons to ETS transcription factor signaling. PLoS Biol *3*, e159.

Hoggan, G., and Hoggan, F.E. (1893). Forked Nerve Endings on Hairs. J Anat Physiol *27*, 224-231.

Honma, Y., Kawano, M., Kohsaka, S., and Ogawa, M. (2010). Axonal projections of mechanoreceptive dorsal root ganglion neurons depend on Ret. Development *137*, 2319-2328.

Hoshino, N., Harada, F., Alkhamrah, B.A., Aita, M., Kawano, Y., Hanada, K., and Maeda, T. (2003). Involvement of brain-derived neurotrophic factor (BDNF) in the development of periodontal Ruffini endings. The anatomical record Part A, Discoveries in molecular, cellular, and evolutionary biology *274*, 807-816.

Hu, J., Huang, T., Li, T., Guo, Z., and Cheng, L. (2012). c-Maf is required for the development of dorsal horn laminae III/IV neurons and mechanoreceptive DRG axon projections. J Neurosci *32*, 5362-5373.

Hu, X., Hicks, C.W., He, W., Wong, P., Macklin, W.B., Trapp, B.D., and Yan, R. (2006). Bace1 modulates myelination in the central and peripheral nervous system. Nat Neurosci *9*, 1520-1525.

Hubbard, S.J. (1958). A study of rapid mechanical events in a mechanoreceptor. J Physiol *141*, 198-218.

Hughes, D.I., Polgar, E., Shehab, S.A., and Todd, A.J. (2004). Peripheral axotomy induces depletion of the vesicular glutamate transporter VGLUT1 in central terminals of myelinated afferent fibres in the rat spinal cord. Brain Res *1017*, 69-76.

Hunt, C.C. (1961). On the nature of vibration receptors in the hind limb of the cat. J Physiol *155*, 175-186.

Ibanez, C.F. (2013). Structure and physiology of the RET receptor tyrosine kinase. Cold Spring Harb Perspect Biol *5*.

Iggo, A. (1985). Sensory receptors in the skin of mammals and their sensory functions. Rev Neurol (Paris) *141*, 599-613.

Iggo, A., and Andres, K.H. (1982). Morphology of cutaneous receptors. Annu Rev Neurosci *5*, 1-31.

Iggo, A., and Muir, A.R. (1969). The structure and function of a slowly adapting touch corpuscle in hairy skin. J Physiol *200*, 763-796.

Iggo, A., and Ogawa, H. (1977). Correlative physiological and morphological studies of rapidly adapting mechanoreceptors in cat's glabrous skin. J Physiol *266*, 275-296.

Ikeda, I., Yamashita, Y., Ono, T., and Ogawa, H. (1994). Selective phototoxic destruction of rat Merkel cells abolishes responses of slowly adapting type I mechanoreceptor units. J Physiol *479 (Pt 2)*, 247-256.

Ikoma, A., Cevikbas, F., Kempkes, C., and Steinhoff, M. (2011). Anatomy and neurophysiology of pruritus. Semin Cutan Med Surg *30*, 64-70.

Imamachi, N., Park, G.H., Lee, H., Anderson, D.J., Simon, M.I., Basbaum, A.I., and Han, S.K. (2009). TRPV1-expressing primary afferents generate behavioral responses to pruritogens via multiple mechanisms. Proceedings of the National Academy of Sciences of the United States of America *106*, 11330-11335.

Jaegle, M., Ghazvini, M., Mandemakers, W., Piirsoo, M., Driegen, S., Levavasseur, F., Raghoenath, S., Grosveld, F., and Meijer, D. (2003). The POU proteins Brn-2 and Oct-6 share important functions in Schwann cell development. Genes Dev *17*, 1380-1391.

Jain, S., Encinas, M., Johnson, E.M., Jr., and Milbrandt, J. (2006). Critical and distinct roles for key RET tyrosine docking sites in renal development. Genes Dev *20*, 321-333.

Janknecht, R. (1996). Analysis of the ERK-stimulated ETS transcription factor ER81. Mol Cell Biol *16*, 1550-1556.

Jensen, R.T., Battey, J.F., Spindel, E.R., and Benya, R.V. (2008). International Union of Pharmacology. LXVIII. Mammalian bombesin receptors: nomenclature, distribution, pharmacology, signaling, and functions in normal and disease states. Pharmacol Rev *60*, 1-42.

Jeon, I.S., Davis, J.N., Braun, B.S., Sublett, J.E., Roussel, M.F., Denny, C.T., and Shapiro, D.N. (1995). A variant Ewing's sarcoma translocation (7;22) fuses the EWS gene to the ETS gene ETV1. Oncogene *10*, 1229-1234.

Jing, S., Wen, D., Yu, Y., Holst, P.L., Luo, Y., Fang, M., Tamir, R., Antonio, L., Hu, Z., Cupples, R., *et al.* (1996). GDNF-induced activation of the ret protein tyrosine kinase is mediated by GDNFR-alpha, a novel receptor for GDNF. Cell *85*, 1113-1124.

Jing, S., Yu, Y., Fang, M., Hu, Z., Holst, P.L., Boone, T., Delaney, J., Schultz, H., Zhou, R., and Fox, G.M. (1997). GFRalpha-2 and GFRalpha-3 are two new receptors for ligands of the GDNF family. J Biol Chem *272*, 33111-33117.

Johansson, R.S., and Vallbo, A.B. (1979). Tactile sensibility in the human hand: relative and absolute densities of four types of mechanoreceptive units in glabrous skin. J Physiol *286*, 283-300.

Johnson, K.O. (2001). The roles and functions of cutaneous mechanoreceptors. Curr Opin Neurobiol *11*, 455-461.

Johnson, K.O., Yoshioka, T., and Vega-Bermudez, F. (2000). Tactile functions of mechanoreceptive afferents innervating the hand. J Clin Neurophysiol *17*, 539-558.

Kawamoto, Y., Takeda, K., Okuno, Y., Yamakawa, Y., Ito, Y., Taguchi, R., Kato, M., Suzuki, H., Takahashi, M., and Nakashima, I. (2004). Identification of RET autophosphorylation sites by mass spectrometry. J Biol Chem *279*, 14213-14224.

Kholodilov, N., Kim, S.R., Yarygina, O., Kareva, T., Cho, J.W., Baohan, A., and Burke, R.E. (2011). Glial cell line-derived neurotrophic factor receptor-alpha1 expressed in striatum in trans regulates development and injury response of dopamine neurons of the substantia nigra. Journal of neurochemistry *116*, 486-498.

Kinkelin, I., Stucky, C.L., and Koltzenburg, M. (1999). Postnatal loss of Merkel cells, but not of slowly adapting mechanoreceptors in mice lacking the neurotrophin receptor p75. Eur J Neurosci *11*, 3963-3969.

Kjaer, S., and Ibanez, C.F. (2003). Identification of a surface for binding to the GDNF-GFR alpha 1 complex in the first cadherin-like domain of RET. J Biol Chem *278*, 47898-47904.

Kjaer, S., Kurokawa, K., Perrinjaquet, M., Abrescia, C., and Ibanez, C.F. (2006). Self-association of the transmembrane domain of RET underlies oncogenic activation by MEN2A mutations. Oncogene *25*, 7086-7095.

Klein, R., Silos-Santiago, I., Smeyne, R.J., Lira, S.A., Brambilla, R., Bryant, S., Zhang, L., Snider, W.D., and Barbacid, M. (1994). Disruption of the neurotrophin-3 receptor

gene trkC eliminates la muscle afferents and results in abnormal movements. Nature *368*, 249-251.

Klein, R.D., Sherman, D., Ho, W.H., Stone, D., Bennett, G.L., Moffat, B., Vandlen, R., Simmons, L., Gu, Q., Hongo, J.A., *et al.* (1997). A GPI-linked protein that interacts with Ret to form a candidate neurturin receptor. Nature *387*, 717-721.

Knibestol, M. (1973). Stimulus-response functions of rapidly adapting mechanoreceptors in human glabrous skin area. J Physiol *232*, 427-452.

Knudson, C.M., Tung, K.S., Tourtellotte, W.G., Brown, G.A., and Korsmeyer, S.J. (1995). Bax-deficient mice with lymphoid hyperplasia and male germ cell death. Science *270*, 96-99.

Koga, K., Chen, T., Li, X.Y., Descalzi, G., Ling, J., Gu, J., and Zhuo, M. (2011). Glutamate acts as a neurotransmitter for gastrin releasing peptide-sensitive and insensitive itch-related synaptic transmission in mammalian spinal cord. Mol Pain *7*, 47.

Kopp, D.M., Trachtenberg, J.T., and Thompson, W.J. (1997). Glial growth factor rescues Schwann cells of mechanoreceptors from denervation-induced apoptosis. J Neurosci *17*, 6697-6706.

Kramer, E.R., Knott, L., Su, F., Dessaud, E., Krull, C.E., Helmbacher, F., and Klein, R. (2006a). Cooperation between GDNF/Ret and ephrinA/EphA4 signals for motor-axon pathway selection in the limb. Neuron *50*, 35-47.

Kramer, I., Sigrist, M., de Nooij, J.C., Taniuchi, I., Jessell, T.M., and Arber, S. (2006b). A role for Runx transcription factor signaling in dorsal root ganglion sensory neuron diversification. Neuron *49*, 379-393.

Krampitz, G.W., and Norton, J.A. (2014). RET gene mutations (genotype and phenotype) of multiple endocrine neoplasia type 2 and familial medullary thyroid carcinoma. Cancer *120*, 1920-1931.

Krimm, R.F., Davis, B.M., Noel, T., and Albers, K.M. (2006). Overexpression of neurotrophin 4 in skin enhances myelinated sensory endings but does not influence sensory neuron number. J Comp Neurol *498*, 455-465.

Kucera, J., Cooney, W., Que, A., Szeder, V., Stancz-Szeder, H., and Walro, J. (2002). Formation of supernumerary muscle spindles at the expense of Golgi tendon organs in ER81-deficient mice. Dev Dyn *223*, 389-401.

Lagerstrom, M.C., Rogoz, K., Abrahamsen, B., Persson, E., Reinius, B., Nordenankar, K., Olund, C., Smith, C., Mendez, J.A., Chen, Z.F., *et al.* (2010). VGLUT2-dependent sensory neurons in the TRPV1 population regulate pain and itch. Neuron *68*, 529-542.

Lallemend, F., and Ernfors, P. (2012). Molecular interactions underlying the specification of sensory neurons. Trends Neurosci *35*, 373-381.

Ledda, F., Paratcha, G., and Ibanez, C.F. (2002). Target-derived GFRalpha1 as an attractive guidance signal for developing sensory and sympathetic axons via activation of Cdk5. Neuron *36*, 387-401.

Ledda, F., Paratcha, G., Sandoval-Guzman, T., and Ibanez, C.F. (2007). GDNF and GFRalpha1 promote formation of neuronal synapses by ligand-induced cell adhesion. Nature neuroscience *10*, 293-300.

LeMaster, A.M., Krimm, R.F., Davis, B.M., Noel, T., Forbes, M.E., Johnson, J.E., and Albers, K.M. (1999). Overexpression of brain-derived neurotrophic factor enhances sensory innervation and selectively increases neuron number. The Journal of neuroscience *19*, 5919-5931.

Levanon, D., Bettoun, D., Harris-Cerruti, C., Woolf, E., Negreanu, V., Eilam, R., Bernstein, Y., Goldenberg, D., Xiao, C., Fliegauf, M., *et al.* (2002). The Runx3 transcription factor regulates development and survival of TrkC dorsal root ganglia neurons. Embo J *21*, 3454-3463.

Li, L., Rutlin, M., Abraira, V.E., Cassidy, C., Kus, L., Gong, S., Jankowski, M.P., Luo, W., Heintz, N., Koerber, H.R., *et al.* (2011). The functional organization of cutaneous low-threshold mechanosensory neurons. Cell *147*, 1615-1627.

Lin, J.H., Saito, T., Anderson, D.J., Lance-Jones, C., Jessell, T.M., and Arber, S. (1998). Functionally related motor neuron pool and muscle sensory afferent subtypes defined by coordinate ETS gene expression. Cell *95*, 393-407.

Liu, Q., Tang, Z., Surdenikova, L., Kim, S., Patel, K.N., Kim, A., Ru, F., Guan, Y., Weng, H.J., Geng, Y., *et al.* (2009). Sensory neuron-specific GPCR Mrgprs are itch receptors mediating chloroquine-induced pruritus. Cell *139*, 1353-1365.

Liu, Y., Abdel Samad, O., Zhang, L., Duan, B., Tong, Q., Lopes, C., Ji, R.R., Lowell, B.B., and Ma, Q. (2010). VGLUT2-dependent glutamate release from nociceptors is required to sense pain and suppress itch. Neuron *68*, 543-556.

Livak, K.J., and Schmittgen, T.D. (2001). Analysis of relative gene expression data using real-time quantitative PCR and the 2(-Delta Delta C(T)) Method. Methods *25*, 402-408.

Loewenstein, W.R., and Mendelson, M. (1965). Components of Receptor Adaptation in a Pacinian Corpuscle. J Physiol *177*, 377-397.

Lou, S., Duan, B., Vong, L., Lowell, B.B., and Ma, Q. (2013). Runx1 controls terminal morphology and mechanosensitivity of VGLUT3-expressing C-mechanoreceptors. J Neurosci *33*, 870-882.

Lucarz, A., and Brand, G. (2007). Current considerations about Merkel cells. Eur J Cell Biol *86*, 243-251.

Luo, W., Enomoto, H., Rice, F.L., Milbrandt, J., and Ginty, D.D. (2009). Molecular identification of rapidly adapting mechanoreceptors and their developmental dependence on ret signaling. Neuron *64*, 841-856.

Luo, W., Wickramasinghe, S.R., Savitt, J.M., Griffin, J.W., Dawson, T.M., and Ginty, D.D. (2007). A hierarchical NGF signaling cascade controls Ret-dependent and Ret-independent events during development of nonpeptidergic DRG neurons. Neuron *54*, 739-754.

Madisen, L., Zwingman, T.A., Sunkin, S.M., Oh, S.W., Zariwala, H.A., Gu, H., Ng, L.L., Palmiter, R.D., Hawrylycz, M.J., Jones, A.R., *et al.* (2010). A robust and high-throughput Cre reporting and characterization system for the whole mouse brain. Nat Neurosci *13*, 133-140.

Magdaleno, S., Jensen, P., Brumwell, C.L., Seal, A., Lehman, K., et al. (2006) BGEM: An in situ hybridization database of gene expression in the embryonic and adult mouse nervous system. PLoS Biol 4(4): e86.

Majumdar, I.D., and Weber, H.C. (2011). Biology of mammalian bombesin-like peptides and their receptors. Current opinion in endocrinology, diabetes, and obesity *18*, 68-74.

Maklad, A., Conway, M., Hodges, C., and Hansen, L.A. (2010). Development of innervation to maxillary whiskers in mice. Anatomical record *293*, 1553-1567.

Maksimovic, S., Baba, Y., and Lumpkin, E.A. (2013). Neurotransmitters and synaptic components in the Merkel cell-neurite complex, a gentle-touch receptor. Ann N Y Acad Sci *1279*, 13-21.

Maricich, S.M., Morrison, K.M., Mathes, E.L., and Brewer, B.M. (2012). Rodents rely on Merkel cells for texture discrimination tasks. The Journal of neuroscience *32*, 3296-3300.

Maricich, S.M., Wellnitz, S.A., Nelson, A.M., Lesniak, D.R., Gerling, G.J., Lumpkin, E.A., and Zoghbi, H.Y. (2009). Merkel cells are essential for light-touch responses. Science *324*, 1580-1582.

Marmigere, F., and Carroll, P. (2014). Neurotrophin signalling and transcription programmes interactions in the development of somatosensory neurons. Handb Exp Pharmacol *220*, 329-353.

Maruyama, Y., Harada, F., Jabbar, S., Saito, I., Aita, M., Kawano, Y., Suzuki, A., Nozawa-Inoue, K., and Maeda, T. (2005). Neurotrophin-4/5-depletion induces a delay in maturation of the periodontal Ruffini endings in mice. Arch Histol Cytol *68*, 267-288.

Matsuo, S., Ichikawa, H., Silos-Santiago, I., Kiyomiya, K., Kurebe, M., Arends, J.J., and Jacquin, M.F. (2002). Ruffini endings are absent from the periodontal ligament of trkB knockout mice. Somatosens Mot Res *19*, 213-217.

Matusiak, D., Glover, S., Nathaniel, R., Matkowskyj, K., Yang, J., and Benya, R.V. (2005). Neuromedin B and its receptor are mitogens in both normal and malignant epithelial cells lining the colon. Am J Physiol Gastrointest Liver Physiol *288*, G718-728.

McDonagh, S.C., Lee, J., Izzo, A., and Brubaker, P.L. (2007). Role of glial cell-line derived neurotropic factor family receptor alpha2 in the actions of the glucagon-like peptides on the murine intestine. Am J Physiol Gastrointest Liver Physiol *293*, G461-468.

Mcintyre, A.K. (1980). Biological Seismography. Trends in Neurosciences *3*, 202-205.

Mendelson, M., and Lowenstein, W.R. (1964). Mechanisms of Receptor Adaptation. Science *144*, 554-555.

Meng, X., Lindahl, M., Hyvonen, M.E., Parvinen, M., de Rooij, D.G., Hess, M.W., Raatikainen-Ahokas, A., Sainio, K., Rauvala, H., Lakso, M., *et al.* (2000). Regulation of cell fate decision of undifferentiated spermatogonia by GDNF. Science *287*, 1489-1493.

Merkel, F. (1875). Tastzellen and Tastkoerperchen bei den Hausthieren und beim Menschen. Arch Mikrosc Anat *11*, 636-652.

Michailov, G.V., Sereda, M.W., Brinkmann, B.G., Fischer, T.M., Haug, B., Birchmeier, C., Role, L., Lai, C., Schwab, M.H., and Nave, K.A. (2004). Axonal neuregulin-1 regulates myelin sheath thickness. Science *304*, 700-703.

Mildren, R.L., and Bent, L.R. (2016). Vibrotactile stimulation of fast adapting cutaneous afferents from the foot modulates proprioception at the ankle joint. J Appl Physiol (1985), jap 00810 02015.

Mirsky, R., Woodhoo, A., Parkinson, D.B., Arthur-Farraj, P., Bhaskaran, A., and Jessen, K.R. (2008). Novel signals controlling embryonic Schwann cell development, myelination and dedifferentiation. J Peripher Nerv Syst *13*, 122-135.

Mishra, S.K., and Hoon, M.A. (2013). The cells and circuitry for itch responses in mice. Science *340*, 968-971.

Molliver, D.C., Wright, D.E., Leitner, M.L., Parsadanian, A.S., Doster, K., Wen, D., Yan, Q., and Snider, W.D. (1997). IB4-binding DRG neurons switch from NGF to GDNF dependence in early postnatal life. Neuron *19*, 849-861.

Monk, K.R., Feltri, M.L., and Taveggia, C. (2015). New insights on Schwann cell development. Glia *63*, 1376-1393.

Montano, J.A., Perez-Pinera, P., Garcia-Suarez, O., Cobo, J., and Vega, J.A. (2010). Development and neuronal dependence of cutaneous sensory nerve formations: Lessons from neurotrophins. Microsc Res Tech *73*, 513-529.

Monte, D., Baert, J.L., Defossez, P.A., de Launoit, Y., and Stehelin, D. (1994). Molecular cloning and characterization of human ERM, a new member of the Ets family closely related to mouse PEA3 and ER81 transcription factors. Oncogene *9*, 1397-1406.

Moody, T.W., and Merali, Z. (2004). Bombesin-like peptides and associated receptors within the brain: distribution and behavioral implications. Peptides *25*, 511-520.

Moore, M.W., Klein, R.D., Farinas, I., Sauer, H., Armanini, M., Phillips, H., Reichardt, L.F., Ryan, A.M., Carver-Moore, K., and Rosenthal, A. (1996). Renal and neuronal abnormalities in mice lacking GDNF. Nature *382*, 76-79.

Morrison, K.M., Miesegaes, G.R., Lumpkin, E.A., and Maricich, S.M. (2009). Mammalian Merkel cells are descended from the epidermal lineage. Dev Biol *336*, 76-83.

Mosconi, T.M., Rice, F.L., and Song, M.J. (1993). Sensory innervation in the inner conical body of the vibrissal follicle-sinus complex of the rat. J Comp Neurol *328*, 232-251.

Mountcastle, V.B. (1957). Modality and topographic properties of single neurons of cat's somatic sensory cortex. J Neurophysiol *20*, 408-434.

Munger, B.L., and Ide, C. (1988). The structure and function of cutaneous sensory receptors. Arch Histol Cytol *51*, 1-34.

Nakamura, S., Senzaki, K., Yoshikawa, M., Nishimura, M., Inoue, K., Ito, Y., Ozaki, S., and Shiga, T. (2008). Dynamic regulation of the expression of neurotrophin receptors by Runx3. Development *135*, 1703-1711.

Nave, K.A., and Salzer, J.L. (2006). Axonal regulation of myelination by neuregulin 1. Curr Opin Neurobiol *16*, 492-500.

Nielsen, J., Gotfryd, K., Li, S., Kulahin, N., Soroka, V., Rasmussen, K.K., Bock, E., and Berezin, V. (2009). Role of glial cell line-derived neurotrophic factor (GDNF)-neural cell adhesion molecule (NCAM) interactions in induction of neurite outgrowth and

identification of a binding site for NCAM in the heel region of GDNF. J Neurosci *29*, 11360-11376.

Niu, J., Ding, L., Li, J.J., Kim, H., Liu, J., Li, H., Moberly, A., Badea, T.C., Duncan, I.D., Son, Y.J., *et al.* (2013). Modality-based organization of ascending somatosensory axons in the direct dorsal column pathway. J Neurosci *33*, 17691-17709.

Ogawa, H. (1996). The Merkel cell as a possible mechanoreceptor cell. Prog Neurobiol *49*, 317-334.

Oh, S., Shin, S., and Janknecht, R. (2012). ETV1, 4 and 5: an oncogenic subfamily of ETS transcription factors. Biochim Biophys Acta *1826*, 1-12.

Oppenheim, R.W., Houenou, L.J., Parsadanian, A.S., Prevette, D., Snider, W.D., and Shen, L. (2000). Glial cell line-derived neurotrophic factor and developing mammalian motoneurons: regulation of programmed cell death among motoneuron subtypes. J Neurosci *20*, 5001-5011.

Ozaki, S., and Snider, W.D. (1997). Initial trajectories of sensory axons toward laminar targets in the developing mouse spinal cord. J Comp Neurol *380*, 215-229.

Paixao, S., Balijepalli, A., Serradj, N., Niu, J., Luo, W., Martin, J.H., and Klein, R. (2013). EphrinB3/EphA4-mediated guidance of ascending and descending spinal tracts. Neuron *80*, 1407-1420.

Palmer, C.I., and Gardner, E.P. (1990). Simulation of motion on the skin. IV. Responses of Pacinian corpuscle afferents innervating the primate hand to stripe patterns on the OPTACON. Journal of neurophysiology *64*, 236-247.

Pan, Z.W., and Li, J.C. (2012). Advances in molecular genetics of Hirschsprung's disease. Anat Rec (Hoboken) *295*, 1628-1638.

Paratcha, G., Ledda, F., Baars, L., Coulpier, M., Besset, V., Anders, J., Scott, R., and Ibanez, C.F. (2001). Released GFRalpha1 potentiates downstream signaling, neuronal survival, and differentiation via a novel mechanism of recruitment of c-Ret to lipid rafts. Neuron *29*, 171-184.

Paratcha, G., Ledda, F., and Ibanez, C.F. (2003). The neural cell adhesion molecule NCAM is an alternative signaling receptor for GDNF family ligands. Cell *113*, 867-879.

Pare, M., Behets, C., and Cornu, O. (2003). Paucity of presumptive ruffini corpuscles in the index finger pad of humans. J Comp Neurol *456*, 260-266.

Pare, M., Elde, R., Mazurkiewicz, J.E., Smith, A.M., and Rice, F.L. (2001). The Meissner corpuscle revised: a multiafferented mechanoreceptor with nociceptor immunochemical properties. The Journal of neuroscience *21*, 7236-7246.

Pare, M., Smith, A.M., and Rice, F.L. (2002). Distribution and terminal arborizations of cutaneous mechanoreceptors in the glabrous finger pads of the monkey. J Comp Neurol *445*, 347-359.

Parisi, M.A., and Kapur, R.P. (2000). Genetics of Hirschsprung disease. Curr Opin Pediatr *12*, 610-617.

Patel, A., Harker, N., Moreira-Santos, L., Ferreira, M., Alden, K., Timmis, J., Foster, K., Garefalaki, A., Pachnis, P., Andrews, P., *et al.* (2012). Differential RET signaling pathways drive development of the enteric lymphoid and nervous systems. Sci Signal *5*, ra55.

Patel, K.N., and Dong, X. (2010). An itch to be scratched. Neuron *68*, 334-339.

Patel, O., Shulkes, A., and Baldwin, G.S. (2006). Gastrin-releasing peptide and cancer. Biochimica et biophysica acta *1766*, 23-41.

Patel, T.D., Jackman, A., Rice, F.L., Kucera, J., and Snider, W.D. (2000). Development of sensory neurons in the absence of NGF/TrkA signaling in vivo. Neuron *25*, 345-357.

Patel, T.D., Kramer, I., Kucera, J., Niederkofler, V., Jessell, T.M., Arber, S., and Snider, W.D. (2003). Peripheral NT3 signaling is required for ETS protein expression and central patterning of proprioceptive sensory afferents. Neuron *38*, 403-416.

Pease, D.C., and Pallie, W. (1959). Electron microscopy of digital tactile corpuscles and small cutaneous nerves. J Ultrastruct Res *2*, 352-365.

Pease, D.C., and Quilliam, T.A. (1957). Electron microscopy of the pacinian corpuscle. J Biophys Biochem Cytol *3*, 331-342.

Perez-Pinera, P., Garcia-Suarez, O., Germana, A., Diaz-Esnal, B., de Carlos, F., Silos-Santiago, I., del Valle, M.E., Cobo, J., and Vega, J.A. (2008). Characterization of sensory deficits in TrkB knockout mice. Neurosci Lett *433*, 43-47.

Peters, E.M., Botchkarev, V.A., Muller-Rover, S., Moll, I., Rice, F.L., and Paus, R. (2002). Developmental timing of hair follicle and dorsal skin innervation in mice. J Comp Neurol *448*, 28-52.

Pierchala, B.A., Milbrandt, J., and Johnson, E.M., Jr. (2006). Glial cell line-derived neurotrophic factor-dependent recruitment of Ret into lipid rafts enhances signaling by partitioning Ret from proteasome-dependent degradation. J Neurosci *26*, 2777-2787.

Plaza-Menacho, I., Morandi, A., Robertson, D., Pancholi, S., Drury, S., Dowsett, M., Martin, L.A., and Isacke, C.M. (2010). Targeting the receptor tyrosine kinase RET sensitizes breast cancer cells to tamoxifen treatment and reveals a role for RET in endocrine resistance. Oncogene *29*, 4648-4657.

Polgar, E., Fowler, J.H., McGill, M.M., and Todd, A.J. (1999). The types of neuron which contain protein kinase C gamma in rat spinal cord. Brain Res *833*, 71-80.

Pozas, E., and Ibanez, C.F. (2005). GDNF and GFRalpha1 promote differentiation and tangential migration of cortical GABAergic neurons. Neuron *45*, 701-713.

Quilliam, T.A., and Sato, M. (1955). The distribution of myelin on nerve fibres from Pacinian corpuscles. J Physiol *129*, 167-176.

Rasmusson, D.D., and Turnbull, B.G. (1986). Sensory innervation of the raccoon forepaw: 2. Response properties and classification of slowly adapting fibers. Somatosens Res *4*, 63-75.

Rice, F.L., and Albrecht, P.J. (2008). Cutaneous Mechanisms of Tactile Perception: Morphological and Chemical Organization of the Innervation to the Skin. In The Senses: A Comprehensive Reference (San Diego: Academic Press), pp. 1-32.

Rice, F.L., and Rasmusson, D.D. (2000). Innervation of the digit on the forepaw of the raccoon. J Comp Neurol *417*, 467-490.

Romei, C., Ciampi, R., and Elisei, R. (2016). A comprehensive overview of the role of the RET proto-oncogene in thyroid carcinoma. Nat Rev Endocrinol *12*, 192-202.

Ross, S.E., Mardinly, A.R., McCord, A.E., Zurawski, J., Cohen, S., Jung, C., Hu, L., Mok, S.I., Shah, A., Savner, E.M., *et al.* (2010). Loss of inhibitory interneurons in the dorsal spinal cord and elevated itch in Bhlhb5 mutant mice. Neuron *65*, 886-898.

Rossi, J., Luukko, K., Poteryaev, D., Laurikainen, A., Sun, Y.F., Laakso, T., Eerikainen, S., Tuominen, R., Lakso, M., Rauvala, H., *et al.* (1999). Retarded growth and deficits in the enteric and parasympathetic nervous system in mice lacking GFR alpha2, a functional neurturin receptor. Neuron *22*, 243-252.

Runeberg-Roos, P., and Saarma, M. (2007). Neurotrophic factor receptor RET: structure, cell biology, and inherited diseases. Ann Med *39*, 572-580.

Rutlin, M., Ho, C.Y., Abraira, V.E., Cassidy, C., Bai, L., Woodbury, C.J., and Ginty, D.D. (2014). The cellular and molecular basis of direction selectivity of Adelta-LTMRs. Cell *159*, 1640-1651.

Salzer, J.L. (2015). Schwann cell myelination. Cold Spring Harb Perspect Biol *7*, a020529.

Sanicola, M., Hession, C., Worley, D., Carmillo, P., Ehrenfels, C., Walus, L., Robinson, S., Jaworski, G., Wei, H., Tizard, R., *et al.* (1997). Glial cell line-derived neurotrophic factor-dependent RET activation can be mediated by two different cell-surface accessory proteins. Proceedings of the National Academy of Sciences of the United States of America *94*, 6238-6243.

Santoro, M., and Carlomagno, F. (2013). Central role of RET in thyroid cancer. Cold Spring Harb Perspect Biol *5*, a009233.

Sato, M. (1961). Response of Pacinian corpuscles to sinusoidal vibration. J Physiol *159*, 391-409.

Savonenko, A.V., Melnikova, T., Laird, F.M., Stewart, K.A., Price, D.L., and Wong, P.C. (2008). Alteration of BACE1-dependent NRG1/ErbB4 signaling and schizophrenia-like phenotypes in BACE1-null mice. Proc Natl Acad Sci U S A *105*, 5585-5590.

Saxod, R. (1996). Ontogeny of the cutaneous sensory organs. Microsc Res Tech *34*, 313-333.

Scheibel, M.E., and Scheibel, A.B. (1968). Terminal axonal patterns in cat spinal cord. II. The dorsal horn. Brain Res *9*, 32-58.

Scheibert, J., Leurent, S., Prevost, A., and Debregeas, G. (2009). The role of fingerprints in the coding of tactile information probed with a biomimetic sensor. Science *323*, 1503-1506.

Scherer, S.S., and Wrabetz, L. (2008). Molecular mechanisms of inherited demyelinating neuropathies. Glia *56*, 1578-1589.

Schmittgen, T.D., and Livak, K.J. (2008). Analyzing real-time PCR data by the comparative C(T) method. Nat Protoc *3*, 1101-1108.

Schuchardt, A., D'Agati, V., Larsson-Blomberg, L., Costantini, F., and Pachnis, V. (1994). Defects in the kidney and enteric nervous system of mice lacking the tyrosine kinase receptor Ret. Nature *367*, 380-383.

Scott, A., Hasegawa, H., Sakurai, K., Yaron, A., Cobb, J., and Wang, F. (2011). Transcription factor short stature homeobox 2 is required for proper development of tropomyosin-related kinase B-expressing mechanosensory neurons. J Neurosci *31*, 6741-6749.

Sedy, J., Tseng, S., Walro, J.M., Grim, M., and Kucera, J. (2006). ETS transcription factor ER81 is required for the Pacinian corpuscle development. Dev Dyn *235*, 1081-1089.

Semba, K., Masarachia, P., Malamed, S., Jacquin, M., Harris, S., and Egger, M.D. (1984). Ultrastructure of pacinian corpuscle primary afferent terminals in the cat spinal cord. Brain Res *302*, 135-150.

Semba, K., Masarachia, P., Malamed, S., Jacquin, M., Harris, S., Yang, G., and Egger, M.D. (1985). An electron microscopic study of terminals of rapidly adapting mechanoreceptive afferent fibers in the cat spinal cord. J Comp Neurol *232*, 229-240.

Senok, S.S., and Baumann, K.I. (1997). Functional evidence for calcium-induced calcium release in isolated rat vibrissal Merkel cell mechanoreceptors. J Physiol *500 (Pt 1)*, 29-37.

Senok, S.S., Baumann, K.I., and Halata, Z. (1996). Selective phototoxic destruction of quinacrine-loaded Merkel cells is neither selective nor complete. Experimental brain research *110*, 325-334.

Senzaki, K., Ozaki, S., Yoshikawa, M., Ito, Y., and Shiga, T. (2010). Runx3 is required for the specification of TrkC-expressing mechanoreceptive trigeminal ganglion neurons. Mol Cell Neurosci *43*, 296-307.

Shim, W.S., Tak, M.H., Lee, M.H., Kim, M., Koo, J.Y., Lee, C.H., and Oh, U. (2007). TRPV1 mediates histamine-induced itching via the activation of phospholipase A2 and 12-lipoxygenase. J Neurosci *27*, 2331-2337.

Shortland, P., and Woolf, C.J. (1993). Morphology and somatotopy of the central arborizations of rapidly adapting glabrous skin afferents in the rat lumbar spinal cord. J Comp Neurol *329*, 491-511.

Skaper, S.D. (2012). The neurotrophin family of neurotrophic factors: an overview. Methods Mol Biol *846*, 1-12.

Snider, W.D., and Silos-Santiago, I. (1996). Dorsal root ganglion neurons require functional neurotrophin receptors for survival during development. Philos Trans R Soc Lond B Biol Sci *351*, 395-403.

Solorzano, C., Villafuerte, D., Meda, K., Cevikbas, F., Braz, J., Sharif-Naeini, R., Juarez-Salinas, D., Llewellyn-Smith, I.J., Guan, Z., and Basbaum, A.I. (2015). Primary afferent and spinal cord expression of gastrin-releasing peptide: message, protein, and antibody concerns. J Neurosci *35*, 648-657.

Srinivasan, M.A., Whitehouse, J.M., and LaMotte, R.H. (1990). Tactile detection of slip: surface microgeometry and peripheral neural codes. J Neurophysiol *63*, 1323-1332.

Stassart, R.M., Fledrich, R., Velanac, V., Brinkmann, B.G., Schwab, M.H., Meijer, D., Sereda, M.W., and Nave, K.A. (2013). A role for Schwann cell-derived neuregulin-1 in remyelination. Nat Neurosci *16*, 48-54.

Su, P.Y., and Ko, M.C. (2011). The role of central gastrin-releasing peptide and neuromedin B receptors in the modulation of scratching behavior in rats. J Pharmacol Exp Ther *337*, 822-829.

Sukhtankar, D.D., and Ko, M.C. (2013). Physiological function of gastrin-releasing peptide and neuromedin B receptors in regulating itch scratching behavior in the spinal cord of mice. PLoS One *8*, e67422.

Sun, Y.G., and Chen, Z.F. (2007). A gastrin-releasing peptide receptor mediates the itch sensation in the spinal cord. Nature *448*, 700-703.

Sun, Y.G., Zhao, Z.Q., Meng, X.L., Yin, J., Liu, X.Y., and Chen, Z.F. (2009). Cellular basis of itch sensation. Science *325*, 1531-1534.

Suzuki, M., Ebara, S., Koike, T., Tonomura, S., and Kumamoto, K. (2012). How many hair follicles are innervated by one afferent axon? A confocal microscopic analysis of palisade endings in the auricular skin of thy1-YFP transgenic mouse. Proc Jpn Acad Ser B Phys Biol Sci *88*, 583-595.

Szeder, V., Grim, M., Halata, Z., and Sieber-Blum, M. (2003). Neural crest origin of mammalian Merkel cells. Dev Biol *253*, 258-263.

Tachibana, T., and Nawa, T. (2002). Recent progress in studies on Merkel cell biology. Anat Sci Int *77*, 26-33.

Takahashi-Iwanaga, H. (2000). Three-dimensional microanatomy of longitudinal lanceolate endings in rat vibrissae. J Comp Neurol *426*, 259-269.

Takahashi, M., Ritz, J., and Cooper, G.M. (1985). Activation of a novel human transforming gene, ret, by DNA rearrangement. Cell *42*, 581-588.

Talbot, W.H., Darian-Smith, I., Kornhuber, H.H., and Mountcastle, V.B. (1968). The sense of flutter-vibration: comparison of the human capacity with response patterns of mechanoreceptive afferents from the monkey hand. Journal of neurophysiology *31*, 301-334.

Taniguchi, H., He, M., Wu, P., Kim, S., Paik, R., Sugino, K., Kvitsiani, D., Fu, Y., Lu, J., Lin, Y., *et al.* (2011). A resource of Cre driver lines for genetic targeting of GABAergic neurons in cerebral cortex. Neuron *71*, 995-1013.

Tansey, M.G., Baloh, R.H., Milbrandt, J., and Johnson, E.M., Jr. (2000). GFRalpha-mediated localization of RET to lipid rafts is required for effective downstream signaling, differentiation, and neuronal survival. Neuron *25*, 611-623.

Tapper, D.N. (1965). Stimulus-response relationships in the cutaneous slowly-adapting mechanoreceptor in hairy skin of the cat. Experimental neurology *13*, 364-385.

Taraviras, S., Marcos-Gutierrez, C.V., Durbec, P., Jani, H., Grigoriou, M., Sukumaran, M., Wang, L.C., Hynes, M., Raisman, G., and Pachnis, V. (1999). Signalling by the RET receptor tyrosine kinase and its role in the development of the mammalian enteric nervous system. Development *126*, 2785-2797.

Taylor-Blake, B., and Zylka, M.J. (2010). Prostatic acid phosphatase is expressed in peptidergic and nonpeptidergic nociceptive neurons of mice and rats. PloS one *5*, e8674.

Tessarollo, L., Vogel, K.S., Palko, M.E., Reid, S.W., and Parada, L.F. (1994). Targeted mutation in the neurotrophin-3 gene results in loss of muscle sensory neurons. Proc Natl Acad Sci U S A *91*, 11844-11848.

Tessler, A., Himes, B.T., Soper, K., Murray, M., Goldberger, M.E., and Reichlin, S. (1984). Recovery of substance P but not somatostatin in the cat spinal cord after unilateral lumbosacral dorsal rhizotomy: a quantitative study. Brain Res *305*, 95-102.

Tomlins, S.A., Rhodes, D.R., Perner, S., Dhanasekaran, S.M., Mehra, R., Sun, X.W., Varambally, S., Cao, X., Tchinda, J., Kuefer, R., *et al.* (2005). Recurrent fusion of TMPRSS2 and ETS transcription factor genes in prostate cancer. Science *310*, 644-648.

Treanor, J.J., Goodman, L., de Sauvage, F., Stone, D.M., Poulsen, K.T., Beck, C.D., Gray, C., Armanini, M.P., Pollock, R.A., Hefti, F., *et al.* (1996). Characterization of a multicomponent receptor for GDNF. Nature *382*, 80-83.

Tronche, F., Kellendonk, C., Kretz, O., Gass, P., Anlag, K., Orban, P.C., Bock, R., Klein, R., and Schutz, G. (1999). Disruption of the glucocorticoid receptor gene in the nervous system results in reduced anxiety. Nat Genet *23*, 99-103.

Trupp, M., Belluardo, N., Funakoshi, H., and Ibanez, C.F. (1997). Complementary and overlapping expression of glial cell line-derived neurotrophic factor (GDNF), c-ret proto-oncogene, and GDNF receptor-alpha indicates multiple mechanisms of trophic actions in the adult rat CNS. J Neurosci *17*, 3554-3567.

Tsui-Pierchala, B.A., Ahrens, R.C., Crowder, R.J., Milbrandt, J., and Johnson, E.M., Jr. (2002). The long and short isoforms of Ret function as independent signaling complexes. J Biol Chem *277*, 34618-34625.

Tsui, C.C., Gabreski, N.A., Hein, S.J., and Pierchala, B.A. (2015). Lipid Rafts Are Physiologic Membrane Microdomains Necessary for the Morphogenic and Developmental Functions of Glial Cell Line-Derived Neurotrophic Factor In Vivo. J Neurosci *35*, 13233-13243.

Uesaka, T., Nagashimada, M., and Enomoto, H. (2013). GDNF signaling levels control migration and neuronal differentiation of enteric ganglion precursors. J Neurosci *33*, 16372-16382.

Uesaka, T., Nagashimada, M., Yonemura, S., and Enomoto, H. (2008). Diminished Ret expression compromises neuronal survival in the colon and causes intestinal aganglionosis in mice. J Clin Invest *118*, 1890-1898.

van Weering, D.H., and Bos, J.L. (1997). Glial cell line-derived neurotrophic factor induces Ret-mediated lamellipodia formation. J Biol Chem *272*, 249-254.

Wada, E., Way, J., Lebacq-Verheyden, A.M., and Battey, J.F. (1990). Neuromedin B and gastrin-releasing peptide mRNAs are differentially distributed in the rat nervous system. J Neurosci *10*, 2917-2930.

Wada, E., Way, J., Shapira, H., Kusano, K., Lebacq-Verheyden, A.M., Coy, D., Jensen, R., and Battery, J. (1991). cDNA cloning, characterization, and brain region-specific expression of a neuromedin-B-preferring bombesin receptor. Neuron *6*, 421-430.

Wada, E., Wray, S., Key, S., and Battey, J. (1992). Comparison of gene expression for two distinct bombesin receptor subtypes in postnatal rat central nervous system. Mol Cell Neurosci *3*, 446-460.

Wang, S.D., Goldberger, M.E., and Murray, M. (1991). Plasticity of spinal systems after unilateral lumbosacral dorsal rhizotomy in the adult rat. J Comp Neurol *304*, 555-568.

Weerakkody, N.S., Mahns, D.A., Taylor, J.L., and Gandevia, S.C. (2007). Impairment of human proprioception by high-frequency cutaneous vibration. J Physiol *581*, 971-980.

Weerakkody, N.S., Taylor, J.L., and Gandevia, S.C. (2009). The effect of high-frequency cutaneous vibration on different inputs subserving detection of joint movement. Exp Brain Res *197*, 347-355.

Wellnitz, S.A., Lesniak, D.R., Gerling, G.J., and Lumpkin, E.A. (2010). The regularity of sustained firing reveals two populations of slowly adapting touch receptors in mouse hairy skin. Journal of neurophysiology *103*, 3378-3388.

Wende, H., Lechner, S.G., Cheret, C., Bourane, S., Kolanczyk, M.E., Pattyn, A., Reuter, K., Munier, F.L., Carroll, P., Lewin, G.R., *et al.* (2012). The transcription factor c-Maf controls touch receptor development and function. Science *335*, 1373-1376.

Willem, M., Garratt, A.N., Novak, B., Citron, M., Kaufmann, S., Rittger, A., DeStrooper, B., Saftig, P., Birchmeier, C., and Haass, C. (2006). Control of peripheral nerve myelination by the beta-secretase BACE1. Science *314*, 664-666.

Willis, W.D., and Coggeshall, R.E. (2004). Sensory mechanisms of the spinal cord, 3rd edn (New York: Kluwer Academic/Plenum Publishers).

Winkelmann, R.K., and Breathnach, A.S. (1973). The Merkel cell. J Invest Dermatol *60*, 2-15.

Woo, S.H., Baba, Y., Franco, A.M., Lumpkin, E.A., and Owens, D.M. (2012). Excitatory glutamate is essential for development and maintenance of the piloneural mechanoreceptor. Development *139*, 740-748.

Woodbury, C.J., Ritter, A.M., and Koerber, H.R. (2001). Central anatomy of individual rapidly adapting low-threshold mechanoreceptors innervating the "hairy" skin of newborn mice: early maturation of hair follicle afferents. J Comp Neurol *436*, 304-323.

Worby, C.A., Vega, Q.C., Zhao, Y., Chao, H.H., Seasholtz, A.F., and Dixon, J.E. (1996). Glial cell line-derived neurotrophic factor signals through the RET receptor and activates mitogen-activated protein kinase. J Biol Chem *271*, 23619-23622.

Worley, D.S., Pisano, J.M., Choi, E.D., Walus, L., Hession, C.A., Cate, R.L., Sanicola, M., and Birren, S.J. (2000). Developmental regulation of GDNF response and receptor expression in the enteric nervous system. Development *127*, 4383-4393.

Wu, J., and Janknecht, R. (2002). Regulation of the ETS transcription factor ER81 by the 90-kDa ribosomal S6 kinase 1 and protein kinase A. J Biol Chem *277*, 42669-42679.

Yamashita, Y., Akaike, N., Wakamori, M., Ikeda, I., and Ogawa, H. (1992). Voltage-dependent currents in isolated single Merkel cells of rats. J Physiol *450*, 143-162.

Yang, J., Runeberg-Roos, P., Leppanen, V.M., and Saarma, M. (2007). The mouse soluble GFRalpha4 receptor activates RET independently of its ligand persephin. Oncogene *26*, 3892-3898.

Yoshikawa, M., Murakami, Y., Senzaki, K., Masuda, T., Ozaki, S., Ito, Y., and Shiga, T. (2013). Coexpression of Runx1 and Runx3 in mechanoreceptive dorsal root ganglion neurons. Dev Neurobiol *73*, 469-479.

Yu, T., Scully, S., Yu, Y., Fox, G.M., Jing, S., and Zhou, R. (1998). Expression of GDNF family receptor components during development: implications in the mechanisms of interaction. J Neurosci *18*, 4684-4696.

Zelena, J. (1978). The development of Pacinian corpuscles. J Neurocytol *7*, 71-91.

Zelena, J. (1980). Rapid degeneration of developing rat Pacinian corpuscles after denervation. Brain Res *187*, 97-111.

Zelena, J. (1982). Survival of Pacinian corpuscles after denervation in adult rats. Cell Tissue Res *224*, 673-683.

Zelena, J. (1984). Multiple axon terminals in reinnervated Pacinian corpuscles of adult rat. J Neurocytol *13*, 665-684.

Zelena, J. (1994). Nerves and Mechanoreceptors (London: Chapman & Hall).

Zelena, J., Halata, Z., Szeder, V., and Grim, M. (1997). Crural Herbst corpuscles in chicken and quail: numbers and structure. Anat Embryol (Berl) *196*, 323-333.

Zelena, J., Jirmanova, I., Nitatori, T., and Ide, C. (1990). Effacement and regeneration of tactile lamellar corpuscles of rat after postnatal nerve crush. Neuroscience *39*, 513-522.

Zhang, J., Eto, K., Honmyou, A., Nakao, K., Kiyonari, H., and Abe, S. (2011). Neuregulins are essential for spermatogonial proliferation and meiotic initiation in neonatal mouse testis. Development *138*, 3159-3168.